



**Studies on Equilibrium and Dynamic
Characteristics of New Adsorption Pairs**

Yong Zhong

This dissertation has been submitted to the University of Warwick in the fulfillment of the requirements for the award of the degree of PhD in engineering Studies. Submitted July 2006

Table of Contents

Nomenclature		i
Acknowledgements		iv
Declaration		v
Abstract		vi
Chapter 1 Introduction		
1.1	History of sorption refrigeration system	2
1.2	Sorption system types	4
1.3	Variety of working pairs	7
1.4	Research objective	9
1.5	Thesis structure	10
Chapter 2 Literature Review		
2.1	Introduction	12
2.2	Adsorption cycles	13
2.2.1	Basic cycle	15
2.2.2	Heat and Mass Recovery Cycles	22
2.3	Adsorption pairs	42
2.3.1	Activated carbon-ammonia systems	44
2.3.2	Activated carbon-methanol systems	46
2.3.3	Silica-gel/water and silica-gel methanol systems	48
2.3.4	Zeolite-water systems	49
2.4	Heat and mass transfer	52
2.5	Previous work in University of Warwick	59
2.6	Summary	67
Chapter 3 Theory		
3.1	Introduction	80
3.2	Principles of adsorption	81
3.3	Adsorption equation of state	85
3.3.1	The Langmuir equation	86
3.3.2	Freundlich isotherm	88
3.3.3	The BET equation	89
3.3.4	Polanyi potential theory	91
3.3.5	The Dubinin-Radushkevich equation	93
3.3.6	The Dubinin-Astakhov equation	94

3.3.7	Improved adsorption equation	96
3.4	Thermodynamic relationships	105
3.4.1	The Clausius-Clapeyron equation	105
3.4.2	Enthalpy of vaporization	107
3.4.3	Enthalpy of adsorption	108
3.5	Summary	110

Chapter 4 Assessment of New Pairs Based on Equilibrium Data

4.1	Introduction	117
4.2	Properties of adsorbates and adsorbents	118
4.3	Experimental apparatus for determining equilibrium adsorption properties	126
4.4	Test with CO ₂ as refrigerant	131
4.5	Alumina – NH ₃	140
4.6	Metallic salt compounds in host matrices	142
4.6.1	BaCl ₂ - Vermiculite	142
4.6.2	Carbon and Calcium Chloride – NH ₃	154
4.6.3	CaCl ₂ +Alumina – NH ₃	163
4.6.4	CaCl ₂ – NH ₃	170

Chapter 5 Dynamics of Adsorption Pairs under Isothermal Conditions

5.1	Introduction	189
5.2	Theory of the dynamics of sorption	191
5.3	Experimental studies	197
5.3.1	Experimental apparatus and procedure	197
5.3.2	Carbon – Ammonia	200
5.3.3	C + CaCl ₂ – Ammonia	204
5.3.4	Vermiculite + BaCl ₂ – Ammonia	205
5.4	Simulation of the dynamics of sorption in Vermiculite – BaCl ₂	214
5.4.1	Description of the mathematical model	214
5.4.2	Data fits	217

Chapter 6 Dynamics of Vermiculite – BaCl₂ in a Lab-Scale Adsorption System

6.1	Introduction	238
6.2	Test rig description	239
6.3	Test procedure and conditions	243
6.4	Experimental results and analysis	247

Chapter 7 Simulation of Sorption in Vermiculite – BaCl₂

7.1	Physical model	259
-----	----------------	-----

7.2	Modeling equations	263
7.3	Simulated results	272
7.4	Prediction of behavior in a sorption generator	290

Chapter 8	Conclusion	295
-----------	------------	-----

Appendices

Appendix A	Matlab program of data fits for D-A equation	299
Appendix B	Matlab program to contour the isosteres of Test Sample	302
Appendix C	Matlab program to simulate the adsorption system using CO ₂ as refrigerant	303
Appendix D	Matlab Program to calculate the concentration of carbon	307
Appendix E	Matlab program to simulate transient heat transfer in a single tube with supplied p, twall vs. time	308
Appendix F	Matlab program to simulate the performance of a compact adsorption bed with idealized cycle	318

Nomenclature

A	Freundlich constant in equation (3-6); differential molar work of adsorption in equation (3-12); the slope of the saturated adsorbate line on the Clapeyron diagram in equation (3-56) and (4-5); area of conduction for sample in equation (6-2); cross-sectional area of flow in equation (7-2)
A_{fw}	heat transfer area between the wall and heat transfer fluid
A_{wc}	heat transfer area between the wall and reaction bed
B	pore size
c_p	specific heat at constant pressure
c_{pf}	specific heat capacity of the heat transfer fluid
c_{pw}	specific heat capacity of the wall
c_{pc}	specific heat capacity of compound adsorbent in chapter 7
c_v	specific heat at constant volume
C	resistant constant due to chemical reactor
C_{ad}	resistant constant during adsorption process
C_{de}	resistant constant during desorption process
C_{ps}	specific heat of the sample in chapter 6
C_{pa}	specific heat of adsorbed ammonia in chapter 6
D	Fickian diffusivity
D_0	intra-particle diffusivity of sorbate
D_h	hydraulic diameter of channel
E	parameters of the distribution function in equation (3-13)
f	fugacities
g	Gibbs free energy
h	enthalpy; convective heat transfer coefficient in equation (7-1)
H	heat of sorption
k	constant determined by the surface of the adsorbent in equation (3-11); constant determined by the characteristics of both adsorbent and adsorbate in equation (3-36); thermal conductivity of the fluid in equation (7-1)
k_a	adsorption constant
k_d	desorption constant
k_s	thermal conductivity of the sample
K	mass transfer coefficient in equation (5-20)
K_{ad}	mass transfer coefficient during adsorption process
K_{de}	mass transfer coefficient during desorption process
K_d	apparent diffusion time constant
K_L	effective LDF mass transfer coefficient
K_Q	effective QDF mass transfer coefficient
L	latent heat
\dot{m}	heat transfer fluid mass flow rate

m	mass
m_a	mass of active carbon in equation (4-16); mass of alumina in equation (4-20); mass of adsorbed ammonia in chapter 6
m_c	mass of compound adsorbent
m_g	mass of free gaseous ammonia
m_r	mass of liquid ammonia in receiver
m_t	mass change of adsorbent at time t in chapter 5; total mass of ammonia in the system in chapter 6
m_∞	final mass change of adsorbent in chapter 5
M_c	mass of the compound adsorbent
M_f	mass of the heat transfer fluid
M_w	mass of the wall
n	constant determined by adsorption pairs in chapter 3
p	pressure
p_{ev}	evaporator pressure
p_{con}	condensing pressure
$p_{transition}$	pressure of phase transition
q	specific heat transfer
Q	heat transfer
Q_c	useful cooling power in equation (4-6)
r	position of the sample cell from the centre
r_c	radius of the adsorbent particle
R	specific gas constant at the system pressure and temperature
R_0	radius of particle or crystal
s	entropy
t	Celsius temperature of adsorbent bed in chapter 4; time in the other parts
t_f	thickness of the heat transfer fluid channel, metal wall and adsorbent
t_w	thickness of the metal wall
t_c	thickness of the adsorbent
T	temperature
T_w	mean temperature of the wall
T_c	temperature of adsorbent
T_f	mean temperature of heat transfer fluid
T_{fin}	inlet temperature of the heat transfer fluid respectively
T_{fout}	outlet temperature of the heat transfer fluid respectively
T_{LMTD}	temperature change in the heat transfer fluid, calculated by equation 7-5
T_{sat}	saturation temperature
u	internal energy
U	heat transfer coefficient
U_{fw}	heat transfer coefficient between the wall and heat transfer fluid
U_{wc}	heat transfer coefficient between the wall and adsorbent
v	velocity
V	volume

V_0	total pore volume
W_0	whole volume of the adsorption space
x	concentration
\bar{x}	average adsorbate content in the sample
$\bar{x}(t)$	average adsorbate concentration in the adsorbent particle at time t
x^*	final equilibrium adsorbate concentration in the adsorbent particle in equation (5-1)
x_0	limiting adsorption capacity in chapter 3; initial equilibrium adsorbate concentration in the adsorbent particle in chapter 5, 6, 7

Greek Letters

θ	surface coverage or friction filling of the micro-pores in equation (3-2)
ε	potential energy
β	affinity coefficient determined by the adsorbent-adsorbate pair in equation (3-11)
ρ	density
ρ_s	sample density
ρ^*	density of the substance adsorbed at a limiting micro filling
μ	viscosity

Common Dimensionless Variables

Nu	Nusselt number = hd/k
Re	Reynolds number = $\rho vd/\mu$

Acknowledgement

I would like to express my gratitude to my supervisor, Prof. Robert Critoph, for his support, patience, and encouragement throughout my graduate studies. It is not often that one finds an advisor and colleague that always finds the time for listening to the little problems and roadblocks that unavoidably crop up in the course of performing research. His technical and editorial advice was essential to the completion of this dissertation and has taught me innumerable lessons and insights on the workings of academic research in general.

The friendship of Dr. Roger Thorpe and Dr. Zacharie Tamainot-Telto is much appreciated and has led to many interesting and good-spirited discussions relating to this research. In particular, I would like to thank them for their help during my dynamic experiments and mass measurement.

I would like to also thank Yana and Lina, their support and encouragement was in the end what made this dissertation possible. The help of all my friends will be greatly appreciated.

Last, but not least, I would like to express my deepest gratitude and love to my family for their dedication and the many years of financial support during my studies. This dissertation is dedicated to them.

Declaration:

I confirm that, except where indicated through the proper use of citations and references, this is my own original work. I confirm that, subject to final approval by the Board of Examiners of the Institute of engineering studies, a copy of this Dissertation may be placed upon the shelves of the library of the University of Warwick and may be circulated as required.

Signed:

Date:

Abstract

In this thesis, research on kinetic and equilibrium state properties of some new adsorption pairs and non-equilibrium models are investigated.

In the first part, the equilibrium characteristics of adsorption pairs using carbon dioxide as adsorbate are studied. The results showed that the performance of this kind of adsorption system is poor due to the low latent heat of carbon dioxide.

New composite ammonia adsorbents, 12.3 wt. % CaCl_2/C (3C), 17 wt. % $\text{CaCl}_2/\text{Alumina}$ (SWS), and 59 wt. % $\text{BaCl}_2/\text{vermiculite}$, were synthesized and studied. It was found that the modification of host matrices by the salt dramatically increases the ammonia uptake.

Hysteresis between the synthesis and decomposition reaction was found and the van't Hoff equation was applied to describe the hysteresis.

In the second part, kinetic experiments of the composite ammonia adsorbent, 59 wt. % $\text{BaCl}_2/\text{vermiculite}$, were performed under isothermal conditions and conditions that would be experienced in a real system. Based on the experimental data, a modified linear driving force (LDF) model is used to simulate the dynamics of adsorption pair. In the model, two resistant constants were obtained empirically from the experimental data.

In the third part, the dynamic model of concentration change with heat and mass transfer equation were used to simulate the performance of adsorption system. The results were

very encouraging with a maximum *COP* of around 0.8 and a maximum *SCP* of around 600W kg^{-1} in an air conditioning application with one-bed basic cycle.

Further studies could focus on the commercial analysis of this promising material in air conditioning. A real lab-scale compact bed could be set up and tested for the performance of adsorption pairs.

Keyword: **Adsorption, Equilibrium, Kinetics, Hysteresis, Modified linear driving force model, Simulation**

Chapter 1 Introduction

The objective of this project is to evaluate the equilibrium and kinetic characteristics of adsorption cooling systems utilising some new adsorption pairs and to obtain a practical numerical model to predict performance of a real adsorption system using data obtained from laboratory-scale experiments.

This chapter reviews the history of the adsorption systems and the challenges at present, connected with environmental problems concerning the ozone layer depletion and global warming due to the emission of CFCs, HFCs and CO₂ from traditional refrigeration units as well as the poor performance of adsorption systems. Due to its energy saving and environmental benefits, adsorption refrigeration could be an excellent replacement for traditional units in the foreseeable future.

1.1 History of sorption refrigeration system

The history of sorption refrigeration goes back to the middle of 19th century when Michael Faraday first demonstrated the system in 1848 utilising ammonia and silver chloride as working pair [1]. Little further research developed until the early years of 20th century when Plank and Kuprianoff described a practical adsorption system by adsorbing methanol into active carbon [2]. Subsequently sorption refrigerators were commercially available in the 1920s. In 1929, Hulse and Miller described an adsorption system in the United States for the air conditioning system of railway carriages [3, 4]. Silica gel-sulphur dioxide was chosen as an adsorbent/adsorbate pair. However, following the advent of cheap reliable compressor and electrical motors, sorption systems fell out of favour. Half a century passed and little research development was carried out on sorption systems.

With the concerns over the ozone layer depletion due to CFCs, global warming due to HFCs and CO₂, since 1970s and up to the present day, interest in sorption systems has increased gradually [5]. Sorption systems which use environmentally friendly refrigerants instead of CFCs will be an ideal replacement for the classical vapour compression machines.

At present, solid sorption systems in some ways seem a more promising choice. They can efficiently use natural gas or solar energy as a primary energy source, and they have no significant moving parts, so the machine will operate silently and safely and be easy to maintain. Of course, there are some disadvantages of the gas-solid sorption system proposed, such as poor heat transfer capacity in the bed, which results in low specific cooling power and huge volume of the solid adsorbent and poor heat transfer capacity

between beds, which leads to a significant reduction in the performance of the adsorption system.

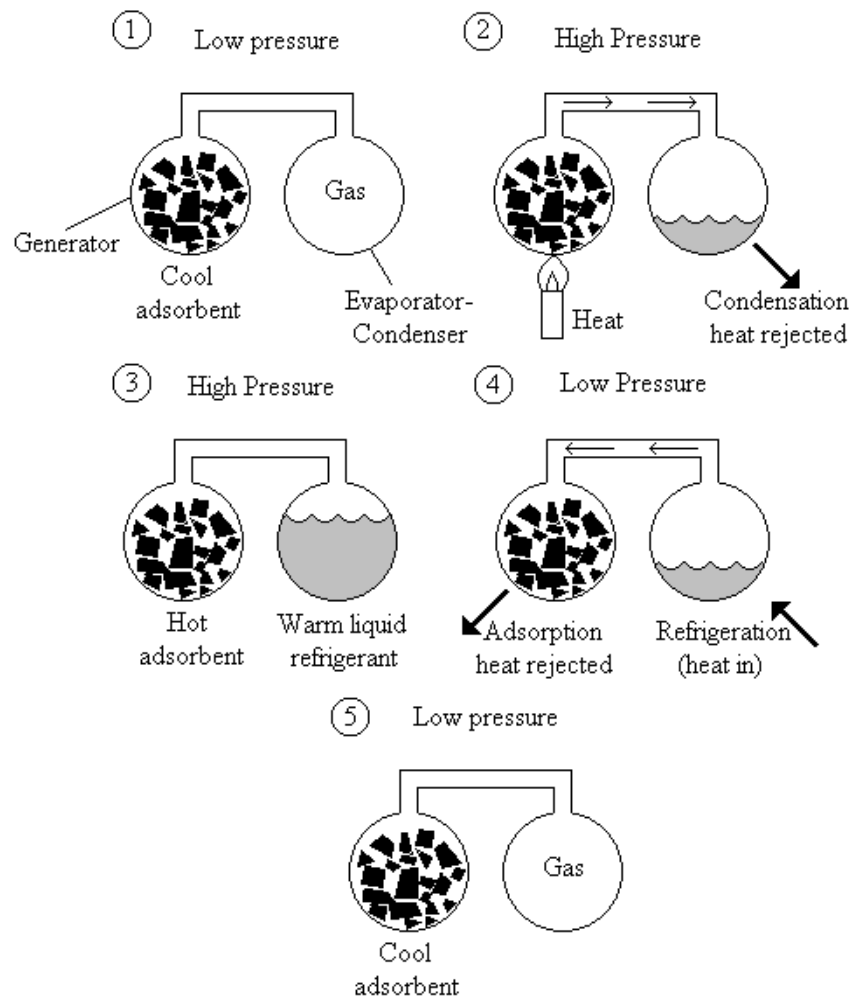
Therefore, recent researches have focused on the following challenges [6]:

- To improve heat transfer in the adsorbate-bed, thereby reducing size and cost
- To improve regeneration heat transfer between beds, thereby increasing COP

1.2 Sorption system types

Sorption systems are the machine used to produce cold energy storage with minimal pollution and energy losses. All sorption cycles can be thought of as using a ‘chemical compressor’ rather than a mechanical one [6]. The simplest form of adsorption refrigerator consists of two linked vessels, both of which contain refrigerant and one of which is also filled with adsorbent as shown in figure 1-1 [6].

Figure 1-1 Basic adsorption cycle



This basic system is comprised of two linked containers, one of which contains the solid adsorbent and is termed the generator and the other is the combined evaporator and condenser in which the refrigerant is evaporated and condensed. Initially the system is at a low temperature and pressure and the adsorbent contains a high concentration of refrigerant whilst the condenser-evaporator contains only refrigerant gas (figure 1-1(1)). The generator is then heated which raises the system pressure and causes refrigerant to be desorbed which passes to the condenser-evaporator where it condenses (figure 1-1(2, 3)). The condensing refrigerant rejects heat, which produces a useful heat output if the system is to be used as a heat pump.

Cooling the generator back down to its initial temperature completes the cycle and causes the adsorbent to re-adsorb the refrigerant (figure 1-1(4, 5)). The cooling also reduces the system pressure and causes the liquid refrigerant in the condenser-evaporator to evaporate and absorb heat. This produces the useful cooling effect if the system is to be used as a refrigerator.

Although absorption systems have higher COP (Coefficient of Performance) and greater specific cooling power, adsorption refrigeration systems still stand their ground for many reasons. The first advantage of solid adsorbents is that they are totally non-volatile unlike most liquid absorbents [6]. One of the two conventional liquid absorption cycle pairs uses ammonia as the refrigerant and water as the adsorbent. In the generation phase, when a concentrate ammonia-water solution is heated, the ammonia is driven off but the vapour contains a few percent of water. This must be removed in a rectifier, which preferentially condenses most of the water vapour and returns it to the generator. Unfortunately this reduces the energy efficiency as well as requiring additional heat exchangers within the

system. The other commonly used pair uses water as refrigerant and Lithium Bromide solution as the sorbent in air conditioning applications. It does not suffer from the problem, since LiBr is effectively non-volatile. However, the pair does have limitations due to the crystallisation limits of LiBr in water. In very hot climate where heat rejection temperature is higher than about 35°C, the pair cannot be used unless additives are used to move the crystallisation boundary [6].

The major advantage that solid sorbent have over liquid system is the large range of available sorption pairs suitable for various applications [6]. The number of liquid absorbent – refrigerant pairs that give reasonable performance is very limited and governed by unalterable chemistry and physics. When using physical adsorption, almost any refrigerant may be used and in principle an adsorbent can be manufactured with the optimal pore size distribution for the particular application.

1.3 Variety of working pairs

The choice of adsorbent and refrigerant pairs will have a great effect on the performance of adsorption systems. Critoph [7] and Srivastava and Eames [8] present a useful discussion of working pairs.

There is a wide range of possible adsorbent/refrigerant pairs but the choice will be governed by factors such as high storage capacity, high thermal stability within the working condition, good thermal conductivity, and high specific power output. They also have a small specific volume and are non-corrosive and non-toxic (environmentally friendly), have a low viscosity and surface tension and low cost. Lebrum and Neveu [9] suggested the following criteria to be considered in a selection of an appropriate working pair:

- economic criteria (cost of working pair itself or cost of equipment)
- performance criteria (temperature rise, specific power production, mass of working pair)
- cost and performance criteria (specific power per unit mass and unit area of exchange surface and temperature rise by unit mass or unit area of exchange surface)

According to the above description, the suitable adsorbents are porous that should adsorb a large amount of refrigerant fluid from the vapour phase and present some additional characteristics: wide concentration change over a small temperature range, reversibility of adsorption process for many cycles, low cost and good thermal conductivity. There are many materials that are suitable to apply in the adsorption system, such as carbon, zeolite

and silica gel. However, by their nature, micro-porous adsorbents always are good insulators. And in order to achieve a rapid cycling, the heat transfer capacity of the adsorbent needs to be improved.

Many ideas have been put forward in order to improve the heat transfer capacity, such as adding high conductivity material into the adsorbent bed, incorporating fins and heat transfer structure into the bed, using metallic foams in conjunction with adsorbents and so on. The details will be discussed in chapter 2.

Another important element is the refrigerant. Ideally, the chosen refrigerant should have a vapour pressure slightly higher than atmospheric at the evaporation temperature. Also, the vapour pressure at the condensing temperature should not be excessively high so as to minimise the size and strength of system components required. Generally speaking, the refrigerant should have high latent heat and good thermal stability. The refrigerants commonly considered in adsorption system are water, methanol, and ammonia.

1.4 Research objective

This project concentrates mainly on the evaluation of equilibrium and kinetic characteristics of new adsorption pairs suitable for a prototype heat driven adsorption refrigeration system. The research gives useful information for the further study on commercial adsorption machine using the new sorption pairs.

The objectives can be further detailed as following:

- Investigate possible adsorbent/refrigerant pairs and adsorption cycles
- Design and construct a pilot-scale adsorption refrigeration system using for equilibrium and kinetic experiments.
- Evaluate the performance of the adsorption system
- Develop a mathematical model for calculation of the behaviour of a real adsorption system.

1.5 Thesis structure

This thesis includes the following contents. In chapter 2, previous research on adsorption pairs, adsorption cycles and heat and mass transfer are reviewed, which give a panoramic view of the current adsorption research and also provide useful information for the selection of adsorption pairs used in the project. Chapter 3 is mainly focused on the study of the mechanism and thermodynamics of the adsorption process. Chapter 4 is concentrated on the equilibrium study of adsorption systems using CO₂ and NH₃ as refrigerant. Chapter 5 and 6 are involved in the dynamics of adsorption pairs under isothermal condition and in a real laboratory-scale adsorption system. A modified LDF (Linear Driving Force) model is proposed and verified. Based on the study of chapter 5 and 6, a mathematical model is set up to simulate the performance of a compact adsorption bed using BaCl₂ – NH₃ as adsorption pairs. The results are shown in chapter 7.

References:

- [1] S.D. Waszkiewicz, Adsorption refrigeration system using zeolite and methanol, PhD dissertation, University of Bristol, 2003
- [2] R. Plank, Kuprianoff J. In die Kleinltemaschine. Berlin: Springer-Verlag, 1960
- [3] G.E. Hulse, Freight car refrigeration by an adsorption system employing silica gel. Refrig. Engnr, p.17, 1929
- [4] E.B. Miller, The development of silica gel refrigeration, Am. Soc. Refrig. Engnr, p.17, 1929
- [5] F. Meunier, Solid sorption: an alternative to CFC's. Heat Recovery Systems and CHP, vol.13, pp.289- 295 1993,
- [6] R.E. Critoph, Adsorption refrigeration and heat pumps, In: Carbon Materials for Advanced Technologies, Edited by Timothy D. Burchell, pp.303-340, PERGAMON, 1999
- [7] R.E. Critoph, Evaluation of alternative refrigerant—adsorbent pairs for refrigeration cycles, Appl. Therm. Engng, vol.16 (11), pp.891-900, 1996
- [8] N.C. Srivastava, I.W. Eames, A review of adsorbents and adsorbates in solid-vapour adsorption heat pump systems, Applied Thermal Engineering, vol.18, pp. 707 -714, 1998
- [9] P. Neveu, M. Lebrun, High efficiency process for solid–gas thermochemical heat pumps, Fourth Congress of Chemical Engineering, Karlsruhe, Germany, pp. 16-21, 1991

Chapter 2 Literature Review

2.1 Introduction

The primary objective of this review is to provide fundamental understanding of the current adsorption systems, and show the further development in this area. The work of other researchers in the adsorption field is reviewed so as to provide an indication of present developments and techniques. Based on this foundation, the aim of the following literature review is to ensure that the subsequent research is able to provide a positive and original contribution to the overall body of research knowledge.

2.2 Adsorption cycle

Many researchers have investigated the thermodynamics of solid adsorption cycles in order to improve cycle efficiency, and overall cycle performance. Many adsorption cycles have been proposed varying from simplest intermittent cycles to more complex systems utilising internal heat regeneration and thermal wave systems. The performance of adsorption system can be expressed in the form of cycle Coefficient of Performance (COP). In summary, the frequently cited adsorption refrigeration cycles are [1]:

- (a) The basic cycle, which is an intermittent refrigeration cycle when operated with one bed.
- (b) The continuous heat recovery cycle, which is usually operated with two adsorption beds. The adsorption bed to be cooled will transfer heat to the adsorption bed to be heated and this heat transfer between two beds includes sensible heat and heat of adsorption. This heat recovery process is useful in increasing COP. Multi-beds could be adopted to get even more heat recovery and thereby much higher COP.
- (c) The Thermal wave cycle [2], in which it is assumed that a high temperature gradient exists along an adsorption bed. For a two-bed system, high temperature thermal fluid flows into the adsorption bed and exchanges heat with the bed so that the fluid cools rapidly after heat exchanging. After being cooled by the ambient surrounding, the fluid flows into another adsorption bed, recovers heat so that at the exit of the bed the thermal fluid become hot and the temperature will be very close to the temperature of the heat source. In this design less heat is added to the system, and less heat released to the environment, thus the heat recovery ratio is high and the COP is significantly increased.

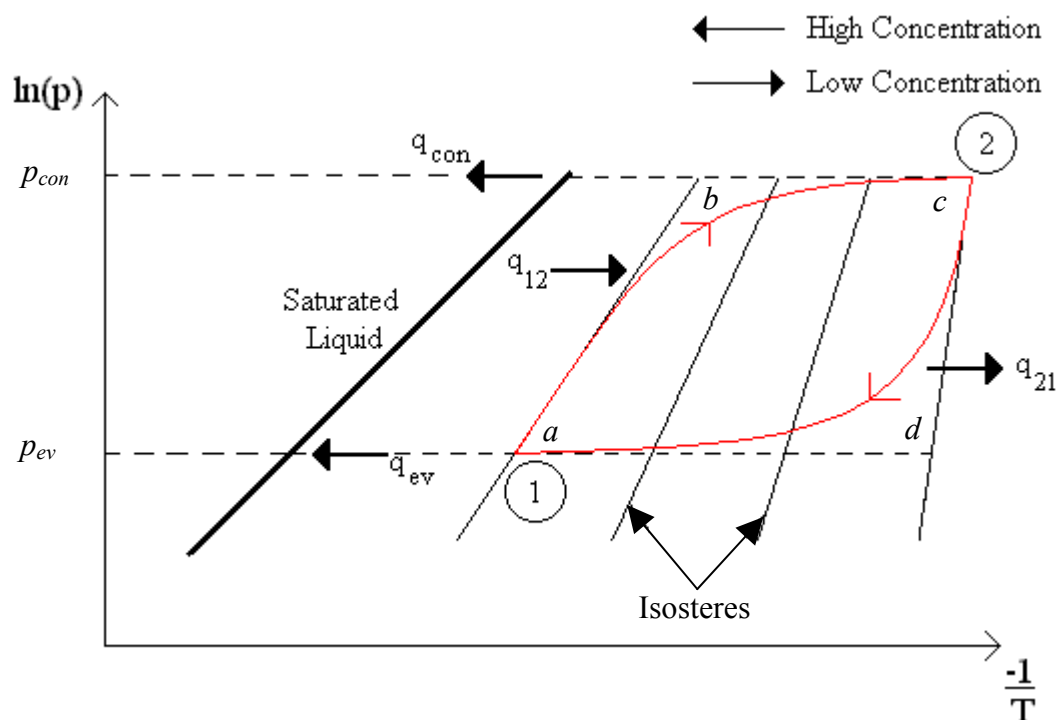
- (d) The convective thermal wave cycle [3]. The concept is the same as thermal wave cycle; however, the thermal fluid is the refrigerant itself. Thus the heat transfer between thermal fluid and adsorption bed is direct contact heat transfer, which is incorporated with mass transfer in the system.
- (e) The cascading cycle [4, 5], in which working pairs might be zeolite-water/activated carbon-methanol, zeolite-water/silica gel-water or zeolite-water/zeolite-water. A heat source (at around 200 °C) drives the high temperature stage adsorption refrigeration cycle (typically 100-200 °C for zeolite-water). The sensible heat and the adsorption heat of the high temperature stage drives the low temperature stage.

2.2.1 Basic cycles

Usually the basic cycle consists of one adsorbent bed which is alternately heated and cooled and produces an intermittent cooling or heating effect. During the heating phase of the cycle, the thermal energy is supplied to provide sensible heat and latent heat for the desorption of the adsorbate [7].

The adsorbent bed exchanges heat with a heat source at high temperature and a heat sink at low temperature. But the complete adsorption system has an evaporator and a condenser that rejects heat to the environment. So the system exchanges heat with another heat sink and a heat source at low temperature. Hence, the refrigerant transfers heat in the adsorbent bed, condenser and evaporator. The cycle is thus a four-temperature cycle, shown in Figure 2-1.

Figure 2-1: Clapeyron diagram of basic adsorption cycle



The mass ratio of adsorbent to adsorbate at equilibrium is a function of the adsorption pressure and adsorbent temperature, i.e. $x = f(p, T)$. According to the analysis in the adsorption process, a set of equations can be applied [8]:

- Isothermal adsorption, $x = f(p)_T$, mainly applied in micro-porous adsorption in industrial equipment
- Isobaric adsorption, $x = f(T)_p$, is used in the design of generation processes [8].
- Isosteric process, $p = f(p, T)_x$, is suitable for the calculation of heat of adsorption and desorption

The isosteric and isobaric adsorption equations are the basic for design and simulation of an adsorption refrigeration process. A basic adsorption cycle can be represented with the aid of the p - T diagram as it is shown in figure 2-1.

The cycle consists of four processes [9]:

(a) Heating and pressurisation (figure 2-1(*a-b*))

At this stage, the adsorbent contains a large concentration of refrigerant. The adsorbent bed receives heat, thus the temperature increases and the adsorbent temperature increases as well. This heating induces a pressure increase from the evaporator pressure (p_{ev}) to the condensing pressure (p_{con}). The generator pressure increases from the evaporating pressure. The mass in the generator is considered to remain constant until the condensing pressure is reached, although the concentration may decrease slightly if the refrigerant is able to be desorbed into any void volume present in the system.

(b) Heating and desorption (figure 2-1(*b-c*))

At this stage, the adsorbent bed continues receiving heat while it is connected to the condenser, thus the condenser pressure prevails within the system. Further increase in the adsorbent temperature induce desorption of the refrigerant vapour and the vapour is driven out from adsorbent bed. This desorbed vapour condenses and heat is rejected to the second heat sink at an intermediate temperature. The mass of refrigerant in the generator is no longer constant and the concentration decreases as the temperature increases from the lower generating temperature to the upper generating temperature.

(c) Cooling and Depressurisation (figure 2-1(*c-d*))

At this stage, the adsorbent bed is cooled. The adsorbent temperature decreases, which induces a change in pressure from the condensing pressure (p_{con}) to the evaporator pressure (p_{ev}). The mass in the generator is considered to remain constant until the evaporating pressure is reached, although the concentration may increase slightly if the refrigerant is able to be adsorbed from any void volume present in the system.

(d) Cooling and Adsorption(figure 2-1(*d-a*))

At this stage, the adsorption bed is cooled while connected to the evaporator, thus the evaporator pressure prevails within the system. The adsorbent temperature continues decreasing, which induces adsorption if the refrigerant vapour (the vapour is driven in the adsorbent bed). This adsorbed vapour is vaporized in the evaporator. The evaporator heat is supplied by the heat source at low temperature. The mass of refrigerant in the generator

is no longer constant and the concentration increases as the temperature decreases from the initial adsorption temperature to the final adsorption temperature. This stage is similar to the evaporation in traditional compression cycles.

For most purposes, analysis of the cycle gives an adequate estimate of the COP and cooling or heating power per kg of adsorbent. COP is the term of Coefficient of Performance.

In generally, it can be defined as following:

$$\text{In cooling: } COP_C = \frac{\text{cooling_power}}{\text{input_power}}$$

$$\text{In heating: } COP_H = \frac{\text{heating_power}}{\text{input_power}}$$

Considering the processes occurring in basic cycle in sequence [9]:

(a) Processes *a-b*: Isostatic heating

The heat input per unit mass of adsorbent in the isosteric heating phase when the concentration x_{conc} is given by [8]:

$$q_{ab} = \int_{T_a}^{T_b} (c_{pc} + x_{conc} c_{va}) dT \quad (2-1)$$

where:

c_{pc} - Specific heat of adsorbent, possible the function of temperature.

x_{conc} - Maximum concentration, obtained at point *a* by using the evaporating pressure and bed temperature T_a in the Dubinin-Astakhov equation.

c_{va} - Specific heat of adsorbed phase at constant volume.

T_a - Minimum cycle temperature (K).

T_b - Temperature at start of desorption (K).

The integrated terms are simply the specific heat of the unit mass of adsorbent and its associated adsorbate. The specific heat at constant volume has been used for the adsorbate since, theoretically, there is no expansion of the adsorbate volume and the heat required to raise the temperature is the change in internal energy. In practice, although there will be some expansion, the use of specific heat at constant pressure c_{pc} can be considered as a good approximation. Temperature T_b can be easily calculated since the ratio of T/T_{sat} is constant along an isostere [8], hence:

$$\frac{T_a}{T_{ev}} = \frac{T_b}{T_{con}} \quad (2-2)$$

(b) Process b - c : Isobaric heating

The heat input per unit mass of adsorbent in the isobaric heating phase where the concentration varies is given by [8]:

$$q_{bc} = \int_{T_b}^{T_c} (c_{pc} + xc_{pa}) dT + \int_{x_{dil}}^{x_{conc}} H dx \quad (2-3)$$

where x_{dil} is the minimum concentration and H is the heat of desorption per unit mass of adsorbate. H at any point on b - c or d - a can be derived from the slope of the isostere on the Clapeyron diagram:

$$H = R \left(\frac{\partial [\ln(p)]}{\partial \left(\frac{1}{T} \right)} \right)_x \quad (2-4)$$

where: R - The specific gas constant at the system pressure and temperature.

Taking into account that the ratio T/T_{sat} is constant along an isostere then H can be expressed as a multiple of the latent heat L of the refrigerant at the system pressure [8]:

$$H = L \frac{T}{T_{sat}} \quad (2-5)$$

(c) Process $c-d$: Isosteric cooling

The heat rejected per unit mass of adsorbent in isosteric process $c-d$ is analogous to the heat input in process $a-b$ [8]:

$$q_{cd} = \int_{T_d}^{T_c} (c_{pc} + x_{dil} c_{va}) dT \quad (2-6)$$

where T_d may be calculated from:

$$\frac{T_d}{T_{ev}} = \frac{T_c}{T_{con}} \quad (2-7)$$

(d) Process $d-a$: Isobaric cooling

The heat rejected per unit mass of carbon in the isobaric process $d-a$ is analogous to process $b-c$ [8]:

$$q_{da} = \int_{T_a}^{T_d} (c_{pc} + x c_{pa}) dT + \int_{x_{dil}}^{x_{con}} [H - (h_{gasbed} - h_{gasev})] dx \quad (2-8)$$

where:

h_{gasbed} - Gas enthalpy evaluated at the bed temperature (J/kg)

h_{gasev} - Gas enthalpy evaluated at the evaporator (J/kg)

The second bracketed term in the second integral takes account of the cooling effect on the bed of the cold gas entering from the evaporator.

(e) Cooling (evaporation)

The cooling and the heat rejected in the condenser are evaluated by considering the mass of refrigerant desorbed and then adsorbed per unit mass of adsorbent during every cycle.

The net concentration change is $x_{dil} - x_{conc}$. The useful cooling obtained from it is:

$$q_{ev} = (x_{conc} - x_{dil})(h_{gasev} - h_{liquidcon}) \quad (2-9)$$

where:

h_{gasev} - Specific enthalpy of gas leaving the evaporator (kJ/kg)

$h_{liquidcon}$ - Specific enthalpy of the condensed liquid (kJ/kg)

(f) Condensation heat

The heat rejected at the condenser is the sum of the condensation heat and that required to cool the gas down to the condensing temperature. Since the gas is desorbed at a range of temperatures between T_b and T_c , the heat rejected is evaluated as [8]:

$$q_{con} = - \int_{x_{dil}}^{x_{conc}} h_{gas} dx + h_{liquid}(x_{conc} - x_{dil}) \quad (2-10)$$

where:

h_{gas} - Gas enthalpy evaluated at the (varying) bed temperature

h_{liquid} - Saturated liquid enthalpy in the condenser

In practice, there is only a small error if the hot gas is all assumed to leave the bed at the mean temperature of T_b and T_c .

Hence, the COP in cooling (COP_C) or heating (COP_H) for a basic refrigeration cycle can be calculated by:

$$COP_C = \frac{q_{ev}}{q_{ab} + q_{bc}} \quad (2-11)$$

$$COP_H = \frac{q_{con} + q_{cd} + q_{da}}{q_{ab} + q_{bc}} \quad (2-12)$$

The two-bed continuous cycle operates with the beds out of phase, to provide continuous cooling power. In thermodynamic terms, it is identical to the basic cycle and has the same COP. Heat can be recovered internally to improve the cycle performance.

2.2.2 Heat and mass recovery cycles

The usefulness of an adsorption cycle machine depends both on the COP(Coefficient of Performance), which will affect the operating costs, and also on the SCP(Specific Cooling Power), which will be related with the system size and influence the capital cost [9].

Therefore, numerous developments on the basic cycle of adsorption refrigeration have been investigated. These include continuous cycle, multiple bed cycle, thermal wave cycle, convective thermal wave cycle and cascade cycle [10, 11]. The continuous cycles include the continuous heat regenerative cycle, the continuous mass recovery cycle and the heat and mass recovery cycle.

The heat regenerative cycle can recover some of the adsorption heat during phase switching between the adsorption and desorption beds. In this process, a temperature gradient between two beds is essential, so that heat can be usefully transferred between them and thermal energy recovered. The heat rejected by one bed can be used to provide some of the heat required by the other bed. In addition, the heat transfer fluid has to be circulated between the adsorbent and heat sources.

Mass recovery is used to convey gaseous refrigerant from the bed with high pressure to the bed with lower pressure just before phase switching. It is apparent that mass recovery is beneficial to improving the adsorption quantity of a cycle [12].

For energy analysis in an adsorption refrigeration cycle, the degree of heat regeneration is represented by the coefficient of r . In general [12, 14]:

$$r = \frac{Q_{reg} - Q_{reg}^*}{Q_{reg}} = \frac{Q_{re}}{Q_{reg}} \quad (2-13)$$

In which Q_{reg} is the required heat for desorption in the cycle without heat regeneration, Q_{reg}^* is the required heat with regeneration and Q_{re} is the exchanged heat during heat regeneration. We can easily find that r indicates the effect of heat regeneration on cooling performance of the cycle as follows.

$$COP^* = \frac{COP}{1 - r} \quad (2-14)$$

In this equation, COP^* is the cooling performance of the adsorption refrigeration cycle with heat regeneration (in the absence of regenerator, $r = 0$). COP is the cooling performance of the basic cycle.

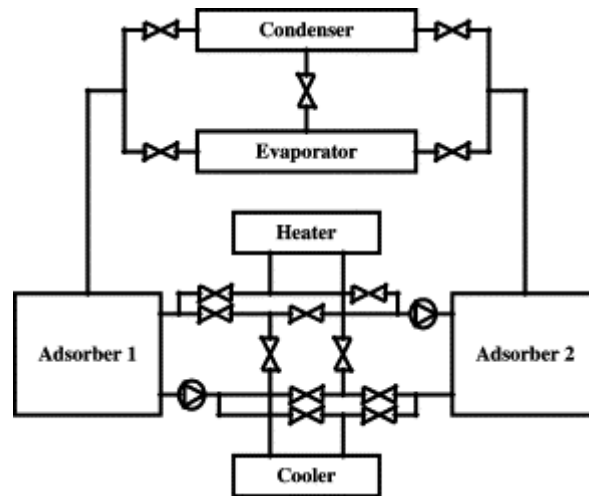
In practice, both mass recovery and heat regeneration are frequently used to improve performance.

➤ Heat regeneration cycle

In the basic continuous adsorption cycle two adsorbent beds are heated and cooled out of phase in order to provide continuous heating or cooling. Meunier and Douss [4, 13] first systematically looked at the potential gain in COP that might be obtained by such heat recovery, both as function of the temperature difference between the beds donating and receiving heat and of the number of the beds in which the heat can be transferred between.

A quasi-continuous adsorption refrigeration system with heat recovery was investigated by Wang et al. [14, 15] and the flow path is shown in figure 2-2. While adsorber 1 is cooled and connected to the evaporator to realize adsorption refrigeration in evaporator, the adsorber 2 connected to the condenser is heated to obtain heating-desorption-condensation. The condensed refrigerant liquid flows into evaporator via a flow control valve. The operation phase can be changed, and the go-between will be a short time heat recovery process. Two pumps are used to drive the thermal fluid in the circuit between two adsorbers (the connection to the heater and cooler are blocked during this process).

Figure 2-2 Schematics of heat recovery two beds adsorption refrigeration system [14]



Jones [19] suggested an improvement to the process by installing more than two adsorbers into the system. The operating principle of the cycle remains the same, relying on heat transfer flowing between the adsorbers and the desorbers. Compared to the basic cycle, heat recovery in this process is only effective if the heat transfer fluid temperature leaving the adsorbers is sufficiently high. Simulation results have shown that the maximum value of the COP depends on the number of adsorbers and desorbers installed. The analysis was further extended to a system containing six adsorbers and six desorbers at the same test temperature conditions (evaporation at 5 °C and condensation at 35 °C) and it was possible to obtain COPs in the range of 1.16 [20].

In order to simplify the management of the cycles and obtain good heat regeneration between adsorption and desorption, systems with several elementary adsorbers coupled with evaporators/condensers and rotated about a central axis, have been proposed [21, 22].

Maier-Laxhuber [23] proposed a rotary system which, in principle, can be used for continuous production of cold based on a single effect adsorption cycle. Erickson [24]

adapted the principle of the rotary system to a double effect chemical reaction cycle operating at three pressure levels. Although there is a problem for the practical management of the air flows, i.e. the heat transfer fluid used in rotary systems, these processes seem highly attractive as continuous cooling effect as well as high COP, in the range of 1, can be obtained.

Based on above reasons, Ebbeson [25] proposed a rotary process which is designed for continuous operation with the concept of a heat regeneration developed for solid sorption cold production systems. The theoretical COP was about 0.9, which is comparatively low, due to the consideration of the thermal masses and thermal pinches necessary for heat exchange between the air and the elementary modules.

Recently, Critoph [26] describes the operation of a continuous multiple-bed regenerative adsorption system. The complete system, consisting of 32 modules was modelled in detail. The design has not yet been optimized but a parametric study has revealed the way in which key parameters affect COP and SCP. The effect of five major parameters such as thermal capacity ratio, number of modules, temperature of air leaving the heater, generator heat transfer coefficient and the evaporator air inlet temperature were reported.

Great numbers of beds allow more regeneration of heat but the benefit of increasing the number of beds drops off rapidly. Table 2-1 below taken from Meunier[13] shows how the COP changes with numbers of beds in a particular case.

Table 2-1 Various in cooling COP of a zeolite-water regeneration cycle with evaporating, condensing, adsorption rejection and maximum desorption temperatures 0 °C, 40 °C, 50 °C and 350 °C respectively [13]

Number of beds	Cooling COP
1	0.425
2	0.684
4	1.008
6	1.293
∞	1.852

➤ Cycle with mass recovery

In a two-bed cycle, the two beds are working out of phase. At the end of each half cycle, one bed is at the end of desorption process P_{con} [1, 12, 27]. It is hot with high pressure. The other is under adsorption process, so it is cold with low pressure P_{ev} . Therefore, the high pressure adsorbent bed needs to be cooled and depressurised while the low-pressure one needs to be heated. The refrigerant vapour will flow from the high pressure bed to the low pressure one. So the pressure in the high pressure adsorbent bed decrease due to mass outflow and this will again cause desorption in the generator. Meanwhile, the pressure in the low-pressure adsorbent bed increases due to mass flow and will cause further adsorption. The mass flow will maintained until the two beds reach the same pressure,

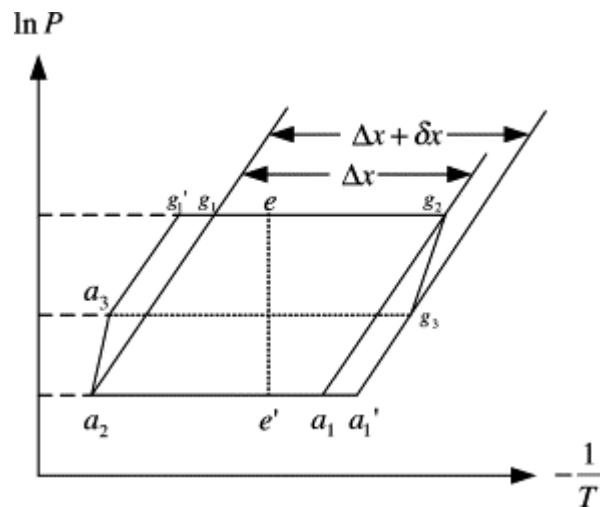
$$P_m \approx \frac{(P_{con} + P_{ev})}{2}$$

basic cycle.

This mass recycle process is expected to accelerate the circulation and enhance the cycle cooling power, because the mass flow is direct, so the equilibration of mass is faster than that of the basic cycle [28, 29, 30].

To simplify the analysis, it is necessary to suppose that all the processes of adsorption refrigeration in figure 2-3 are in equilibrium and the heat transfer capacity of the heat transfer fluid can be ignored (heat transfer fluid is used for heating and cooling the adsorbent beds). In practice, the process of mass recovery would need to be maintained for quite a long time.

Figure 2-3 Diagram of mass recovery cycle [27]



The mass recovery cycle ($a_2-a_3-g'_1-g_1-g_2-g_3-a'_1-a_1-a_2$) is an extended form of a two bed basic cycle or two bed heat recovery cycle ($a_2-g_1-g_2-a_1-a_2$ shown in figure 2-3), and the cycled mass is increased from Δx to $\Delta x + \delta x$, which causes the refrigeration effect to increase. The principle of these cycles can be described using figure 2-3. The very first part of each half cycle is the mass recovery process (path g_2-g_3 and a_2-a_3). Then the heat

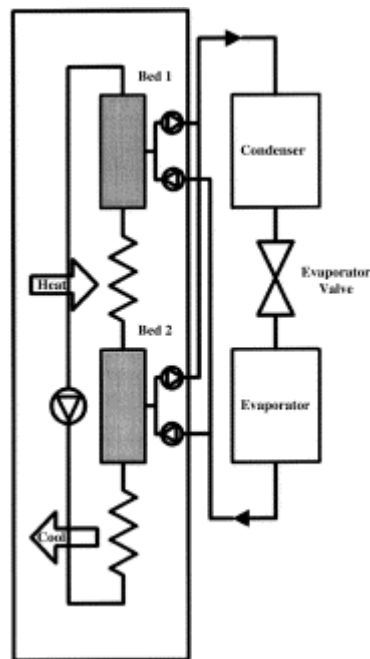
recovery process proceeds: heat is transferred from the hot adsorber to the cold one (path g_3-e'). As a consequence, the hot adsorber is first depressurized (path $g_3-a'_1$), it then adsorbs vapour from the evaporator. Meanwhile, the cold adsorber is first pressurized (path $a_3-g'_1$), and then vapour that is desorbed passes into the condenser (path g'_1-e).

Theoretically, the heat recovery process develops until the adsorbers reach the same temperature. Actually, there still remains a temperature difference between the adsorbers at the end of this period. Then, for closing each half cycle, the adsorbers are, respectively, connected to the heat source and heat sink (path $e-g_2$ and $e'-a_2$). The second half-cycle is performed the same way except that the adsorbers now exchange their roles. Due to this process, about 35% of the total energy transmitted to each adsorber can be internally recovered, including part of the latent heat of sorption [27, 30].

➤ Thermal wave

A practical means of approaching the performance of multiple bed cycles that only requires two beds is the thermal wave approach patented by Shelton [31] and illustrated in Figure 2-4. The simulation of the cycle by Shelton showed that the heat regenerative ratio and COP for the heat pump are as high as 70% and 1.87, respectively. Many researchers have studied the cycle [32 - 34]. The thermal wave utilises a simple heat transfer fluid circulating loop for heating and cooling the two adsorbent beds, in which part of the adsorbent heat can be recovered from the bed being cooled to the bed being heated.

Figure 2-4 Thermal wave cycle [31]



Heating and cooling of the adsorbent beds is no longer direct but via a heat transfer fluid such as high temperature oil. The oil passes through special heat exchangers in each of the beds and through two convectional heat exchangers outside the beds. The main function of the heat exchangers is to combine a large area of heat transfer surface with a low oil flow rate. One of the external heat exchangers allows the oil to be heated by a gas flame, while the other removes heat, either to supply the heating load (in the case of the heat pump) or to be rejected (in the case of the refrigeration). There is also a reversible pump, which is used to circulate the oil in either direction round the loop.

The cycle consists of two phases. In the first, suppose the pumping to be anticlockwise, that is to say: initially bed 1 is cold (maximum adsorbent concentration) and bed 2 is hot (minimum adsorbent concentration). When the cycle starts, the oil recovers heat from bed 2 and has a further heat addition from the gas heat exchanger and then proceeds to heat bed

via the special heat exchanger within it. Bed 1 desorbs refrigerant which passes to the condenser (giving a useful heat output in the case of a heat pump) and bed 2 adsorbs gas from the evaporator, which provides cooling. In the following phase of the cycle, the pump is reversed and bed 1 is cooled (adsorbing) and bed 2 is heated (desorbing) in a similar fashion until the original conditions are reached and the pump then can again be reversed.

Up to now, the description could apply to simple but limited heat recovery between the beds. However, the system can achieve much better performance than this due to the combination of the special design of the internal bed heat exchangers and the low oil flow rate. A hot slug of oil entering a cold region of the bed cools rapidly and leaves the bed cold. If the oil has a very low thermal capacity flow rate and there is little conduction within the bed then a thermal wave will pass through it. Conversely, high conduction rates normal to the oil flow are necessary in order to achieve a good ratio of adsorbent to heat exchanger mass. The wave front will propagate through the bed, all of the carbon upstream if the wave hot (low concentration) and that downstream cold (high concentration). The wave velocity is much less than that of the oil flowing through the bed.

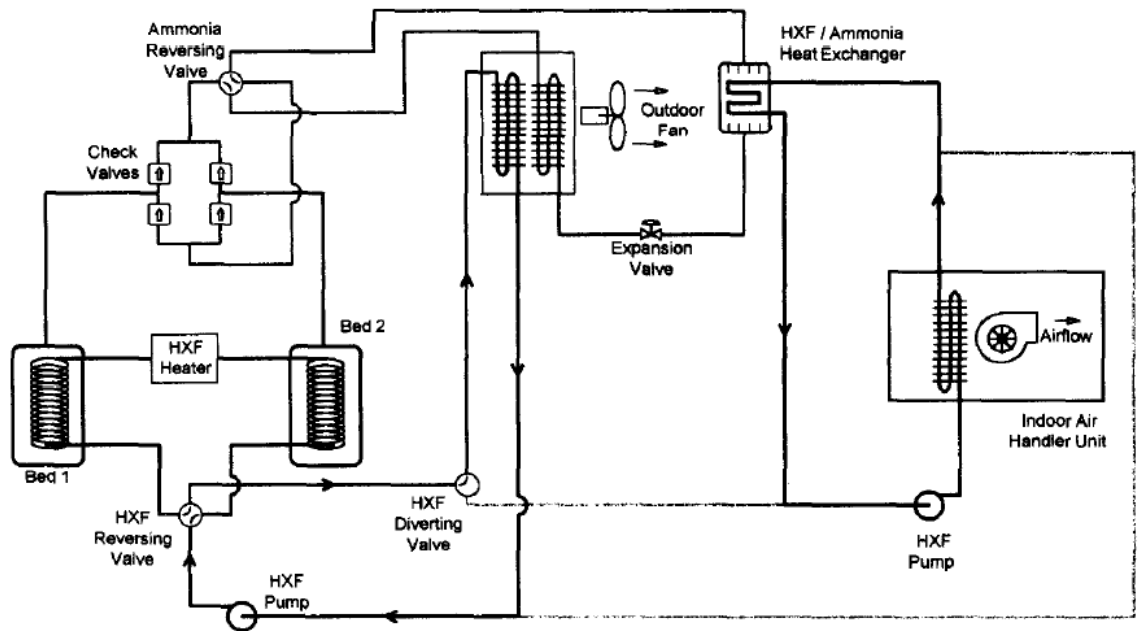
The oil emerging from the bed heat exchanger will be cold until the wave reaches the end of the cycle and a rapid temperature rise in the oil will be observed as the wave 'breaks through'. At this stage, the pump is reversed for the second half of the cycle and the bed is cooled as a cold wave front passes back down the bed in the opposite direction.

According to the above discussion, the great merit of thermal wave is that it recycles the maximum amount of heat, giving the maximum thermal efficiency. Whilst the bed exchangers are thermally massive, the energy used to heat them is to some extent recycled

along with the heat from the bed and the practical efficiency is high. However, a low velocity heat transfer fluid would greatly decrease the power density of the system. Moreover, the heat transfer coefficient between the fluid and the adsorbent bed is limited by the characteristic of porous adsorbent.

Miles [16] obtained an experimental COP of 0.8 for the activated carbon/ammonia system with an evaporation temperature and a condensation temperature of about 5 and 35 °C respectively. Miles and Shelton [32] set up a two-bed system which uses the activated carbon/ammonia sorbent/sorbate pair using thermal wave cycle, which is shown in figure 2-5 (HXF in the figure is the abbreviation for heat transfer fluid). The system performance was measured at eight different conditions in accordance with the ANSI 221.40.4 Standard [112] and COP of 0.76 has been achieved [32]. At the same time, Istria et al. [17] achieved approximately the same theoretical value for these temperatures with the multi-salt system. Pons et al. [18] investigated the zeolite - water adsorption system under the fixed test temperature and offers the best possible theoretical maximum COP of 1.5. Pons and Poyelle [6] also discussed an advanced adsorption cycle, where vapour is internally recovered between the two adsorbers by heat regeneration. Two pairs were evaluated: activated carbon AC35/methanol and zeolite NaX/water. In the case of thermal wave the COP achieved for zeolite/water is 0.92 and for carbon/methanol is 0.61.

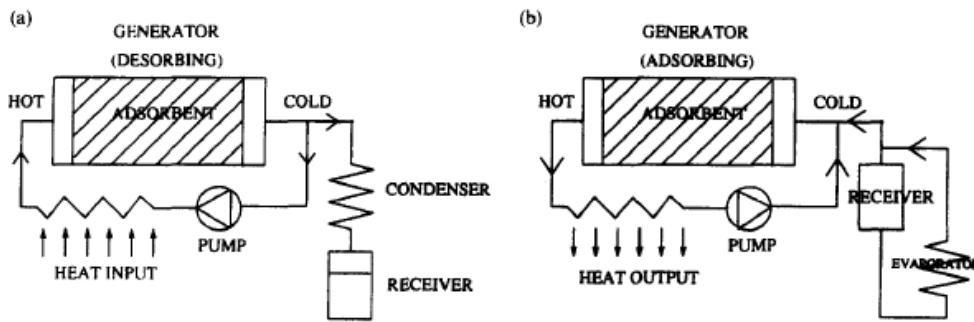
Figure 2-5 Scheme of adsorption system using thermal wave cycle [32]



➤ Convective thermal waves

In the convective cycle proposed by Critoph [35], the thermally massive heat exchangers in the adsorbent beds are not required. Rather than heating the bed directly, it is possible to heat the refrigerant gas outside the bed and to heat the sorbent. Although the bed has very poor conductivity, the carbon (or other adsorptive) grains have a very high surface area which can be used for convective heat transfer. For a carbon-ammonia bed, the ammonia can be heated externally to the bed in a convectional heat exchanger and then pumped through the bed, where it rapidly gives up its heat to the carbon. In the process, it will desorb a little more ammonia. The cold ammonia issuing from the other end of the bed completes the circuit by returning to the gas heater via the pump. This is illustrated in figure 2-6.

Figure 2-6 (a) Cycle in desorption phase. (b) Cycle in adsorption phase [35]



Because of the high surface of the grains, the heat transfer per unit mass of bed is higher than that for conventional heat exchangers. There is also the advantage that there are no heat exchangers, which would consume heat. It is possible to switch the external gas heat exchangers between the adsorbing and desorbing loops so that they are in continuous use rather than being heated and cooled periodically. Thus, their thermal mass has no negative effect.

Additionally, a thermal wave is generated in the bed in a similar fashion to that of the thermal wave system. However, it is more similar to conventional gas regenerators, which also exhibit thermal waves. In order to use the recovery heat, it is necessary to transfer it from the cooling bed loop to the heating bed loop. It was proposed to do this with a gas-to-gas heat exchanger, and is denoted by the vertical 'heat input' and 'heat output' arrow in figure 2-6.

Only one phase of the cycle is shown in figure 2-6, in which bed 1 is heated (desorbing, figure 2-6(a)) and bed 2 is cooled (adsorbing, figure 2-6(b)). The clockwise flow of refrigerant in the loop for bed 1 takes the gas through the recuperator where heat is

recovery from bed 2, the external heat exchanger, where heat from a gas flame is added and into bed 1. The refrigerant gas emerges cold from this bed until the thermal wave starts to break through.

In bed 2, the circulation of hot gas from the bed passes through the inter-loop heat exchanger, through the external cooler (which provides some of the useful output of a heat pump system) and back into bed 2. The gas emerging from the bed remains hot until the thermal wave starts to break through, at which time it undergoes a rapid drop in temperature.

When the two thermal waves start to break through, the opposite phase of the cycle begins. Valves are switched which effectively swap the two beds over so that bed 1 is cooled and bed 2 is heated.

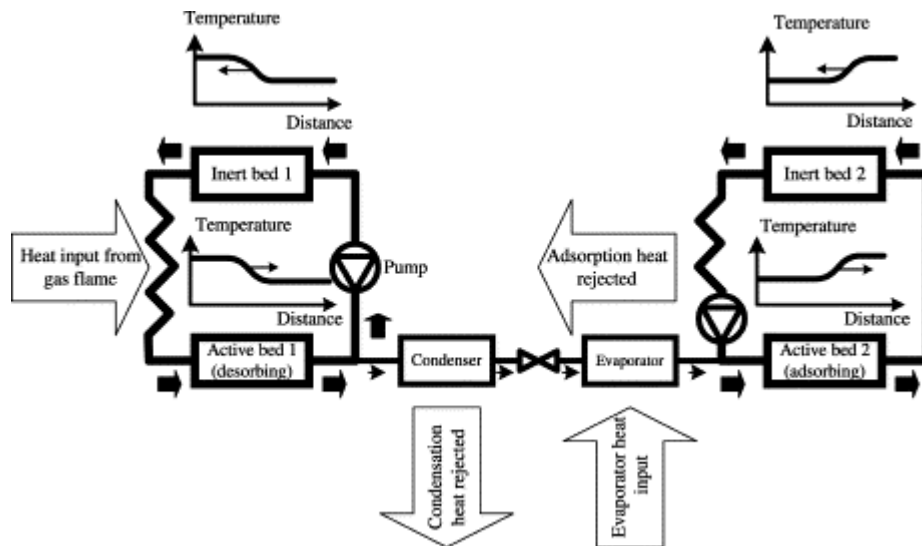
The advantages of this concept are [36, 37]:

1. The cycle is highly regenerative and hence highly efficient.
2. There is no complex and expensive heat exchanger within each bed.
3. There is no added thermal mass due to the use of heat exchangers.
4. The high heat transfer rate allows rapid cycle times which result in the plant being more compact and less expensive to produce.

One disadvantage of the system described is the need for the gas-to-gas heat exchanger required to transfer recovery energy between the fluid loops. It could be both large and expensive and there might be matching problems when the heat rejected by one bed is not

required at the same time the other bed. Critoph and Thorpe [36, 37] suggested the use of an inert packed bed regeneration to overcome the problems, as shown in figure 2-7.

Figure 2-7 Adsorption refrigeration system with convective thermal wave cycle



Heat is no longer passed from loop 1 to loop 2, but, instead, the heat recovery from each active bed in desorption is stored in an inert bed and is passed back to the active bed in the next desorption phase. The inert bed could be as simple as a cylinder packed with steel balls.

In figure 2-7, active bed 1 is being heated (desorbing) and active bed 2 is being cooled (adsorbing). Flow in loop 1 is anti-clockwise with cold gas coming out of active bed 1 where it is pre-heated, through the heat exchanger where it is supplied with heat from the gas flame, and back into active bed 1 where it transfers heat to the adsorbent. There are thermal waves in both beds, which ensure the optimum recycle heat. At the same time as active bed 1 is being heated, it desorbs gas which passes through the check valve to the condenser. This produces part of the output of a heat pump or is simply rejected if the

machine is a refrigerator. When hot gas starts to break out of active bed 1 the cycle enters the next phase. Whilst active bed 1 is being heated, active bed 2 is being cooled by a clockwise flow of gas. In an analogous process hot gas leaves active beds, passes to inert bed 2 where it is cooled (making a thermal wave progress down into inert bed 2), pass through the external cooler where it is further cooled (and giving useful heat output in the case of the heat pump) and re-enters active bed as cold gas. Whilst this process is occurring the active bed simultaneously adsorbs gas from the evaporator producing useful cooling.

When both of these processes (heating of active bed 1 and cooling of active bed 2) are complete, the other stage of the cycle takes place in which active bed 1 is cooled and active bed 2 is heated. This is achieved by the switching valves so that the dotted flow paths replace the adjoining paths shown by solid lines.

The advantages of this system are [9]:

1. The four packed beds are in effect heat exchangers of very high surface area but of minimum cost and are very compact.
2. There are only four conventional heat exchangers and this is the minimum number allowed by thermodynamics. In addition to an evaporator and condenser, one is needed to get high grade heat in and one to reject the heat if adsorption to the environment.
3. The cycle is highly regenerative since the packed beds act like large counter flow heat exchangers. This results in good energy efficiency (i.e. high COP).

Critoph [38] proposed a numerical investigation on a convective thermal wave with two 'active' beds filled with activated carbon and the two 'inert' beds packed with non-reactive

particles such as steel balls. The high degree of regeneration, which is possible, leads to good COP. Thermodynamic modelling, based on measured heat transfer data, predicts a COP of 0.9 when evaporating at 5 °C and condensing at 40 °C, with the generating temperature of 200 °C. However, the experimental result [39] shows that the COP (0.57-0.79) and power (1.07-1.49 kW) are lower than had been hoped (COP=0.9, SCP=5kW). Critoph [39] explains that due to a higher than anticipated pressure loss in the heat exchangers, the mass flow in the circuit is less than the design value. For this reason, the power is lower and as a consequence the thermal losses of the machine are more significant than they would be.

➤ Multi-stage and cascading cycle

The adsorption cycles discussed in previous sections are applicable only to a single stage cycle. The single stage cycle systems have certain limitations. That is, they can not effectively utilize high temperature heat sources and do not perform well at very low temperatures. Hence, to improve the system performance under such situations, adsorptive processes may be adapted for advanced cycles, such as, multi-stage and cascading cycle.

The basic idea of a multi-stage cycle is to perform the desorption–condensation processes and evaporation–adsorption processes at different temperature/pressure levels by using the ‘same working pair’. The internal re-use of heat of condensation or adsorption can increase the system performance significantly. Another practical cycle that can make good use of high temperature heat source is the ‘cascading cycle’, which operates with ‘different working pairs’ (either liquid/liquid or solid/liquid), such as zeolite–water/activated carbon–methanol, or zeolite–water/silica gel–water, etc. A typical three-bed adsorption system

using cascading cycle is shown in figure 2-8 [40]. These cascading cycles are applied to situations especially, when there exists a large temperature difference between the heat source/ambient and the temperature in the evaporator/refrigeration space. For such situations, it may not be practical to use single stage cycle. Hence, one way of dealing with such situations is to perform the evaporation/refrigeration process in stages, that is, to have two or more cycles that operate in series at different temperature levels (cascading), which is shown in figure 2-9. A high temperature heat source (e.g. boiler) is used to drive the high temperature stage adsorption refrigeration cycle. The low temperature stage adsorption refrigeration is driven by sensible heat and heat of adsorption obtained from high temperature stage. To minimize the contribution of sensible heat, special care has been attached to the heat management of the adsorbers; n -adsorber cycles operating with a single evaporator and a single condenser have been proposed with sequences of heat recovery between adsorbers.

Douss [40] experimented with a refrigerator in which a zeolite-water high temperature input cycle drove a carbon-methanol low temperature cycle. Critoph and Turner [41] carried out a theoretical analysis of a cascaded cycle using zeolite –ammonia. These cycles and the multiple bed cycles all seek to input heat at higher temperatures only and to reject heat at lower temperatures only. Thermodynamic considerations imply that this will lead to higher theoretical COP. Rockenfeller [42] has suggested triple cascade chemical adsorption cycles in which theoretical refrigeration COP's as high as 1.2 are possible.

Figure 2-8 Scheme of experimental unit using cascading cycle [42]

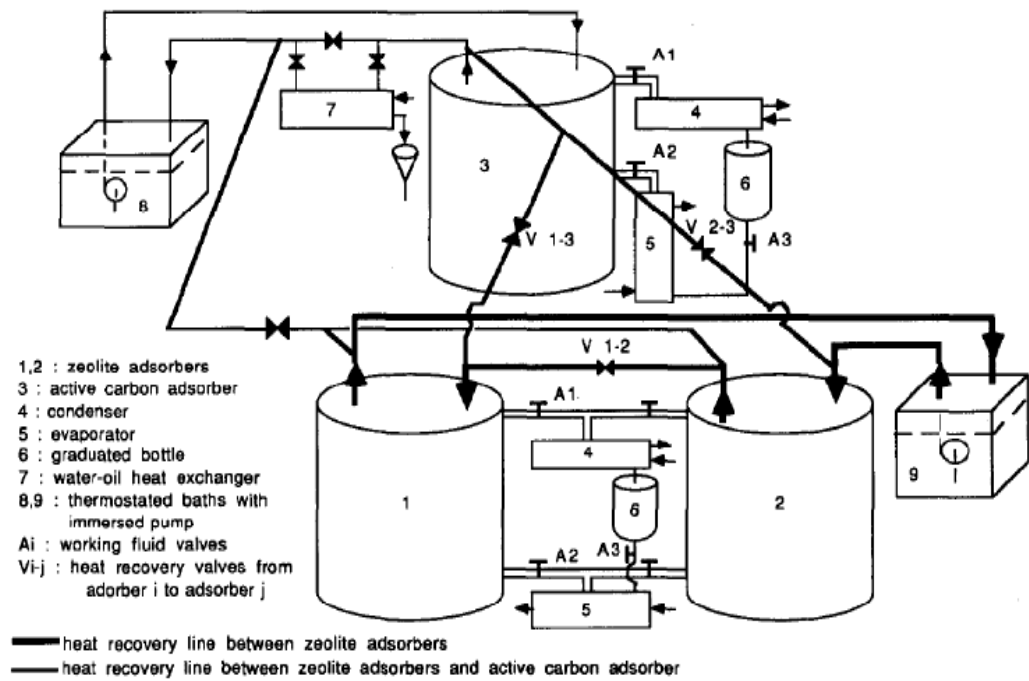
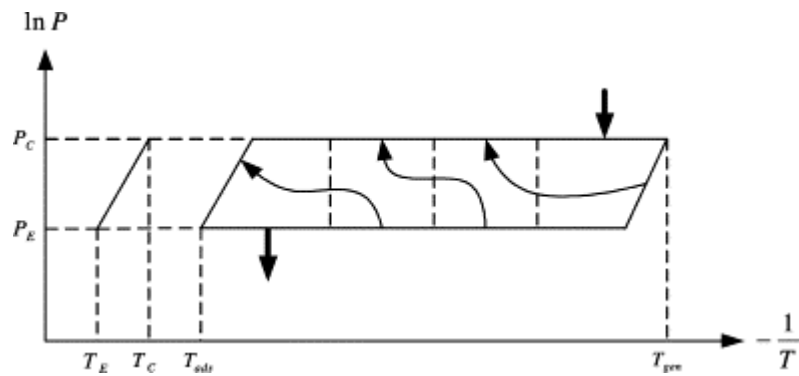


Figure 2-9 n -Adsorber cascading cycle



Meunier [43] computed the first and second law efficiencies of cascading cycles using the zeolite/water pair and found that the performance of the adsorption system (COP and SCP) was a function of the number of cascades. Zeigler [44] proposed a cascading two-stage sorption system contain a zeolite/water pair in the high temperature stage and a lithium bromide/water pair in the low temperature stage. Moss and Shahidullah [45] proposed a two-stage cycle containing a zeolite/water pair in the high temperature stage and a calcium

chloride/methanol pair in the low temperature stage. Meunier [46] presented four cases of cascading solid adsorbent cycles operating at high regenerating temperatures. One of these cycles is a double effect zeolite/water cycle and the three other cycles consist in a low temperature active carbon/methanol cycle. Production of refrigeration is possible at around -10°C with a COP as high as 0.85.

2.3 Adsorption pairs

The choice of adsorbent/adsorbate pair is important. Many researchers examine different working pairs in the basic adsorption system [47, 48].

The most useful refrigerants are those that have the highest latent heats, since the maximum possible cooling that may be obtained in a single cycle in which the refrigerant is completely desorbed and then re-adsorbed is given by the product of the refrigerant's latent heat and the mass of refrigerant which completely fills the micropores [9].

Refrigerants with a higher latent heat per unit volume should therefore in general give better performance, unless the limiting concentration in a particular adsorbent is prohibitively low and means that a refrigerant with a lower latent heat but a higher limiting concentration may give a better performance.

Table 2-2 lists some common refrigerants with high latent heats and is split into high-pressure refrigerants in the top section and sub-atmospheric refrigerants in the bottom section [9]

Refrigerant	Boiling Point (°C) (at 1 bar)	Latent Heat (kJ/kg)	Latent Heat Per Unit Volume (kJ/m ³)
Ammonia	-34	1368	932
Formaldehyde	-19	768	626
R32	-52	382	463
Chlorine	-34	288	450
R22	-41	235	331
Water	100	2258	2163
Sulphur Trioxide	45	508	905
Methanol	65	1102	872

From the table it may be seen that water, ammonia and methanol have the best performance.

In many respects water is the ideal refrigerant, having the highest latent heat and being non-toxic. It may be used with zeolites and silica gels. However, its low vapour pressure can present problems [49].

1. The minimum evaporating temperature is a few degrees Celsius and so applications are limited to air conditioning and chilling.
2. The system pressure is always sub-atmospheric and a small ingress of air prevents the system from working. This does not prevent conventional LiBr absorption chillers from working, but they have devices to scavenge air from the machine. If there is no air removal, then an adsorption chiller needs to be hermetically sealed for life.

Ammonia has less than half the latent heat of water and so is not as thermodynamically efficient but its higher vapour pressure ensures that there are no mass transfer limitations in cycle times down to the order of 1 min. It is environmentally friendly and may be used for cooling down to about -40°C . It is stable in the presence of adsorbents to at least 200°C . Its disadvantages are [49]:

- (a) it is toxic and not normally used within residential or office spaces;
- (b) it may not be used together with copper or its alloys, although steel and aluminium are acceptable.

In many ways methanol lies somewhere between water and ammonia in its applicability [49]. It has higher vapour pressure than water (although sub-atmospheric), can be used at ice-making temperatures, and does not have the toxicity and compatibility problems of

ammonia. It is unstable at temperatures much higher than 120°C. It may be used with activated carbons, silica gels, and certain zeolites.

Due to the advantage and limitation of different refrigerants, water, ammonia and methanol would be used in different adsorption for specific purpose. The most commonly used adsorption pairs are: activated carbon/ammonia, activated carbon/methanol, zeolite/water and silica gel/water [48].

2.3.1 Activated carbon-ammonia systems

Investigations in the use of charcoal-ammonia are apparently more recent-mainly during the 1990s. One of the biggest groups is from the University of Warwick with Professor R. E. Critoph as the co-ordinator. Considerable research had been carried out to improve the heat transfer, COP, SCP and system cost. Important findings are described below.

Critoph [50] developed a solar refrigerator using a carbon/ammonia cycle in 1994. A bank of 75W incandescent lamps simulated the solar radiation. Experimental results show that the largest calculated COP had a value of 0.33 at a constant irradiance of 925W/m², whilst the lowest value of 0.24 was obtained at a diurnal irradiance of 500W/m².

As a continuation of the work, Tamainot-Telto and Critoph [51] presented a prototype solar energy collector for sorption refrigeration. The system consists of two reflectors, two absorbers and a single glazing cover. The absorber is made of seamless steel tube covered in a selective surface (absorptance 0.95) and contains aluminium fins, activated carbon and

ammonia. The concentration ratio of the collector is about 2.4. It was designed for a solar power input of about 500W and could provide a cooling power up to 120W.

Thereafter, Critoph [52] tested ammonia, R32 and butane as refrigerants in new monolithic carbon adsorbents. This included a coconut-shell based carbon known as Sutcliffe Speakman 208C, a compressed, monolithic form of the 208C, and a PVDC (polyvinylidene chloride), which can be compressed into shape and carbonised without cracking or deforming. The results show that the COP of ammonia was 0.365, three times greater than that of R32 and butane. For the adsorbents, monolithic carbon always gave slightly better performance than 208C in COP and only required about 75% of the pressure-vessel volume. The PVDC based carbon had marginally better performance than the carbon monolith at high temperature around 200°C.

Then, Tamainot-Telto and Critoph [53] constructed a prototype of an adsorbing cooling machine that used an activated carbon-ammonia pair. A finned aluminium steam channel permits heat transfer to a monolithic carbon. The maximum COP and the specific cooling power over the whole cycle were 0.12 and 60W/kg carbon. One reason for the low COP value was because the generating temperature was low and there was no heat recovery between the heating and the cooling phase.

Jones [54] used a novel carbon-moulding technique and incorporated a thermal wave-regeneration concept employed in the drying of gas streams; a small unit consuming 0.51 kg of charcoal produced 293 W cooling with an adsorbent heating and cooling cycle of 6 minutes, with ammonia as the adsorbate. With R22 and R134a as adsorbates, cooling rates of 113 and 99 W were reported. Jones [54] also reported that larger multi-bed systems

were under development which could have a cooling COP of 1.0. Miles and Shelton [55] were involved in a similar development work. They claimed to have achieved a heating COP of 1.21 and a cooling COP of 0.76, using a two-bed system with half-cycle time of 2.6 min.

In order to improve the heat transfer effectiveness, finned tubes are used instead of a simple flat-bed [56], which had an outer diameter of 53 mm and relatively length ($L=0.2$ m). The system was tested at various operating conditions, and was shown to be optimum, when the condensation temperature of and regeneration temperature were 20 and -5°C , respectively.

2.3.2 Activated carbon-methanol systems

A solar-powered adsorption system using activated carbon methanol pair was investigated by Delgado et al. [57] in France. With an exposed area of 4m^2 solar collector area, it would produce nearly 25 kg ice in a day. While the thermodynamic COP was 0.4, the overall system COP was only 0.15. Li and Sumathy [58] had presented the description and operation of a solar-powered ice-maker with the solid adsorption pair of activated carbon and methanol using a basic adsorption cycle. A domestic type of charcoal was chosen as the adsorbent, and a simple flat-plate collector with an exposed area of 0.92 m^2 was employed to produce about 4-5 kg ice per day at an evaporator temperature of about -6°C . The above system could achieve solar refrigeration COP of about 0.1-0.12. A similar experiment was performed by Pons et al. [7] with activated carbon and methanol as the working pair and the condensers used were of air-cooled type. The system was loaded with 130 kg of activated carbon, which produced around 30-35 kg of ice on sunny days. The

system employed flat-plate collector having an exposed area of 6 m^2 and was packed with charcoal at a ratio of 20 kg m^{-2} . It was reported that the system COP was about 0.12 and was comparable with Delgado's results.

They further extended their work at Agadir, Morocco and demonstrated the operation of a mini-ice maker which could produce about 4 kg of ice a day. The limitation of the performance was mainly due to the ambient temperature, and an increase in the ambient temperature beyond 23°C reduced the system performance significantly.

Since 1986, at AIT Bangkok, Exell et al. [59] have worked extensively on the development of a charcoal-methanol system. With just 1 m^2 collector area, the system could produce 4 kg of ice a day. The COP of the system was about 0.123 which is marginally better than the systems reported by other researchers. With a similar collector of area (0.92 m^2), Meunier et al. [60] as well as Cacciola and Restuccia [61] also carried out many experimental investigations on development of activated carbon-methanol adsorption machines. Their observations were similar to that reported by Pons and Guillemot.

Antonio and Daguinet [62] also performed an experimental study on an adsorption solar cooling system using the activated carbon-methanol pair. The solar powered ice maker consists of the following basic components: a reactor containing an adsorptive bed coupled to a static solar collector covered by Transparent Insulation Material (TIM), a condenser and an evaporator. A uniform pressure model for the reactor is considered. The bed's radial temperature distribution is determined by means of a one-dimensional numerical method based on a finite difference technique. The results show that the TIM covers' system proved to be about 40% more efficient than the single cover solar system. The average net

solar COP was 0.13 and ice production per square meter of solar collection surface was about 7-10 kg/day for the TIM cover system during the six month considered period.

Wang et al [63] also proposed an activated carbon-methanol pair together with spiral plate heat exchangers as a prototype heat regenerative adsorption refrigerator. The adsorption system uses 12kg activated carbon and has a cycle time of 40min. The experimental results show the system can make more than 1kg ice per kg adsorbent per day.

2.3.3 Silica-gel/water and silica-gel methanol systems

Since early 1980s, the work on silica-gel/water systems have been popular and lot of work was carried out mainly in Japan. In an effort to utilize solar heat, Sakoda and Suzuki [64] achieved a solar COP of about 0.2 with a solar collector $500 \times 500 \times 50 \text{ mm}^3$, packed with 1 kg of silica-gel particles and with 1.5 kg of distilled water in the evaporator. On a clear day with total solar insulation of $19.3 \text{ MJ m}^{-2} \text{ day}^{-1}$, it was estimated that a COP of about 0.4 can be possible just with 0.4 m^2 solar collector.

Hisaki et al. [65], utilizing the benefits of multi-bed cycle, manufactured a 34.5 kW adsorption chiller and ice thermal storage system, comprising two adsorption units, an evaporator and a condenser. Both adsorbers were installed in an evacuated hermetic enclosure, and each adsorber was alternatively heated and cooled in a cycle time of 7 min. The COP of the system was found to be 0.4. Based on the above approach, Saha et al. [66], also had worked on a 10 kW system using silica gel as the working media. The silica gel was packed around finned tubes and the experiments had shown that each adsorption/desorption cycle takes nearly 3-13 min and heat-exchange cycle is about 30 s.

The system could achieve a COP of 0.48 and was found that the COP tends to rise with cycle time above 5 min and with the flow rate of chilled water.

A solar powered refrigeration system with a 0.25 m² flat plate collector has been developed [56]. This system would realize an evaporating temperature of 5°C when the condensation temperature was around 35°C and the attained regeneration temperature was 100°C. Ortel and Fischer [67] used methanol with silica gel instead of water, so that the system could operate at an evaporating temperature below 0°C. It was found that a two-chamber silica-gel/water system could be operated by methanol also, but because of methanol's inferior thermodynamic properties the COP of the system was considerably reduced by about 30%.

Chua et al. [68] examined a twin bed adsorption chiller. The system uses silica gel packed around the fins of the heat exchanger tubes, and water. The cycle time and the bed switching time were investigated as a critical part of system performance. Tangkensisirin et al. [69] proposed the silica gel-water couple for solar-powered adsorption cooling.

Metallic solar collectors with fins have been used to increase the thermal conductivity in solar collectors. The addition of activated carbon to the silica gel improves desorption rate and the regeneration temperature of the packed bed. Matsushita et al. [70] has developed a commercialised silica gel-water chiller.

2.3.4 Zeolite-water systems

Since the late 1970s, significant efforts were made by Tchernev [71] to develop a solar-powered natural-zeolite/water system. Natural zeolites, with a heat of adsorption of 2.8MJ kg⁻¹, were found to be more suitable for cooling systems than synthetic zeolites having a

heat of adsorption of 4.2MJ kg^{-1} . This is due to the fact that with lower heat of adsorption the adsorbent bed can be cooled more effectively, which in turn results in better adsorption of refrigerant. This air-conditioning system with the exposed collector area of 1 m^2 could produce ice at a rate of 6.8 kg day^{-1} . Tchernev [71] also designed and tested a solar adsorption machine with different combinations of working media. Flat plate collector having an exposed area of 2.44 m^2 was used to produce 100 kg of ice per day. An additional 1.5 m^2 flat plate collector was used along with the system to refrigerate milk. However, its performance was found to be unsatisfactory, which was due to the presence of inert gas inside the zeolite bed chamber.

In France, Grenier et al. [72] had developed a system using a simple solar collector with an area of 20 m^2 containing 360 kg of NaX zeolite for a cold storage plant. The cold production during evaporation was 1.93MJ m^{-2} and net production was only about 1.88MJ m^{-2} when the incident radiation was 17.8MJ m^{-2} . The operation conditions were set to a condensation temperature of 32°C , evaporating temperature at 1°C and the regeneration temperature at 118°C . The system could attain a net solar COP of 0.105 , while its cycle COP was 0.38 . Tather and Erdem-Senatalar [73] also utilized zeolite-water as working pair and reported that, the system could operate successfully if the ambient temperature is less than 20°C . In the literature [58] it is mentioned that Guilleminot et al. tried to use zeolite composites to replace zeolite as an adsorbent and two different composites with different ratios was used in his study. (i) 65% of zeolite+ 35% of metallic foam; (ii) 70% of zeolite+ 30% of natural expanded graphite. It was expected that, the latter combination resulted in a better performance [58]. A similar performance was noticed by Poyelle et al. [74], who found that, if the evaporation temperature is set to -4°C , the required ambient temperature should not exceed 30°C .

Meunier [60] had been a pioneer in the field of adsorption. Initially, in 1979, his group theoretically analyzed the zeolite and water pair and found that the COP depends largely on the condensation temperature, followed by evaporation temperature and then the regeneration temperature. In 1984, they developed an adsorption machine which was operated at different temperature conditions. When $T_C=30^\circ\text{C}$, $T_E=5^\circ\text{C}$ and $T_R=70^\circ\text{C}$, the system could attain a COP of 0.14, while when the T_C and T_E was set to 48 and 121°C , respectively, the COP reduced drastically to 0.04. Further work was continued and in 1986, they had attempted to use various working media like Z13X and Z4AX-water in order to improve the performance of the system.

A detailed thermodynamic model had been developed by Cacciola and Restuccia [61] to obtain all the data needed during the design step of an adsorption machine. Using this model, it is possible to calculate the operative conditions, the energy balance in each component of the machine and the COP.

Lu et al. [75-77] also research on an adsorption cold storage system with zeolite-water working pair. This system is used for providing air conditioning for the driver's cab of an internal combustion locomotive. Unlike a normal adsorption air conditioner, the system starts running with the adsorption process, during which the cold energy stored is discharged, and ends running with the generation process. The adsorbent temperature decreases during the cold storing period between two runs. The refrigeration power output for the whole running cycle is about 4.1 kW. Such a system is quite energetically efficient and is comparatively suitable for providing discontinuous refrigeration capacity when powered by low grade thermal energy, such as industrial exhausted heat or solar energy.

2.4 Heat and mass transfer

For adsorption systems, whether refrigeration or heat pumping, the heat and mass transfer within the systems are crucial to the performance achieved. Increasing compactness by reducing the cycle time to minutes rather than hours demands high heat transfer coefficients. Additionally, the various regenerative cycles above all demands heat transfer between beds in order to achieve competitive COP. This also requires good heat transfer, and a low approach temperature between beds.

However, the conventional adsorbent beds always have low thermal conductivity. The poor heat transfer in an adsorber and its strong effect on system performance pose a major challenge. Some reports [74, 78, 79] stated that the main difficulty preventing the full commercial success of such systems is knowing how to obtain a good heat transfer rate between the solid bed and the heating/cooling fluid. This depends on the geometry of the heat exchanger, the shape and the thermal conductance of the solid adsorbent.

There are mainly two types of resistance to heat transfer in a system. The first one occurs at the metal-adsorbent interface and depends on the physical contact between the materials. The lack of good contact between the metal surface and the adsorbent creates a steep thermal gradient at the interface. The inefficient heat exchange is mainly due to the shape of the adsorbent particles, generally spheres or cylinders, which do not allow a good contact between the adsorbent solid surface and the metal of the heat exchanger. In order to reduce this thermal resistance, a suitable shape of the solid bed with a smooth surface should be sought. The second resistance is associated with heat transfer inside the

adsorbent bed and is inversely proportional to the thermal conductivity of the bed, which is generally low.

The sections below consider both the fundamentals of thermal conductivity in conventional granular beds and contact resistance between the materials and some of the means available to achieve the required improvement.

Zhu et al. [80, 81] and Wang et al. [82] introduced poly-aniline, which has the advantage of superior thermal conduction characteristics, into zeolite to increase the thermal conductivity of the solid adsorbent fixed bed. The thermal conduction of the zeolite/poly-aniline complex is about 4 times higher than that of the zeolite alone. In contrast to the granular adsorbent, the thermal conduction of a shaped adsorbent increases by about 30%, while there is no noticeable decrease in the adsorption capacity. This result represents great progress toward industrial application. However, it is not enough only to increase the adsorbent's thermal conduction: the contact resistance interface between the two surfaces must also be reduced as the heat resistance inside the adsorbent is progressively decreased. Zhu and Wang [83] present a further development on decreasing the thermal contact resistance at the interface. Exerting certain pressure or spreading adhesive on the interface reduces the contact resistance. They investigated some methods for improving the heat transfer at the interface between the copper surface and the adsorbent granule, such as applying an exerting pressure on the surface.

Cacciola et al. [84] have also investigated heat and mass transfer in a adsorption syetem. Many physical conductivity enhancements have been proposed varying from the addition of conductive powders and granules, creating more consolidated beds, addition of

expanded graphite or graphite fibres, addition of metallic foams sintering in metallic powders to general metallic inserts. He also indicated that the thermal contact between the heat exchange surface and the bed itself is vital for good system performance and therefore elected to use a solid block of adsorbent material.

According to Jones [85], relatively short cycle times and increased thermal conductivity were achieved by moulding the chosen adsorbent to a finned aluminium tube using a specially formulated binder. Hinotani et al. [86] and Spinner [87] also discuss the improvement of heat transfer within adsorption beds by the use of heat pipes. Hu et al. [88] utilised a polymer (poly-aniline) of high conductivity to enhance the thermal conductivity of the microporous granule zeolite by 3 times. Fang et al. [89] presented a method to improve the mass and heat transfer by treating the active carbon physically. Zhu et al. [81] studied the improvement of heat conduction inside the solar-powered adsorber. Antonetti [90] showed that metallic coatings could enhance the thermal contact conductance. Peterson [91] investigates the influence of the thermal contact conductance and thermal conductivity of anodised aluminium coatings. Hammad and Habali [92] stated that augmenting heat transfer is important in the design of a solar powered vaccine cabinet. The study of Qu et al. [16] showed the importance of decreasing the resistance of the heat and mass transfer in a waste heat recovery system using adsorption refrigeration cycles.

Metal powder may also be mixed in with the hydride followed by compression and optional sintering to improve conductivity [93]. The thermal contact resistance between the adsorbent bed and exchangers can be reduced by using metallic foams or anisotropic graphite materices which are well bonded to the bed walls [93]. The use of consolidated bed and metallic foams for improving bed conductivity are also mentioned by Guilleminot

et al. [94]. They suggested that performance can be improved to a certain extent with granular beds by utilising bimodal mixtures to reduce the voids and porosity between grains thus improving thermal conductivity. The grain size may also be reduced in order to improve the wall heat transfer coefficient. However, only small improvements in thermal conductivity tend to be obtained for bimodal mixtures of the low conductivity materials that are generally found as adsorbents [95]. Metallic foams can be combined with granules to improve conductivity but these tend to suffer from high thermal contact resistance between the foams and the granules.

The heat transfer to and from the adsorbent bed can be optimised by selection of a suitable heat exchangers. Cacciola et al. [70] and Wang et al. [96] chose to use a plate type of heat exchanger, building the bed from a stack of solid adsorbent bricks and heat exchanger plates. This can provide good thermal contact between the adsorbent and the heat transfer surfaces. The experimental results show that this machine can provide 4-5 kg ice after receiving 14–16 MJ radiation energy with a 0.75 m² collector, while it can provide 7-10 kg ice after receiving 28–30 MJ radiation energy with a 1.5 m² collector. Cacciola and Restuccia [97] and Meunier [98] investigate a number of different types of heat exchanger including finned tube, plate and shell and tube. Shell and tube heat exchangers have the advantage of being relatively cheap and easily available and have been used by a number of researchers. It is difficult to obtain a good thermal contact between the fins of the heat exchanger and the adsorbent bed. However, if some methods for forming the fins and consolidated adsorbent together could be found thus binding them more tightly, this problem could be minimised.

The need for higher bed conductivity has led to research aimed at producing carbons that combine high packing density and improved conductivity. If a monolithic block of carbon adsorbent can be produced which eliminated void spaces, there are several advantages [9]:

- More carbon can be contained within a given pressure vessel
- The surface heat transfer coefficient can be dramatically increased since the gas space between fin or tube and the adsorbent can be greatly reduced or eliminated
- The 'bed' conductivity becomes that of the 'grain' since there is a continuous solid conduction path

Mauran et al. [99] report the value for bed thermal conductivity as high as $40\text{Wm}^{-1}\text{K}^{-1}$ which is considerably larger than the best values obtained for unconsolidated beds.

Tamainot-Telto and Critoph [53] also investigate such monolithic carbon produced by Sutcliffe Speakman Carbons. Powder activated carbon is mixed with a polymeric binder, compressed in a die and fired to produce a monolith of the desired shape, with a density of 713 kg/m^3 and conductivity of 0.33 W/mK . A heat transfer coefficient of $200\text{W/m}^2\text{K}$ has been measured between the blocks and aluminium fins. Consolidated beds also yield considerable improvements in the bed-wall heat transfer coefficient as a result of the improved thermal contact. Hence, consolidated beds should allow large increases in SCP (Specific Cooling Power). However, when using consolidated adsorbent beds, reduction in mass transfer with increasing bed consolidation may counteract the improvement. Some researchers apply some methods to minimize the adverse effect. Groll [93] and Cacciola et al. [84] suggest utilising porous gas tubes, channels or arteries within the solid adsorbent bed to improve mass transfer. Additionally slots and channels may be cut in the heat transfer surfaces to promote mass transfer [53]. Overall, in order to improve the heat transfer between the heat transfer fluid and the bed itself, the thermal conductivity of the

bed needs to be increased as well as the rate of heat transfer between the heat transfer surfaces and the bed.

A novel method for improving heat transfer through adsorbent bed has been proposed by Critoph [35-39]. This involves utilising forced convection to yield higher heat transfer rates by pumping the adsorbate in alternate directions through the adsorbent bed. However, this system is considerably more complex than more conventional systems.

The adsorption process discussed so far has concerned physical adsorption in which relatively weak van der Waals bonding occurs between the adsorbate and adsorbent. In chemical adsorption however, a chemical bond is formed between the adsorbent and adsorbate. Unfortunately, chemical adsorbents undergo large volume changes during adsorption and desorption and eventually continual cycling renders them impermeable and the reaction rate is limited by kinetics [100].

Recently a family of new composite sorbents has been developed for multiple applications that include thermal energy storage, adsorption heat pump etc. These materials, so called hybrid material, are two-phase systems which consist of a porous host matrix with open pores and a metallic salt impregnated into its pores. Due to their physical structure the materials take an intermediate position between solid adsorbents and pure metallic salts and can be organized in a way to demonstrate the best features of both systems. A large variety of host matrices (such as silica gel, alumina, active carbon, vermiculite, etc.) and salts (CaCl_2 , LiBr , CoCl_2 , BaCl_2 , etc) are expected to give many possibilities to controllably change the sorbent properties in a wide range to fit the demands of a particular application [101]. Research shows that host matrices can effectively restrict the swelling

and disintegration and so improve the performance of adsorption systems [102-107]. This kind of material will be of practical significance for the design of a chemical heat pump of better performance. The details of these materials will be discussed in chapter 4.

2.5 Previous work in University of Warwick

For a number of years research at Warwick University has been focussed on the development of adsorption heat pumps and refrigerators, specifically those utilising active carbon as the adsorbent and ammonia as the adsorbate. A great deal of experience and expertise has been gained in the modelling, designing and building of such machines. The research can provide useful information for choosing proper adsorption pairs and cycles that are the subject of the research presented here and so that the work is worth reviewing.

Generally speaking, the research has been focussed in four main areas:

- Development of monolithic carbon beds rather than granular beds to improve bed conductivity;
- Developing machines that employ convective heat transfer to the beds;
- Developing machines with multiple beds, with regenerative heat transfer between them to improve COP.
- Developing a plate heat exchanger utilising monolithic carbon, which will facilitate rapid cycling and lead to high specific heating and cooling powers

Monolithic carbon

The pores in active carbon allow the adsorbate vapour to be filled in and drained out. But the pores were also partially attributable to the low conductivity of the carbon, causing low thermal conductivity of granular carbon beds.

Research had been carried out at Warwick to produce monolithic carbons that were utilised in compact adsorption beds. Powdered carbon is bound and compressed, giving a higher packing density which means that a greater mass of carbon is contained within a given volume and therefore more refrigerant may be adsorbed, which means a more compact machine can be applied.

The compaction into a monolith also reduces the volume of gas filled voids and creates a solid conduction path, increasing conductivity from 0.1 to $0.6 \text{ Wm}^{-1}\text{K}^{-1}$ [101]. The elimination of the gas filled voids also gives more direct contact between the adsorbent material and the generator walls, thereby reducing the thermal contact resistance between them [101].

Further work at Warwick has achieved additional improvements in heat transfer to the bed by incorporating aluminium fins within the monolithic carbon bed. Figure 2-10 shows a cross section through the generator. This generator has an effective conductivity of $20 \text{ Wm}^{-1}\text{K}^{-1}$ and has achieved a specific cooling power (SCP) of 200 W/kg [101].

Figure 2-10 Cross section through a laminated generator, employing monolithic carbon adsorbent and aluminium fins to improve heat transfer [101]



Convective thermal wave machine

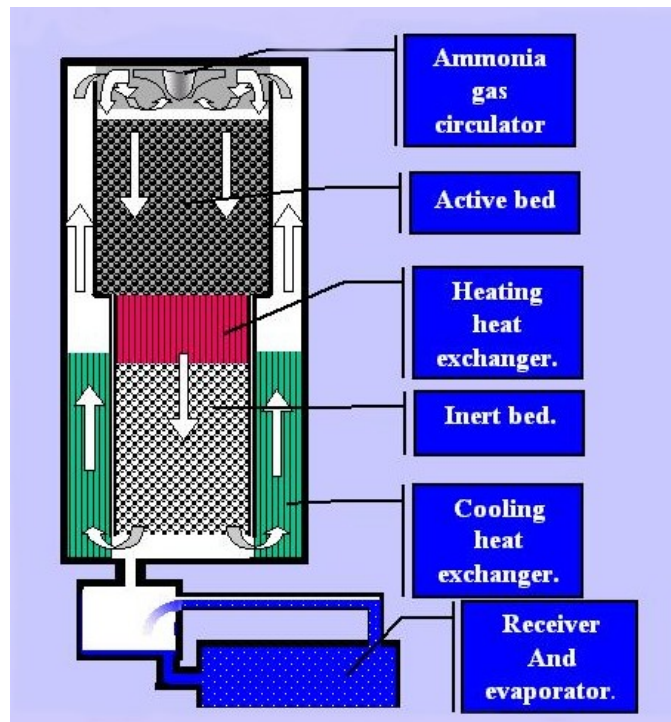
The convective thermal wave was the first developed at the University of Warwick to improve both the COP and specific cooling power of adsorption machines, and has been patented by Critoph and Thorpe [38].

Figure 2-11 shows a schematic of a 10kW carbon-ammonia convective thermal wave chiller that is currently under construction. The beds in the convective thermal wave chiller are heated and cooled by passing the refrigerant itself through them with a gas circulator and regeneration of heat to improve the COP is achieved by storing heat in an inert bed [36]. The details of this adsorption cycle have been described in the previous part.

The benefits of this design are that all of the components, with the exception of the gas circulator, are standard components and it is relatively compact and should produce in the

region of 10kW of cooling and fit within a 1m³ volume, giving a power density of approximately 10 litres/W. The effective heat regeneration should also give a relatively high COP, which has been conservatively estimated at 0.8 [101].

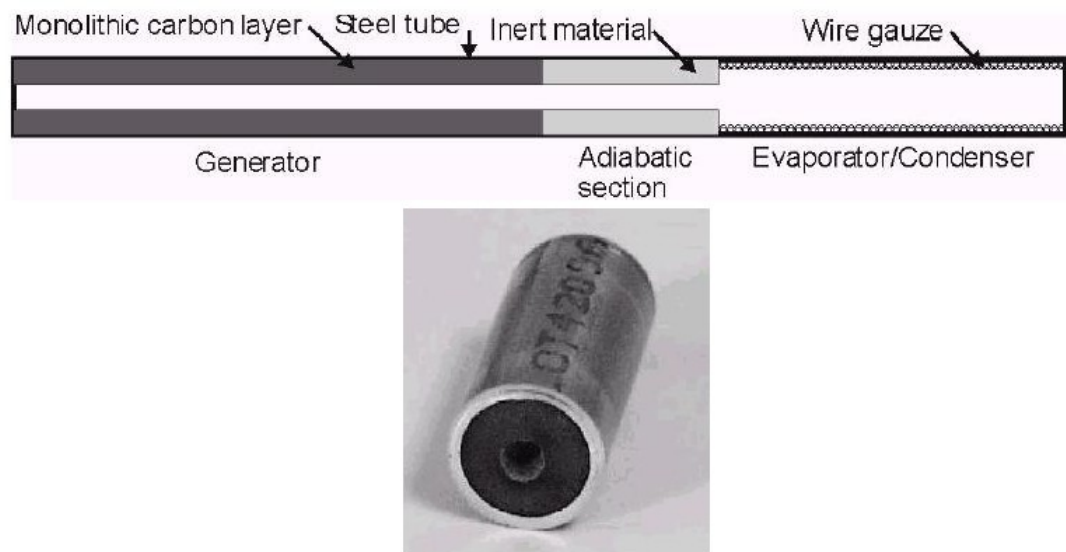
Figure 2-11 Schematic of 10kW convective thermal wave chiller [101].



Multiple bed regenerative adsorption air conditioner

Another machine currently under development at the University of Warwick employs multiple beds with heat regeneration between them in order to improve the COP. The beds are in the form of modules as illustrated in figure 2-12.

Figure 2-12 Section through and a schematic of a single sorption module [108]



The module is made from a 12.7mm diameter stainless steel tube which is lined with a 500 mm long, 3 mm thick layer of monolithic carbon at one end which forms the generator. The other end of the tube forms the evaporator-condenser in which the ammonia refrigerant is condensed and evaporated. The configuration of the modules within the prototype air conditioner is shown in figure 2-13.

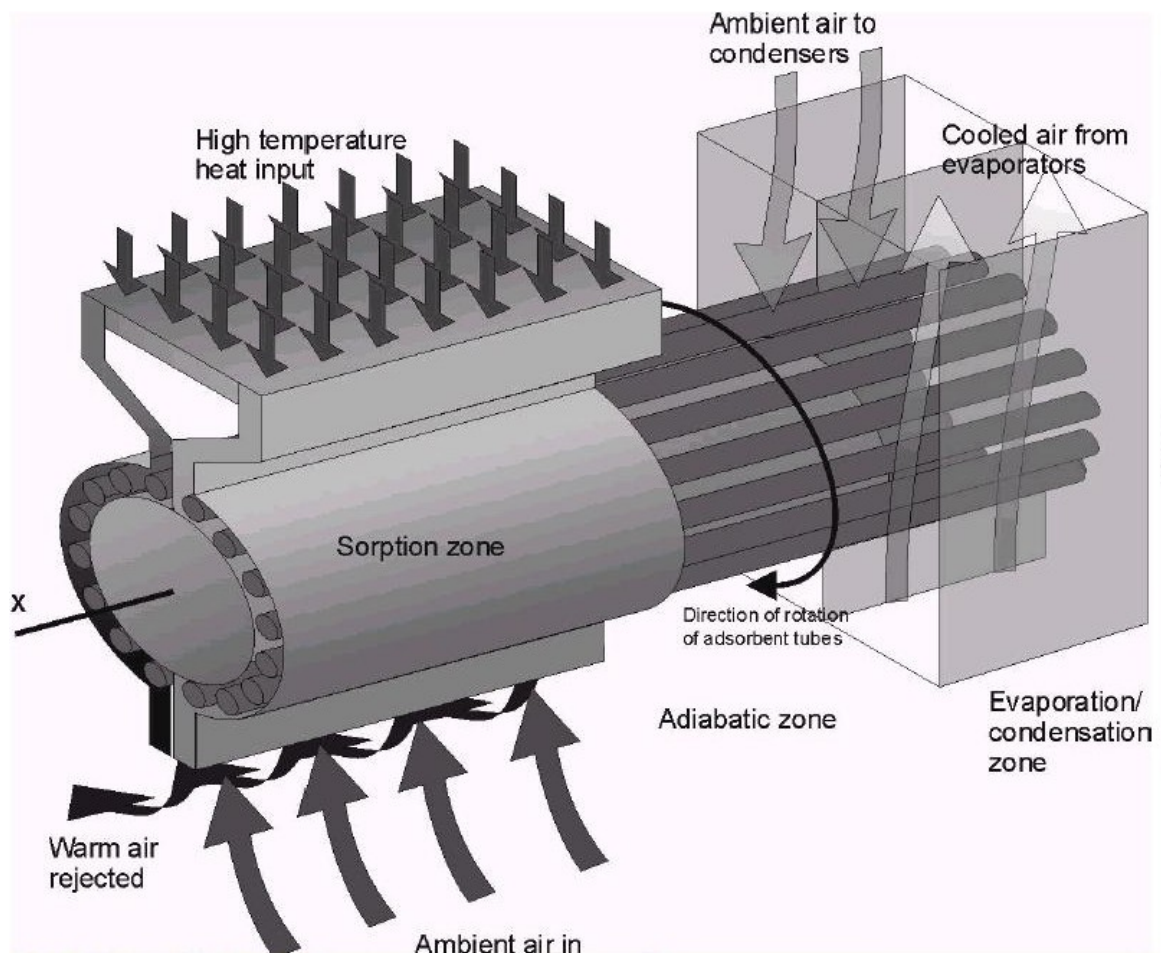
The modules are mounted on a circular carousel that is slowly rotated about its central axis, which moves the modules between the adsorption zone of the machine in which ambient air is blown over the generator sections of the modules and the desorption zone in which air at 200°C is blown over them.

In the adsorption zone ambient air cools the modules and causes ammonia to be adsorbed which reduces the pressure and causes the condensed ammonia in the condenser-

evaporator to boil and absorb heat. Air passed over the condenser-evaporator sections of the modules whilst in the adsorption zone is thereby cooled.

The ambient air passed over the modules in the adsorption zone is heated in cooling the modules and this is the means by which heat is regenerated. The air from the adsorption zone emerges at around 135°C and is further heated in a heater to 200°C before being passed through the desorption zone.

Figure 2-13 Schematic of multiple bed regenerative air conditioner [101]



In the desorption zone the air from the heater heats the generator sections of the modules and causes ammonia to be desorbed which increases the pressure and causes ammonia to condense in the condenser-evaporator sections of the modules and reject heat.

Simulation of the machine with a computer model has predicted a high cooling COP of 0.85 with 400W of cooling power, which corresponds to a SCP of 180 Wkg^{-1} [101].

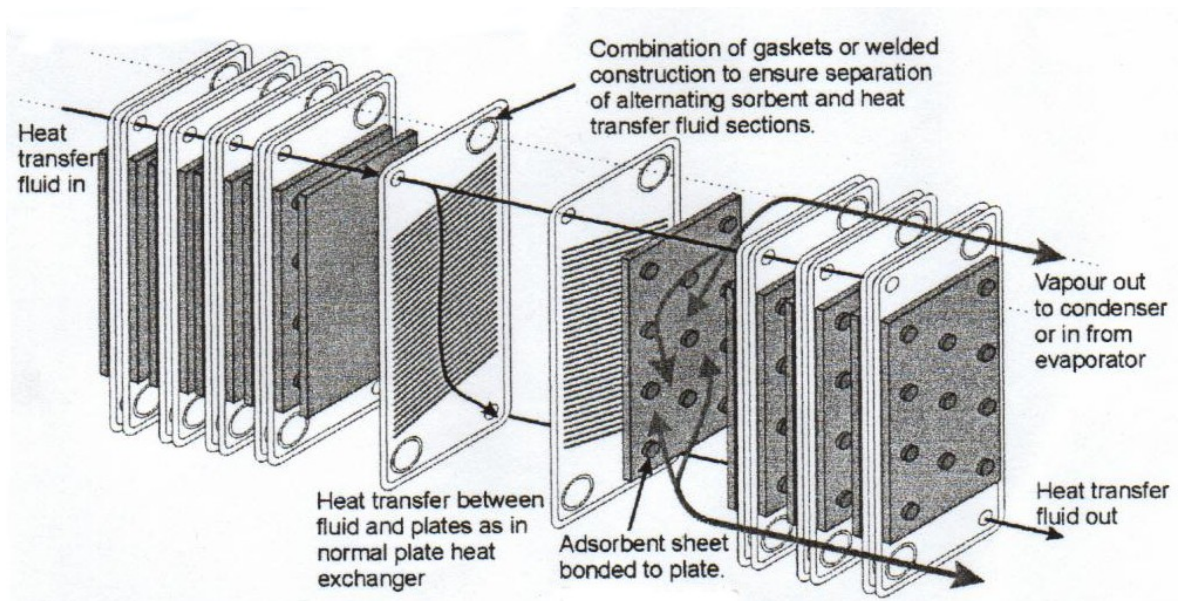
Critoph [109] predicts that with more complex configurations performance may be further improved.

One of the major advantages of this system is that it uses a number of identical low cost modules, enabling machines of varied size and power to be manufactured cost effectively simply by varying the number of modules employed.

Compact plate heat exchanger utilising monolithic carbon

A compact adsorption bed to improve the performance of adsorption systems has been under construction at Warwick University. The structure of the plate heat exchanger which is used in the simulation is shown in figure 2-14 [110]. The heat transfer fluid is pumped between two metal plates to heat and cool the adsorbent beds. The refrigerant, ammonia, is condensed and evaporated in separate sections. The heat rejected from the condensing ammonia during desorption and the heat absorbed by the evaporating ammonia during adsorption is transferred through the condenser - evaporator plates to and from heat transfer fluid [111].

Figure 2-14 Configuration of the plate heat exchanger for the generator bed [111]



This configuration should give good heat transfer to the carbon layers, especially if they are made sufficiently thin, and it should be possible to achieve short cycle times and high specific cooling or heating powers. The separating metal plates may be made thin by allowing equalization of pressure between the heat transfer fluids and the refrigerant, thus preventing a pressure imbalance that would deform them. Their thermal masses can thereby be made low, further decreasing the cycle time and improving COP (since less energy is wasted in heating up the plates every cycle) [110].

Simulations showed that it should be possible to construct a monolithic carbon–ammonia refrigeration system utilising a simple non-regenerative cycle with a COP typically about 0.3 and SCP better than 2000 W kg^{-1} carbon [110].

2.6 Summary

This chapter focused on the previous general study involved in adsorption heat pumps. The thermodynamics of the various solid adsorption cycles with a view to improving cycle efficiency, cycling time and overall cycle performance is studied. Most used adsorption pairs with particular emphasis on the principle of heat transfer enhancement were also discussed thoroughly. Finally, the previous work at Warwick University is reviewed.

References:

- [1] R.Z. Wang, Performance improvement of adsorption cooling by heat and mass recovery operation., *International Journal of Refrigeration*, vol. 24, pp.602-611, 2001
- [2] S.V. Shelton, W.J. Wepfer, *Solid-vapour air conditioning technology*, IEA Air Conditioning Conference, Tokyo, pp.525-535, 1990
- [3] R.E. Critoph, A forced convection regenerative cycle using the carbon-ammonia pair, *Proceeding of the Symposium: Solid sorption refrigeration*, pp.97-102, 1992
- [4] N. Doss, F. Meunier, L. Sun, Predictative model and experimental results for a two-adsorption air conditioning, *Industrial and Engineering Chemistry Research*, vol. 27(2), pp.310-316, 1988
- [5] R.Z. Wang, Study on a four-bed cascade adsorption refrigeration cycle capable of COP over 1.1, *Proceeding of 20th International Congress of Refrigeration*, 19-24 September, Sydney, 1999
- [6] M. Pons, F. Poyelle, Adsorptive machines with advanced cycles for air conditioning or cooling applications, *International Journal of Refrigeration*, vol.22(1), pp. 27-37, 1999
- [7] M. Pons, J.J. Gulleminot, Design of an experimental solar-powered solid-adsorption ice maker, *JSEE, ASME*, vol.108, pp. 332-337, 1986
- [8] R.Z. Wang, Q.B. Wang, Adsorption mechanism and improvements of the adsorption equation for adsorption refrigeration pairs, *International Journal of Energy Research*, vol. 23, pp. 887-898, 1999

- [9] R.E. Critoph, Adsorption refrigeration and heat pumps, In: Carbon Materials for Advanced Technologies, Edited by Trimothy D. Burchell, pp.303-340, PERGAMON, 1999
- [10] F. Zeigler, Recent developments and future prospectus of sorption heat pump systems, International Journal of Thermal Science, vol.38 (3), pp.191-208, 1999
- [11] F. Meunier, Adsorption heat pump technology: possibilities and limits, proceedings of TSHPC'99, pp.25-35, 24 -26 March, Munich, Germany, 1999
- [12] W. Wang, T.F. Qu, R. Z. Wang, Influence of degree of mass recovery in adsorption refrigeration cycles, Applied Thermal Engineering, vol.21, pp. 439-452, 2001
- [13] F. Meunier, Second law analysis of solid adsorption heat pump operating on reversible cascade cycle: application to the zeolite-water pair. Heat Recovery System, vol.5 (2), pp133-141, 1985
- [14] R.Z. Wang, Adsorption refrigeration research in Shanghai Jiao Tong University, Renewable Sustainable Energy Rev, vol.5(1), pp. 1-37, 2001
- [15] R.Z. Wang, Performance improvement of adsorption cooling by heat and mass recovery operation, Int J Refrigeration, vol.24, pp. 602-611, 2001
- [16] D.J. Miles, D.M. Sanborn, G.A.S. Nowakowski and V. Shelton, Gas-fired sorption heat-pump development, Heat Recovery Syst CHP, vol.13(4), pp. 347-351, 1993
- [17] S. Istria, J. Castaing and P. Neveu, Energetic analysis, application field and performance of a new thermochemical sorption cycle: the multisalt system, Appl Thermal Engng, vol.16(1), pp. 875-889, 1996
- [18] M. Pons, Y. Feng, Characteristic parameters of adsorptive refrigeration cycles with thermal regeneration, Appl Thermal Engng, vol.17(3), pp. 289-298, 1997

- [19] J.A. Jones, Regenerative adsorbent heat pump, US Patent 5046319, 1991
- [20] J.A. Jones, In: Proceedings of the Solid Sorption Refrigeration, Paris, In: Proceedings of the Solid Sorption Refrigeration, Paris, pp. 126–35, 1992
- [21] H. Lotz, Continuously operating and adsorption refrigeration plant, especially for operation by waste heat of combustion engines or the like, US Patent 4478057, 1984
- [22] M. Duran, Chemisorption air conditioner, US Patent 4574874, 1986
- [23] P. Maier-Laxhuber, Continuously acting adsorption devices and process for their operation, US Patent 4660629, 1987
- [24] D.C. Erickson, Rotary trisorption heat pump, US Patent 5279359, 1994
- [25] B. Ebbeson, Sorption device, US Patent 5431716, 1995.
- [26] R.E. Critoph, Simulation of a continuous multiple-bed regenerative adsorption cycle, Int J Refrigeration vol.24, pp. 428–437, 2001
- [27] R.Z. Wang, Adsorption refrigeration, China Machine Press, pp.63-104, 2002
- [28] S. Szarzynski, Y. Feng, M.Pon, Study of different internal vapour transports for adsorption cycles with heat regeneration, Int. J. Refrigeration, vol.20 (6), pp390-401, 1997
- [29] T.F. Qu, R.Z. Wang, W. Wang, Study on heat and mass recovery in adsorption refrigeration cycles, Applied Thermal Engineering, vol.21 (4), pp439-452, 2001
- [30] T.F. Qu, W. Wang, S.G. Wang, Y.X. Xu, J.Y. Wu, R.Z. Wang, Research of the mechanism of mass recovery in adsorption refrigeration cycles and a new theoretical model, Proceedings of the International Sorption Heat Pump Conference, pp.639-644, September 24-27, Shanghai, China, 2002
- [31] S. Shelton, Solid adsorbent heat pump system, US Patent No. 4,610,148, September 1986

- [32] D.J. Miles, S. Shelton, Design and testing of a solid-sorption heat-pump system. Applied Thermal Engineering, vol.16, pp. 389–394, 1996
- [33] L.M. Sun, Y. Feng, M. Pon, Numerical investigation of adsorption heat pump with thermal wave heat regeneration under uniform pressure conditions, Int. J. Heat and Mass Transfer, vol.40 (2), pp.281-293, 1997
- [34] M. Pon, S. Szarzynski, An adsorption cooling system with heat regeneration: experimental and numerical study, Proc. of the International Sorption Heat Pump Conference, Munich, Germany, March 24-26, pp.625-630, 1999
- [35] R.E. Critoph, Forced convection adsorption cycles, Applied Thermal Engineering, vol.18, pp.799-807, 1998
- [36] R.E. Critoph, Forced convection enhancement of adsorption cycles, Heat Recovery Systems & CHP, vol.14 (4), pp.343-350, 1994
- [37] R.E. Critoph, Forced convection adsorption cycle with packed bed heat regeneration. International Journal of Refrigeration, vol.22, pp.38-46,1999
- [38] R.E. Critoph, R.N. Thorpe, U.K., Paten 9419202.8, 1994
- [39] R.E. Critoph, R.N. Thorpe, Experimental results from a forced convective adsorption heat pump/air conditioner. Proceedings of the International Sorption Heat Pump Conference, Munich, Germany, March 24-26, pp.555-559, 1999
- [40] N. Douss, F. Meunier, Experimental study of cascading adsorption cycles, Chemical Engineering Science, vol.44, pp.225-235, 1989
- [41] R.E. Critoph, L. Turner, Performance of ammonia-activated carbon and ammonia zeolite heat pump adsorption cycles, Proceedings of Pompes a Chaleur Chimiques De Hautes Performances, Perpignan, Lavoisier, Paris, pp.202-211, 1989

- [42] U. Rockenfeller, et al, Advanced heat pump staging for complex compound chemi-sorption systems, Proceedings of Solid Sorption Refrigeration, Paris, IIR, pp.153-159, 1992
- [43] F. Meunier, Heat recovery systems, vol.5, pp.133-141, 1985
- [44] F. Zeigler, Adsorption experts meeting, Paris, pp.20-23, 1985
- [45] G. Moss, M. Shahidullah, Proceedings of International Workshop on Heat Transformation and Storage, Ispra, 9-11 Oct., pp.295-309, 1988
- [46] F. Meunier, Theoretical performances of solid adsorbent cascading cycles using the zeolite-water and active carbon-methanol pairs: four case studies, Heat recovery systems, vol.6 (6), pp.491-498, 1986
- [47] S.B. Riffat, C.F. Afonso, A.C. Diveira, D.A. Reay, Natural refrigerants for refrigeration and air conditioning systems, Applied Thermal Engineering, vol.17 (1), pp.33-42, 1997
- [48] N.C. Srivastava, I.W. Eames, A review of adsorbents and adsorbates in solid vapour adsorption heat pump systems, Applied Thermal Engineering, vol.18 (9-10), pp.707-714, 1998
- [49] R.E. Critoph, Y. Zhong, Review of trends in solid sorption refrigeration and heat pumping technology, Proc. IMechE Part E: J. Process Mechanical Engineering, vol.219, pp.1-6, 2005
- [50] R.E. Critoph, An ammonia carbon solar refrigerator for vaccine cooling, Renewable Energy, vol.5 (1), pp.502-508, 1994
- [51] Z. Tamainot-Telto, R.E. Critoph, Solar sorption refrigerator using a CPC collector, Renewable Energy, vol.16, pp.735-738, 1999
- [52] R.E. Critoph, Evaluation of alternative refrigerant-adsorbent pairs for refrigeration cycles, Applied Thermal Engineering, vol.16 (11), pp.891-900, 1996

- [53] Z. Tamainot-Telto, R.E. Critoph, Adsorption refrigeration using monolithic carbon-ammonia pair. *International Journal of Refrigeration*, vol.20 (2), pp.146-155, 1997
- [54] J.A. Jones, Carbon/ammonia regenerative adsorption heat pump, *International Absorption Heat Pump Conference*, ASME-AES, pp. 449-455, 1993
- [55] D.J. Miles, S.V. Shelton, Design and testing of a solid sorption heat pump system, *Applied Thermal Engineering*, vol.16, pp. 389-394, 1996.
- [56] A.O. Dieng, R.Z. Wang, Literature review on solar adsorption technologies for ice-making and air-conditioning purposes and recent developments in solar technology, *Renewable Sustainable Energy Rev.*, vol.5 (4), pp.313-342, 2001
- [57] R. Delgado, A. Choisier, P. Grenier, I. Ismail, F. Meunier, M. Pons, Etude de cycle intermittent charbon actif/methanol en vue de la realisation d'une machine a fabriquer de la glace fonctionnant a l'energie solaire, *Proc Meetings IIR Commissions E1-E2*, Jerusalem, pp.185-191, 1982
- [58] Z.F. Li and K. Sumathy, A solar powered ice maker with the solid adsorption pair of activated carbon and methanol. *Int. J. Energy Res.*, vol.23, pp.517-527, 1999
- [59] R. Exell, S.C. Bhattacharya, Y.R. Upadhyaya, Research and development of solar powered desiccant refrigeration for cold storage applications, *Asian Institute of Technology*, Bangkok, AIT Research Report, No.265, 1993
- [60] F. Meunier, Solid sorption heat powered cycles for cooling and heat pumping applications, *Applied Thermal Eng.*, vol.18, pp. 715-729, 1998
- [61] G. Cacciola, G. Restuccia, Reversible adsorption heat pump: a thermodynamic model, *Int. J Refrigeration*, vol.18 (2), pp.100-106,1995

- [62] P.F.L. Antonio, M. Daguene Performance of a new solid adsorption ice maker with solar energy regeneration, *Energy Conversion and Management*, vol. 41(15), pp.1625-1647, 2000
- [63] R.Z. Wang, J.X. Xu, Y. Teng, W. Shi, Experiment on a continuous heat regenerative adsorption refrigerator using spiral plate heat exchanger as adsorbers, *Applied Thermal Engineering*, vol.18(1), pp.13-23, 1998
- [64] A. Sokoda, M. Suzuki, Simultaneous transport of heat and adsorbate in closed type adsorption cooling system utilizing solar heat, *J. Sol. Energy Eng.*, vol.108, pp.239-245, 1986
- [65] H. Hisaki, N. Kobayashi, Y. Yonezawa, A. Morikawa, Development of ice-thermal storage system using an adsorption chiller, *Int. Absorption Heat Transfer Conf, ASME-AES*, vol.31, pp.439-444, 1993
- [66] B.B. Saha, E.C. Boleman, T. Kashiwagi, Experimental investigation of silica gel-water adsorption refrigeration cycle- the influence of operating conditions on cooling output and COP. *ASHRAE Trans.*, No.101, pp. 425-431, 1995
- [67] K. Ortel, M. Fischer, Adsorption cooling system for cold storage using methanol and silica gel, *Proceedings of the International Heat Powered Cycles Conference*, University of Nottingham, UK, pp.15–17, 1997
- [68] H. Chua., Modelling the performance of two-bed, silica gel-water adsorption chillers, *International Journal of Refrigeration*, vol.22, pp.194-204, 1999
- [69] V. Tangkongsirish, A. Kanzawa, T. Watanabe, A solar-powered adsorption cooling system using silica gel-water mixture, *Energy*, vol.23 (5), pp.347-353, 1998
- [70] S. Matsushita, Adsorption chiller using low temperature heat source, *Energy Conservation*, vol.39 (10), p.96, 1987

- [71] D. Tchernev, Solar air conditioning and refrigeration systems utilizing zeolites, Proc. Meetings of IIR Commissions E1-E2, pp.209-215, Jerusalem 1982
- [72] P.H. Grenier, J.J. Guilleminot, F. Meunier, M. Pons, Solar powered solid adsorption cold store, ASME J Solar Energy Eng., vol.110, pp.192-197,1998
- [73] M. Tather, A. Erdem-Senatalar, The effects of thermal gradients in a solar adsorption heat pump utilizing the zeolite-water pair, Applied Thermal Eng., vol.19, pp.1157-1172, 1999
- [74] F. Poyelle, J.J. Guilleminot, F. Meunier, Experimental tests and predictive model of an adsorptive air conditioning unit, Int. Eng. Chem. Res., vol.38, pp. 298-309, 1999
- [75] Y.Z. Lu, R.Z. Wang, M. Zhang, S. Jiangzhou, zeolite/water⁴. Adsorption cold storage system with zeolite-water working pair used for locomotive air conditioning, Energy Conversion and Management, vol.44 (10), pp.1733-1743, 2003
- [76] Y.Z. Lu, R.Z. Wang, S. Jianzhou, Y.X. Xu , J.Y. Wu, Practical experiments on an adsorption air conditioner powered by exhausted heat from a diesel locomotive, Applied Thermal Engineering, vol.24(7), pp.1051-1059, 2004
- [77] S. Jiangzhou, R.Z. Wang, Y.Z. Lu, Y.X. Xu, J.Y. Wu, Z.H. Li, Locomotive driver cabin adsorption air-conditioner, Renewable Energy, vol. 28 (11), pp.1659-1670, 2003
- [78] Y.K. Tan, D.S. Zhu, An experimental study and simulation on adsorption heat pump cycle process, Science et Technique du Froid, vol.1, pp.129-134, 1992
- [79] M. Tatlier, A novel approach to enhance heat and mass transfer in adsorption heat pump using zeolite-water pair, Microporous and Mesoporous Materials, vol.27, pp.1-10, 1999

- [80] D.S. Zhu, Y.K. Tan, Investigation of heat and mass transfer in heat pump adsorber, J. Chem. Industry & Engineering (Chinese), vol.2, pp.212-217, 1993
- [81] D.S. Zhu, S.W. Wang et al., An experimental study of heat conduction enhancement on the solar-powered absorber, Acta Energiæ Solaris Sinica, vol.2, pp.186-190, 1998
- [82] L.J. Wang, D.S. Zhu, Y.K. Tan, Heat transfer enhancement on the adsorber of adsorption heat pump, Adsorption, vol.5, pp.279-286, 1999
- [83] D. S. Zhu, S. W. Wang, Experimental investigation of contact resistance in adsorber of solar adsorption refrigeration, Solar Energy, vol.73 (3), pp.177-185, 2002
- [84] G. Cacciola, G. Cammarata, A. Fichera, G. Restuccia, Advances on innovative heat exchangers in adsorption heat pumps, Solid Sorption Refrigeration Symposium, Paris, pp.221-226, 18-20 Nov., 1992
- [85] J.A. Jones, Sorption refrigeration research at JPL/NASA, Solid Sorption Refrigeration Symposium, Paris, pp.126-135, 18-20 Nov., 1992
- [86] K. Hinotani, K. Kanatani, K. Matsumoto, M. Kume, Development of Solar actuated zeolite refrigeration system, Research Centre, Sanyo Electric Co. Ltd, Hirakata, Osaka 573, Japan
- [87] B. Spinner, Application of new concepts for the development of gas solid sorption machines, CNRS-IMP, LEA-SIMAP, University of Perpignan (France), 1996
- [88] E. Hu, D.S. Zhu, Enhancement of thermal conductivity by using polymer zeolite in solid adsorption heat pumps, J. Heat Transfer, vol.8, pp.627-629, 1997
- [89] L.G. Fang, D.S. Zhu, Y.K. Tan, Mass and heat transfer enhancement of adsorbent in adsorption refrigeration, J. Chem. Eng.(In Chinese), vol.12, pp. 17-22, 1998

- [90] V.M. Antonetti, Enhancement of thermal contact conductance by metallic coatings: theory and experiment, *J. Heat Transfer*, vol.8, pp.513-519, 1985
- [91] G.P. Peterson, Measurement of the thermal contact conductance and thermal conductivity of anodized aluminium coatings, *J. Heat Transfer*, vol.8, pp. 579-585, 1990
- [92] M. Hammad, S. Habali, Design and performance study of a solar energy powered vaccine cabinet, *Applied Thermal Engineering*, vol.18, pp.1785-1798, 2000
- [93] M. Groll, Solid Sorption Machines for CFC-Free Generation of Heat and Cold (An Overview), 1st ISMHT-ASME Heat and Mass Transfer Conference, Bombay, 1994
- [94] J.J. Guilleminot, A. Choisier, J. B. Chalfen, S. Nicolas, Heat Transfer Intensification in fixed bed adsorber, *Heat Recovery Systems & CHP*, vol.13 (4), pp.297-300, 1993
- [95] J.J. Guilleminot, J.M. Gurgel, Heat transfer intensification in adsorbent beds of adsorption thermal devices, Proceedings of the 12th Annual International Solar Energy Conference, Miami, USA, ASME, New York, pp.69-74, 1990
- [96] M. Li and R.Z. Wang, Heat and mass transfer in a flat plate solar solid adsorption refrigeration ice maker, *Renewable Energy*, vol.28 (4), pp.613-622, 2003
- [97] G. Cacciola, G. Restuccia, Progress on adsorption heat pump, *Heat Recovery Systems & CHP*, vol.14 (4), pp.409-420, 1994
- [98] F. Meunier, Solid sorption: an alternative to CFC's, *Heat Recovery Systems & CHP*, vol.13 (4), pp.289-295, 1993
- [99] S. Mauran, P. Prades, F. L' Haridon, Heat and mass transfer in consolidated reacting beds for thermochemical systems, *Heat Recovery Systems & CHP*, vol.13 (4), pp.315-319, 1993

- [100] R.E. Critoph, Carbon-ammonia sorption systems-previous experience, current projects and challenges for the future, Proceedings of the Int. Heat Pump Conference 2002, Shanghai, China, Sep 24-27 2002
- [101] Yu.I Aristov, G. Restuccia, G. Cacciola, V.N. Parmon, a family of new working materials for solid sorption air conditioning systems, Applied Thermal Engineering, vol. 22, pp.191-204, 2002
- [102] M. Tokarev, L. Gordeeva, V. Romannikov, I. Glaznev, Y. Aristov, New composite sorbent CaCl_2 in mesopores for sorption cooling/heating, Int J. Therm Sci, vol. 41, pp.470–474, 2002
- [103] S.O. Enibe, O.C. Iloeje, Heat and mass transfer in porous spherical pellets of CaCl_2 for solar refrigeration, Renewable Energy, vol.20, pp.205-224, 2000
- [104] L.W. Wang, R.Z. Wang, J.Y. Wu, K. Wang, Compound adsorbent for adsorption ice maker on fishing boats, International Journal of Refrigerator, vol. 27, pp. 401 – 408, 2004
- [105] Z.S. Lu, R.Z. Wang, L.W. Wang and C.J. Chen, Performance analysis of an adsorption refrigerator using activated carbon in a compound adsorbent, Carbon, vol. 44(4), pp.747-752, 2005
- [106] J. Trudel, S. Hosatte, M. Ternan, Solid - gas equilibrium in chemical heat pumps: the NH_3 - CoCl_2 system, Applied Thermal Engineering, vol. 19, pp.495 – 511, 1999
- [107] A. Marty, Etude par microcalorimétrie de la réactivité de deux ammoniacates de chlorure de manganèse, J. Therm. Anal., vol. 37, pp.479 – 498, 1991

- [108] R.E. Critoph, Z. Tamainot-Telto, Laboratory demonstration of a multiple bed regenerative adsorption cycle air conditioner, Proceedings of the Int. Heat Pump Conference 2002, Shanghai, China Sep 24-27 2002
- [109] R.E. Critoph, Multiple bed regenerative adsorption cycle using the monolithic carbon–ammonia pair, Applied Thermal Engineering, vol.22(6), pp.667-677, 2002
- [110] R.E. Critoph, S.J. Metcalf, Specific cooling power intensification limits in ammonia-carbon adsorption refrigeration systems, Applied Thermal Engineering, vol.24, pp.661-678, 2004
- [111] S.J. Metcalf, Simulation of the Effect of Generator Heat Transfer Parameters on Power Density and Efficiency in Multiple-Bed Regenerative Carbon-Ammonia Sorption Heat Pump, International Sorption Heat Pump Conference, June 22-24, 2005, Denver, USA
- [112] ANSI Standard Z21.40.4. In: *Standard for Performance Testing and Rating of Gas Fired Air Conditioning and Heat Pumping Appliances*, American National Standards Institute, New York (1994)

Chapter 3 Theory

3.1 Introduction

In the following chapter the physical process of ‘adsorption’ is explained. The adsorption equations of state and thermodynamic relationships available are presented together with numerical models.

3.2 Principles of adsorption

Although certain phenomena associated with adsorption were known in ancient times, the first quantitative observations were carried out by Scheele [1] in 1773 and Fontana [2] in 1777 who reported some experiments of the uptake of gases by charcoal and clays.

The modern application of adsorption is connected with Lowitz's observation [3, 4], who used charcoal for decolorisation of tartaric acid solutions as result of organic impurities uptake. Systematic studies of adsorption that date from the work by de Saussure [5, 6] started in 1814. He came to the conclusion that all types of gases are taken up by porous substances such as sea-foam, cork, charcoal, asbestos, and this process is accompanied by the evolution of heat. Thus, he discovered the exothermic character of adsorption processes, and he was the first to pay attention to the commonness of adsorption. Moreover, de Saussure observed that gases which undergo condensation readily are taken up to the greatest extent by porous substances.

Of very few papers from the 19th century, there should be mentioned those by Chappuis [7-9], Joulian [10] and Kayser [11, 12]. Chappuis measured the adsorption of ammonia on charcoal and asbestos at a constant temperature. He also found that sulphur dioxide, carbon dioxide and air are taken up by charcoal depending on the pressure of the gas. He made the first calorimetric measurement of heat evolved during wetting of adsorbents by liquids. This problem was also studied by Pouillet [13], Junck [14], Fitzgerald [15], Lagergren [16], Gaudechon [17] and Dewar [18, 19].

The term 'adsorption' was proposed by du Bois-Reymond but introduced into literature by Kayser [11, 12]. During the next few years, the terms 'isotherm' and 'isothermal curve' were used to describe the results of adsorption measurements at constant temperature. Kayser also developed some theoretical concepts which became basic for the monomolecular adsorption theory.

McBain [20] introduced the term 'absorption' in 1909, to determine a much lower uptake of hydrogen by carbon than adsorption. He proposed the term 'sorption' for adsorption and absorption. It is not always possible to distinguish between these two phenomena and to define them precisely. In doubtful cases, the term 'sorption' and consequently the terms 'sorbent', 'sorbate' and 'sorptive' should be used.

Practical application of adsorption processes is based mainly on selective uptake of individual components from their mixtures by other substances. Selective adsorption was discovered by Tswett in 1903 [21]. He took advantage of this phenomenon to separate chlorophyll and other plant pigments by means of silica materials. This separation was possible due to different adsorption affinity of silica gel with regard to various pigments. The technique proposed by Tswett has been called as 'column solid liquid adsorption chromatography'. This discovery was not only the beginning of a new analytical technique, but also the origin of a new field of surface science.

Brunauer [22] defined adsorption as following: "when the gas or vapour is brought in contact with an evacuated solid takes up a part of it. The molecules that disappear from the gas phase either enter the inside of the solid or remain on the outside, attached to its surface." The former phenomenon is called absorption, the latter is called adsorption. The

two often occur simultaneously; the total uptake of the gas is then designated by the term of sorption. The solid that takes up the gas or vapour is called the adsorbent, the gas or vapour attached to the surface of the solid is called the adsorbate. Most adsorbents are highly porous bodies with tremendously large internal surfaces. If the gas enters the inside of a solid two things may happen: either the gas merely dissolves in it, forming a solid solution or it reacts chemically with the solid and forms a compound.

Ponec [23], Oscik [24], Ruthven [25] and Suzuki [26] also explain the term of adsorption. They reckon that adsorption is a surface phenomenon occurring at the interface of two phases. Cohesive forces, including Van der Waals forces and hydrogen bonding, act between the molecules of all substances. Surface forces or unbalanced forces at the phase boundary cause changes in concentration of molecules at the solid/fluid interface [27]. The solid and the fluid adsorbed on its surfaces are referred to as adsorbent and adsorbate respectively. Adsorption due to a physical process is generally called as physical adsorption, or physisorption. In chemical process, adsorption is often called as chemical adsorption or chemisorption. And all types of sorption are exothermic.

Ruthven [25] and Wang [27] present some features, which distinguish physical adsorption from chemical adsorption. The details are shown as,

Table 3.1 Physical and chemical adsorption [25]

Physical Adsorption	Chemical Adsorption
Low heat of adsorption (< 2 or 3 times latent heat of evaporation)	high heat of adsorption (> 2 or 3 times latent heat of evaporation)
Non specific	Highly specific
Monolayer or multilayer. No dissociation of adsorbed species. Only significant at relatively low temperature	Monolayer only. May involve dissociation. Possible over a wide range of temperature
Rapid, non-activated, reversible. No electron transfers although polarisation of adsorbate may occur	Activated, may be slow and irreversible. Electron transfers leading to bond formation between sorbate and surface

Desorption is brought about by either an increase in temperature or a decrease in external partial pressure; some processes of chemical adsorption are irreversible. The general term sorption can be used when both adsorption and absorption occurs simultaneously.

Depending on adsorbent and adsorbate phases, adsorption system may be classified as solid/gas, liquid/gas, solid/liquid and liquid/liquid.

3.3 Adsorption equation of state

The equation for physical adsorption can be classified into three types [28]:

- (a) Adsorption equations based on adsorption speed, which are typically based upon single molecular layer adsorption.
- (b) Thermodynamic adsorption equations, which are based on Polanyi adsorption potential theory and the Dubinin mini-pore filling theory
- (c) Adsorption equations based on capillary condensation theory, which does not consider the effect of energy distribution around the adsorbent surface, but treats the mini-pores as capillaries. A good example is the Kelvin equation.

There are also some empirical equations [27,28], of which one example is based upon the assumption that the adsorption capacity is a function of temperature and pressure, but the two parameters affect the adsorption independently, that is to say,

$x = f(T, p) = f_1(T)f_2(p)$. The disadvantage of such equations is that a large quantity of experimental work is needed, and the assumption cannot always express the adsorption characteristics properly.

The available theories commonly used to describe the adsorption cycles include the theories of Polanyi, Dubinin-Radushkevich (D-R) and Dubinin-Astakhov (D-A). Many adsorption equations have been derived from these theories. These equations deal with physical adsorption of gases and vapours and give the most important characteristics of industrial sorbents that include, among others, pore volume, pore size or energy distribution and specific surface area. These very specific curves can be interpreted to obtain information concerning the adsorption mechanism strictly connected with

interactions between adsorbent and adsorbate molecules, and they give the opportunity to assess the efficiency of industrial adsorbents applied in separation, purification and other utilitarian processes.

To understand these equations, let us first introduce some basic concepts of adsorption.

- (a) Henry's law. For an adsorption process on a uniform surface at sufficiently low concentrations (such that all molecules are isolated from their nearest neighbours), where, the equilibrium relationship between fluid phase and adsorbed phase concentrations will always be linear [29, 23].
- (b) Gibbs' theory. This is based on the ideal gas law, in which the adsorbate is treated in microscopic and bi-dimensional form and provides a general relation between spreading pressure and adsorbed phase concentration. In this concept, volume in the bulk phase is replaced by the area and the pressure is replaced by the so-called 'spreading pressure'. By assuming some forms of thermal equation of state relating the number of moles of adsorbate, the area and the spreading pressure and using them in the Gibbs equation, a number of fundamental equations can be derived, such as the linear isotherm, the Volmer isotherm, etc.

3.3.1 The Langmuir equation

The simplest and by far the most widely used expression for physical adsorption from either gas or liquid solution is the Langmuir equation [29]. The Langmuir equation initially derived from kinetic studies was based on the assumption that on the adsorbent surface there is a definite and energetically equivalent statement when both the adsorption and

desorption rates are the same. The assumptions used for deriving the expressions are as following [29]:

1. Adsorption of adsorbate molecules takes place at well-defined localized states
2. All the adsorption sites are identical (energetically), and each site accommodates one adsorbate molecule only
3. There are no lateral interactions (i.e., interactions between neighbouring adsorbed adsorbate molecules)

The adsorption and desorption rates are assumed to be [29]:

$$\text{Rate of adsorption: } k_a p(1 - \theta) \quad (3-1)$$

$$\text{Rate of desorption: } k_d \theta \quad (3-2)$$

where $\theta = \frac{x}{x_0}$ and

k_a - the adsorption constant

k_d - the desorption constant

θ - the surface coverage or fraction filling of the micro-pores

x - the adsorbed phase concentration at equilibrium

x_0 - the adsorption capacity of the adsorbent

p - the partial pressure in the gas phase

At equilibrium:

$$k_a p(1 - \theta) = k_d \theta \quad (3-3)$$

Rearranging equation (3-3) becomes:

$$\theta = \frac{x}{x_0} = \frac{Kp}{1 + Kp} \quad (3-4)$$

where $K = \frac{k_a}{k_d}$

While at low adsorbate concentration ($x \ll x_0$), Henry's law is obeyed and the equation becomes:

$$\theta = Kp \quad (3-5)$$

The Langmuir equation is limited to single monolayer adsorption and assumes no interaction between nearby molecules on the surface. Later some attempts were made to generalise the Langmuir equation by taking into account lateral interactions among adsorbed molecules, their mobility and the energetic surface heterogeneity of the solids. The Langmuir equation itself should be considered, however, as a useful equation that corresponds to the so-called ideal localised monolayer. The ideal localised monolayer model, despite its obvious imperfections, occupies a central position in surface and adsorption science. It allowed for a start of comprehensive theoretical studies, the aim of which was and still is a search for more and more perfect and real descriptions of experimental adsorption systems.

3.3.2 Freundlich isotherm

Another type of the equation commonly used is Freundlich isotherm expression [29]:

$$x = Ap^{1/n} \quad (3-6)$$

The Freundlich equation is the simplest equation for data representation. It does have some defects, namely, it fails to observe Henry's law behaviour in the limiting situations of $p \rightarrow 0$. But it is the first empirical equation used to describe adsorption isotherms.

Incidentally, the so-called Freundlich adsorption isotherm was actually proposed by Boedecker in 1895 [30] as an empirical equation. This equation is known in literature as the Freundlich's equation, because Freundlich [31] assigned great importance to it and popularised its use.

The Langmuir expression can be modified in several ways to improve its fit with experiments. One of them is the Langmuir-Freundlich expression:

$$\theta = \frac{x}{x_0} = \frac{Kp^{1/n}}{1 + Kp^{1/n}} \quad (3-7)$$

This equation contains three parameters: x_0 , K , n and for certain type of data (adsorption of hydrocarbons on activated carbon [32]) is found to be better in data correlation compare with either Langmuir or Freundlich equations used separate[29].

3.3.3 The BET equation

Brunauer, Emmett and Teller developed the BET theory [33]. As is in the case of Langmuir isotherm, the theory is based on the concept of an adsorbed molecule, which is not free to move over a surface and which exerts no side forces on adjacent molecules of adsorbate. The BET theory does allow different numbers of adsorbed layers to build up on different parts of the surface.

The principal assumption of the BET theory is that the Langmuir equation applies to every adsorption layer. Like the Langmuir theory, the first adsorption layer is formed on an array of surface sites of uniform energy. The major simplifying assumptions deal with the foundation, that beginning from the second adsorbed layer the condensation heat is equal to the evaporation heat of gas and that the ratio between the rate constant of uptake from one layer and the condensation of a lower situated layer for all the layers starting from the second one. The BET isotherm represents a generalisation of the Langmuir isotherm, to some extent. The BET equation can be represented as:

$$\theta = \frac{x}{x_0} = \frac{K\left(\frac{p}{p_s}\right)}{\left[1 + (K-1)\left(\frac{p}{p_s}\right)\right]\left[1 - \left(\frac{p}{p_s}\right)\right]} \quad (3-8)$$

where p_s denotes the saturation vapour pressure of the adsorbate at the prevailing temperature.

The advantage of the BET equation is that it can be fitted to different shapes of adsorption isothermal. But this equation is not applicable under supercritical conditions, i.e., if the temperature is beyond the critical temperature of the adsorbate. For this reason, it is seldom used for data correlation and representation.

In summary, the BET theory, despite many restrictions, was the first attempt to create a universal theory of physical adsorption [34]. It describes the entire course of the isotherm including the areas of monomolecular adsorption, polymolecular adsorption and capillary condensation. Unfortunately, the last region is described in an unsatisfactory way, particularly, if the solid is of a heterogeneous porous structure that comprises pores of various capillary widths. This theory cannot be applied to adsorption at temperatures

higher than the critical temperature because it is not possible to assume equality of heats of adsorption and condensation as well as stability of the adsorption coefficient ratio with regard to individual adsorption layers.

The Langmuir and BET theories, originating from one common assumption, assume the existence of an interface geometrical surface on which mono- or multilayer adsorption takes place. The basic geometrical parameter applied to flat macroscopic adsorbents is their surface area.

3.3.4 Polanyi potential theory

The original potential theory, as postulated by Polanyi [35], is based upon the potential energy distribution around the adsorbent surface, which is a theoretical model to describe multi-molecular layer adsorption. Because the adsorbed layer has a multilayer character, therefore it is not two-dimensional as follows from the Langmuir theory, but it possesses a definite volume and applies to the van der Waals equation. According to this theory, the adsorbed layer is considered as a 'thick', multilayer film of decreasing density and increasing distance from the solid surface. The basic concept of the Polanyi theory includes the adsorption potential and the characteristic adsorption curve. This characteristic curve presents a simple relationship between the adsorption potential and the distance from the solid surface. This relationship was named as the characteristic adsorption equation. The aforementioned distance may be expressed in terms of volume units of the adsorbed phase. Polanyi assumed that the adsorption potential is independent of temperature over a wide temperature range. It means that the characteristic curve of adsorption is temperature independent, too. Such a statement follows from the fact, that the Van der Waals forces are

also independent of temperature. However, for polar adsorbates this does not always hold true.

Later, Dubinin [36] further developed this model; thus this theory is now also called as Dubinin-Polanyi adsorption potential theory. According to Polanyi's assumption, the adsorption potential energy ε is independent of temperature, that is:

$$\left(\frac{\partial \varepsilon}{\partial T}\right)_{V_s} = 0 \quad (3-9)$$

where V_s is adsorption volume, the potential function $\varepsilon = f(V_s)$ is suitable for all temperature ranges for a known gas, and is thus called the characteristic adsorption function.

This assumption was verified for non-polar adsorption and for a polar system with low coverage [27]. Based on the Polanyi assumption [35], potential ε can be presented around the surface of the adsorbent. Adsorbed gas exists in a compressed state by the attractive forces acting from the surface (where $\varepsilon \approx \varepsilon_{\max}$) to a certain distance (where $\varepsilon = 0$) into the surrounding space. In this case, the adsorbate exists in a compressed state and its density is not constant, being the maximum at the solid surface and a minimum at $\varepsilon = 0$. Polanyi reckoned that the adsorption potential ε might be represented by the equation for isothermal work of compression:

$$\varepsilon = RT \ln \frac{p_2(T)}{p_1(T_{sat})} \quad (3-10)$$

where:

p_2 - Pressure of the compressed adsorbate on an equal-potential surface, which equals the saturation pressure at T

- p_1 - Vapour-adsorbate equilibrium pressure corresponding to T_{sat} , the fluid temperature at the evaporator or condenser
- T - Adsorbent bed temperature

Therefore, ε is a function of P and T for a certain adsorbate. The equilibrium adsorption capacities is $x = \frac{M_a}{M_c} = \frac{\rho V_s}{M_c}$, where ρ is a density of the liquid adsorbate at the adsorbent temperature, M_a and M_c are the mass of adsorbate and adsorbent respectively. Thus the adsorption potential energy ε can be expressed as $\varepsilon = f_1(V_s) = f_2(x)$ or we can write $x = f(\varepsilon)$, where x is the equilibrium adsorption capacities.

3.3.5 The Dubinin-Radushkevich equation

Dubinin and Radushkevich [36] suggest that the adsorption potential in the Polanyi Potential Theory can be expressed as a Gaussian distribution function (D-R equation):

$$x = x_0 \exp\left(-k\left(\frac{\varepsilon}{\beta}\right)^2\right) \quad (3-11)$$

where x_0 is the limiting adsorption capacity, k is a constant determined by the surface of the adsorbent, and β is the affinity coefficient which is determined by the adsorbent-adsorbate pair. The DR equation is very useful to describe the adsorption characteristics of most industrial adsorbents which have a complex and well-developed porous structure including pores of different shapes and widths, but where micropores play the most significant role in the structure. However, For carbonaceous solids resulting from a high degree of burn-out during activation, the degree of heterogeneity increases because of a

wider pore size distribution, and for such cases the DR equation does not describe well the equilibrium data.

Jing and Exell [37] reported that the DR representations of their experimental data from several activated carbon samples with methanol tested in the temperature range of 30-120°C at two different pressures yielded curves that are convex downwards but convex upwards for un-activated carbon/methanol. This implies that the DR model cannot yield adsorption data with reasonable accuracy for use in engineering system design. Critoph [38] also reported that some deviations from such linear plots occur in practice. Therefore, Dubinin and Astakhov [39] proposed another equation (DA).

3.3.6 The Dubinin-Astakhov equation

This theory [39] is based upon the concept of the temperature invariance of a characteristic curve, which can express the distribution of the degree of filling, θ , of the volume of the adsorption space versus A , the differential molar work of adsorption. The observation of temperature invariance follows experimental observations, originally noted by Polanyi, but with a different interpretation. The differential molar work of adsorption can be determined as a decrease in Gibbs' free energy ($A = -\Delta G$):

$$A = RT \ln \left(\frac{p_s}{p} \right) \quad (3-12)$$

where p_s is the pressure of the saturated vapour of the substance at temperature T , and p is the equilibrium pressure.

The characteristic curve equation of the theory can be represented as follows:

$$\theta = \exp(-kA^2) = \exp\left[-\left(\frac{A}{E}\right)^2\right] \quad (3-13)$$

An equivalent form of the equation above is:

$$\theta = \frac{x}{x_0} \quad (3-14)$$

where x is the adsorption rate at temperature T and equilibrium pressure p , while x_0 is the limiting adsorption rate corresponding to the filling of the whole volume of the adsorption space W_0 , or of the micro-pore volume. Terms k or E are parameters of the distribution function ($E = 1/\sqrt{k}$). The limiting adsorption rate x_0 depends on the temperature as a result of the thermal expansion of the substance adsorbed. The temperature changes of W_0 are neglected. Let ρ^* be the density of the substance adsorbed at a limiting micro filling [27], then:

$$x_0 = W_0 \rho^* \quad (3-15)$$

According to Dubinin and Nikolav [27], the term ρ^* is calculated to a good approximation from a set of the physical constants of the substance.

Later, Dubinin and Astakhov suggested a quasi-Gaussian distribution equation based on the theory of mini-pores filing, which is suitable for a distribution of the adsorption mini-pores size:

$$x = x_0 \exp\left(-\left(\frac{\varepsilon}{E}\right)^n\right) \quad (3-16)$$

This is called the D-A equation, in which there are three constants. Dubinin suggested that n can be an integer between 2 and 6, but actually, experimental results show that n can be even a decimal fraction between 2 and 6 [27]; E is the characteristic adsorption work determined by the energy properties of the adsorption system. This equation is simple but is only suitable for adsorbents with uniform surfaces and weak polar adsorbates.

3.3.7 Improved adsorption equation

There are several non-idealities in practice that influence the accuracy of the above theories, and merit further corrections [27].

(a) Consideration of the polarity of adsorbate

The common refrigerant adsorbates in adsorption refrigeration are methanol, water, and ammonia. The values of their polar moment are 1.7, 1.8 and 1.5 respectively [27]. So they are all strongly polar gases. Regarding the state equation of the polar gases, the Martin-Hou equation (M-H equation) is commonly used. The constants in the M-H equation can be determined easily, and can be allied over a wide range of condition. It has been shown that the relative error of the M-H equation is less than 1% if it is used for non-hydrocarbon gases, and it is more suited for the polar molecules such as water, methanol and ammonia et al. [27]. The M-H equation can be expressed as following:

$$p = \sum_{i=1}^5 \frac{f_i(T)}{(V-b)^i} = \frac{RT}{V-b} + \frac{A_2 + B_2T + C_2 \exp\left(-\frac{KT}{T_c}\right)}{(V-b)^2} + \frac{A_3 + B_3T + C_3 \exp\left(-\frac{KT}{T_c}\right)}{(V-b)^3} + \frac{A_4}{(V-b)^4} + \frac{A_5 + B_5T + C_5 \exp\left(-\frac{KT}{T_c}\right)}{(V-b)^5} \quad (3-17)$$

The constants in the equation are shown in the table below.

Table 3.2 Constants of M-H equation for various refrigerants [27, 28]

M-H constants	Methanol	Water	Ammonia
$A_2 \times 10^7$	-1.181884	-0.7347924	-0.51407794
$A_3 \times 10^9$	0.9823941	0.3367519	0.25238453
$A_4 \times 10^{10}$	-4.911565	-0.6221217	-0.71432305
$A_5 \times 10^{11}$	-10.96970	-0.9647009	-0.64790943
$B_2 \times 10^4$	0.9605366	0.4867358	0.47427270
$B_3 \times 10^8$	-5.55264	-2.162056	-1.1981187
$B_5 \times 10^8$	41.58169	2.432953	1.1981187
$b \times 10^2$	0.1265582	0.06601304	0.10464551
$C_2 \times 10^8$	-4.55933	-2.37388	-1.1226807
$C_3 \times 10^{10}$	5.609259	1.365615	0.79905689
$C_5 \times 10^{13}$	-8.947510	-0.4708418	-0.40828723
K	5.475	5.475	5.0

(b) Modification of the assumption of an idea gas

Wang and Wang [28] proposed improvements to the adsorption equations. They considered the real behaviour of vapour of the main refrigerants. Ammonia, Water and methanol vapours are not ideal gases, as a result the desorption rate was modified by

including the fugacity instead of the pressure. Then the real adsorption potential can be expressed as:

$$\varepsilon_r = RT \ln \left(\frac{f_1}{f_2} \right) \quad (3-18)$$

f_1 and f_2 are the fugacities that replace pressures P_1 and P_2 respectively. The authors considered the polarity of the refrigerant by introducing the M-H state equation of polar gases. And the distribution of the adsorption micro-pores was considered to be a Gaussian normal distribution. The expression is:

$$x = x_0 \exp \left(-RT \frac{\ln \left(\frac{f_1}{f_2} \right)}{E_x} \right)^{n_x} \quad (3-19)$$

Where E_i , n_i are two constants varied with different adsorption pairs and can be determined by fitting the experimental data [28].

(c) Considerations of non-uniform distribution of adsorption micro-pores

The modified D-R equation with fugacity is [27, 28]:

$$x = x_0 \exp \left(-k \left(\frac{\varepsilon}{\beta} \right)^2 \right) = x_0 \exp \left(-B \left(\frac{T^2}{\beta^2} \ln^2 \left(\frac{f_0}{f} \right) \right) \right) \quad (3-20)$$

Considering that most of the commonly used materials, such as activated carbon, and zeolite, have a heterogeneous collection of micro-pores, adsorption should be expressed in the form of a sum of contributions from different pore sizes,

$$x = \sum_j x_{0j} \exp \left(-k_j \left(\frac{\varepsilon_j}{\beta} \right)^2 \right) = \sum_j x_{0j} \exp \left(-B_j \left(\frac{T^2}{\beta^2} \ln^2 \left(\frac{f_0}{f} \right) \right) \right) \quad (3-21)$$

where $B_j = k_j R^2$, x_{0j} and B_j correspond to a given size of micro-pores. For the sake of mathematical convenience, the continuous distribution $f(B)$ for the adsorption concentration x_{0j} , and $x_{0j} = f(B_j)\delta B_j$ can be used. The sum is then replaced by the integral:

$$\int_0^{\infty} f(B)dB = 1 \quad (3-22)$$

For a given size of micro-pore characterized by B_j , the adsorption equation can be treated as $x_j = x(T, p, B_j)$. For an adsorption surface, the total adsorption capacity can be integrated with the characteristic adsorption of micro-pores multiplied by its distribution to get:

$$x = \int_0^{\infty} x(T, p, B)f(B)dB \quad (3-23)$$

Two groups of adsorption pores with different distributions are discussed.

- (1) Uniform distribution of pore sizes (examples are activated carbon fibre, carbon molecular sieve)

The pore size are limited to a small range $[B_1, B_2]$, so the pore distribution function can be assumed as a constant, $f(B) = \text{const}$ and $B_1 < B < B_2$, $\Delta B = B_2 - B_1 \rightarrow 0$. Therefore, we can get a distribution as:

$$f(B) = \frac{1}{B_2 - B_1} \quad (3-24)$$

Thus the total adsorption capacity can be expressed as:

$$x = \int_0^{\infty} \frac{1}{B_2 - B_1} x(T, p, B) dB \quad (3-25)$$

In the limit that the range of pore size is sufficiently narrow $\Delta B \rightarrow 0$, and so that

$x(T, p, B) = \text{const} = x_B$, ($B_1 < B < B_2$) in this range. The simple form obtained is [27, 28]:

$$x = x_i = x_{i0} \exp \left[- \left(\frac{RT \ln \left(\frac{f_0}{f} \right)}{E_i} \right)^{n_i} \right] \quad (3-26)$$

(2) Non-uniform distribution of pore sizes in adsorbent surface (examples are activated carbon, zeolite etc.)

The non-uniform pore adsorption can be treated as collection of pores of various sizes. The random distribution of pore sizes can usually be supposed as a Gaussian normal distribution with a half-width of Δ [27, 28, 40]:

$$f(B) = \frac{1}{\Delta \sqrt{2\pi}} \exp \left[- \frac{(B - B_0)^2}{2\Delta^2} \right] \quad (3-27)$$

where B_0 is a constant. In this equation, the characteristic pore size B is corresponding to

the adsorption capacity $x(T, p, B) = x_{B_0} \exp \left(-k \left(\frac{\varepsilon}{\beta} \right)^2 \right)$, therefore,

$$x = \int_0^{\infty} f(B) x_{B_0} \exp(-By) dB \quad (3-28)$$

where, $y = \left(\frac{T}{\beta} \right)^2 \ln^2 \left(\frac{f_0}{f} \right)$

Thus, the total adsorption concentration of the pores in the solid can be given by the normalized condition:

$$x_0 = \int_0^{\infty} f(B)x_{B_0} dB \quad (3-29)$$

From a mathematical point of view, the general expression $x = \int_0^{\infty} f(B)x_{B_0} \exp(-By)dB$ is an integral of a Laplace type equation with the D-R equation as ma core. This yields a Gaussian-based equation for the filling of the pores [40]:

$$x = x_0 \exp(-B_0y) \exp\left(\frac{y^2 \Delta^2}{2}\right) [1 - \text{erf}(z)]/2 \quad (3-30)$$

This is a modified equation, where $z = \left(y - \frac{B_0}{\Delta^2}\right) \frac{\Delta}{2}$, and $\text{erf}(z)$ is the error function.

This equation contains three parameters x_0, B_0 and Δ , which can be determined by adsorption experiments [41].

(d) Modified D-A equation

According to the theory of the Dubinin-Radushkevich [36], the volume V occupied by the adsorbate is related to the total pore volume V_0 and adsorption potential ε by the following relation:

$$V = V_0 \exp\left[-\left(\frac{B}{\beta^2}\right)\varepsilon^2\right] \quad (3-31)$$

where:

β - the affinity coefficient, taken a ratio of the adsorbate molar volume at the temperature T to that of a reference gas (normally benzene) at the same temperature

B - a function of the adsorbent microstructure

According to Polanyi's theory, the adsorption potential ε can be expressed as:

$$\varepsilon = RT \ln \frac{p_2(T)}{p_1(T_{sat})}$$

$$\text{Therefore, } V = V_0 \exp \left[- \left(\frac{B}{\beta^2} \right) \left(RT \ln \frac{p_2(T)}{p_1(T_{sat})} \right)^2 \right] \quad (3-32)$$

In addition, the correlation between temperature and pressure for saturated adsorbate can be represented for example by the Clausis-Clapeyron equation [42]:

$$\ln(p) = A - \frac{C}{T} \quad (3-33)$$

where, A and C depend on the adsorbate.

Substituting all this into D-R equation and introducing the density $\rho(T)$, the mass adsorbed $M(T, T_{sat})$ becomes:

$$M(T, T_{sat}) = M_0(T_{sat}) \exp \left[- \left(\frac{B}{\beta^2} \right) \left(RC \frac{T}{T_{sat}} - RC \right)^2 \right] \quad (3-34)$$

where $M_0(T_{sat}) = V_0(T_{sat})\rho(T_{sat})$ because $\rho(T)$ is constant as $\rho(T_{sat})$ around the surface of the adsorbent when $T = T_{sat}$

To allow a better fit to some adsorbent characteristics, an extension of the equation is introduced as in the following equation, which employs a variable index n instead of 2:

$$M(T, T_{sat}) = M_0(T_{sat}) \exp \left[- \left(\frac{B}{\beta^2} \right) \left(RC \frac{T}{T_{sat}} - RC \right)^n \right] \quad (3-35)$$

Introducing the mass ratio x of the adsorbed mass to the mass of adsorbent in this equation, and writing it in a simple form, the above equation becomes:

$$x(T, T_{sat}) = x_0(T_{sat}) \exp \left[- k \left(\frac{T}{T_{sat}} - 1 \right)^n \right] \quad (3-36)$$

where k represents value of $\left(\frac{B}{\beta^2} \right) (RC)^n$, which determined by the characteristics of both adsorbent and adsorbate and which is independent of temperature.

In summary, different equilibrium equation should be used according to different adsorption pairs. The equations mostly used by researchers to fit the experimental data are presented in Table 3-3.

Table 3-3 Equilibrium Equations for different adsorption pairs

Equilibrium equation	Adsorbent/adsorbate Pairs	References
$\ln(p) = a(w) + b(w)/T$	4A zeolite/water, 13X Zeolite/water, AC/Methanol	Caccicola[43,44], Hajji[44,46], Zhang[47,48,49]
Freundlich equation,	Silica gel/water	Cho[50], Saha[51], Chua[52]
D-R equation	Zeolite Nax/water, AC/ammonia, Zeolite Nax/ammonia	Meunier[53], Pon[54]
Modified D-R equation	AC/methanol, AC/ethanol, AC/ethane, AC/ammonia	Luo[55], Tim[56], Qi[57], Critoph[58, 59]

D-A equation	Zeolite/water, AC/ammonia,SO ₂ ,amine, methanol, methyl	Wang[28], Liobet[60], Critoph[38], Tatlier et al.[61]
Modified D-A equation	AC/ butane, R22, ammonia, methanol, Zeolite/water	Critoph[62], Tim[56] , Qu et al.[63], Chahbani [64], Anyanwu et al.[65]
Langmuir equation	Silica gel/water	Ng et al.[66]

3.4 Thermodynamic relationships

3.4.1 The Clausius-Clapeyron equation

The Clausius-Clapeyron equation provides the relationship between the enthalpy of vaporization and the pressure and the temperature of a material [41]. The derivation is well known and can be found in standard thermodynamics textbook (e.g. Rogers and Mayhew [41]), which is shown in the following:

The Gibbs free energy is defined as:

$$g = h - Ts \quad (3-37)$$

The definition of enthalpy is:

$$h = u + pV \quad (3-38)$$

Thus: $g = u + pV - Ts$

Differentiating the above equation gives:

$$dg = du + pdV + Vdp - Tds - sdT \quad (3-39)$$

From the first and second law of thermodynamics:

$$q = du + pdV = Tds \quad (3-40)$$

$$\text{so, } du + pdV - Tds = 0 \quad (3-41)$$

$$\text{Therefore, } dg = Vdp - sdT \quad (3-42)$$

With respect to the transition of a liquid phase to a gas phase where the gas phase is assumed to behave as an ideal gas, for an initial equilibrium condition between the gas phase and the liquid phase:

$$\Delta g = g_g - g_l \quad (3-44)$$

For an increase in system pressure and a corresponding increase in temperature to maintain equilibrium, gas and liquid phase equation can be expressed as following:

$$dg_g = V_g dp - s_g dT \quad (3-45)$$

$$dg_l = V_l dp - s_l dT \quad (3-46)$$

When the system in equilibrium state, $dg_g = dg_l$

$$\text{Therefore, } V_g dp - s_g dT = V_l dp - s_l dT \quad (3-47)$$

$$\text{That is to say, } \frac{dp}{dT} = \frac{s_g - s_l}{V_g - V_l} \quad (3-48)$$

The enthalpy of vaporization for an internally reversible isothermal process is:

$$h_v = h_g - h_l = T(s_g - s_l) \quad (3-49)$$

For an ideal gas (as assumed initially):

$$V_g = \frac{RT}{p} \quad (3-50)$$

Assuming that the liquid specific volume V_l is negligible compared to the gas specific volume V_g ($V_l \ll V_g$), so

$$\frac{dp}{dT} = \frac{h_v p}{RT^2} \quad (3-51)$$

This equation expresses the rate of change of equilibrium vapour pressure with equilibrium temperature, which may be rewritten as:

$$h_v = \frac{dp}{dT} \left(\frac{RT^2}{p} \right) \quad (3-52)$$

or, as the Clausius-Claypeyron equation:

$$\frac{d(\ln p)}{dT} = \frac{h_v}{RT^2} \quad (3-53)$$

3.4.2 Enthalpy of vaporisation

Assuming that at the phase between liquid and gas the equilibrium temperature is the saturation temperature, Clausius-Claypeyron equation becomes:

$$\frac{d(\ln p)}{dT_{sat}} = \frac{h_v}{RT_{sat}^2} \quad (3-54)$$

Integrating the above equation and assuming h_v is constant with saturation temperature gives:

$$\ln p = C - \frac{h_v}{RT_{sat}} \quad (3-55)$$

That means a plot of $\ln p$ against $-\frac{1}{T_{sat}}$ should be a straight line with gradient h_v / R .

Let A be the line gradient, thus

$$h_v = RA \quad (3-56)$$

3.4.3 Enthalpy of adsorption

The enthalpy of adsorption can be defined in the same way as the enthalpy of vaporization in the Clausius-Clapeyron equation [27]. For a constant concentration condition at the adsorbent-gas phase interface during a change in pressure and temperature:

$$h_{ads} = \left. \frac{dp}{dT} \right|_x \left(\frac{RT^2}{p} \right) \quad (3-57)$$

For a constant concentration ($x = const$), the T/T_{sat} term in the D-A equation is also constant and hence:

$$\left. \frac{dT_{sat}}{dT} \right|_x = \frac{T_{sat}}{T} \quad (3-58)$$

Therefore:

$$\left. \frac{dp}{dT} \right|_x = \frac{dp}{dT_{sat}} \frac{dT_{sat}}{dT} = \frac{dp}{dT_{sat}} \frac{T_{sat}}{T} \quad (3-59)$$

so,

$$h_{ads} = \frac{dp}{dT_{sat}} \left(\frac{RTT_{sat}}{p} \right) \quad (3-60)$$

According to Clausius-Clapeyron equation,

$$h_v = \frac{dp}{dT_{sat}} \left(\frac{RT_{sat}^2}{p} \right) \quad (3-61)$$

Rearranging the above equation to give dp/dT :

$$\frac{dp}{dT_{sat}} = \frac{h_v p}{RT_{sat}^2} \quad (3-62)$$

Substituting the above equation into $h_{ads} = \frac{dp}{dT_{sat}} \left(\frac{RTT_{sat}}{p} \right)$ gives the enthalpy of adsorption

in terms of enthalpy of vaporization, temperature and saturation temperature, thus:

$$h_{ads} = h_v \left(\frac{T}{T_{sat}} \right) \quad (3-63)$$

Substituting $h_v = RA$ into the above equation gives:

$$h_{ads} = RA \left(\frac{T}{T_{sat}} \right) \quad (3-64)$$

According to Clausius-Clapeyron equation:

$$\left. \frac{d(\ln p)}{dT_{sat}} \right|_x = \frac{h_{ads}}{RT^2} \quad (3-65)$$

Integrating this equation and assuming h_v is constant with temperature, and thus along an isostere ($x = const$), h_{ads} is also constant with temperature:

$$\ln p = C - \frac{h_{ads}}{RT} \quad (3-66)$$

This equation indicates that a plot of $\ln p$ against $-1/T$ should be a straight line with gradient h_{ads}/R .

3.5 Summary

The general theory relating to the research area has been discussed with particular emphasis on the principle of adsorption and the equilibrium equations that describe the adsorbent pore filling process. The thermodynamic relationships and equations relating to the enthalpy of vaporization and enthalpy of adsorption have also been derived. The theory and equations are discussed in this chapter

Reference

(The original source of reference [1-21, 30, 36] is reference [29])

- [1] C.W. Scheele, *Chemische Abhandlung von der Luft und dem Feuer*, 1773, see:
Ostwald's *Klassiker der exakten Wiss*, p.58, 1894
- [2] F. Fontana, *Mem. Mat. Fis. Soc, Ital.*, vol.1, p.679, 1777
- [3] T. Lowitz, *Crell's Chem. Ann.*, vol.1, p.211, 1786
- [4] T. Lowitz, *Crell's Chem. Ann.*, vol.2, p. 36, 1788
- [5] T. de Saussure, *Gilbert's Ann. Phys.*, vol.47, p.113, 1814
- [6] T. de Saussure, *Ann. Phil.*, vol.6, p.241, 1915
- [7] P. Chappuis, *Wied. Ann.*, vol.8, p.1, 1879
- [8] P. Chappuis, *Wied. Ann.*, vol.12, p.161, 1881
- [9] P. Chappuis, *Wied. Ann.*, vol.19, p.21, 1883
- [10] L. Joulian, *Ann. Chim. Phys.*, vol.22, p.398, 1881
- [11] H. Kayser, *Wied. Ann. Phys.*, vol.12, p.526, 1881
- [12] H. Kayser, *Wied. Ann. Phys.*, vol.14, p.450, 1881
- [13] C.M. Pouillet, *Ann. Chim. Phys.*, vol.20, p.141, 1882
- [14] C.G. Junck, *Pogg. Ann.*, vol.125, p.292, 1865
- [15] D. Fitzgerald, *Nature*, vol.49, p.293, 1894
- [16] S. Lagergren, *Kgl. Vetenskaps Akad.*, 24B, 1898
- [17] H. Gaudechon, *Compt. Rend.*, vol.157, p.207, 1913
- [18] J. Dewar, *Proc. R. Soc.*, vol.74, p.122, 1904
- [19] J. Dewar, *Proc. R. Soc.*, vol.74, p.127, 1904
- [20] J.W. McBain, *Phil. Mag.*, vol.18, p.916, 1909

- [21] M.S. Tswett, *Chromatographic Adsorption Analysis: Selected Works*, Ellis Horwood Ltd, 1903
- [22] S. Brunauer, *The adsorption of gases and vapour*, vol.1, Princeton University Press, 1945
- [23] V. Ponec, Z. Knor and S. Cerny, *Adsorption on solid*, Butterworths and Co., London, 1974
- [24] J. Oscik, *Adsorption*, Ellis Horwood Ltd./John Wiley and Sons, 1982
- [25] D.M. Ruthven, *Principles of adsorption and adsorption processes*, John Wiley and Sons, 1984
- [26] M. Suzuki, *Adsorption Engineering*, Elsevier Science Publishers, 1990
- [27] R.Z. Wang, *Adsorption refrigeration*, China Machine Press, 2002
- [28] R.Z. Wang, Q.B. Wang, *Adsorption mechanism and improvements of the adsorption equation for adsorption refrigeration pairs*, *International Journal of Energy Research*, vol.23, pp.887-898, 1999
- [29] C. Tien, *Adsorption calculations and modelling*, Butterworth-Heinemann, 1994
- [30] C. Boedecker, *J. Landw.*, vol.7, p.48, 1895
- [31] H. Freundlich, *Colloid and Capillary Chemistry*, Methuen, London, 1926
- [32] D.P. Valenzuela, A. L. Myers, *Adsorption equilibrium handbook*, Printice-Hall, Englewood Cliffs, NJ., 1989
- [33] S.B. Brunauer, P. Emmett, E. Teller, *Adsorption of gases in multimolecular layers*, *Journal of Am. Chem. Society*, vol.60, p.309, 1938
- [34] K.S.W. Sing, In: J.M. Fraissard, C.W. Conner, *Physical Adsorption: Experiment, Theory and Applications*, NATO ASI Series, Kluwer Academic Publ, Dordrecht, p.3, 1996
- [35] Z. Polanyi, *Electrochemistry*, vol.26, p.370, 1920

- [36] M.M. Dubinin, E.D. Zaverina, L.V. Radushkevich, *Zh.Fiz. Khim*, vol.21, p.1351, 1947
- [37] H. Jing, R. Exell, *Renew Energy*,3(6/7):567–575, 1993
- [38] R. E. Critoph, Performance limitations of adsorption cycles for solar cooling, *Journal of Solar Energy*, vol.41 (1), pp.21–31, 1988
- [39] M.M. Dubinin, V.A. Astakhov, Description of adsorption equilibria of vapours on zeolites over wide ranges of temperature and pressure, *Advances in Chemistry Series 102*, American Chemical Society, pp.69-85, Washington D.C., 1971
- [40] M.M. Dubinin, H. Stoeckli, Homogeneous and heterogeneous micropore structures in carbonaceous adsorbents, *J Colloid Interface Sci.*, vol.75, p.34, 1980
- [41] R.Z. Wang, Adsorption refrigeration in Shanghai Jiao Tong University, *Renewable and Sustainable Energy Review*, vol. 5(1), pp.1-37, 2000
- [42] G.F.C. Rogers, Y. Mayhew, *Engineering thermodynamics : work and heat transfer*, 4th edition, New York : Wiley, 1992
- [43] G. Cacciola, G. Restuccia, Reversible adsorption heat pump: a thermodynamic model, *International Journal of refrigeration*, vol.18 (2), pp.100–106, 1995
- [44] G. Cacciola, G. Restuccia, G. Benthem, Influence of the adsorber heat exchanger design on the performance of the heat pump system, *Applied Thermal Engineering*, vol.19, pp.255–269, 1999
- [45] A. Hajji, S. Khalloufi, Theoretical and experimental investigation of a constant-pressure adsorption process, *International Journal of Heat and Mass Transfer*, vol.38 (18), pp.3349–3358, 1995
- [46] A. Hajji, S. Khalloufi, Improving the performance of adsorption heat exchangers using a finned structure, *International Journal of Heat and Mass Transfer*, vol.39 (8), pp.1677–1686, 1996

- [47] L.Z. Zhang, L. Wang, Effects of coupled heat and mass transfers in adsorbent on the performance of a waste heat adsorption cooling unit, *Applied Thermal Engineering*, vol.19(2), pp.195–215, 1999
- [48] L.Z. Zhang, L. Wang, Momentum and heat transfer in the adsorbent of a waste-heat adsorption cooling system, *Energy*, vol.24, pp.605–624, 1999
- [49] L.Z. Zhang, A three-dimensional non-equilibrium model for an intermittent adsorption cooling system, *Solar Energy*, vol.69 (1), pp.27–35, 2000
- [50] S.H. Cho, J.N. Kim, Modeling of a silica gel/water adsorption cooling system. *Energy*, vol.17 (9), pp.829–839, 1992
- [51] B. Saha, E.C. Boelman, T. Kashiwagi, Computational analysis of an advanced adsorption-refrigeration cycle, *Energy*, vol.20 (10), pp.983–94, 1995
- [52] H.T. Chua HT, K.C. Ng, et al., Modeling the performance of two beds, silica gel-water adsorption chillers, *International Journal of Refrigeration* vol.22, pp.194–204, 1999
- [53] N. Ben Amar, L. Sun, F. Meunier, Numerical analysis of adsorptive temperature wave regenerative heat pump, *Applied Thermal Engineering*, vol.16 (5), pp.405–418, 1996
- [54] L. Sun, M. Pons, Numerical investigation of adsorptive heat pump system with thermal wave heat regeneration under uniform-pressure conditions, *International Journal of Heat and Mass Transfer*, vol.40 (2), pp.281–293, 1997
- [55] L. Luo, D. Tondeur, Transient thermal study of an adsorption refrigeration machine, *Adsorption*, vol.6, pp.93–104, 2000
- [56] S. J. Tim, E. M. David, Modified Dubinin–Radushkevich/Dubinin–Astakhov adsorption equations, *Journal of Colloid and Interface Science*, vol.252, pp.263–268, 2002

- [57] X.H. Ye, N. Qi, Y.Q. Ding, M. Douglas, Prediction of adsorption equilibrium using a modified D–R equation: pure organic compounds on BPL carbon, *Carbon*, vol.41, 681–686, 2003
- [58] R. E. Critoph, Forced convection adsorption cycles, *Applied Thermal Engineering*, vol.18, pp.255–269, 1998
- [59] R.E. Critoph, Forced convection adsorption cycle with packed bed heat regeneration, *International Journal of Refrigeration*, vol.23 (4), pp.260–268, 2000
- [60] J. Liobet, V. Geotz, Rotary system for the continuous production of cold by solid-gas sorption: modeling and analysis of energy performance, *International Journal of Refrigeration*, vol.23, pp.609–625, 2000
- [61] A. Erdem-Senatalar, M. Tatlier, The relationship of the geometric factor in the Dubinin-Astakhov equation with the fractal dimension, *Colloids and Surfaces*, vol.173, pp.51-59, 2000
- [62] Z. Tamainot, R.E. Critoph, Monolithic carbon for sorption refrigeration and heat pump applications, *Applied Thermal Engineering*, vol.21 (1), pp.37-52, 2001
- [63] T. Qu, R.Z. Wang, W. Wang, Study on heat and mass recovery in adsorption refrigeration cycles, *Applied Thermal Engineering*, vol.21(1), pp.439-452, 2001
- [64] M.H. Chahbani, J. Labidi, J. Paris, Effect of mass transfer kinetics on the performance of adsorptive heat pump systems, *Applied Thermal Engineering*, vol.22 (1), pp.23–40, 2002
- [65] E.E. Anyanwu, U.U. Oteh, N.V. Ogueke, Simulation of a solid adsorption solar refrigerator using activated carbon/methanol adsorbent/refrigerant pair, *Energy Conversion and Management*, vol.42, pp.899-915, 2001

[66] K.C. Ng, H.T. Chua, C.Y. Chung, et al., Experimental investigation of the silica gel-water adsorption: isothermal characteristics, *Applied Thermal Engineering*, vol.21 (16), pp.1631-1642, 2001

Chapter 4 Assessment of New Pairs Based on Equilibrium Data

4.1 Introduction

In recent times, the adsorption pair mostly used included ammonia-carbon [1, 2, 3], ammonia-salts [4, 5], methanol-carbon [6, 7], water-silica gel [8, 9] and water-zeolite [10, 11]. One of the most important elements of any refrigeration and heat pump system is the sorption properties of working pairs. Generally speaking, the refrigerant requirements are high latent heat per unit volume and good thermal stability. The refrigerants tested here include ammonia and carbon dioxide. As mentioned before, ammonia has high latent heat and good thermal stability, while CO₂ is one of the few natural refrigerants, which is neither flammable nor toxic. The property of adsorbents is also very important. A suitable adsorbent should have a large adsorption capacity for the selected adsorbate and be easily regenerated regarding the pressure and temperature ranges of operation. Briefly, the adsorption characteristics of adsorbents are determined from the adsorption isotherms.

This chapter focuses on experimental studies on the equilibrium properties of several adsorption pairs. The adsorbents here are including carbon, zeolite, alumina, 3C (Calcium Chloride impregnated into Carbon matrix), SWS (Selected Water Sorbent) and a compound material of BaCl₂ impregnated into vermiculite. The adsorbates tested here are NH₃ and CO₂. The isotherms are the inputs in the prediction of COP. These properties are the basic elements to the performance of adsorption systems.

4.2 Properties of adsorbates and adsorbents

Adsorbates

The refrigerants chosen in the experiments are CO₂ and ammonia. As we know, CO₂ is one of the few natural refrigerants, which is neither flammable nor toxic. It is inexpensive, widely available and does not affect the global environment as many other refrigerants. CO₂ has a GWP=1 (global warming potential, the GWP of HFC is 1000-3000), but the net global warming impact when used as a technical gas is zero, since the gas is a waste product from industrial production. Therefore, CO₂ may be an excellent alternative among the natural refrigerants, especially in applications where the toxicity and flammability of ammonia and hydrocarbons may be a problem. The promising applications of CO₂ refrigeration systems include automotive air conditioning, heat pumps, residential/commercial air conditioning and various refrigeration areas [12, 13].

Ammonia is widely used in adsorption system. The advantages include high enthalpy of vaporisation, stability, wide temperature range and low freezing temperature.

Unfortunately, just as mentioned by Critoph[14], it has draw backs in use such as odour, corrosion and safety risks due to high operating pressure and flammability in certain concentrations. Additionally, the use of ammonia is forbidden or restricted in countries such as Japan while being widely used in countries such the UK and USA. After a process of elimination, Critoph [14] mentioned that ammonia would appear to offer the best high

pressure characteristics. Due to its benefits, ammonia will also be chosen as refrigerant in the experiments.

Adsorbents

There are a number of different adsorbents available. The choice depends on factors such as porosity, permeability, conductivity, heat capacity, compatibility, availability and cost.

There are three main types of solid-gas sorption systems depending on the type of solid adsorbent chosen. They may be classified as systems using physical adsorbents such as active carbon or zeolite, those using chemical compounds which undergo a chemical reaction such as calcium chloride and those based on the dissolution of hydrogen in metal hydrides [15]. Alternatively they may utilise a complex composite adsorbent consisting of a mixture of physical and chemical adsorbents with the inclusion of heat transfer enhancing structure. The adsorbent chosen in the experiments are active carbon, SWS, 3C and compound material of BaCl_2 impregnated into vermiculite.

Among the practical solids used in industries, activated carbon is one of the most complex solids but it is the most versatile because of its extremely high surface area and micro-pore volume. The structure of activated carbon is complex and it is basically composed of an amorphous structure and graphite-like microcrystalline structure. Typical characteristics of activated carbon are listed below.

Table 4-1 Typical characteristics of activated carbon [16]

Density	2.2 g/cm ³
Total porosity	0.71
Macro-pore porosity	0.31
Micro-pore porosity	0.40
Macro-pore volume	0.47 cm ³ /g
Micro-pore volume	0.44 cm ³ /g
Specific surface area	1200 m ² /g
Mean macropore radius	800
Mean micropore half width	1-2 m

Macro-pores having a size range of greater than 100nm are normally not filled with adsorbate by capillary condensation. The volume of macro-pore is usually in the order of 0.2-0.5 cm³/g and the area contributed by the macro-pore is usually very small, of the order of 0.5 m²/g, which is negligible, compared to the area contributed by the micro-pore. They are of no significance in terms of adsorption capacity but they act as transport pores to allow adsorbate molecules to diffuse from the bulk into the particle interior.

Meso-pores have a size range from 2 nm to 100nm, and are readily filled during the region of capillary condensation $\left(\frac{P}{P_0} \geq 0.3\right)$. The volume of meso-pore is usually in the range of 0.1 to 0.4 cm³/g and the surface area is in the range of 10-100 m²/g. Meso-pore contributes marginally to the capacity at low pressure and significantly in the region of capillary condensation. Like macro-pores, meso-pores act as transport pore when capillary

condensation is absent and they act as conduit for condensate flow in the capillary condensation region.

Micro-pores are pores having size less than 2 nm. These pores are slit-shaped and because of their high dispersive force acting on adsorbate molecule they provide space for storing most of adsorbed molecules and the mechanism of adsorption is via the process of volume filling.

The chemical nature of the surface of activated carbon is more complex than the pore network. This property depends on many factors, for example the source of carbon as well as the way the carbon is activated. Activated carbon is made from raw materials which are usually rich in oxygen and therefore many functional groups on activated carbon have oxygen atoms. Moreover, oxygen also is introduced during the course of preparation, for example coal activation by air or gasified by water vapour. The functional groups of an activated carbon can be increased by treating it with some oxidizing agents or decreased by exposing it to a vacuum environment at very high temperature.

Recently a family of new composite sorbents has been developed for multiple applications that include thermal energy storage, adsorption heat pump etc. These materials, so called hybrid material, are two-phase systems which consist of a porous host matrix with open pores and a metallic salt impregnated into its pores. Due to their physical structure the materials take an intermediate position between solid adsorbents and pure metallic salts

and can be organized in a way to demonstrate the best features of both systems. A large variety of host matrices (such as silica gel, alumina, active carbon, vermiculite, etc.) and salts (CaCl_2 , LiBr , CoCl_2 , BaCl_2 , etc) are expected to give many possibilities to controllably change the sorbent properties in a wide range to fit the demands of a particular application [17].

In the study of Kato [18], Calcium oxide/carbon dioxide is used as adsorbent in a packed bed reactor. Results showed that the reactor was capable of storing heat at 900°C by de-carbonation of calcium carbonate and generating up to 997°C by carbonation of calcium oxide. The amount of stored heat in the reactor was 800–900 kJ/kg [18]. Researches also show that the addition of a porous matrix in the chemical adsorbent could improve the adsorption performance. Five different compounds, pure MnCl_2 , a simple mixture of ex-PAN T300 carbon fibres and MnCl_2 (mixture 1), simple mixture of ex-pitch FT700 carbon fibres and MnCl_2 (mixture 2), impregnated ex-pitch FT500 carbon fibres with MnCl_2 (ICF) and intercalation of MnCl_2 into ex-pitch graphitized carbon fibres P120 (GFIC), are studied by Dellerio [22, 23]. The best of all kinetic results are obtained with GFIC and IFC. These two compounds not only provide a very fast reaction but also give a complete reaction by avoiding the agglomeration phenomenon [22, 23].

Calcium chloride is one of the most popular materials used in recent chemical heat pumps. Upon the absorption of ammonia, powdered anhydrous calcium chloride may expand three to four times its original volume, and may subsequently disintegrate into a white powder.

In order to restrict the swelling and disintegration, the absorbent is treated with a cementitious material and prepared as hard porous granules which can withstand multiple cycling of the absorption/generation processes. The performance of CaCl_2 confined to a meso-porous host matrix MCM-41 has been studied by Tokarev [19, 20, and 21]. Results show that the composite material based on CaCl_2 as an impregnated salt and MCM-41 as a host matrix is able to absorb up to 0.75 g of H_2O /g of dry sorbent [21]. That high absorptivity can ensure high values of the energy storage capacity of 2.1kJ/g [21]. Iloeje has also controlled the problem of agglomeration of CaCl_2 by setting 20% CaSO_4 in the adsorbent [24]. A transient experiments and analysis of heat and mass transfer in a CaCl_2 - NH_3 solar powered solid absorption refrigerator has also been undertaken [25, 26]. And simulation was also done by Iloeje [24, 27]. The results show that the host matrices can improve the thermal conductivity of adsorbents effectively.

Wang [28] studied two types of compound adsorbent, granular adsorbent and solidified compound adsorbent, in which CaCl_2 are impregnated into active carbon, for the performance of adsorption on ammonia. The results show that the performance of solidified compound adsorbent is much more stable than that of granular compound adsorbent. This compound material is studied on the adsorption refrigeration performances under two different working conditions, an ice-maker for a fishing boat driven by the waste heat from exhaust gases, and solar ice-maker driven by solar water heating. The obtained average SCP (specific cooling power) and the COP (coefficient of performance) of the refrigerator were measured to be 770.4 W/kg and 0.39 at about -20°C of evaporating

temperature for the former working condition, and they were 161.2 W/kg and 0.12 at about $-15\text{ }^{\circ}\text{C}$ of evaporating temperature for the later working condition [29].

More recently, pseudo-equilibrium hysteresis behaviour (equilibrium lines were a function of solid concentration) was observed between the synthesis reaction and the decomposition reaction for CoCl_2 and ammonia [30]. The widths of the hysteresis loops were found to be a function of heating rate. Extrapolation of the experimental data suggests that the hysteresis might be eliminated entirely by maintaining the temperature for extremely long times. Nevertheless, in all circumstances it appears that the conversion of the salt would be a function of temperature [30]. The experimentally measured bi-variant behaviour was contrary to mono-variant behaviour which had been anticipated and has been discussed in the literature [30]. Hysteresis loops are also observed by Marty [31] for $\text{MnCl}_2 - \text{NH}_3$ system.

These materials have higher sorption capacity in comparison with non-impregnated matrices and better kinetics than the bulk salt. However, the salt swelling due to its reaction with ammonia could destruct the structure of matrix [28, 29], so the choice of a proper host matrix is important from practical point of view. In [46] it was found that one promising inorganic host matrix could be expanded vermiculite, in which the pore volume reaches $3.2\text{cm}^3/\text{g}$. It allows the inserting inside the pores a large amount of salt and reaching the ammonia uptake of 68.5 wt. % (for composite “63.5 wt % CaCl_2 /vermiculite”) [6]. One more very important advantage of vermiculite, which results from its large pore volume, is

that it can efficiently accommodate the salt swelling due to its reaction with ammonia.

In summary, it is necessary to do some precise equilibrium experiments on hybrid material because of the inconsistent information provided from previous literature studies. The materials used here are '3C' (CaCl₂ impregnated into active carbon 208C), SWS (CaCl₂ impregnated into alumina matrix), and a composite material made by BaCl₂ and Vermiculite. These materials are very popular in chemical adsorption system due to the large adsorption of NH₃.

4.3 Experimental apparatus for determining equilibrium adsorption properties

The experimental apparatus is shown in figure 4-1. The simplified schematic flow diagram of the experimental rig is shown in figure 4-3. The adsorbent sample is contained in a small basket, which is suspended inside the sealed steel chamber (shown in figure 4-2).

The chamber is covered by a jacket, which is connected by an oil circulator and control the temperature of the chamber. Four thermocouples within the chamber are used to measure the adsorbent temperature and the wall temperature to ensure the equilibrium state. When a new temperature is selected, readings are only taken when the temperature varieties measured by the four thermocouples are within 0.5 °C for a period of at least 30 minutes.

The system pressure was measured directly with a calibrated Druck PDCR 920 transducer.

The mass of the sample in the basket is measured by Rubotherm magnetic suspension balance. The adsorbate concentration is calculated by the mass change of the sample during the experiment.

Before the tests, adsorbents were dried at 180 °C for at least 10 hours in the air at atmospheric pressure to make sure the water vapour was eliminated from the sample.

During this procedure, the system was kept vacuuming and the sample mass was measured every half an hour. The measurement showed that the sample mass would not change after around 2 hours. After all the vapour was driven out of the system and the test rig was vacuumed, the ammonia was introduced into the system. The sample was then cooled to a setting temperature to start equilibrium test. In these series of test, the experimental sample

(contained in a stainless steel basket) was exposed to pure refrigerants. The system pressure was the saturated pressure of ammonia at the saturated temperature controlled by the water bath, which is shown in figure 4-3. During the experiments, the temperature ranged from 30 to 150°C and the pressure within the steel chamber was from 5 to 20 bar. The following is the detail about system instruments used during the tests.

Thermocouples

In order to monitor system temperatures, four stainless steel sheathed *K* type thermocouples with the diameter of 1.5 mm supplied by TC Ltd were attached to the experimental rig (figure 4-3). The temperature accuracy of the thermocouples was $\pm 0.5^\circ\text{C}$.

Pressure transducers and gauges

Druck PDCR 920 absolute pressure transducers with a 0-35bar range, a resolution of 0.35 bar mV^{-1} and an accuracy of $\pm 1.5\%$ were applied to monitor the pressure.

Data acquisition and control

One Strawberry Tree DATAshuttle (DA-16-8-TC-AO) was employed to acquire the data from thermocouples, pressure transducers. The stated accuracy of the DATAshuttles is

± 0.3 °C on temperature and $\pm 25 \mu\text{V} \pm 0.05\%$ of reading on voltage. The control process and data logging was performed utilising the dedicated WorkBench software running on a standard 486 / Windows98 PC operating in conjunction with the Datashuttles. All of the experimental data was logged at one second intervals (sampling frequency of 1 Hz per channel) and written to local hard-disk for processing and analysis at a later stage.

Figure 4-1 Experimental apparatus for equilibrium tests

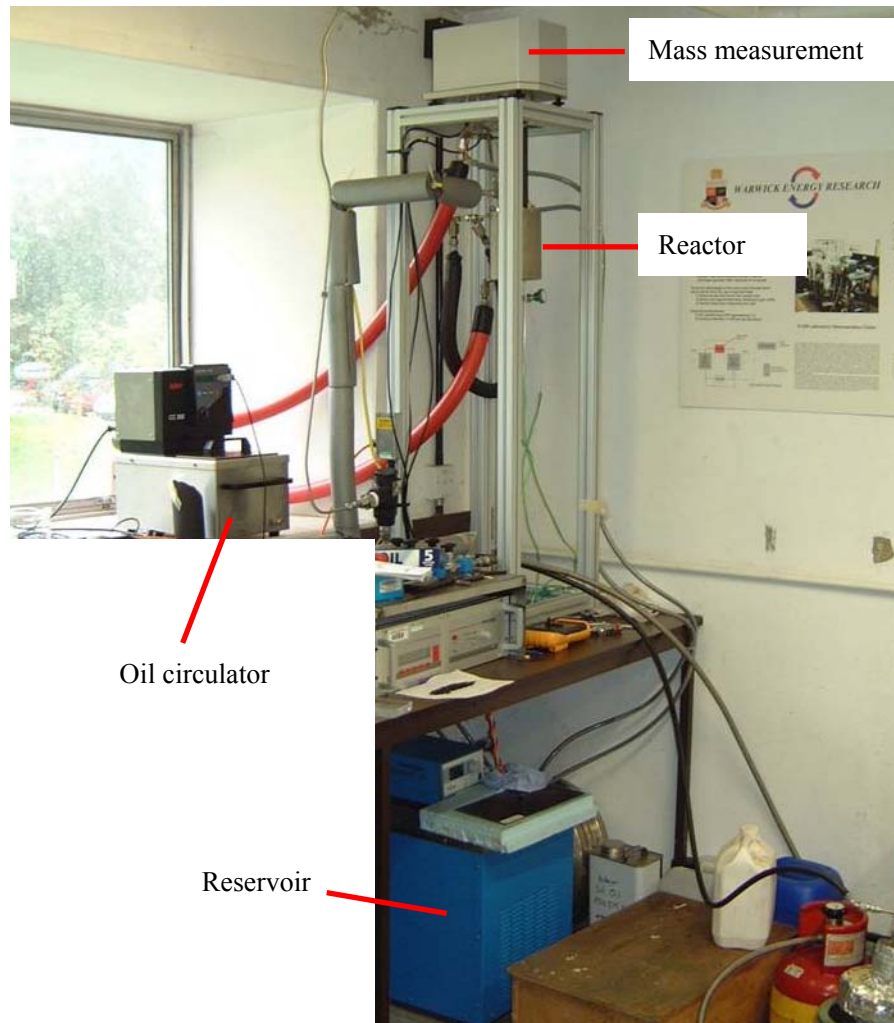


Figure 4-2 Container and the sample

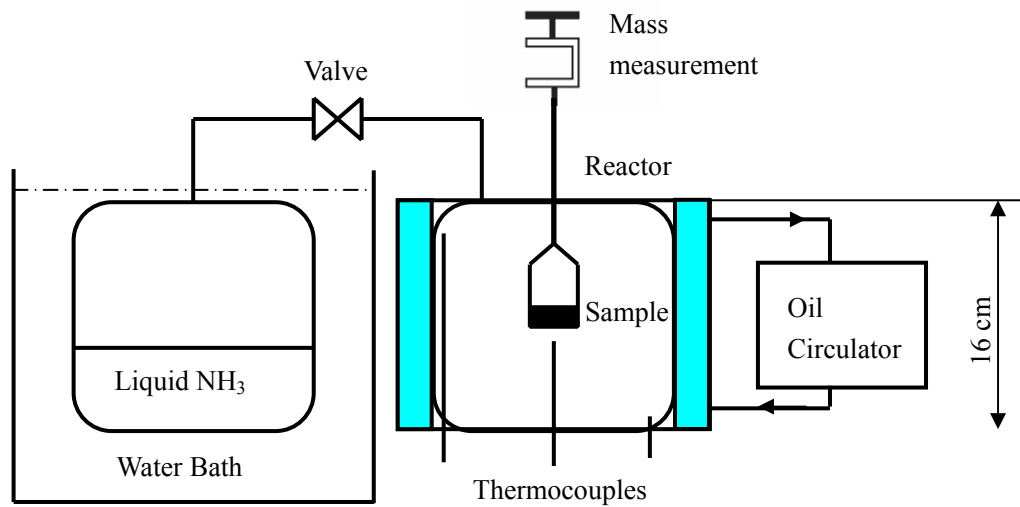
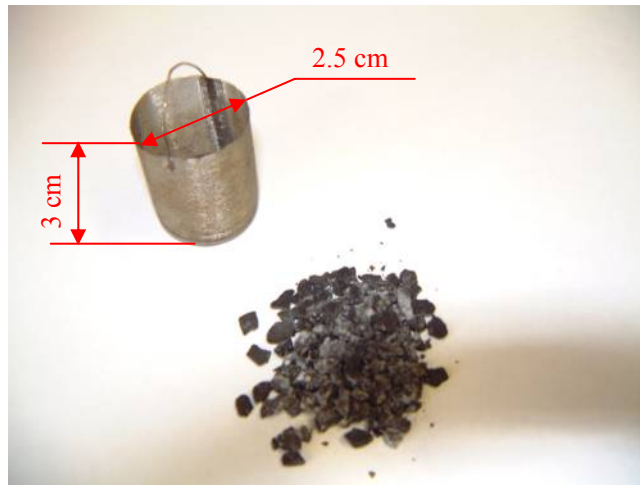
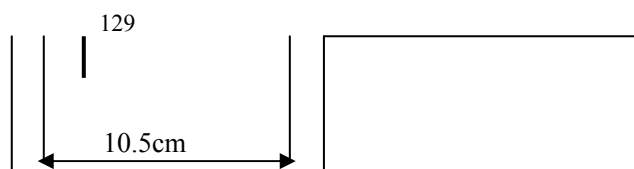


Figure 4-3 Schematic flow diagram of porosity test rig

Mass measurement

A Rubotherm magnetic suspension balance is used to measure the mass of sample in the



basket. The resolution of the equipment is 0.01 mg and the uncertainty less than 0.002%.

The standard deviation of successive measurement is less than ± 0.03 mg.

Before the experiments, the magnetic suspension balance needs to be calibrated. During calibration, the span of balance is adjusted to the changes in ambient conditions. The balance has an internal system for the changing of the calibration weights, which is internally applied by servomotor [50]. Only in zero-point the calibration can be activated. During the calibration, the deviation of the current read out from the target weight is indicated on the screen after the display has stabilised. And we can press the TARE-key to zero the weight display [50].

4.4 Test with CO₂ as refrigerant

As mentioned before, CO₂ is one of the few natural refrigerants, which is neither flammable nor toxic. So CO₂ may be an excellent alternative among the natural refrigerants, especially in applications where the toxicity and flammability of ammonia and hydrocarbons may be a problem.

Three types of different adsorbents were tested. The first was activated carbon, which included Sutcliffe Speakman 208C, NORIT A5798, NORIT 2030 and NORIT RB1. 208C is coconut-shell-based gas adsorption carbon which is very cheap and generally used in our laboratories. The other two kinds of adsorbent are silica gel, which included MD263 and HPV silica, and zeolite, which included zeolite 3A, 4A, 13X and NA-Y. All these adsorbents selected in our porosity experiments are widely used in the recent research on adsorption refrigeration systems [32]. The experimental data on the porosity character of Sutcliffe Speakman 208C is acquired using the new apparatus mentioned above. The other data was obtained previously using a different porosity test rig described in the paper written by Critoph [33].

All the experimental data were fitted to a modified Dubinin-Astakhov equation:

$$x = x_0 \exp \left[-K \left(\frac{T}{T_{sat}} - 1 \right)^n \right] \quad (4-1)$$

where x_0 , K and n are constants for the pair; T_{sat} is the saturation temperature in K; T is the adsorbent temperature in K.

A program written in MATLAB was used to find the values of x_0 , K and n , which minimize the sum of the squares of the differences in concentration predicted by the equation and the measured (Appendix A). The results and the standard estimate of error (SEE) are given in Table 4-2.

Table 4-2 Porosity test results

Adsorbent	Refrigerant	limiting concentration, x_0	K	n	SEE
208C carbon	carbon dioxide	0.3242	2.5135	1.1602	0.0087
NORIT A5798 carbon	carbon dioxide	0.5049	3.5318	1.7473	0.0037
NORIT 2030 carbon	carbon dioxide	0.5929	2.2717	0.7331	0.0109
NORIT RB1 carbon	carbon dioxide	0.5184	2.9064	1.3221	0.0025
MD263 silica	carbon dioxide	0.6591	4.281	0.7887	0.0016
HPV silica	carbon dioxide	0.6257	3.5887	0.3752	0.0025
zeolite 13X	carbon dioxide	0.2741	1.9792	4.3149	0.0074
zeolite 3A	carbon dioxide	0.2139	0.8503	1.8918	0.0048
zeolite 4A	carbon dioxide	0.2754	0.6865	0.4754	0.0043
zeolite NA-Y	carbon dioxide	0.5553	0.7826	0.2054	0.009

The data given in Table 4-2 implies that the carbon dioxide can be well adsorbed by most of the practical adsorbent. And to research on the performance of adsorption system using CO₂ as refrigerant, complete cycle analyse was carried out.

The method used to calculate the heating required and cooling produced follows

Meunier[34] and Critoph and Turner[35]. The concentration is obtained by the use of equation (4-1) and the effective specific heat (dQ/dT) along an isostere is given by:

$$\frac{dQ}{dT} = c_{pc}(T) + xc_{pa} \quad (4-2)$$

c_{pc} is the adsorbent specific heat. In the absence of complete information, the value obtained by Turner [36] for 208C as a function of temperature (K) has been used for all four carbons:

$$c_{pc} = 174 + 2.245T \text{ (J/kg)} \quad (4-3)$$

The value 921 J/kg [37] has been used for all types of silica and the value 836 J/kg [38] has been used for all types of zeolite.

Here, c_{pa} is the adsorbate specific heat. It is commonly assumed similar to the specific heat of the liquid phase at the same temperature [39], but this assumption breaks down at higher than critical temperatures. It could also be argued that c_v is more appropriate than c_p along an isostere [40]. In this work a constant value of 2986 J/kg is taken for carbon dioxide.

During desorption the effective specific heat is given by

$$\frac{dQ}{dT} = c_{pc}(T) + xc_{pa} - H \left(\frac{\partial x}{\partial T} \right)_p \quad (4-4)$$

where H is the heat of desorption, given by

$$H = R(p,T)A \frac{T}{T_{sat}} \quad (4-5)$$

R is the gas constant and A is the slope of the saturated adsorbate line on the Clapeyron diagram; T_{sat} is the saturation temperature corresponding to the system pressure (Figure 4-4, 4-5 and 4-6). In these figures, the isostere lines are produced by the Matlab command ‘contour’ (Appendix B) and the points labelled with ‘+’ are the experimental data.

Figure 4-4 Clapeyron diagram for 208C carbon and carbon dioxide

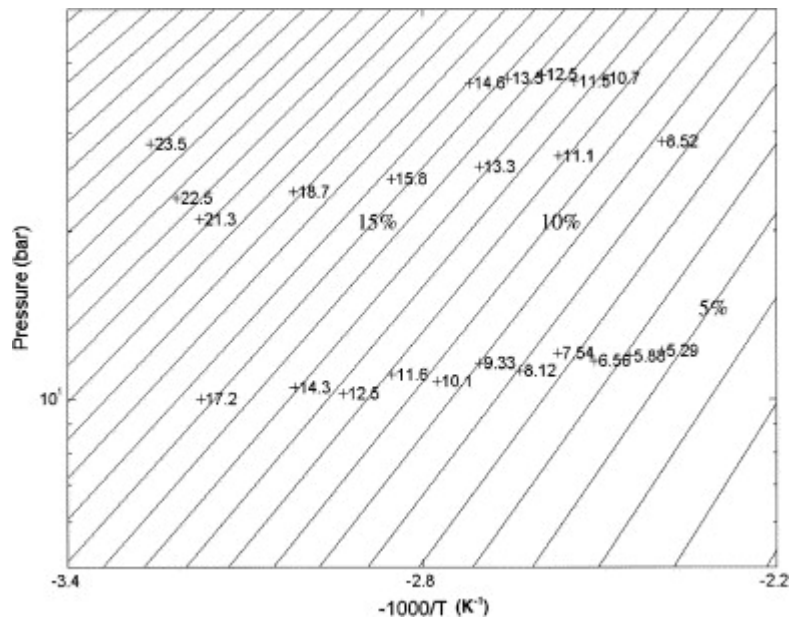


Figure 4-5 Clapeyron diagram for MD263 silica gel and carbon dioxide

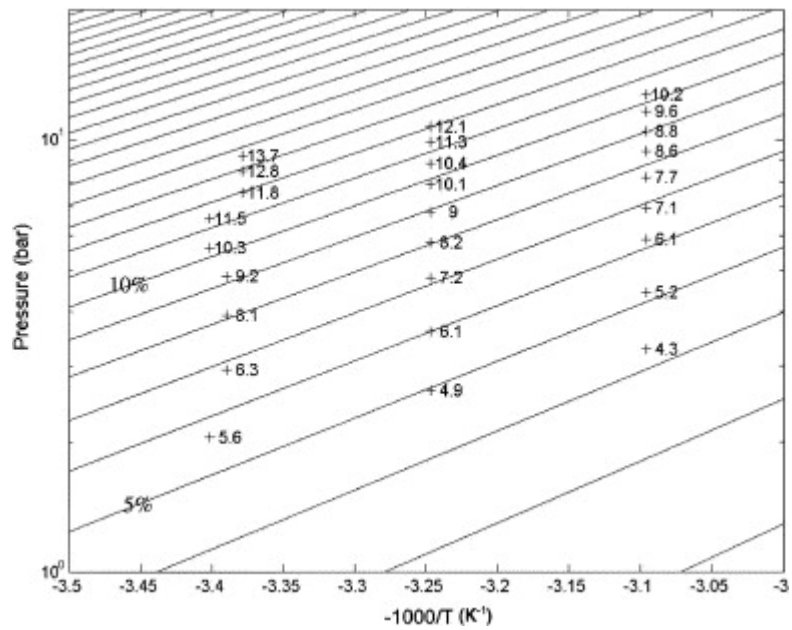
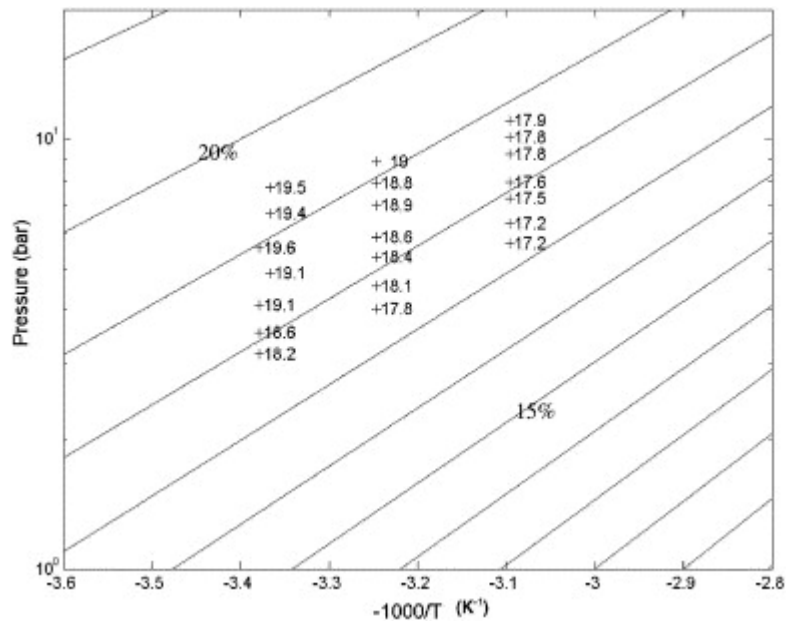


Figure 4-6 Clapeyron diagram for zeolite 3A and carbon dioxide



The effective specific heat is calculated every 1K change in temperature during both the heating and cooling phases. The total heating or cooling load of a bed is simply the integral

of the above equations, actually taken as the sum of the value of effective specific heat calculated every degree. The cooling and the heat rejected in the condenser are evaluated by considering the mass of refrigerant desorbed and then adsorbed per unit mass of adsorbent during every cycle. The net concentration change is $x_{conc} - x_{dil}$. The obtained from it is:

$$Q_c = (x_{conc} - x_{dil})(h_{gasev} - h_{liquidcon}) \quad (4-6)$$

where x_{conc} = maximum concentration; x_{dil} = minimum concentration; h_{gasev} = specific enthalpy of gas leaving the evaporator (kJ/kg) and $h_{liquidcon}$ = specific enthalpy of the condensed liquid (kJ/kg).

The condensing temperature used was 30 °C, which was a little below the critical temperature. The cycle COP is calculated for both a basic (one-bed) cycle and two-bed cycle in which some of the heat of adsorption can be pre-heat the desorbing bed. The assumption is made that the two beds can exchange heat until there is a 10K temperature difference between two beds. A Matlab program is used to modelling the process (Appendix C), and the results are illustrated in figures 4-7 to 4-9, discussed below.

In figures 4-7 – 4-9, the area under the upper curves gives the heat input between any two temperatures and the area under the lower (negative) curves gives the heat rejected. The discontinuities are the changes from isosteric heating to isobaric or vice versa. The quantity of heat that can be transferred from one bed to another, assuming an approach temperature of 10K is also be shown.

Figure 4-7 Cycle heat load for 208C and carbon dioxide with -5°C evaporating and 200°C generating temperatures

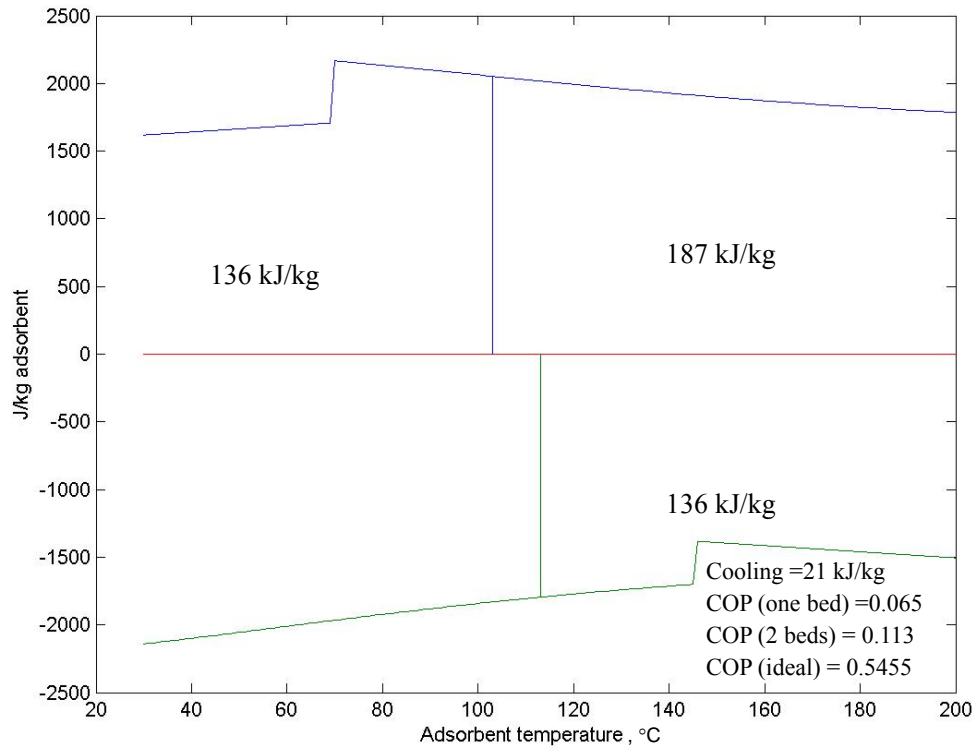


Figure 4-8 Cycle heat load for MD263 and carbon dioxide with -5°C evaporating and 200°C generating temperatures

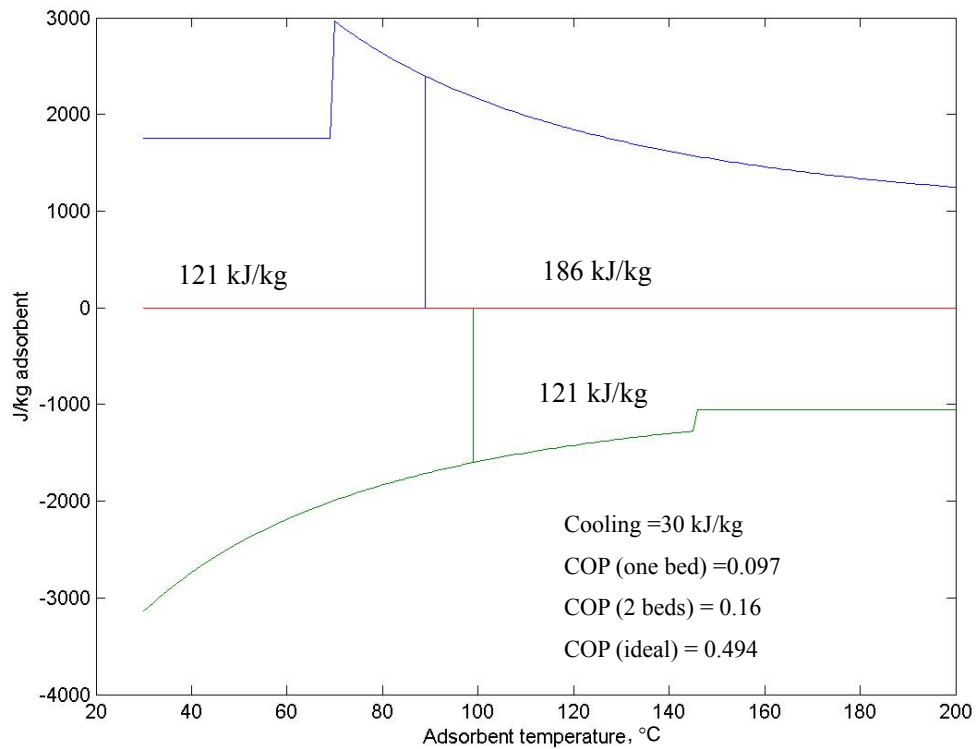
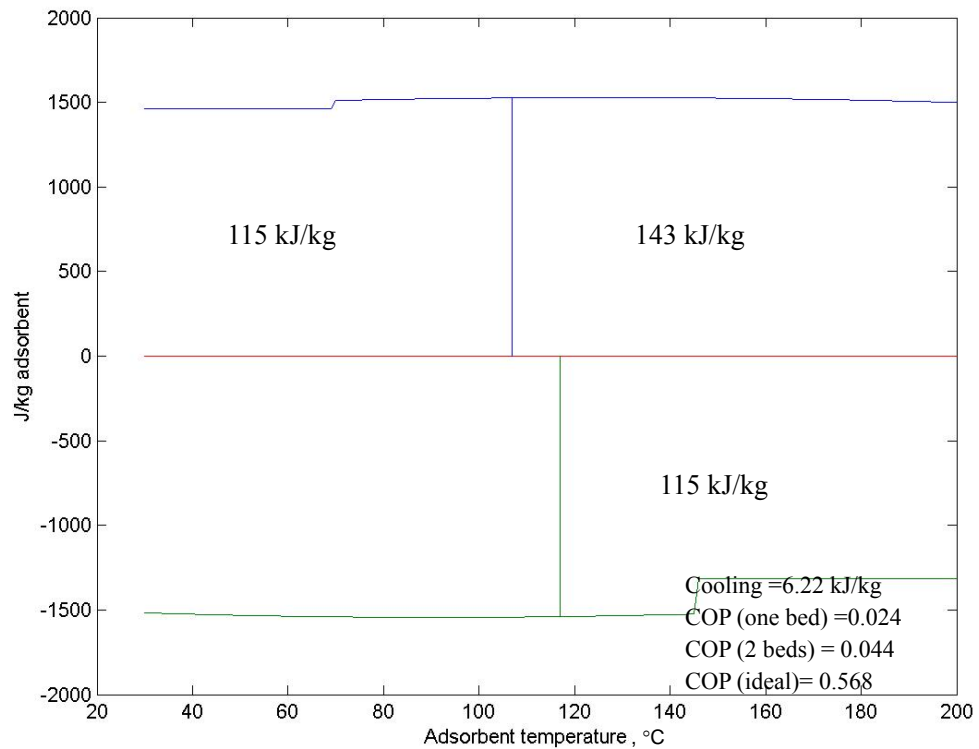


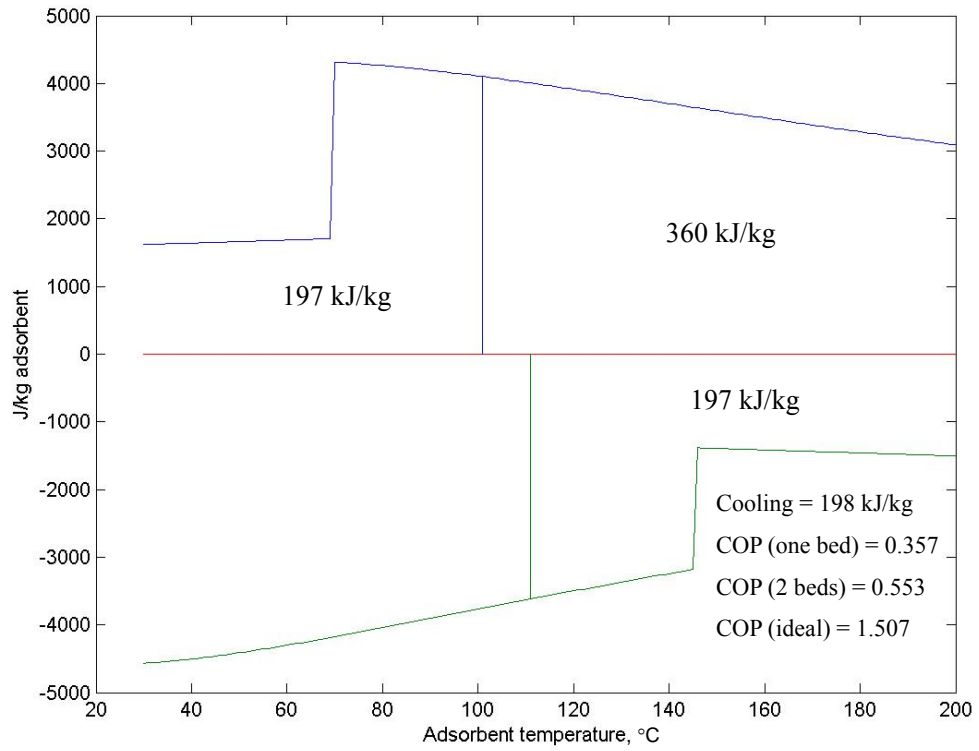
Figure 4-9 Cycle heat load for zeolite 3A and carbon dioxide with -5°C evaporating and 200°C generating temperatures



These figures illustrate that the cycle COPs of these adsorption systems are very low, since the greater concentration swings are negated by the lower latent heat of CO₂. To verify this opinion, artificially set the latent heat of CO₂ to be the same as ammonia (which is about 6 times that of CO₂). The result is shown in figure 4-10, which indicated much higher COP.

These results illustrate that the cycle COPs of these adsorption systems are very low, since the greater concentration swings are negated by the lower latent heat of CO₂. If there are applications where COP is not of primary importance, but toxicity and the ability to use copper is valued, then CO₂ may be useful, but CO₂ is not considered as refrigerant in the following work.

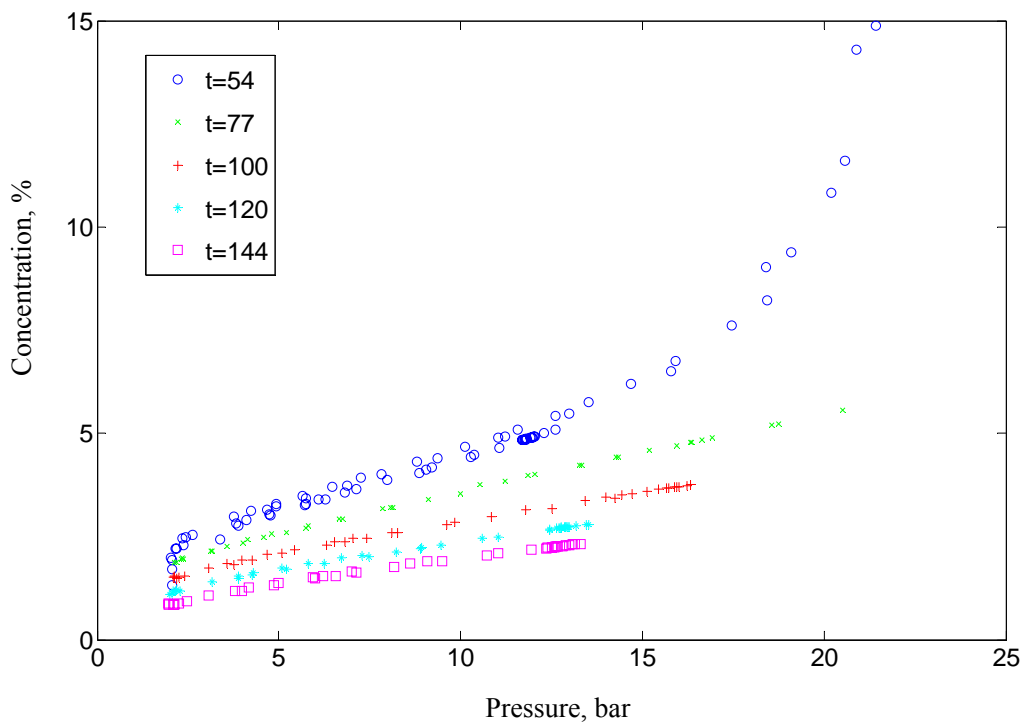
Figure 4-10 Cycle heat load for 208C and carbon dioxide with -5°C evaporating and 200°C generating temperatures (the latent heat of CO₂ has been artificially changed)



4.5 Alumina – NH₃

Equilibrium experiments on alumina and NH₃ are operated at the adsorbent temperature of 54 (blue open circles), 77 (green 'x' points), 100 (red '+' points), 120 (cyan '*' points) and 144°C (magenta open squares), which is shown in figure 4-11. These experiments have been performed, not with the intention of using alumina alone as adsorbent, but in order to interpret results of composite adsorbents that use alumina as the host matrix. The result is used to compare with a hybrid material, which is made by meso-porous alumina with impregnated CaCl₂ into it.

Figure 4-11 Concentration of equilibrium experimental data against saturated temperature



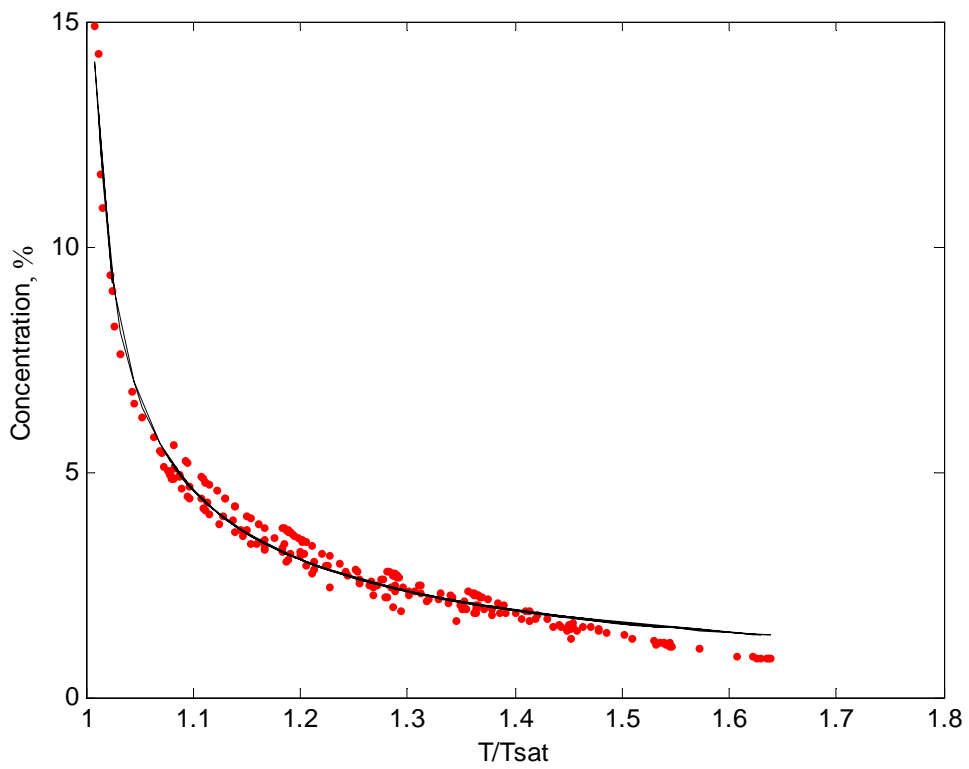
The modified Dubinin-Astakhov equation, equation (4-1), is used to fit the experimental

data. The result is,

$$x = 0.3102 \exp \left[-4.42 \left(\frac{T}{T_{sat}} - 1 \right)^{1.1775} \right] \quad (4-7)$$

The comparison between experimental data and the fit calculated by equation (4-7) is shown in figure 4-12.

Figure 4-12 Comparison between experimental data o and calculation from D-A equation



4.6 Metallic salt compounds in host matrices

4.6.1 BaCl₂ - Vermiculite

BaCl₂ impregnated with vermiculate developed by the Boreskov Institute of Catalysis (Novosibirsk, Russia) was investigated to obtain its equilibrium characteristics. This compound material was prepared by the immersion of the matrix with an aqueous solution of BaCl₂ followed by its drying at 200°C for 5 hours [48]. Unlike many other metallic salt compounds, the chemical reaction between BaCl₂ and NH₃ is quite simple. There are only BaCl₂ → BaCl₂ · 8NH₃ (0/8) adsorption and BaCl₂ · 8NH₃ → BaCl₂ (8/0) desorption.

The equation for the synthesis and decomposition reactions between BaCl₂ and NH₃ is,



Both the decomposition and synthesis temperatures of the ammonia – calcium chloride complex can be determined from the van't Hoff equation, equation (4-9), for the equilibrium of a solid gas reaction [30, 31].

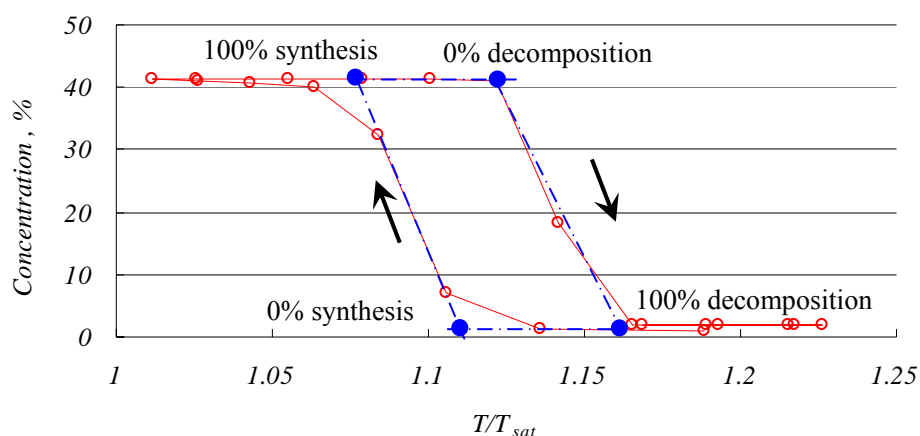
$$\ln p_{\text{NH}_3} = -\frac{\Delta h_R}{RT} + \frac{\Delta s}{R} \quad (4-9)$$

where, Δh_R is the standard enthalpy of reaction, R the molar gas constant, T the temperature, and Δs the standard entropy of the system.

A typical cycle (isothermal adsorption and desorption) which is represented by the open circles in figure 4-13 includes both the synthesis reaction at around 37°C which occurred

when the saturated temperature was increased from -1°C and the decomposition reaction at around 37°C which occurred when the pressure was decreased, thereby decrease the saturation temperature by 3.5K . The arrows show the direction in which the experimental measurements were performed. From figure 4-13, we can see a hysteresis loop was formed.

Figure 4-13 Concentration against T/T_{sat} at around 37°C



Another isothermal hysteresis loop measured at around 43.5°C is shown in figure 4-14. By comparing Figure 4-13 and 4-14, it is seen that as the adsorbent temperature increased, the saturated temperatures for both decomposition and synthesis also increased. This is consistent with the van't Hoff Equation. Hysteresis loops like those in figure 4-13 and 4-14 were observed at other adsorbent temperatures. The circles and squares in figure 4-14 represent the first and second times that the hysteresis loop was repeated. This illustrates that the hysteresis loops can be reproduced. From figure 4-14 and 4-15, it showed that for a specific adsorbent temperature, the reaction of synthesis and decomposition occurred in a range of saturated temperature. In other words, the non-vertical hysteresis loop would

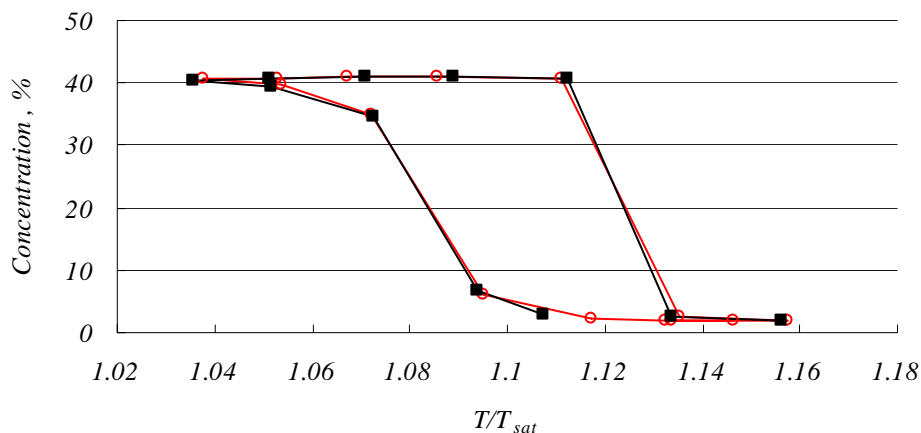
require both temperature and pressure to be specified in order to determine the state of the system. The preceding discussion of the phase rule, van't Hoff equation, suggested the system should be mono-variant. However, our experimental data show that it is definitely bi-variant, not mono-variant.

The concentration change after synthesis is complete in figure 4-13 and 4-14 is 0.4 kg NH₃/kg sample. From the equation applied to describe the sorption process,



The sample consists of 58.7% BaCl₂ and 41.3% vermiculite. That is to say, for 1kg sample, there is 0.587kg BaCl₂ and the adsorbed NH₃ is 0.4 kg. Assume vermiculite does not adsorb NH₃. So $n = \frac{(0.4/17)}{(0.587/207)} = 8.3$, which is a little greater than 8. The decimal fraction, 0.3, may contribute to the adsorption of vermiculate or the experimental error. This result shows that the synthesis and decomposition in figure 4-13 and 4-14 correspond to the 0/8 adsorption and 8/0 desorption.

Figure 4-14 Change of concentration against T/T_{sat} at around 43.5°C



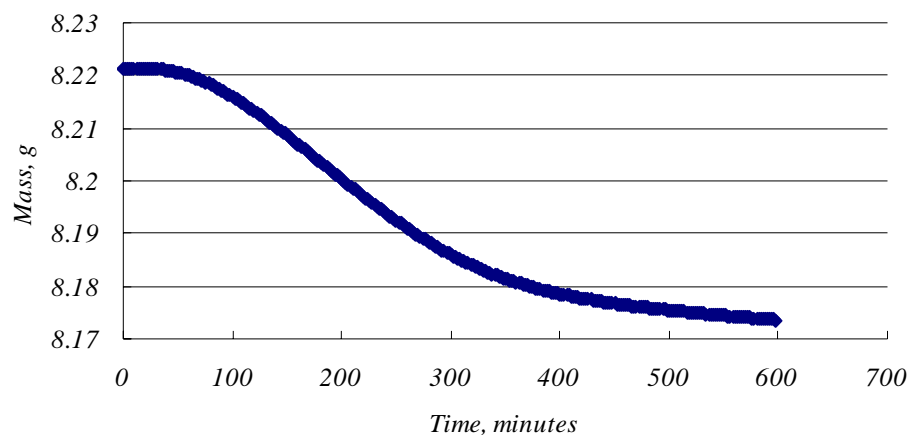
There are at several possible explanations for the hysteresis loop. One explanation is that hysteresis is related to the expansion and contraction of the crystal lattice as the ammonia content in the $\text{BaCl}_2 - \text{NH}_3$ complex changes. The hysteresis loops are somewhat reminiscent of the pore filling - pore emptying phenomena that occur during physical adsorption [41], and these have been ascribed to dimensional changes of the solid [42]. The hysteresis phenomena shown in figure 4-13 and 4-14 may be associated with the expansion of the BaCl_2 salt when the synthesis reaction occurs and the contraction of the $\text{BaCl}_2 \cdot 8\text{NH}_3$ salt when decomposition occurs. The unit cell dimensions increase as the crystal density changes. Hysteresis may be caused by solid phase changes, in which different solid phases have different crystal structures. An activation barrier is necessary to expand the solid, while the work of expansion is not recovered on contraction [30, 31]. The hysteresis area is a measure of the irreversible energy loss during a complete adsorption-desorption cycle [43].

A second explanation for hysteresis is that the measured gas-phase temperature could be

somewhat different to the temperature within the interior of the salt particle. The exothermicity of the synthesis reaction and endothermicity of the decomposition reaction could cause such a temperature difference. In this situation, the solid temperature, T_S , would lag the gas temperature, T_G . In other words, $T_S < T_G$ during decomposition, and $T_S > T_G$ during synthesis. If the temperature lag, $\Delta T = |T_S - T_G|$, increased, then the width of the hysteresis loop would increase.

The time required to approach equilibrium after the saturated temperature had been decreased from -17 to -20°C, and held constant at -20°C for around 10h, is shown in figure 4-15. Initially, the rate of mass gain was rapid but then decreased to a much slower value. After a long time (8 hours) the change of the mass still occurred at a steady rate (1.17 mg/h). The slow rate of reaction is probably caused by the small chemical driving force, $\Delta p = |p_G - p_S|$, where p_G is the ammonia pressure in the gas phase and p_S is the ammonia vapour pressure of the solid at the existing conditions (temperature, extent of solid conversion), given by van't Hoff equation. By definition, the chemical driving force for the reaction at constant temperature becomes small when the gas-phase pressure approaches the solid ammonia vapour pressure. As equilibrium is approached, Δp becomes smaller and the reaction rate becomes slower. If the time to obtain equilibrium state at constant temperature had been extended beyond 10 h to much longer (100 or 1000 h), perhaps real equilibrium may have eventually been attained.

Figure 4-15 Change in mass against time (min) when the saturation temperature was changed from -17 to -20°C at an adsorbent temperature of 22 °C

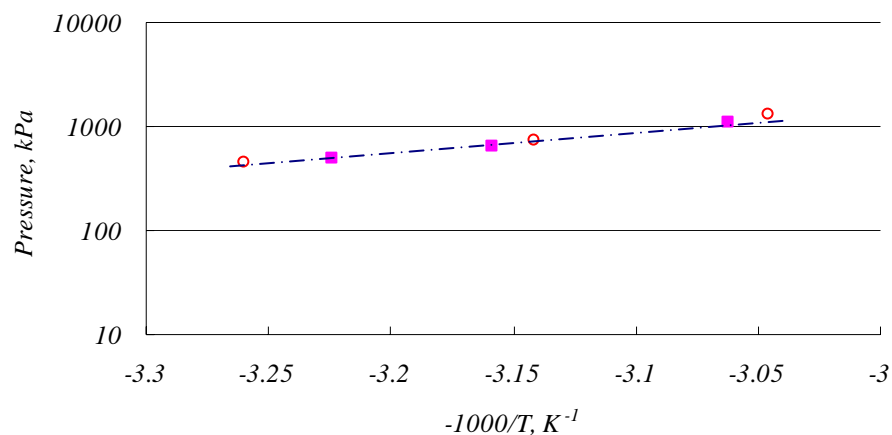


Although the previous suggestion that hysteresis may be caused by a temperature lag between the solid and the gas may be valid for short equilibrium time, it is unlikely to be valid when the temperature is held constant for several hours. The data in figure 4-15 indicate that after 4 hours the reaction rate has become slow, which means that the heat generation rate would also be slow. It also means that little departure from thermal equilibrium would be expected. Therefore, in this case, it is unlikely that temperature lag could be the cause of hysteresis [30]. However, explaining hysteresis in terms of dimensional changes to the lattice would still be a valid possibility [30].

For each hysteresis loop, obtained at a specific adsorbent temperature, four data points were selected, the onset of synthesis (0% synthesis), the termination of synthesis (100% synthesis), the onset of decomposition (0% decomposition), and the termination of decomposition (100% decomposition), which is shown in figure 4-13.

The data for 0% synthesis (open circles) and 0% decomposition (solid squares) are shown in figure 4-16. The 0% synthesis point represents the first molecule of ammonia that reacts with the salt during the synthesis reaction. Similarly the 0% decomposition point represents the first molecule of ammonia that is produced during the decomposition reaction. The position of the starting points for synthesis and decomposition is very important to the equilibrium and dynamics of adsorption pair. These points should not be influenced by either heat transfer or mass transfer because in these cases, there is no heat and mass transfer at all [30]. Also since both 0% synthesis and 0% decomposition are on the same line, one can assume that the same micro-crystallites of the salt are involved in sorbing the first molecule of ammonia during the synthesis reaction and releasing the first molecule of ammonia during the decomposition reaction.

Figure 4-16 Logarithm of ammonia pressure (kPa) vs negative inverse temperature (-1000/K) for 0% synthesis and 0% decomposition



The position of the onset points for synthesis and decomposition, which referred to as a transition line, is very important to determine the equilibrium and dynamical characteristics

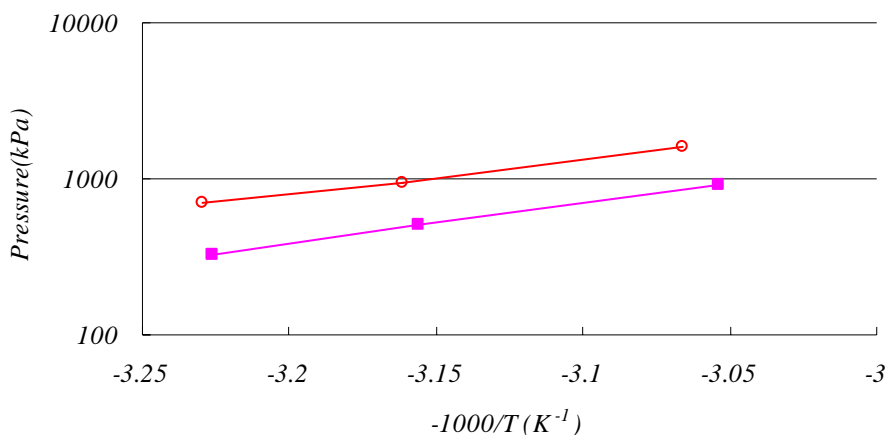
of the adsorption pair. At a specific adsorbent temperature, adsorption happens when the system pressure is greater than onset pressure of synthesis and desorption happens when the system pressure is less than onset pressure of decomposition. The transition line shown in figure 4-16 is equating,

$$\ln p_{NH_3} = 4.9767 \frac{-1000}{T} + 22.257 \quad (4-11)$$

where, T is the temperature of reaction bed.

The data for 100% synthesis (open circle) and 100% decomposition (solid square) are shown in figure 4-17. These data points represent the conditions at which the last molecule reacted during our experiments. The line for 100% synthesis has a slightly smaller slope, which according to equation (4-9), means that $\Delta h_{dec} > \Delta h_{syn}$, where, Δh_{dec} , is the endothermic energy required to break the bonds between the ammonia and the salt. While Δh_{syn} is the exothermic energy released when the ammonia - salt bonds are formed minus the endothermic energy required to expand the lattice of the salt. The smaller slope for 100% synthesis suggests that during decomposition, only the endothermic energy to break the ammonia - salt bond must be supplied instantaneously and the salt can relax to its former dimensions slowly. Therefore, this exothermic relaxation energy may not be available, and it may not contribute to the Δh_{dec} value. A synthesis line having a smaller slope than the decomposition line was also observed by Marty [31] for the $MnCl_2 - NH_3$ system and Ternana [30] for the $CoCl_2 - NH_3$ system.

Figure 4-17 Logarithm of ammonia pressure (kPa) vs negative inverse temperature (-1000/K) for 100% synthesis and 100% decomposition



As discussed by Aristov etc. [48], according to the Gibbs phase rule the number of degrees of freedom ν for the system with k components, f phases and r linearly independent reactions could be calculated as $\nu = k + 2 - f - r$ [30]. This system consists of three components ($BaCl_2$, NH_3 and $BaCl_2 \cdot 8NH_3$) in three phases ($[BaCl_2]_{sol}$, $[NH_3]_{gas}$ and $[BaCl_2 \cdot 8NH_3]_{sol}$). Therefore, the examined system is mono-variant ($\nu = 3 + 2 - 3 - 1 = 1$). That is to say, the same van't Hoff correlation of pressure and temperature will be valid for both synthesis and decomposition reactions. The separate equilibrium lines for synthesis and decomposition observed in figure 4-18 show a departure from what would be expected. There is a slope to both branches of all the hysteresis loops shown in Figure 4-14 and 4-15, in other words, the hysteresis is not vertical for either synthesis or decomposition, even for the hysteresis loop composed of the data points obtained by maintaining a constant temperature for 5 - 8 h. This is a strong indication that both synthesis and decomposition reactions occurred over a range of saturated temperatures. It also means that both temperature and pressure would be required to determine the state of the system.

So the system is bi-variant, rather than mono-variant. It means the examined system is not consistent with what would be predicted by Gibbs phase rule. This inconsistency is also observed in recent studies with other systems [30, 31]. One reason could be the formation of complexes $BaCl_2 \cdot nNH_3$ with variable n , which would add more degrees of freedom for this system. Such complexes are known for bulk crystalline hydrates of barium oxalate [47], but, as to our knowledge, such complexes have not been detected [48]. A more reasonable explanation is that micro crystallites of the confined salt are not homogeneous due to various sizes of these crystallites inside the pores. Each particular micro crystallite crystal undergoes a mono-variant 0/8 synthesis or 8/0 decomposition at its own temperature (pressure) determined by the van't Hoff equation. Thus, the system behaves as bi-variant due to the mentioned non-uniform micro crystallite crystal.

The van't Hoff equation can also be used to describe the termination of synthesis and decomposition,

For 100% synthesis,

$$\ln p_{NH_3} = 5.10 \times \frac{-1000}{T} + 23.05 \quad (4-12)$$

For 100% decomposition,

$$\ln p_{NH_3} = 5.90 \times \frac{-1000}{T} + 24.85 \quad (4-13)$$

The slope of 100% synthesis and decomposition are both larger than those obtained for 0% synthesis and 0% decomposition, that indicates higher activation barrier and stronger reformation of salt structure for micro crystals responsible for sorbing the last NH_3

molecule during the synthesis reaction and releasing the last molecule of ammonia during the decomposition step.

Assuming the transition between 0 and 100% of synthesis and decomposition is linear with the concentration, the equation to describe the processes of synthesis and decomposition can be obtained by combining equations (4-11), (4-12) and (4-13),

For synthesis,

$$\ln p_{NH_3} = (4.98 + 0.3x) \times \frac{-1000}{T} + 22.26 + 2x \quad (4-14)$$

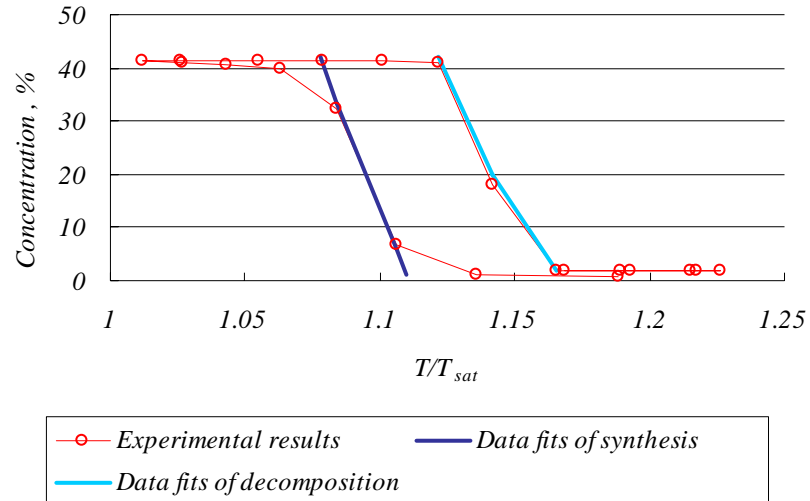
For decomposition,

$$\ln p_{NH_3} = (5.9 - 2.3x) \times \frac{-1000}{T} + 24.85 - 6.5x \quad (4-15)$$

where, x is the concentration of the adsorbent (from 0 to 0.4). These equations provide a relationship between temperature, pressure and concentration (T , p , and x). The state of the hysteresis loop can be determined by specifying two of these variables.

Figure 4-18 shows the comparison between the experimental data and data fits of equation (4-14) and (4-15). The results show that the data fits are consistent with experimental data. That is to say, equations (4-14) and (4-15) can be used to describe the processes of synthesis and decomposition.

Figure 4-18 Comparison between experimental results and data fits of synthesis and decomposition processes at the adsorbent temperature of 37°C



In a real chemical heat pump, the temperature will be changed at a substantial rate to provide a reasonably large chemical driving force, which means non-equilibrium statement and hysteresis loops. In practice, the equation (4-11) is of more practical significance for the design of a chemical heat pump using the $\text{NH}_3 - \text{BaCl}_2$ system. And it can be used to predict the onset of the phase change.

4.6.2 Carbon and Calcium Chloride – NH₃

'3C' (Carbon and Calcium Chloride) refers to a composite made in the University of Warwick consisting of Calcium Chloride impregnated in a carbon matrix. The carbon is granular, reflecting the form of its precursor material (coconut husk) with a typical grain dimension of 3mm. The loading of CaCl₂ on the 3C is 12.3% by weight. The 3C material was prepared by soaking dried active carbon with a saturated solution of calcium chloride in methanol at ambient temperature and atmospheric pressure for 17 hours. The composite was then heated to 150 °C and dried under vacuum [49]. After the methanol was removed from the sample, the mass of composite was measured and CaCl₂ content was deduced [49].

The essential difference between this material and the BaCl₂ – vermiculite material mentioned in part 4.6.1 is that the carbon host material is highly micro-porous, so that both physical adsorption with the carbon and chemical adsorption with the CaCl₂ are both significant.

In order to test the adsorption performance under equilibrium conditions, repeated experiments were performed with the temperature of adsorbent at 104, 115, 126, 143, 153, 160, 168, 177, 186, 194, 202, 211, 220 and 229°C, the saturation temperature of the reservoir within the temperature range -15 to 45°C. Results are shown in figure 4-19 and 4-20, where t is the temperature of the adsorbent bed (°C) and x is the concentration of

adsorbent (kg/kg). The arrows show the direction in which the experimental measurements were performed. Hysteresis loops were observed when the temperatures of adsorbent were above 200°C. But for the temperature of adsorbent between 100 and 200°C, the data points collapse to approximate a single curve with the saturated temperature ranging between -15 and 45°C when concentration is plotted against saturated temperature.

The adsorption quantity of CaCl₂ in experimental sample for hysteresis loops is computed by the adsorption quantity of compound adsorbent and a Matlab program to calculate the concentration of activated carbon, which is provided by professor Critoph and attached in Appendix D. Then the adsorption quantity of CaCl₂ in experimental sample is,

$$x = \frac{m_c \times x_c - m_a \times x_a}{m_c - m_a} \quad (4-16)$$

where x (kg/kg) is the adsorption quantity of CaCl₂ in test sample, m_c (kg) is the mass of compound adsorbent, x_c (kg/kg) is the adsorption quantity of compound adsorbent, m_a (kg) is the mass of active carbon, x_a (kg/kg) is the adsorption quantity of active carbon. The calculated results of isothermal condition are shown in figure 4-21. The black arrows show the direction in which the experimental measurements were performed. It is seen that as the adsorbent temperature increased, the saturated temperatures for both decomposition and synthesis transition also increased.

Figure 4-19 Concentration of 3C against saturated temperature when the temperatures of adsorbent are between 100 and 200°C

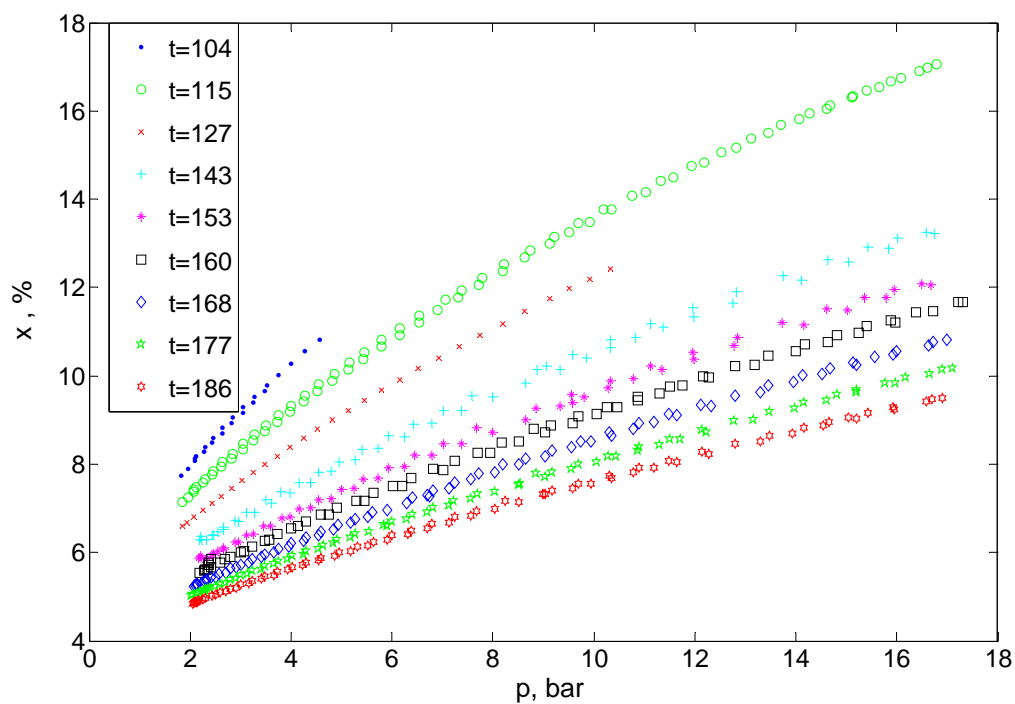


Figure 4-20 Concentration of 3C against saturated temperature when the temperatures of adsorbent are above 200°C

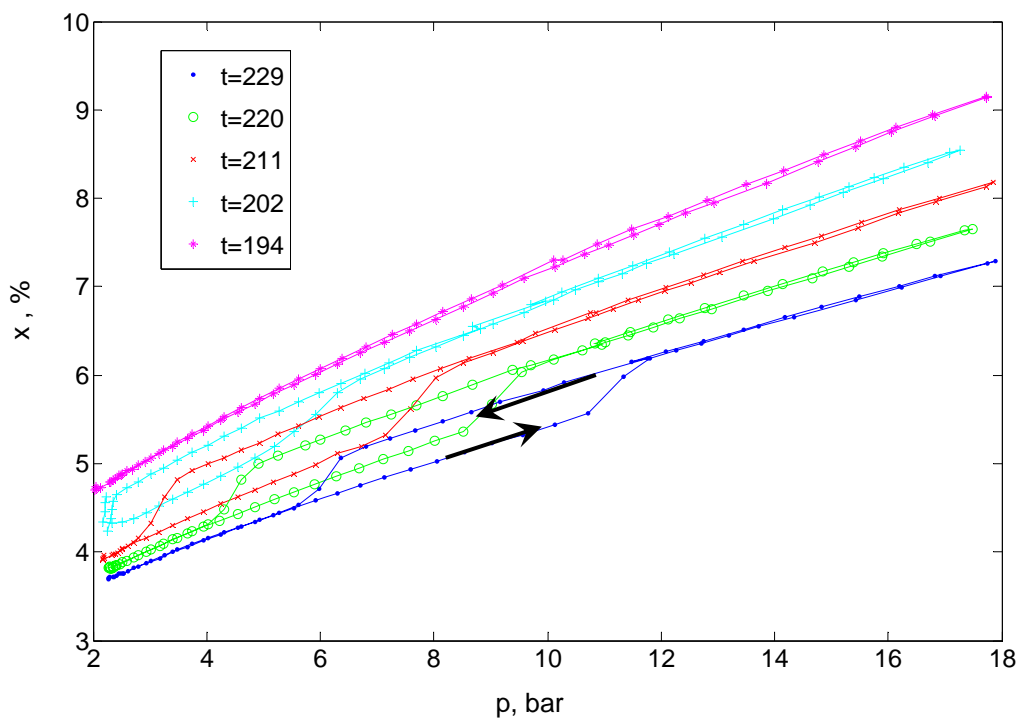
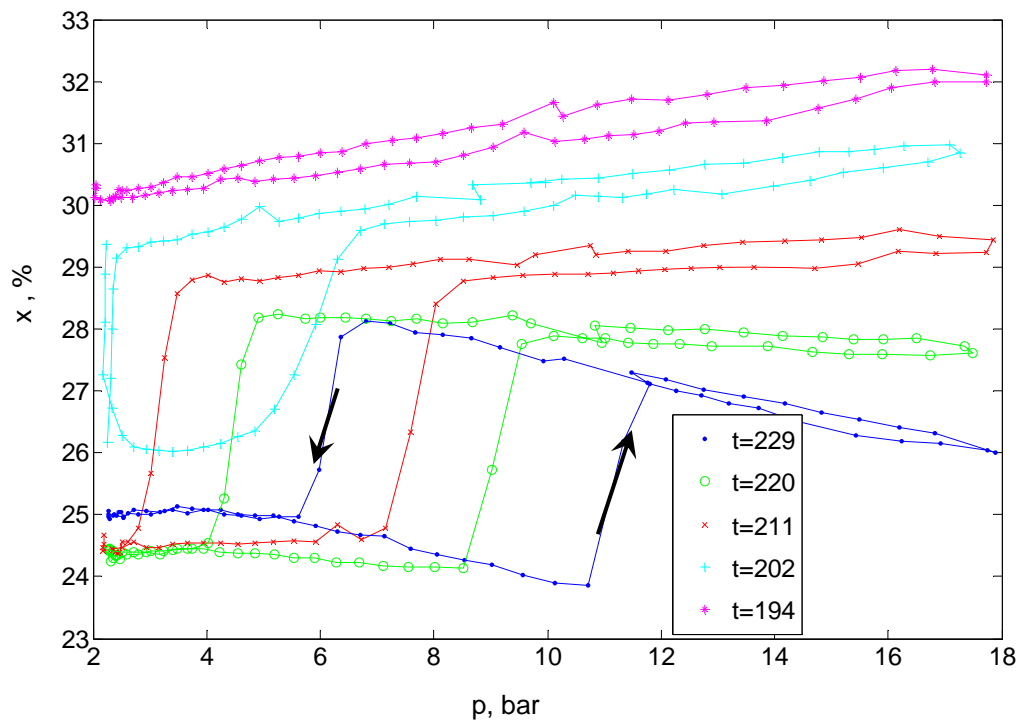
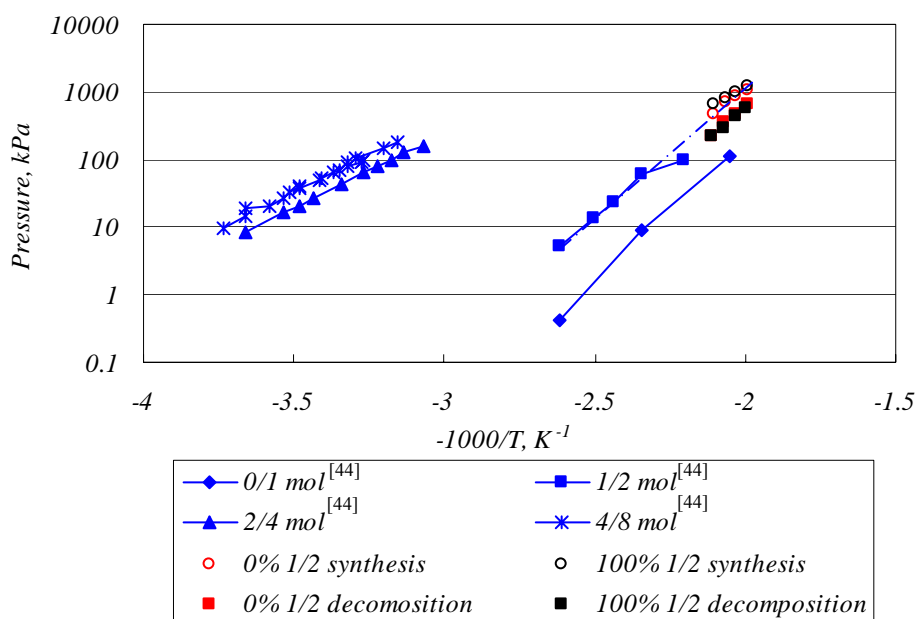


Figure 4-21 Adsorption quantity of CaCl_2 in test sample against saturated temperature when the temperatures of adsorbent are above 200°C



At low pressure CaCl_2 absorbs NH_3 in the molar proportions ($\text{NH}_3/\text{CaCl}_2$) of 1, 2, 4 and 8. The transition points for these phases are given for low pressures in [44] and at atmospheric pressure, from a range of sources by [45]. The comparison between the low pressure data from the references and the experimental data of the 0% (red open circles), 100% synthesis (black open circles), 0% (red solid squares) and 100% decomposition (black solid squares) is shown in figure 4-22. It shows that the transition during the experiments is 1/2 transition.

Figure 4-22 Comparison between transition data under low pressure from literature [44] and those under high pressure of our experiments

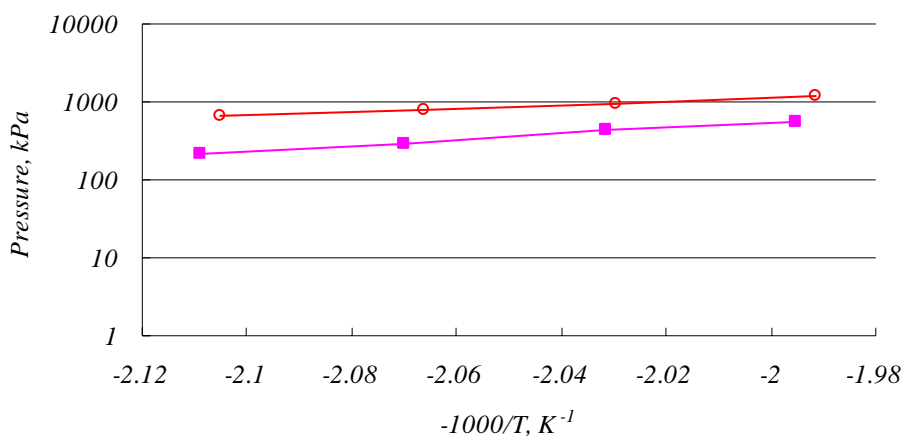


The experimental results also showed that the step changes in concentration are lower than would be expected if all the CaCl_2 were available during reaction and in the same state. The concentration change is only 5% for the 1/2 synthesis and decomposition during the experiments while the expected concentration change should be about 15%. This may be mainly due to the expansion of CaCl_2 on the surface of the sample, which will prevent NH_3 penetrating into the sample and contacting with CaCl_2 inside. The concentration change may approach the expected value if the sample is exposed in NH_3 vapour for a sufficient long time. But fortunately, this inaccurate concentration change would not affect the determination of transition line.

The data for 100% synthesis (open circle) and 100% decomposition (solid square) are

shown in figure 4-23. These data points represent the conditions at which the last molecule reacted during our experiments. Similar to $\text{BaCl}_2 - \text{NH}_3$, the line for 100% synthesis also has a smaller slope.

Figure 4-23 Pseudo-equilibrium lines for 100% synthesis and 100% decomposition



Similarly, the van't Hoff equation can be used to describe the termination of synthesis and decomposition,

For 100% synthesis,

$$\ln p_{\text{NH}_3} = 5.2153 \frac{-1000}{T} + 17.468 \quad (4-17)$$

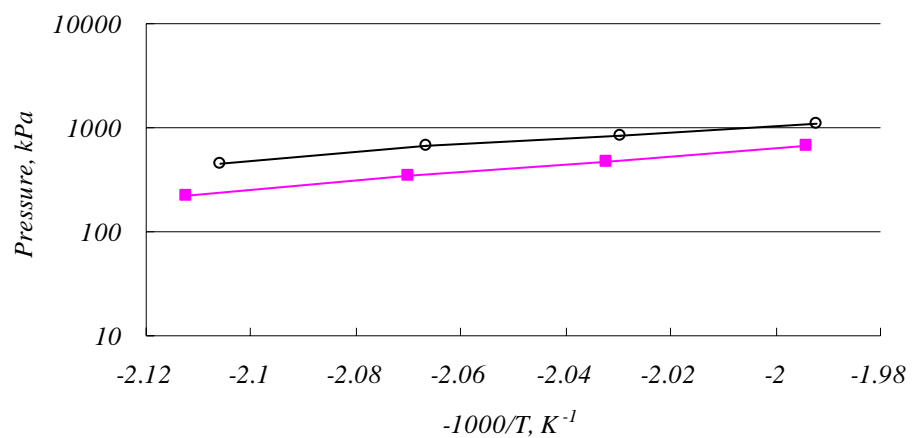
For 100% decomposition,

$$\ln p_{\text{NH}_3} = 8.2221 \frac{-1000}{T} + 22.734 \quad (4-18)$$

The data for 0% synthesis (open circles) and 0% decomposition (solid squares) are shown in figure 4-24. In principle, these points should not be influenced by either heat transfer or mass transfer so that a single line of logarithm of pressure against negative inverse temperature should be expected. While from figure 4-24, we can see that, under the same

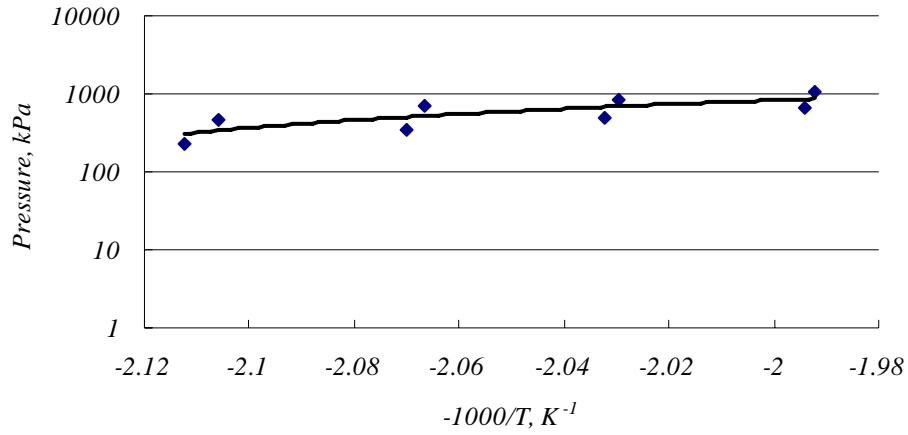
temperature, the pressure for 0% synthesis is greater than that for 0% decomposition. This contradiction may be attributed to the short equilibrium time for experimental point, which is just around 1 hour and not enough to obtain real equilibrium state.

Figure 4-24 Logarithm of ammonia pressure (kPa) vs negative inverse temperature (-1000/K) for 0% synthesis and 0% decomposition



The position of the onset points of 0% synthesis and decomposition is very important to determine the equilibrium and dynamical characteristics of the adsorption pair. An imaginary single straight line which presents the onset points of both synthesis and decomposition are fitted with the experimental data for both synthesis and decomposition, which is shown in figure 4-25.

Figure 4-25 Imaginary line to fit both 0% synthesis and 0% decomposition experimental data

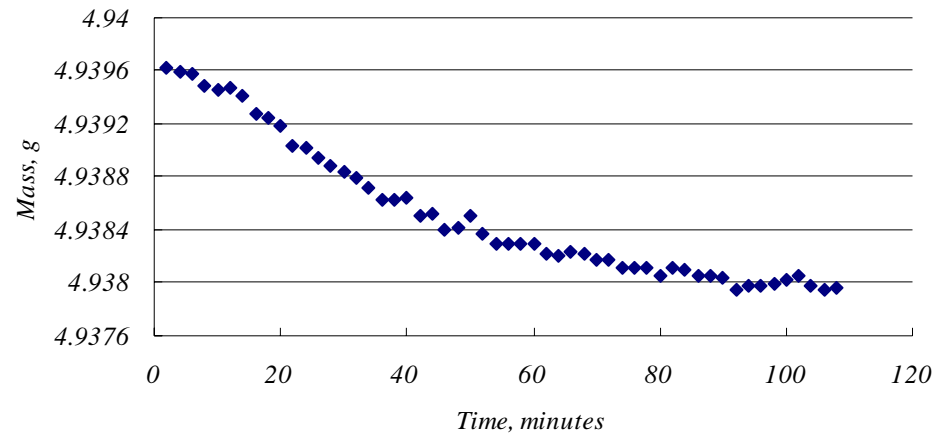


The position of the onset point for synthesis and decomposition can be calculated by,

$$\ln p_{NH_3} = 8.5657 \frac{-1000}{T} + 23.849 \quad (4-19)$$

The time required to approach equilibrium after the saturated temperature had been decreased from 0 to $-2^{\circ}C$, and held constant at $-2^{\circ}C$ for around 2h, is shown in figure 4-26. Initially, the rate of mass gain was rapid but then decreased to a slower but steady rate (0.33 mg/h). It shows that if the time at constant temperature was extended to much longer time (100 or 1000 h), perhaps real equilibrium may have eventually been attained.

Figure 4-26 Change in mass against time (min) when the saturated temperature changed from 0 to -2°C at an Adsorbent Temperature of 220°C



4.6.3 CaCl₂+Alumina – NH₃

Equilibrium experiments have also been carried on with another metallic salt compound. The experimental sample supplied by Boreskov Institute of Catalysis is made from mesoporous alumina with CaCl₂ impregnated into the material, which is named 'SWS'. The percentage of the mass of CaCl₂ in the sample was 17%. In order to test the adsorption performance under equilibrium conditions, repeated experiments were performed with the temperature of adsorbent controlled to 58, 62, 66, 69, 77, 87, 99 and 110°C and the saturation temperature of the reservoir within the temperature range -15 to 45°C. Results are shown in figure 4-27, where t is the temperature of the adsorbent bed (°C) and x is the adsorption quantity of adsorbent (kg/kg). The lower branch of the experimental results at each temperature represents measurements obtained by progressive addition of gas to the system and the upper branch by progressive withdrawal. For the temperature of adsorbent between 54 and 100°C, hysteresis loops are observed. While the temperature is above 100°C, under our experimental conditions, there is no obvious hysteresis loop.

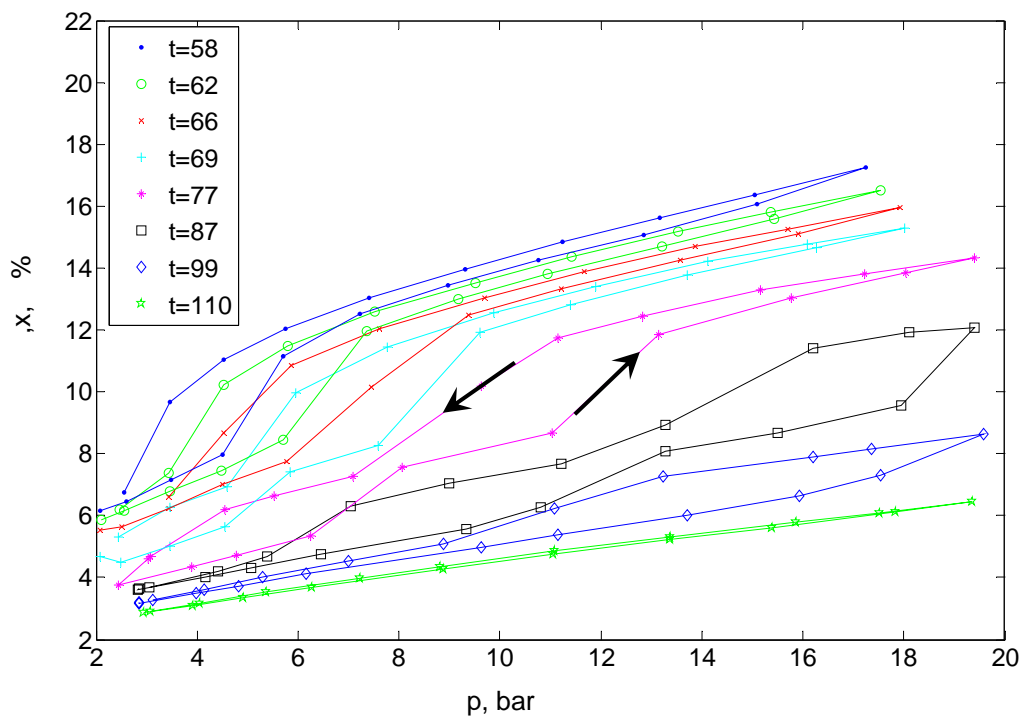
The adsorption quantity of the CaCl₂ in compound material (CaCl₂+Alumina) during the equilibrium experiments can be calculated by removing the alumina adsorption contribution from compound adsorbent,

$$x = \frac{m_c \times x_c - m_a \times x_a}{m_c - m_a} \quad (4-20)$$

where x (kg NH₃/kg CaCl₂) is the adsorption quantity of CaCl₂ in the compound material, m_c (kg) is the mass of compound adsorbent, x_c (kg NH₃/kg adsorbent) is the adsorption

quantity of compound adsorbent, m_a (kg) is the mass of alumina, x_a (kg NH₃/kg Alumina) is the adsorption quantity of alumina, which is calculated from equation (4-7). The experimental results of isothermal condition are shown in Figure 4-28. Hysteresis loops and two transitions are observed in the figures.

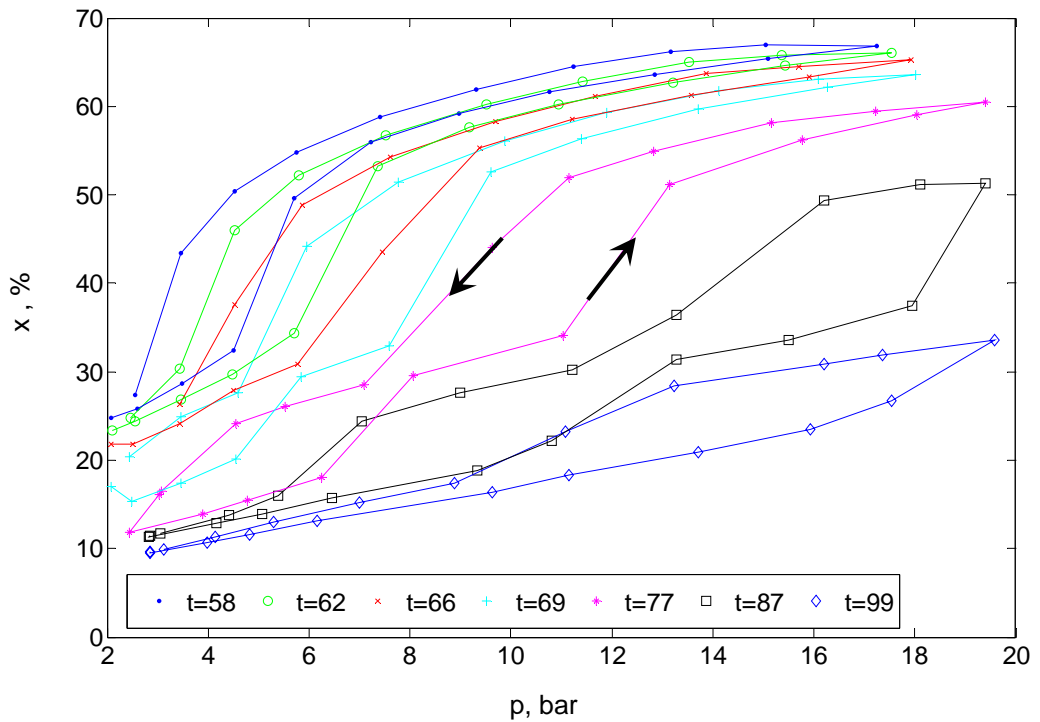
Figure 4-27 Concentration of SWS against saturated temperature



The alumina host matrix is mainly meso-porous [3] and figure 4-12 confirms this, in that there is not a high uptake of ammonia, and most of the uptake is at low values of T/T_{sat} (less than 1.05). Conversely, the carbon matrix is highly micro-porous. It is manufactured for gas adsorption and has good uptake at higher values of T/T_{sat} . The calcium chloride is therefore in a different state in each of the matrices investigated. The fact that the change in concentration on SWS occurs over a wider temperature range than the step changes of

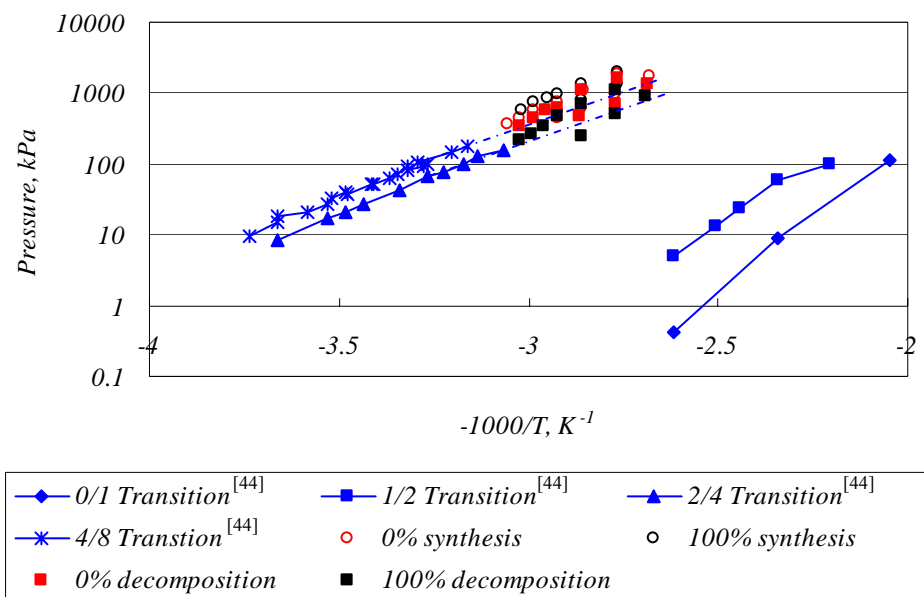
the bulk salt is understood to be caused by the way that the salt is constrained within the pores [3]. No distinct phases that are not present in the bulk salt were detected.

Figure 4-28 Adsorption quantity of CaCl_2 in test sample against saturated temperature



The experimental data of the 0% (red open circles), 100% synthesis (black open circles), 0% (red solid squares) and 100% decomposition (black solid squares) are compared with the transition data under low pressure. The result is shown in figure 4-29. It shows that the transitions during the experiments are 2/4 and 4/8 transition. As we mentioned before, due to the expansion of CaCl_2 on the surface, the experimental results also showed that the step changes in concentration are lower than would be expected if all the CaCl_2 were available during the reaction and in the same state.

Figure 4-29 Comparison between transition data under low pressure from literature [44] and those under high pressure of our experiments



The data for 100% synthesis (open circle) and 100% decomposition (solid square) of 2/4 and 4/8 transitions are shown in figure 4-30 and 4-31 respectively. These data points represent the conditions at which the last molecule reacted during our experiments. Similar to $BaCl_2 - NH_3$, the line for 100% synthesis also has a smaller slope.

Figure 4-30 Pseudo-equilibrium lines for 100% synthesis and decomposition of 2/4 transition

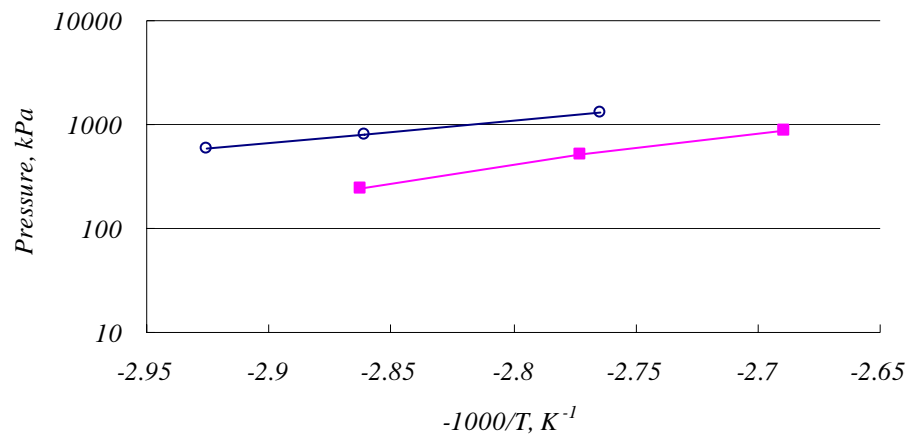
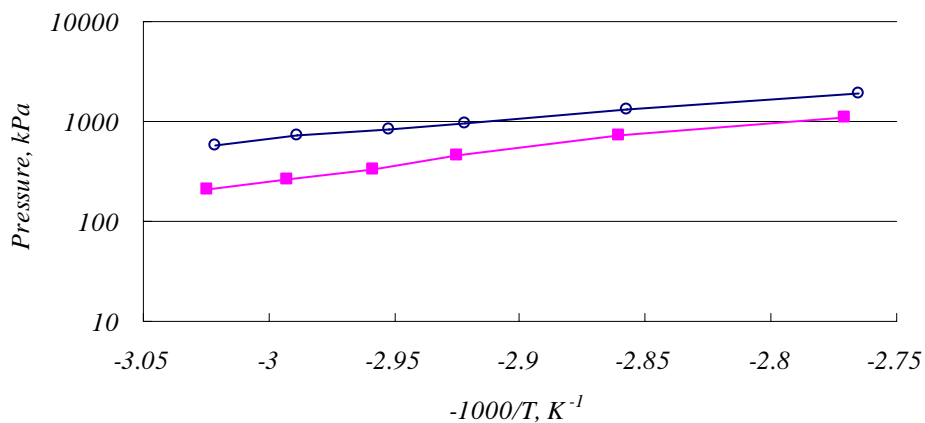


Figure 4-31 Pseudo-equilibrium lines for 100% synthesis and decomposition of 4/8 transition



Similarly, van't Hoff equation can be used to describe the termination of synthesis and decomposition,

For 100% synthesis of 2/4 transition,

$$\ln p_{NH_3} = 5.111 \frac{-1000}{T} + 21.32 \quad (4-21)$$

For 100% decomposition of 2/4 transition,

$$\ln p_{NH_3} = 7.46 \frac{-1000}{T} + 26.87 \quad (4-22)$$

For 100% synthesis of 4/8 transition,

$$\ln p_{NH_3} = 4.657 \frac{-1000}{T} + 20.47 \quad (4-23)$$

For 100% decomposition of 4/8 transition,

$$\ln p_{NH_3} = 6.74 \frac{-1000}{T} + 25.767 \quad (4-24)$$

The data for 0% synthesis (open circles) and 0% decomposition (solid squares) of 2/4 and 4/8 transitions are shown in figure 4-32 and 4-33 respectively. In principle, these points should not be influenced by either heat transfer or mass transfer so that a single line of logarithm of pressure against negative inverse temperature should be expected, which is consistent with the experimental data.

Figure 4-32 Pseudo-equilibrium lines for 0% synthesis and decomposition of 2/4 transition

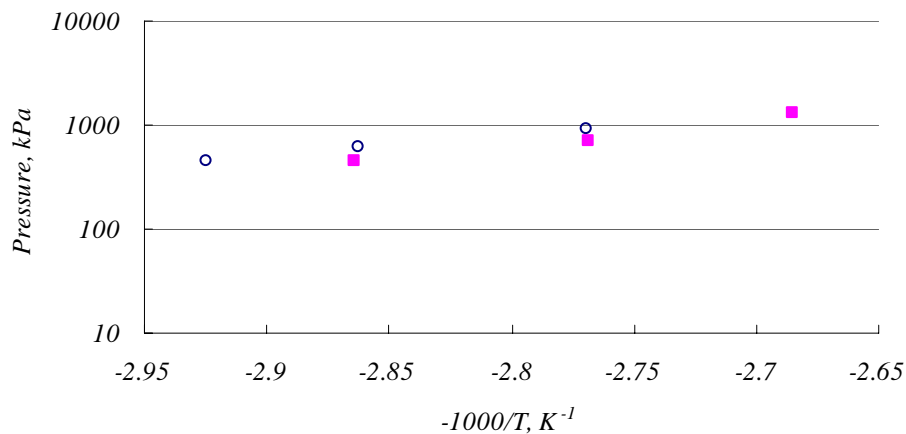
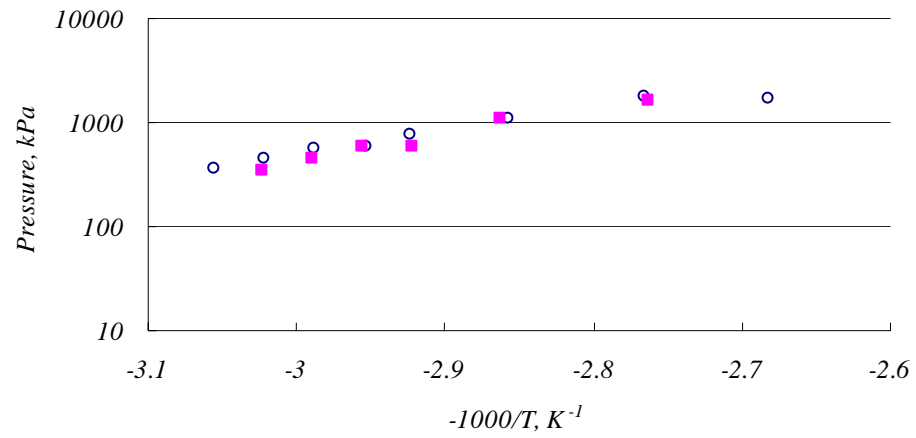


Figure 4-33 Pseudo-equilibrium lines for 0% synthesis and decomposition of 4/8 transition



The position of the onset points for synthesis and decomposition is very important to the equilibrium and dynamical characteristics of the adsorption pair. It can be calculated by fitting a straight line to the experimental data shown in figure 4-33 and 4-34,

For 2/4 transition,

$$\ln p_{NH_3} = 4.4914 \frac{-1000}{T} + 19.175 \quad (4-25)$$

For 4/8 transition,

$$\ln p_{NH_3} = 4.9782 \frac{-1000}{T} + 21.096 \quad (4-26)$$

4.6.4 CaCl₂ – NH₃

In order to compare with the compound material, repeated experiments on pure CaCl₂ were performed with the temperature of adsorbent controlled at 67, 74, 85, 136 and 203°C, the saturation temperature of the reservoir within the temperature range -15 to 45°C. The sample material with the purity of general purpose grade was obtained from Fisher Scientific in the form of anhydrous lumps. Because CaCl₂ will aggressively take up moisture from the atmosphere, the sample was stored in a sealed bottle. To make sure that the water vapor were eliminated from the sample and system, the adsorption system was heated and vacuumed for a long time, normally 25 hours. The experimental results are shown in figure 4-34, where t is the temperature of the adsorbent bed (°C) and x is the concentration of adsorbent (kg NH₃ /kg CaCl₂). The arrows show the direction in which the experimental measurements were performed. Hysteresis loops is observed when the temperature of adsorbent is above 200°C. But for the adsorbent temperature between 100 and 200°C, the data points collapse to approximate a single curve when concentration is plotted against t_{sat} .

The experimental data of the 0% (red open circles), 100% synthesis (black open circles), 0% (red solid squares) and 100% decomposition (black solid squares) are also compared with the transition data under low pressure, which is shown in figure 4-35. Three transitions are observed from the experimental data. They are 1/2, 2/4, 4/8 synthesis and decomposition.

Figure 4-34 Concentration of pure CaCl₂ on NH₃ against saturated temperature

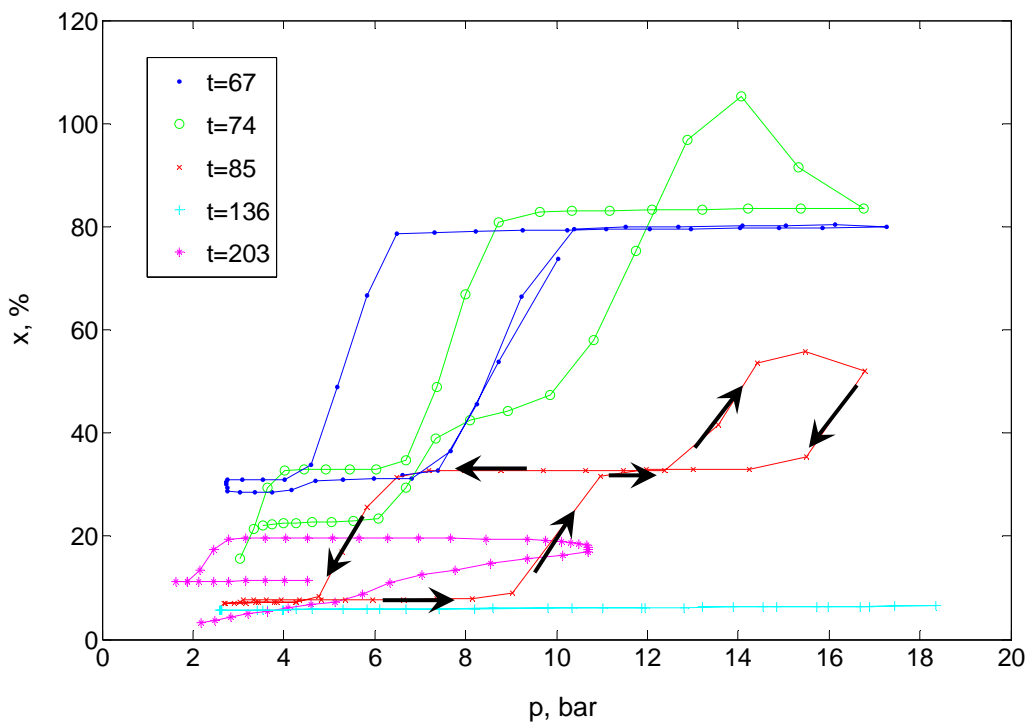
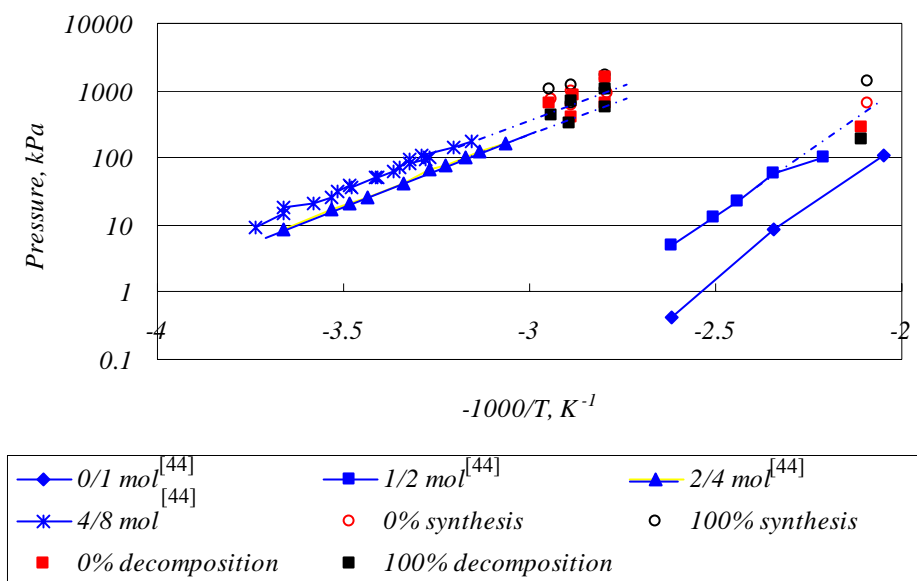


Figure 4-35 Comparison between transition data under low pressure from literature [44] and those under high pressure of our experiments



The pseudo-equilibrium lines for 100% synthesis (open circle) and 100% decomposition (solid square) of 2/4, 4/8 transition are shown in figure 4-36 and 4-37. These data points represent the conditions at which the last molecule reacted during our experiments. While for 1/2 transition, there is only one data point, which is not sufficient to draw a line.

Similarly, the van't Hoff equation can be used to describe the termination of synthesis and decomposition,

For 100% synthesis of 2/4 transition,

$$\ln p_{NH_3} = 5.47 \frac{-1000}{T} + 22.3 \quad (4-27)$$

For 100% decomposition of 2/4 transition,

$$\ln p_{NH_3} = 6.8 \frac{-1000}{T} + 25.6 \quad (4-28)$$

For 100% synthesis of 4/8 transition,

$$\ln p_{NH_3} = 4.253 \frac{-1000}{T} + 19.47 \quad (4-29)$$

For 100% decomposition of 4/8 transition,

$$\ln p_{NH_3} = 6.3 \frac{-1000}{T} + 24.6 \quad (4-30)$$

Figure 4-36 Pseudo-equilibrium lines for 100% synthesis and decomposition of 2/4 transition

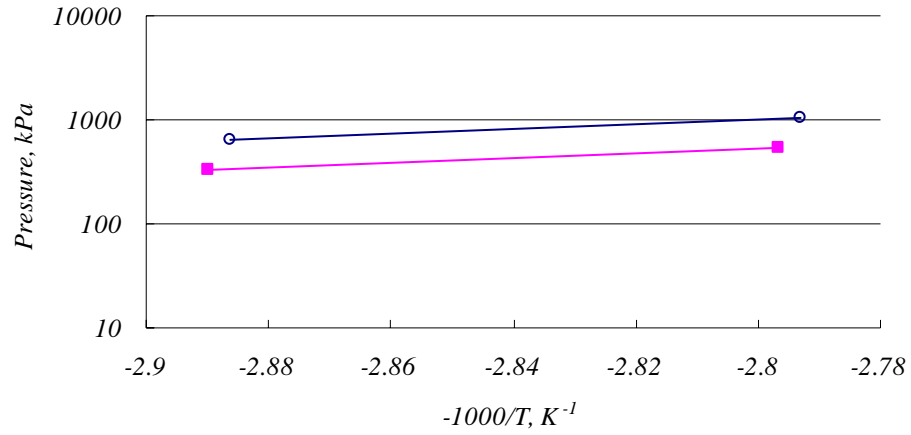
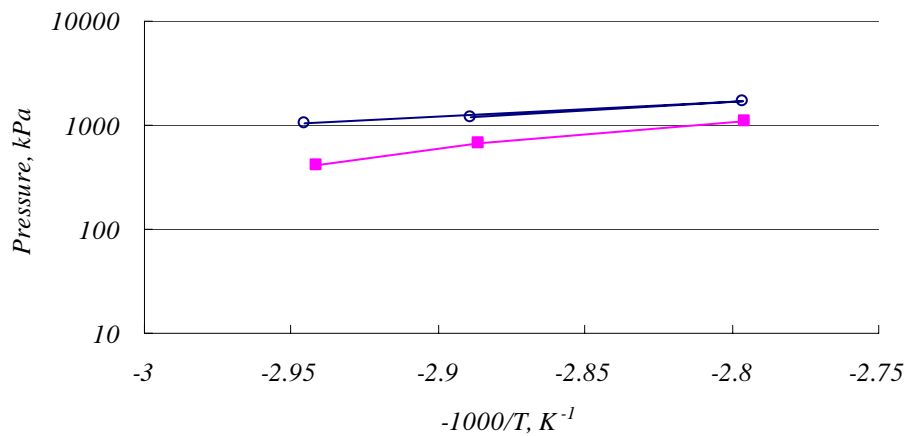


Figure 4-37 Pseudo-equilibrium lines for 100% synthesis and decomposition of 4/8 transition



The data for 0% synthesis (open circles) and 0% decomposition (solid squares) of 2/4, 4/8 transition are shown in figure 4-38 and 4-39. In principle, these points should not be influenced by either heat transfer or mass transfer so that a single line of logarithm of pressure against negative inverse temperature should be expected, which is consistent with the experimental data

Figure 4-38 Pseudo-equilibrium lines for 0% synthesis and decomposition of 2/4 transition

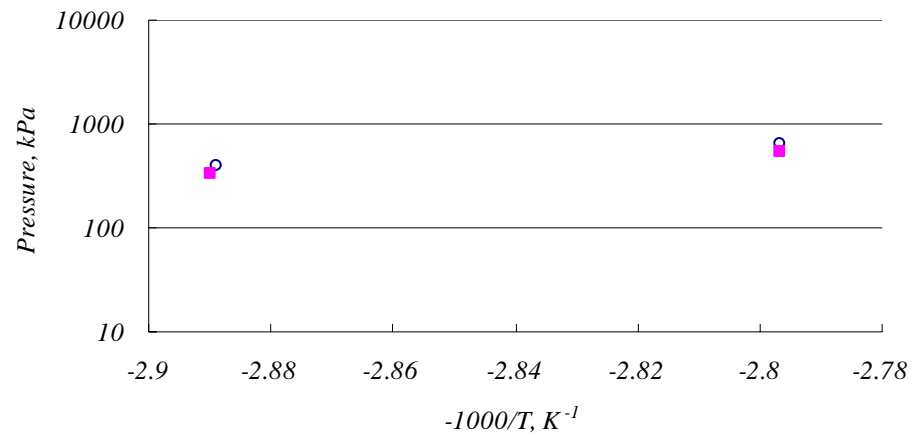
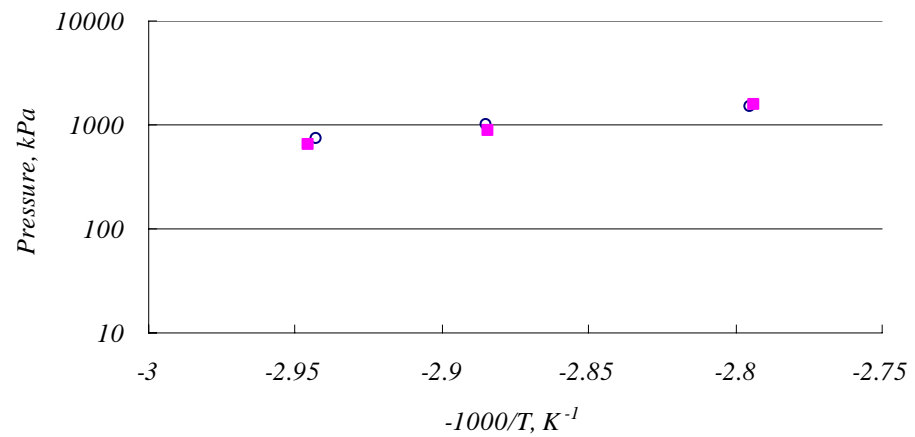


Figure 4-39 Pseudo-equilibrium lines for 0% synthesis and decomposition of 4/8 transition



The position of the onset points for synthesis and decomposition is fitted with the van't Hoff equation, which is,

For 2/4 transition,

$$\ln p_{NH_3} = 4.8931 \frac{-1000}{T} + 20.322 \quad (4-31)$$

For 4/8 transition,

$$\ln p_{NH_3} = 5.2539 \frac{-1000}{T} + 22.001 \quad (4-32)$$

Compared the results of SWS and pure CaCl_2 , the equations used to describe the equilibrium characteristics of SWS, equations (4-21) – (4-26), and pure CaCl_2 , equations (4-27) – (4-32) are almost the same. To get general results, the experimental data of 3C, SWS and pure CaCl_2 are put together to evaluate the equilibrium characteristics of CaCl_2 . The molar proportions ($\text{NH}_3/\text{CaCl}_2$) when CaCl_2 absorbs NH_3 are 1, 2, 4 and 8. Generally speaking, for saturation temperature of the reservoir within the temperature range -15 to 50°C, which covers most applications using real chemical adsorption heat pump, the transition from 1 mole to 2 moles mainly happens when the adsorbent temperature is over 200°C; The transitions from 2 to 4 moles and 4 to 8 moles mainly happened when the adsorbent temperature is lower than 100°C; While for the temperature of adsorbent below 240°C, which is the highest temperature in our experiments, no transition from 0 moles to 1 moles are observed. For a real heat pump, the operation temperature is always below 240°C. The results discussed in this chapter can provide enough information to describe the equilibrium character for a real adsorption system.

The onset positions of the transitions are important because they provide useful information for dynamic test, which are provided by,

For 1/2 transition,

$$\ln p_{\text{NH}_3} = 8.5657 \frac{-1000}{T} + 23.849 \quad (4-33)$$

For 2/4 transition,

$$\ln p_{\text{NH}_3} = 5.2539 \frac{-1000}{T} + 22.001 \quad (4-34)$$

For 4/8 transition,

$$\ln p_{NH_3} = 4.9782 \frac{-1000}{T} + 21.096 \quad (4-35)$$

The comparison between the experimental data and the equation (4-33), (4-34) and (4-35) is shown in figure 4-40, 4-41 and 4-42 respectively.

Figure 4-40 Comparison between the 0% synthesis and decomposition experimental data and equation (4-33) for 1/2 transition

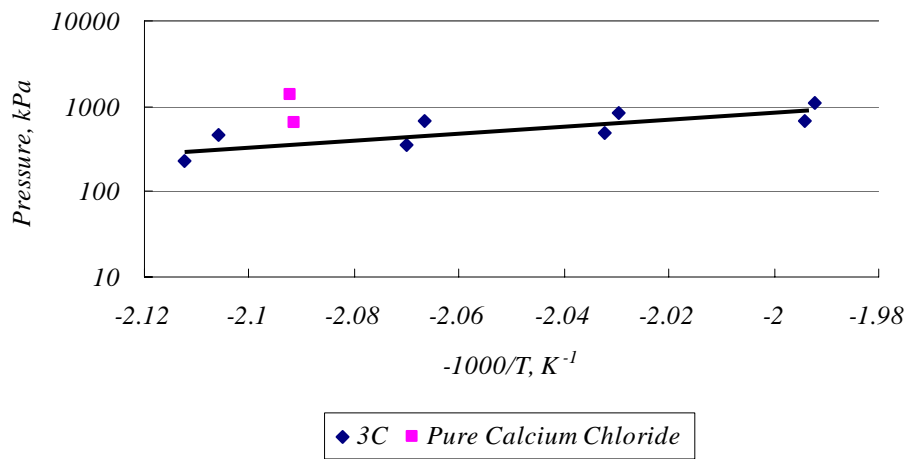


Figure 4-41 Comparison between the 0% synthesis and decomposition experimental data and equation (4-34) for 2/4 transition

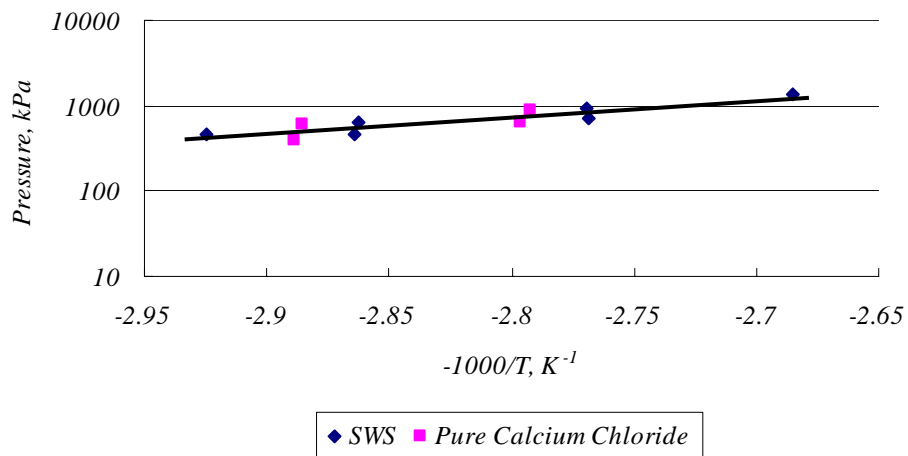
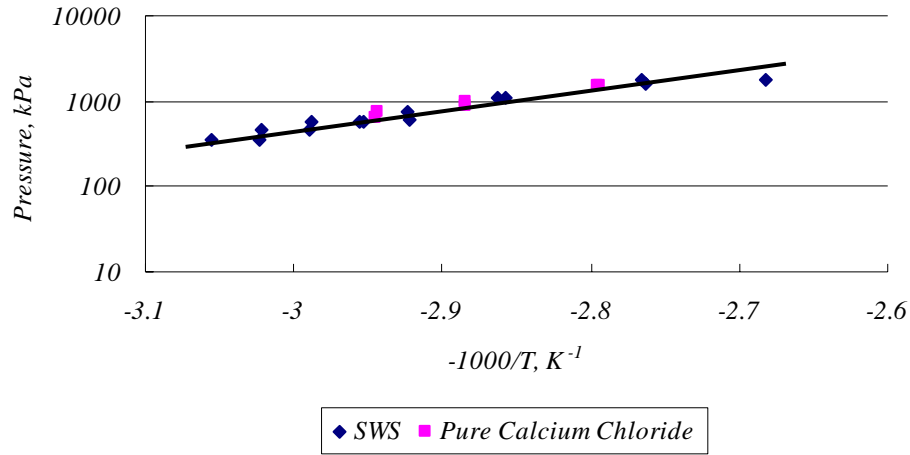


Figure 4-42 Comparison between the 0% synthesis and decomposition experimental data and equation (4-35) for 4/8 transition



Similarly, the terminal positions of the transitions can be calculated by,

For 100% synthesis of 1/2 transition,

$$\ln p_{NH_3} = 5.10 \times \frac{-1000}{T} + 23.05 \quad (4-36)$$

For 100% decomposition of 1/2 transition,

$$\ln p_{NH_3} = 5.90 \times \frac{-1000}{T} + 24.85 \quad (4-37)$$

For 100% synthesis of 2/4 transition,

$$\ln p_{NH_3} = 4.5128 \times \frac{-1000}{T} + 20.078 \quad (4-38)$$

For 100% decomposition of 2/4 transition,

$$\ln p_{NH_3} = 6.8411 \times \frac{-1000}{T} + 26.098 \quad (4-39)$$

For 100% synthesis of 4/8 transition,

$$\ln p_{NH_3} = 5.1353 \times \frac{-1000}{T} + 21.351 \quad (4-40)$$

For 100% decomposition of 4/8 transition,

$$\ln p_{NH_3} = 5.7858 \times \frac{-1000}{T} + 22.341 \quad (4-41)$$

The comparison between the experimental data and the equation (4-36) - (4-41) is shown in figure 4-43 - 4-48.

Figure 4-43 Comparison between the 100% synthesis experimental data and equation (4-36) for 1/2 transition

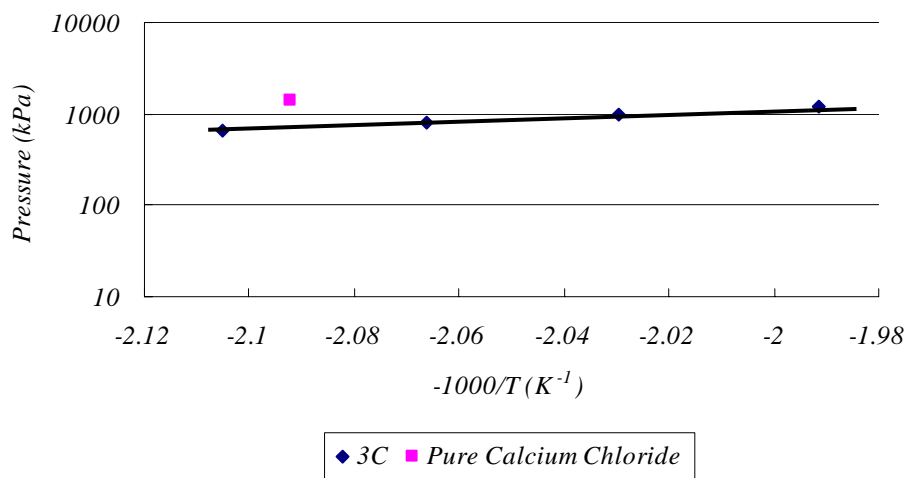


Figure 4-44 Comparison between the 100% decomposition experimental data and equation (4-37) for 1/2 transition

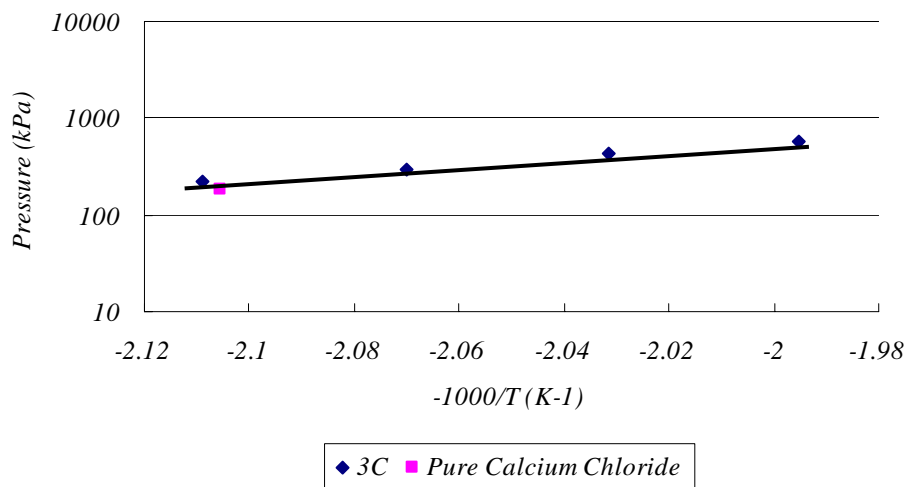


Figure 4-45 Comparison between the 100% synthesis experimental data and equation (4-38)

for 2/4 transition

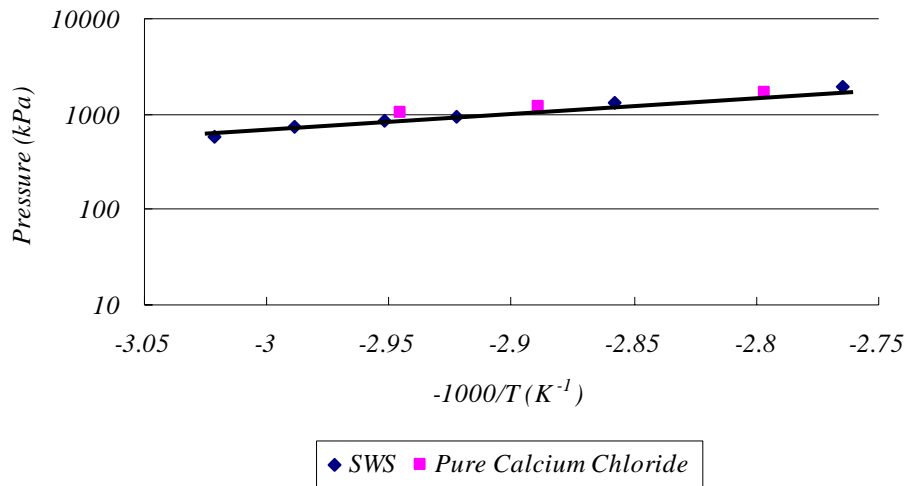


Figure 4-46 Comparison between the 100% decomposition experimental data and equation

(4-39) for 2/4 transition

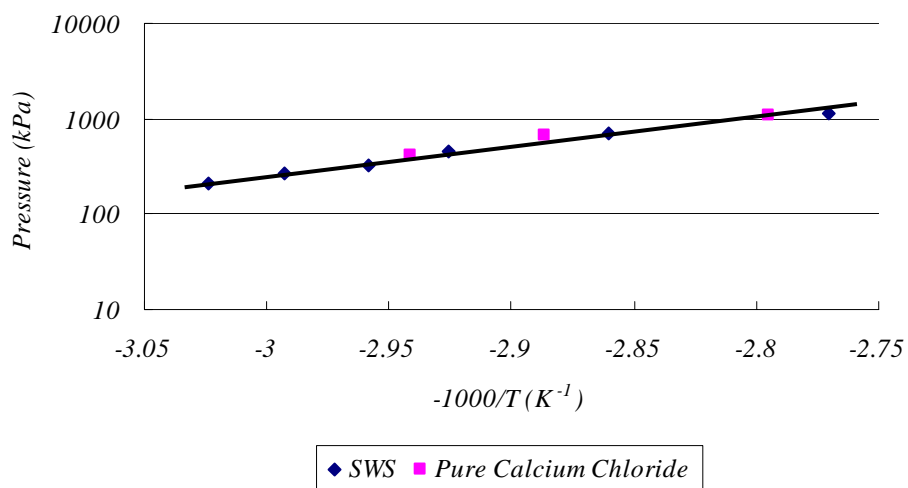


Figure 4-47 Comparison between the 100% synthesis experimental data and equation (4-40) for 4/8 transition

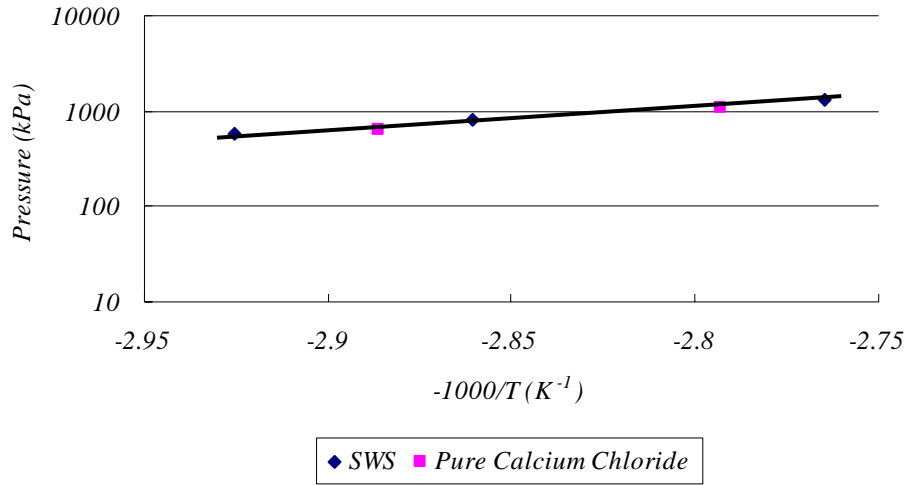
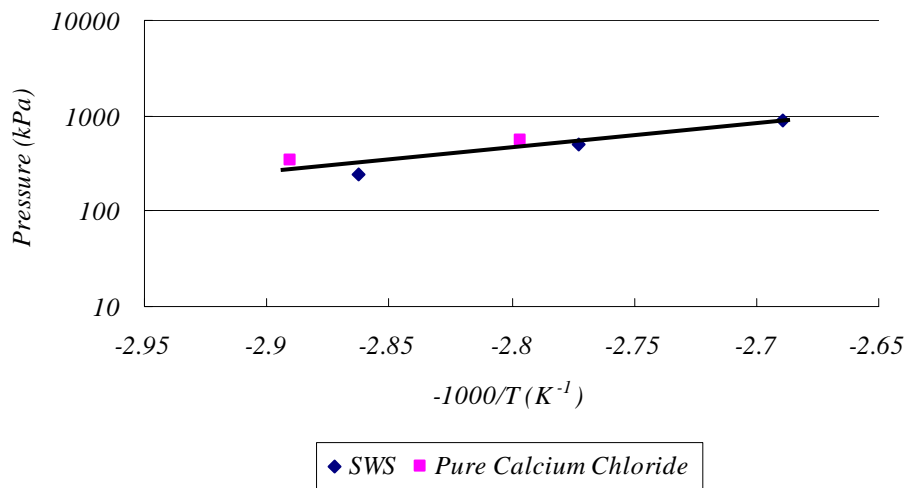


Figure 4-48 Comparison between the 100% decomposition experimental data and equation (4-41) for 4/8 transition



Assuming the transitions between 0 and 100% of synthesis and decomposition are linear with the concentration, the equation to describe the processes of synthesis and decomposition can be obtained by combining equations to determine the onset and

terminal position of the reaction.

For 1/2 synthesis,

$$\ln p_{NH_3} = (8.5657 - 23.1(x - 0.15)) \times \frac{-1000}{T} + 23.85 - 5.3(x - 0.15) \quad (4-42)$$

For 1/2 decomposition,

$$\ln p_{NH_3} = (4.513 + 27.02(x - 0.15)) \times \frac{-1000}{T} + 20.8 + 25.15(x - 0.15) \quad (4-43)$$

For 2/4 synthesis,

$$\ln p_{NH_3} = (5.24 - 0.34(x - 0.3)) \times \frac{-1000}{T} + 22 - 0.325(x - 0.3) \quad (4-44)$$

For 2/4 decomposition,

$$\ln p_{NH_3} = (5.9 - 2.215(x - 0.3)) \times \frac{-1000}{T} + 24.85 + 9.5(x - 0.15) \quad (4-45)$$

For 4/8 synthesis,

$$\ln p_{NH_3} = (4.98 + 3.1(x - 0.6)) \times \frac{-1000}{T} + 21.1 + 8.3(x - 0.6) \quad (4-46)$$

For 4/8 decomposition,

$$\ln p_{NH_3} = (5.79 - 1.35(x - 0.6)) \times \frac{-1000}{T} + 22.34 - 2.1(x - 0.6) \quad (4-47)$$

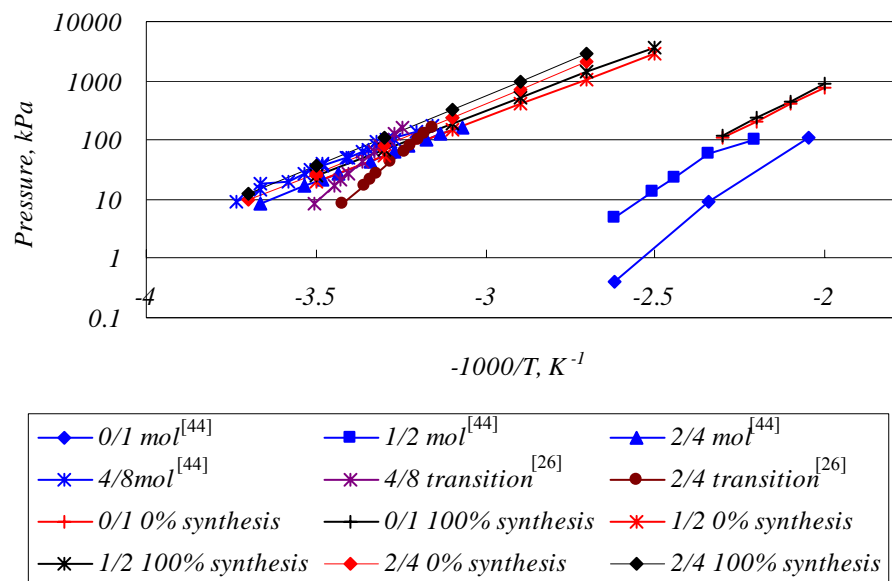
In the equations above, x is the concentration of CaCl_2 between the onset and termination of the reaction, 0.15 is the concentration of adsorbent when CaCl_2 absorbs NH_3 in the molar proportions of 1; 0.3 is the concentration of adsorbent when CaCl_2 absorbs NH_3 in the molar proportions of 2 and 0.6 is the concentration of adsorbent when CaCl_2 absorbs NH_3 in the molar proportions of 4. These equations provide relationship between temperature, pressure and concentration (T , p , and x).

The experimental data of the start and end of the synthesis transitions are compared with

the data under low pressure [44, 45] and the equation to describe transitions provided by Enibe and Iloeje [26]. The results are shown in figure 4-49. From figure 4-49, we can see that the imaginary lines for the transitions from our experimental data are very similar to those under low pressure. They are the almost the extension of the fitting line under low pressure, while the research of Enibe and Iloeje [26] deviated our results.

In summary, the experiments on some metallic salt compounds in which CaCl_2 is impregnated into different kinds of materials provide more useful information for the equilibrium characteristics of CaCl_2 . The equations used to determine the reaction processes provide useful information to evaluate the position of onset and termination of the transitions theoretically.

Figure 4-49 Comparison of experimental data with the data from literature



Reference:

- [1] G.E. Hulse, Freight Car Refrigeration by an adsorption system employing silica gel, Refrigerating Engineer, vol.17, 1924
- [2] R.E. Critoph, An ammonia carbon solar refrigerator for vaccine cooling, Renewable Energy, vol.5(1), pp.502-508, 1994
- [3] Z. Tamainot-Telto, R.E. Critoph, Adsorption refrigeration using monolithic carbon-ammonia pair, International Journal of Refrigeration, vol.20(2), pp.146-155, 1997
- [4] B. Spinner, Les transformateurs thermo-chimiques a ammoniac. Proc. Symp. le Froid a Sorption Solide, Paris, 1992
- [5] U. Rockenfeller, L.D. Kirol, P. Sarkisian., Advanced heat pump staging for complex compound chemisorption systems. Proc. Symp. le Froid a Sorption Solide, Paris, 1992
- [6] Z.F. Li, K. Sumathy, A solar powered ice maker with the solid adsorption pair of activated carbon and methanol. Int. J. Energy Res., vol.23, pp.517-527, 1999
- [7] R. Exell, S.C. Bhattacharya, Y.R. Upadhyaya, Research and development of solar powered desiccant refrigeration for cold storage applications, Asian Institute of Technology, Bangkok, AIT Research Report, no.265, 1993
- [8] B.B. Saha, S. Koyama, J. B. Lee, Performance evaluation of a low-temperature waste heat driven multi-bed adsorption chiller, International Journal of Multiphase Flow, vol.29(8), pp.1249-1263, 2003
- [9] A. Akahira, K.C. A. Alam, Y. Hamamoto, Mass recovery adsorption refrigeration

- cycle-improving cooling capacity, *International Journal of Refrigeration*, vol.27(3), pp.225-234, 2004
- [10] P.H. Grenier, J.J. Guilleminot, F. Meunier et al., Solar powered solid adsorption cold store, *ASME J Solar Energy Eng.*, vol.110, pp.192-197,1998
- [11] M. Tather, A. Erdem-Senatalar, The effects of thermal gradients in a solar adsorption heat pump utilizing the zeolite-water pair, *Applied Thermal Eng.*, vol.19, pp.1157-1172, 1999
- [12] P. Neksa, CO₂ heat pump systems, *International Journal of Refrigeration*, vol.25, pp.421-427, 2002
- [13] M.H. Kim, J. Pettersen, C.W. Bullard, Fundamental process and system design issues in CO₂ vapor compression systems, *Progress in Energy and Combustion Science*, vol. 30, pp.119-174, 2004
- [14] R.E. Critoph, Performance limitations of adsorption cycles for solar cooling, *Solar energy*, vol. 41(1), pp.21-31, 1988
- [15] F. Meunier, Solid sorption: An alternative to CFC's, heat recovery system & CHP, vol.13 (4), pp. 289 – 295, 1993.
- [16] D.Do Duong, *Adsorption analysis: equilibria and kinetics*, London: Imperial College Press, 1998.
- [17] Yu.I Aristov, G. Restuccia, G. Cacciola, V.N. Parmon, a family of new working materials for solid sorption air conditioning systems, *Applied Thermal Engineering*, vol.22, pp.191-204, 2002
- [18] Y. Kato, M. Yamada, T. Kanie, Y. Yoshizawa, Calcium oxide/carbon dioxide

- reactivity in a packed bed reactor of a chemical heat pump for high-temperature gas reactors, *Nucl Eng Des*, vol.210, pp.1–8, 2001
- [19] A. El Atifi, Ph. Touzain, P. Mathonnet, Etude du couple compose d'insertion du graphite-chlorure de manganese/ ammoniac pour le stockage chimique de la chaleur, *Rev. Phys. Appl.*, vol.21, pp.603–607, 1986
- [20] Ph. Touzain, D. Sarneo, T. Deller, Etude de l'efficacite des systemes de pompes a chaleur chimique ammoniacchlorures metalliques-carbones, in: *Proc. 19th Intern. Congr. Refriger.*, IVb, pp. 1270–1276, 1995
- [21] M. Tokarev, L. Gordeeva, V. Romannikov, I. Glaznev, Y. Aristov, New composite sorbent CaCl_2 in mesopores for sorption cooling/heating, *Int J. Therm Sci*, vol.41, pp.470–474, 1986
- [22] T. Deller, D. Sarneo, Ph.A. Touzain, Chemical heat pump using carbon fibers as additive. Part I: enhancement of thermal conduction. *Appl Therm Eng.*, vol.19, pp.991–1000, 1999
- [23] T. Deller, Ph.A. Touzain, Chemical heat pump using carbon fibers as additive. Part II: study of constraint parameters. *Appl Therm Eng.*, vol.19, pp.1001–1011, 1999.
- [24] Iloeje OC, Ndili AN, Enibe SO. Computer simulation of a CaCl_2 solid-adsorption solar refrigerator. *Energy*, vol.20(11), pp.1141–1151, 1995
- [25] S.O. Enibe, O.C. Iloeje, Transient analysis and performance prediction of a solid absorptionsolar refrigerator, *Solar Energy*, vol. 61, pp.43-59, 1997
- [26] S.O. Enibe, O.C. Iloeje, Heat and mass transfer in porous spherical pellets of

- CaCl₂ for solar refrigeration, *Renewable Energy*, vol.20, pp.205-324, 2000
- [27] S.O. Enibe, O.C. Iloeje, COSSOR – a transient simulation program for a solid absorption solar refrigerator, *Renewable Energy*, vol.19, pp.413-434, 2000
- [28] L.W. Wang, R.Z. Wang, J.Y. Wu, K. Wang, Compound adsorbent for adsorption ice maker on fishing boats, *International Journal of Refrigerator*, vol.27, pp.401 – 408, 2004
- [29] Z.S. Lu, R.Z. Wang, L.W. Wang and C.J. Chen, Performance analysis of an adsorption refrigerator using activated carbon in a compound adsorbent, *Carbon*, vol. 44(4), pp.747-752, 2005
- [30] J. Trudel, S. Hosatte, M. Ternan, Solid - gas equilibrium in chemical heat pumps: the NH₃ - CoCl₂ system, *Applied Thermal Engineering*, vol.19, pp.495 – 511, 1999
- [31] A. Marty, Etude par microcalorime trie de la re activite de deux ammoniacates de chlorure de manganese, *J. Therm. Anal.*, vol.37, pp.479 – 498, 1991
- [32] J. Llobet, V. Goetz. Rotary system for the continuous production of cold by solid-gas sorption: modeling and analysis of energy performance. *International Journal of Refrigeration*, vol.23, pp.609–25, 2000
- [33] N.C. Srivastava, I.W. Eames, A review of adsorbents and adsorbates in solid-vapour adsorption heat pump systems, *Applied Thermal Engineering*, vol.18, pp.707-714, 1998
- [34] F. Meunier, Second law analysis of solid adsorption heat pump operating on reversible cascade cycle: application to the zeolite-water pair. *Heat Recovery System*, vol.5(2), pp.133-141, 1985

- [35] R.E. Critoph, H.L. Turner, Performance of ammonia-activated carbon and ammonia zeolite heat pump adsorption cycles, Proc. Pompes a Chaleur Chimiques De Hautes Performances, Perpignan, September 1989. Lavoisier, Paris
- [36] L. Turner, Improvement of activated charcoal-ammonia adsorption heat pumping/refrigeration cycles. Investigation of porosity and heat /mass transfer characteristics, Ph.D. Thesis, University of Warwick, UK, 1992
- [37] K.C. Ng, H.T. Chua, C.Y. Chung et al., Experimental investigation of the silica gel-water adsorption isotherm characteristics, Applied Thermal Engineering, vol.21(16), pp.1631-1642, 2001
- [38] N.B. Amar, L.M. Sun, F. Meunier, Numerical analysis of adsorption temperature wave regenerative heat pump, Applied Thermal Engineering, vol.16(5), pp. 405-418, 1996
- [39] R.E. Critoph, Adsorption refrigeration and heat pumps, In: Carbon Materials for Advanced Technologies, Edited by Trimothy D. Burchell, pp.303-340, PERGAMON, 1999
- [40] R.E. Critoph, Evaluation of alternative refrigerant-adsorbent pairs for refrigeration cycles, Applied Thermal Engineering, vol.16(11), pp.891-900, 1996
- [41] L.W. Wang, R.Z. Wang, J.Y. Wu, K. Wang, The adsorption character of $\text{CaCl}_2\text{-NH}_3$ pairs and its application in the refrigeration, Science in China, vol.34(3), pp.268~279, 2004
- [42] S.J. Gregg, K.S.W. Sing, Adsorption, surface area and porosity, Academic Press, 1982

- [43] A.W. Adamson, Physical chemistry of surfaces, Wiley, New York, 1997
- [44] E.W. Washburn, International Critical Tables of Numerical Data, Physics, Chemistry and Technology, Knovel, 2003
- [45] P. Touzain, Thermodynamic values of ammonia-salts reactions for chemical salts heat pumps, Proceedings of the International Sorption Heat Pump Conference, Munich, Germany, 1999
- [46] V.E. Sharonov, J.V. Veselovskaya, Yu.I. Aristov, Ammonia sorption on composites "CaCl₂ in inorganic host matrix": isosteric chart and its performance, Int. J. Low Carbon Techn., vol.1(2), 2006
- [47] V.E. Sharonov, A.G. Okunev, Yu.I. Aristov, Kinetics of CO₂ sorption by the composite material K₂CO₃-in-porous alumina, React.Kinet.Cat. Lett., vol. 82(2), pp. 363-370, 2004
- [48] V.E. Sharonov, J.V. Veselovskaya, Yu.I. Aristov, Y. Zhong, R.E. Critoph, New composite adsorbent of ammonia "BaCl₂ in vermiculate" for adsorptive cooling, CHP (2006), Proc. HPC06, Newcastle, 2006
- [49] R.N. Thorpe, R.E. Critoph, Y. Zhong, Sorption of ammonia on calcium chloride / alumina and calcium chloride / active carbon composite materials, International Sorption Heat Pump Conference, Denver, USA, June 2006
- [50] Operating instructions of magnetic suspension balance, RUBOTHERM Comp., p.16, German

Chapter 5 Dynamics of Adsorption Pairs under Isothermal Conditions

5.1 Introduction

It is essential to obtain accurate kinetics of adsorption pairs. For a real adsorption chiller, accurate isotherms, isosteric heat of adsorption and the kinetic characteristics of adsorption and desorption are the key factors to determine the performance of the system [1]. With these key data, the numerical modelling of the processes of the real adsorption system can be computed accurately with greater confidence [2]. However, most of previous studies on adsorption heat pumps have been performed using steady-state concepts, while a real adsorption system can hardly reach the equilibrium state because of the short cycle time.

Dawoud and Aristov carried on the kinetic study on water sorption on loose grains of composite sorbent CaCl_2 confined to meso-porous silica for various grain sizes (between 0.34 and 3.2 mm) and various salt contents (12.6-33.7 wt.%) [3]. Experimental measurements were performed in a constant pressure unit based on a microbalance under isothermal external conditions [4]. The results showed evidence of a remarkable enhancement of the sorption rate and apparent diffusion constant with the decrease in the particle size and salt content. The kinetic characteristic sorption times were used to evaluate the specific power generated inside adsorbent grains during the water sorption [4]. Aidoun and Ternan did some experimental study on the effect of the kinetic characteristics of $\text{CoCl}_2 - \text{NH}_3$ working pairs on the performance of the chemical heat pump [5]. The

experimental results showed that the rate of the synthesis reaction in a chemical heat pump is controlled by the rate of diffusion of ammonia gas into the chemical salt [6]. A shrinking core model is suggested to describe the synthesis reaction in the chemical heat pump [6].

This chapter focuses on experimental studies on the kinetics of several adsorption pairs mentioned in chapter 4. A mathematic model is also applied to fit the experimental data. The results provided useful information to understand the dynamics of chemical sorption.

5.2 Theory of the dynamics of sorption

The design and modelling of the adsorption processes require numerical solutions of a set of partial differential equations involving time and spatial variables. The theoretical background of the mathematical models that have been developed to represent sorption kinetic behaviour can be found in many references [7-28].

These mathematical models are based on the following assumption. The heat transfer in the adsorbent particles is rapid and the heat sink to surrounding medium is intensive, the particle can be considered isothermal. Since the intrinsic interaction between adsorbate and adsorbent is commonly very fast, the rate of sorption is controlled by adsorbate vapour diffusion in adsorbent meso-pores [8].

The Linear Driving Force (LDF) model for gas adsorption kinetics is frequently and successfully used for analysis of adsorption column dynamic data and for adsorptive process designs because it is simple, analytic, and physically consistent. This model was first introduced by Gluekauf [25]. According to the LDF model, the rate of adsorption of adsorbate into adsorbent particles is given by [9]:

$$\frac{d\bar{x}(t)}{dt} = K_L (x^* - \bar{x}(t)) \quad (5-1)$$

where, $\bar{x}(t)$ is the average adsorbate concentration in the adsorbent particle at time t , x^* is the final equilibrium adsorbate concentration in the adsorbent particle, K_L is called effective LDF mass transfer coefficient and usually given by [25, 27],

$$K_L = \frac{15D_0}{R_0^2}$$

where D is intra-particle diffusivity of sorbate, cm^2/s ; R_0 is radius of particle or crystal, cm

For a step change in pressure at time zero (The gas phase pressure is instantaneously changed from P_0 to P_1 at time zero, and then it is held constant at that value during the constant pressure experiment), the analytical solution for equation (5-1) is given by,

$$\frac{\bar{x}(t) - x_0}{x^* - x_0} = 1 - e^{-K_L t} \quad (5-2)$$

where x_0 , x^* are, respectively, the initial and final equilibrium adsorbate concentrations in the adsorbent particle at the start and end of the batch dynamic experiment.

Another well known model to describe the kinetics of adsorption system is the isothermal Fickian diffusion (FD) model, which Gluekauf used to get the LDF model. For uniform spherical adsorbent particles the transient diffusion equation may be written in the form [8]:

$$\frac{\partial x}{\partial t} = \frac{1}{r^2} \frac{\partial}{\partial r} \left(r^2 D \frac{\partial x}{\partial r} \right) \quad (5-3)$$

in which the Fickian diffusivity, D , can be calculated by “Darken equation” [8],

$$D = B \left(\frac{d \ln p}{d \ln x} \right)_T, \text{ for constant temperature, T} \quad (5-4)$$

where $\frac{d \ln p}{d \ln x}$ represents simply the gradient of the equilibrium isotherm in logarithmic coordinates. Fickian diffusion can be assumed to be independent of concentration. This is generally valid for a small change in the adsorbed phase concentration and under conditions of Knudsen diffusion it is valid even when the concentration change is large [8].

So equation (5-3) can be simplified to,

$$\frac{\partial x}{\partial t} = D \left(\frac{\partial^2 x}{\partial r^2} + \frac{2}{r} \frac{\partial x}{\partial r} \right) \quad (5-5)$$

For a step change in pressure at time zero, the solution of equation (5-5) is well known [7]:

$$\frac{m_t}{m_\infty} = \frac{\bar{x} - x_0}{x_\infty - x_0} = 1 - \frac{6}{\pi^2} \sum_{n=1}^{\infty} \frac{1}{n^2} \exp\left(-\frac{n^2 \pi^2 Dt}{r_c^2}\right) \quad (5-6)$$

where \bar{x} is the average adsorbate content in the sample which depends on time, r_c is the radius of the adsorbent particle. The equation (5-6) may also be written in equivalent form,

$$\frac{m_t}{m_\infty} = \frac{\bar{x} - x_0}{x_\infty - x_0} = 6 \left(\frac{Dt}{r_c^2} \right)^{0.5} \left[\frac{1}{\sqrt{\pi}} + 2 \sum_{n=1}^{\infty} \text{ierfc} \left(\frac{nr_c}{\sqrt{Dt}} \right) \right] - \frac{3Dt}{r_c^2} \quad (5-7)$$

where the function *ierfc* is given by,

$$\text{ierfc}(x) = \frac{1}{\sqrt{\pi}} \left[\exp(-x^2) - x(1 - \text{erf}(x)) \right] \quad (5-8)$$

$$\text{and } \text{erf}(x) = \frac{2}{\sqrt{\pi}} \int_0^x e^{-\xi^2} d\xi \quad (5-9)$$

This form is more convenient for short times, since, the summation in equation (5-6) converges very slowly when t is small. A simplified expression for the initial region of the sorption curve may be obtained by neglecting the higher order terms in equation (5-7):

$$\frac{m_t}{m_\infty} \approx \frac{6}{\sqrt{\pi}} \sqrt{\frac{Dt}{r_c^2}} \quad (5-10)$$

This corresponds physically to the case when the concentration front has not yet reached the centre of the particle so that the diffusion occurs as in a semi-infinite medium. Equation

(5-10) can be used for determining the apparent diffusion time constant $K_d = \frac{D}{r_c^2}$.

In the long time region, all terms except the first one in the series of exponential terms in (5-6) became negligible so that the sorption curve approaches the asymptotic form,

$$\frac{m_t}{m_\infty} = 1 - \frac{6}{\pi^2} \exp\left(-\frac{\pi^2 D t}{r_c^2}\right) \quad (5-11)$$

from which it is apparent that a plot of $\ln(1-m_t/m_\infty)$ versus t gives at long t a straight line with the slope $-\frac{\pi^2 D}{r_c^2}$. In practice this limiting form is somewhat less useful than expression (5-10) since any distribution of particle size leads to curvature of the semi-logarithmic plot. Furthermore, the long time region of the sorption curve is more sensitive than the initial region to the intrusion of thermal effects [8].

The solutions of the Fickian diffusion model (FD model) are frequently used to obtain D from the experimental uptake data. It should, however, be emphasized that these solutions are rigorously applicable only for isothermal uptakes and for the case where D is not a function of concentration, x . Otherwise, the calculated values of diffusivity will be erroneous even though the model may fit the data fairly well. Recently many experimental studies had been conducted to test the validity of the model. The results show that the model can fit the data fairly well. Rynders et al. [12] and Mohr et al. [13] researched on the kinetics of adsorption system using the isotope exchange technique, where the process is truly isothermal and the effective adsorption isotherms for the isotopes are linear. The results showed that FD model describes the process very well for diffusion of simple gases

in zeolites.

It is generally assumed that the FD model is fundamentally adequate to describe gas sorption kinetics [9]. However, the model imposes formidable mathematical complication in adsorptive process design because the equation (5-3) and (5-4) have to be integrated at the adsorbent particle level. And the above integration process must be repeated over many cycles of operation in order to establish the final cyclic-steady-state separation performance of the overall process. Also all practical adsorption systems operate under non-isothermal condition. So the above described integrations must be carried out by coupling the solutions of simultaneous mass, heat, and momentum balance equations at the particle, column, and steady state cyclic operation levels [9]. As a result, the FD model will generally require large computational times for process simulation under realistic conditions. J. Crittenden studied FD models in the 1980s. He showed that simulations could be accelerated by orders of magnitude with the Orthogonal Collocation method, in which mass transfer of the adsorbate and the particle was treated at column levels [28]. However, the lack of experimental data to justify the model was a big problem.

On the other hand, the LDF model is much simpler and most importantly it eliminates the integration step at the particle level so it can significantly reduce the computational times required for realistic process simulations. This model with a lumped mass transfer coefficient is very frequently used for practical analysis of dynamic data and for adsorptive process design because it is simple, analytical, and physically consistent. Of course, the

LDF model may not fit the experimental data very well because its assumption and simplification sometimes are not consistent with the reality. To obtain better match with experimental data, many researches had been conducted to empirically modify the form of LDF model. The Quadratic Driving Force (QDF) model is one of them [14]. The rate of adsorption into the adsorbent particle by this empirical model is given by,

$$\frac{d\bar{x}(t)}{dt} = K_Q \frac{\left((x^*)^2 - (\bar{x}(t))^2 \right)}{2\bar{x}(t)} \quad (5-12)$$

where K_Q is the effective QDF mass transfer coefficient at adsorbate concentration of $\bar{x}(t)$ and temperature T , x^* is the final equilibrium concentration.

In summary, the Fickian Diffusion (FD) model is often used for analyzing isothermal gas uptake by adsorbents in order to estimate a diffusivity parameter. The Linear Driving Force (LDF) model with a lumped mass transfer coefficient, on the other hand, is very frequently used for practical analysis of column dynamic data and for adsorptive process design because of its simple, analytical, and physically consistent. To obtain better match with the experimental data, modification may be applied to the LDF model. It is also worth pointing out that in LDF and FD model, the chemical reaction of adsorbate and adsorbent are not considered. To describe the dynamics of chemisorption system, these models will have to be modified.

5.3 Experimental studies

5.3.1 Experimental apparatus and procedure

Active carbon, 3C, SWS and a composite material of BaCl₂ and vermiculite were tested to determine the kinetic characteristics of adsorption system using NH₃ as adsorbate.

The simplest experimental method to determine the kinetics of sorption system involves the measurement of sorption curve, under isothermal conditions, for a small sample of the adsorbent subjected to a step change in the sorbate pressure. The real experimental apparatus used for dynamic tests is the same as that used for equilibrium experiments, which are shown in figure 4-1 and 4-2. To make sure that the sample is in isothermal conditions, a new sample container is used, which consists of one fixed component and one moving part, as is shown in figure 5-1. The container made tight contact with the sample by screwing the moving part up and down to make sure the sample is at constant temperature.

The typical experimental run was as follows. The sample was heated up to 180°C for 10 hours and then cooled down to the measuring temperature under continuous pumping ($P \approx 5$ mbar). Then the measuring cell with the sample was disconnected from the pump and connected to an evaporator maintained at a setting temperature between -20 and 50°C for a long time until the system reach equilibrium state. At the beginning of the dynamic tests,

the valve separating the reactor and the reservoir closed and the saturated temperature of the reservoir was changed to a new value. After the adsorbent material and the refrigerant in the reactor had attained thermal and chemical equilibrium, the valve between the reactor and reservoir was opened. The pressure changed to the pressure of the reservoir, causing a rapid rate of concentration change, because the adsorbent bed was at conditions far from equilibrium. The values of temperature, pressure and mass change during this process were recorded. After the kinetic curve had been recorded, the evaporator was disconnected from the measuring cell and its temperature was increased to fix the proper pressure for the next kinetic test and so on.

Figure 5-1 Diagram of the sample holder



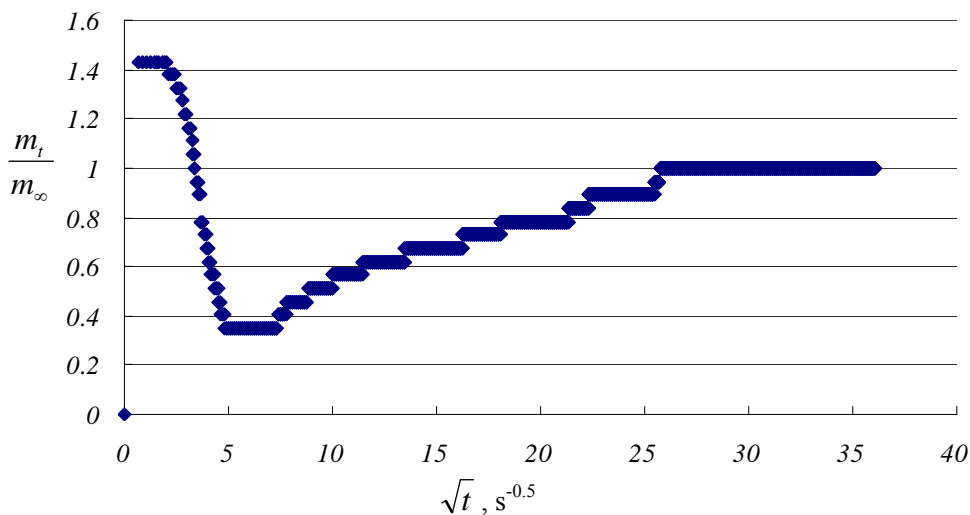
During the test, the system should first be kept in equilibrium state. To ensure this

equilibrium state, thermocouples within the reactor were used to measure the adsorbent temperature, the temperatures of the sample material at the top and bottom of the chamber and the wall temperature. During the test, it is not considered as equilibrium state unless the temperature variations measured by these thermocouples are within 0.5 °C for a period of at least 30 minutes. The frequency of data reading is 2.5 Hz. The control process and data logging was performed utilising the dedicated WorkBench software running on a standard 486 / Windows98 PC operating in conjunction with the DATAshuttles.

5.3.2 Carbon 208C - Ammonia

Typical kinetic curves of ammonia adsorption plotted as m_t/m_∞ (the definition is shown in equation 5-7) vs. \sqrt{t} are presented in figure 5-2, in which the temperature of the adsorption system is 94°C. The system showed different performance in the first 25seconds, which was beyond the explanation of dynamic characteristics. This may be due to the limitation of experimental apparatus. During the dynamic tests, the pressure change of the system would disturb the mass measurement. It would take several seconds for the magnetic suspension balance, which was used as mass measurement in the tests, to obtain reasonable measurement. So the measured experimental data in the first 25 seconds will be disregarded.

Figure 5-2 Plot of the ammonia sorption curves in the form m_t/m_∞ vs. \sqrt{t} . T=94°C,



The reasonable experimental data after 25seconds were used for the analysis. The Fickian Diffusion model was used to fit the experimental data. Firstly we calculated the apparent

diffusion time constant $K_D = \frac{D}{r_c^2}$ from the slope of the initial region of the sorption curve,

which is given by $A = \frac{6}{\sqrt{\pi}} \sqrt{\frac{D}{r_c^2}}$. Then the obtained K_D was used to calculate the $\frac{m_t}{m_\infty}$

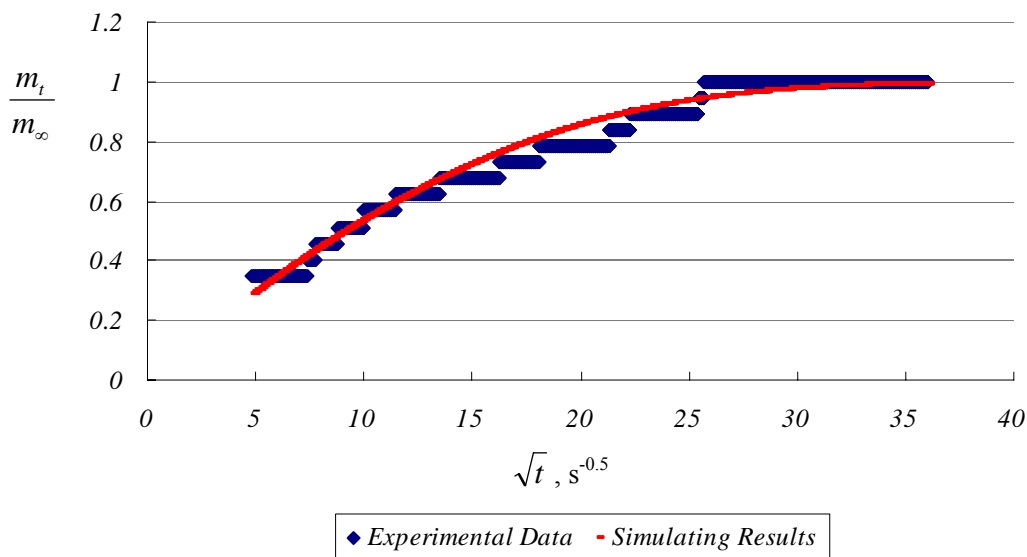
from equation (5-6). To get a good approximation, the first ten terms were chosen in the

calculation, that is to say, $\frac{m_t}{m_\infty} = \frac{\bar{x} - x_0}{x_\infty - x_0} = 1 - \frac{6}{\pi^2} \sum_{n=1}^{10} \frac{1}{n^2} \exp\left(-\frac{n^2 \pi^2 D t}{r_c^2}\right)$. The comparison

between the experimental data and the results from mathematical model were shown in

figure 5-3, in which K_D is calculated to be 0.000369.

Figure 5-3 Comparison between the experimental data and the results from mathematic model



Similarly, at the temperature of 71°C, the experimental data after 25 seconds were also

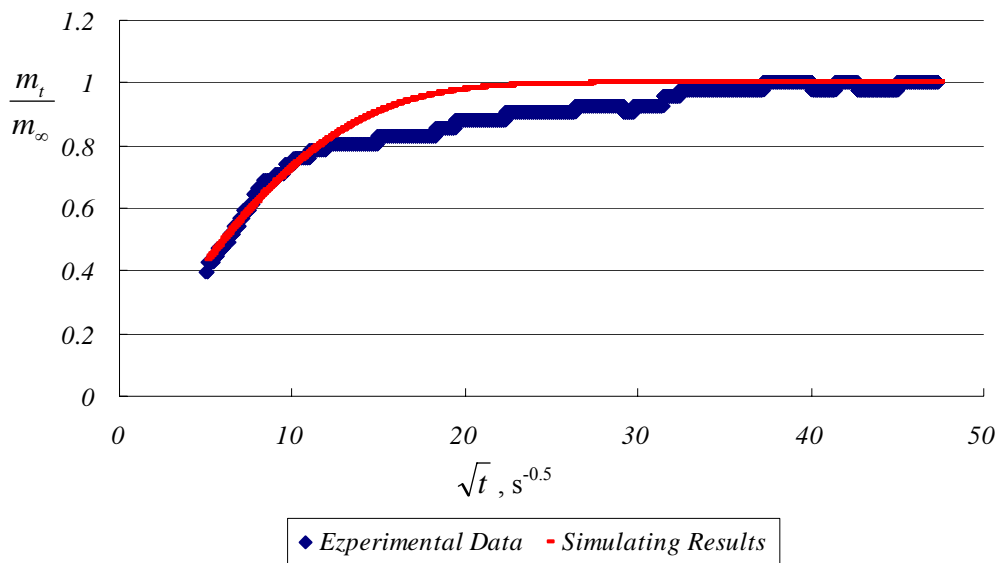
used for the calculation of the slope $A = \frac{6}{\sqrt{\pi}} \sqrt{\frac{D}{r_c^2}}$ and the apparent diffusion time

constant $K_D = \frac{D}{r_c^2}$. The comparison between the experimental data and the results from

FD model were shown in figure 5-4, in which K_D is calculated to be 0.000873.

From the comparison above, in the first 25 seconds, the concentration change is around 30% of the overall concentration change during the experiments. Also the comparison shows that results from mathematical model fit experimental data fairly well. It means the abandoned experimental data in the first 25seconds would not cause significant deviation between the experimental data and mathematical model. It means that the equipment described in chapter 5.3.1 can be used to determine the dynamics of adsorption pairs.

Figure 5-4 Comparison between the experimental data and the results from FD model



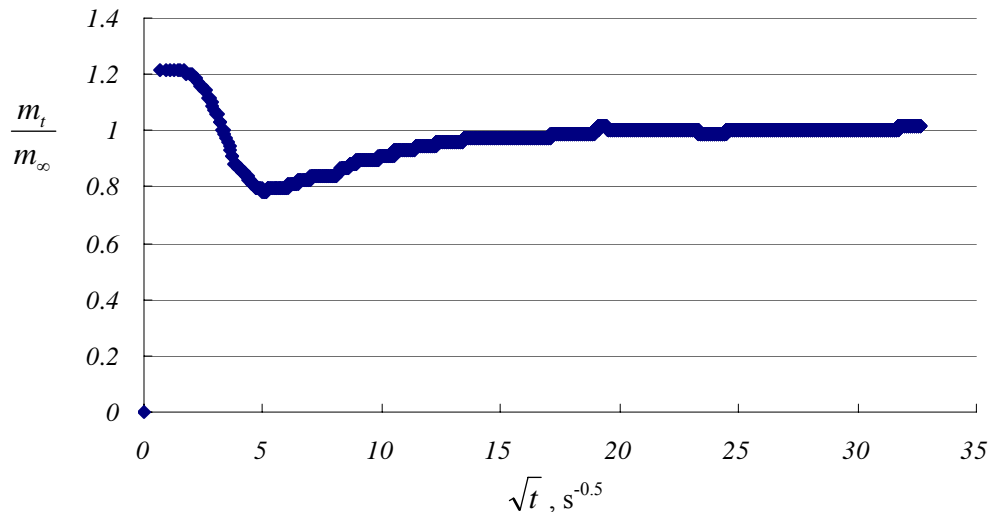
The results obtained from the kinetic experiments of active carbon may not be accurate. However, they provide useful information to choose available adsorption pairs, which can be used in the experimental apparatus mentioned above. In a word, for a specific adsorption pair, if the concentration change in the first 25seconds is small and can be

ignored compared to the overall concentration change so that the limitation of experimental apparatus will not greatly affect the results.

5.3.3 C + CaCl₂ - Ammonia

3C is also used as adsorbent to test the kinetic character of ammonia adsorption. The typical kinetic curve plotted as m_t/m_∞ vs. \sqrt{t} is shown in figure 5-5, in which the temperature of adsorption system was 88°C. Similarly, due to the limitation of experimental apparatus, the system showed different performance in the first 25seconds. Within the first 25 seconds, the concentration change is around 75% of the overall concentration change during the experiments. It means that the results from the experiments can not provide sufficient information to determine the kinetics of 3C adsorption on ammonia.

Figure 5-5 Plot of the ammonia sorption curves in the form m_t/m_∞ vs. \sqrt{t} . T=88°C,



5.3.4 Vermiculite + BaCl₂ - Ammonia

Another adsorbent to test the kinetic character of ammonia adsorption is the composition material consisting of BaCl₂ and vermiculite mentioned in chapter 4.6.1. The change of concentration against time at the sample temperature of around 37°C is shown in figure 5-6. Before the valve is open, the pressure of the system is around 5bar, while the pressure of the condensing reservoir is kept at around 2.15bar. After the valve is open, the system pressure dropped quickly and then kept at the pressure of condensing reservoir, which is shown in figure 5-7. In the first 25 seconds, the system showed different performance due to the limitation of experimental apparatus. But the concentration change in the first 25seconds is small and can be ignored compared to the overall concentration change. The limitation of experimental apparatus had just a little effect on the analysis.

From the figure 5-6, the concentration of the salt in the reactor decreased when decomposition occurred and the evolved ammonia left the reactor. The concentration change of the adsorbent was around 38% during a period of 20 minutes and then no more ammonia was released from sample and the concentration kept at 2.5%, which is considered as the contribution of vermiculite to the ammonia concentration.

The pressure variation with time is shown in figure 5-7. The change of the calculated adsorbent temperature against time is also shown in figure 5-8. The calculated

temperature decreased from 37.4 to 35.3°C for around 15 minutes. During this period of time, the endothermic reaction of decomposition caused the adsorbent temperature to decrease. To calculate the temperature, the sample and container are considered adiabatic and the temperature change is assumed mainly to be caused by the endothermic reaction of decomposition. So the temperature change can be calculated by the energy balance equation,

$$\left(\dot{m}_s c_{ps} + \dot{m}_b c_{pb} \right) \Delta T = \Delta H \Delta x' \quad (5-13)$$

where, \dot{m}_s is the sample mass, g; c_{ps} is the specific heat of the sample, 1000 J kg⁻¹ K⁻¹; \dot{m}_b is the mass of the container, g; c_{pb} is the specific heat of the container, 452 J kg⁻¹ K⁻¹; T is the temperature of the sample, °C; t is time, seconds; x' is the mole concentration of the sample, molNH₃/molsample, and ΔH is the heat of reaction, 43.67kJ/mol [26].

During the tests, the sample mass, is around 0.2g, the mass of the container is around

11.2g. So $\Delta T = \frac{(0.2 \times 8 \times 17 / 208) \times 43.67 \times 1000}{0.2 \times 1000 + 11.2 \times 452} = 1.1$, which is approximately

consistent with the experimental results. Of course, the temperature change of sample calculated above is not accurate, but it provides useful information to explain the experimental results.

Figure 5-6 Concentration change against time at 37°C

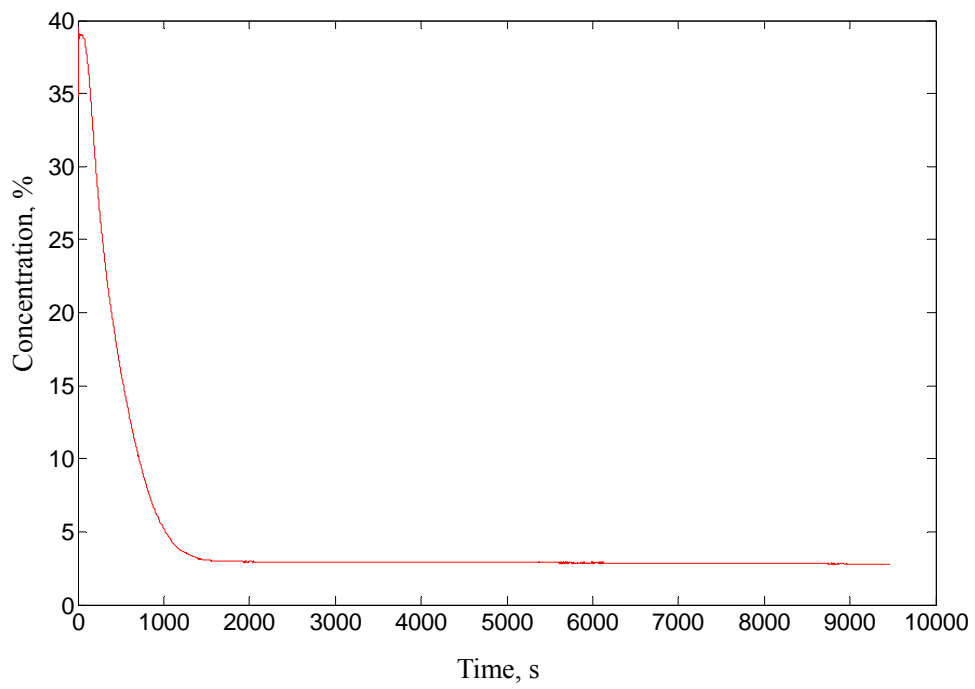


Figure 5-7 Pressure change against time at 37°C

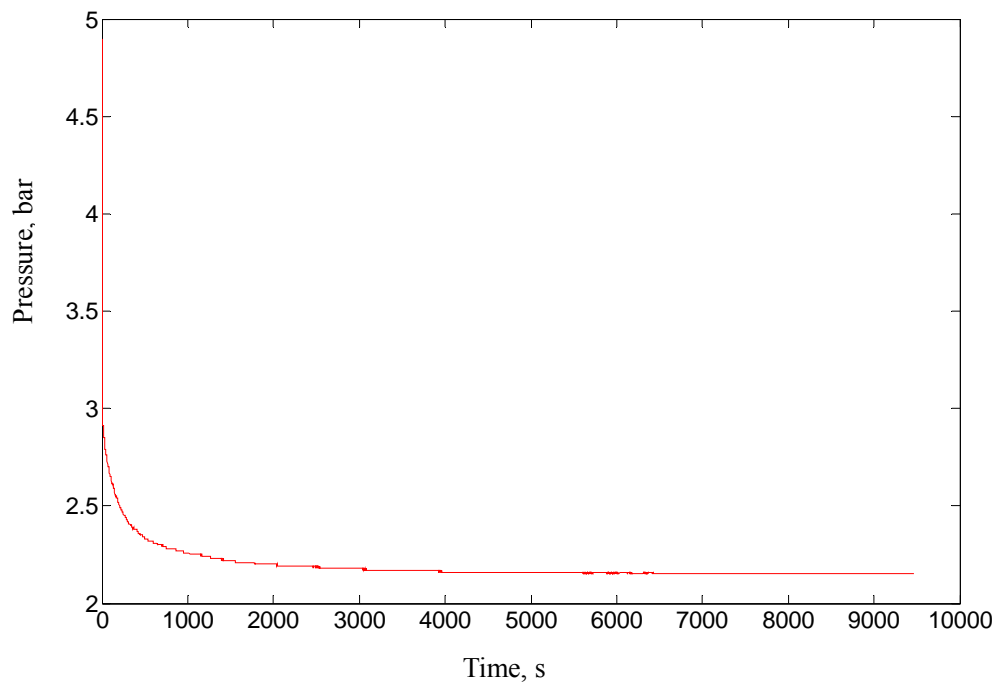
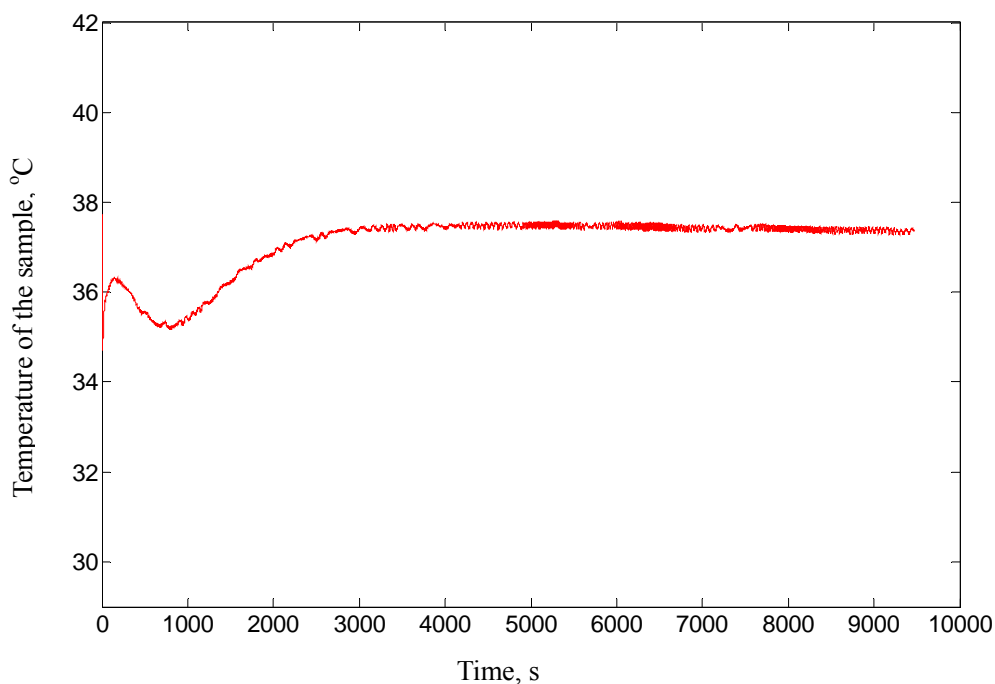


Figure 5-8 Temperature change against time at 37°C



The concentration change for decomposition kinetic experiments at the sample temperature of around 44.8 and 53.4°C are shown in figure 5-9 and 5-10. Before the valve is open, the pressures of the system are at around 9.2 and 10.8bar respectively, while the pressure of the condensing reservoir is kept at around 2.7 and 4.11bar respectively. Similarly, after a transition time of approximately 10 minutes, the curve for the concentration change shifted from a straight line to an exponential curve. The concentration change of the adsorbent was around 38% during a period of 20 minutes and then no more ammonia was released from sample and the concentration kept at 2.5%.

Figure 5-9 Concentration change for decomposition against time at 44.8°C

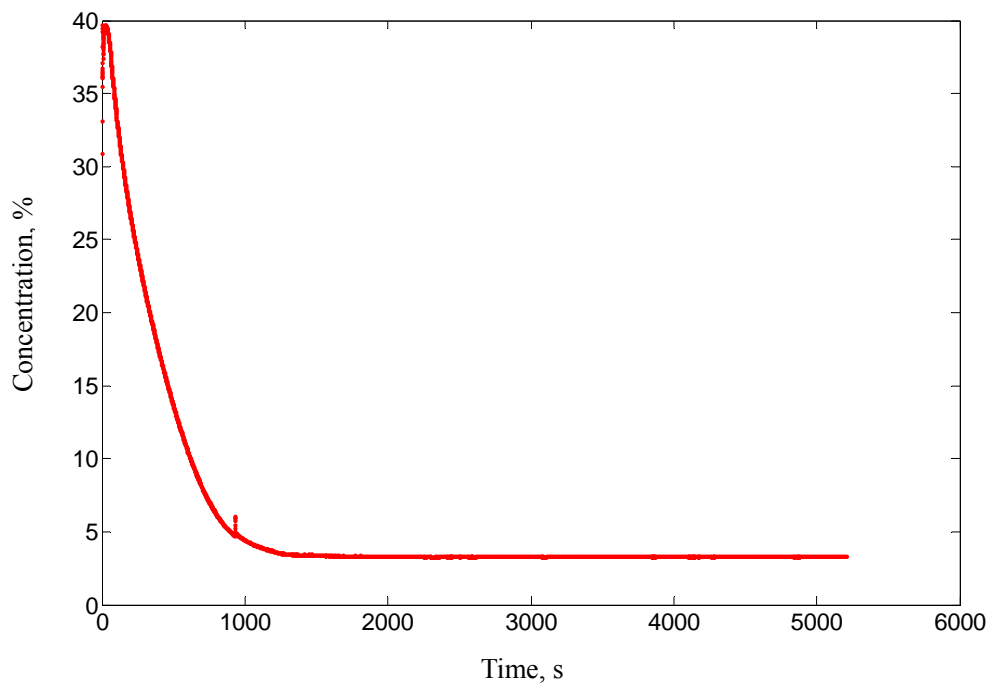
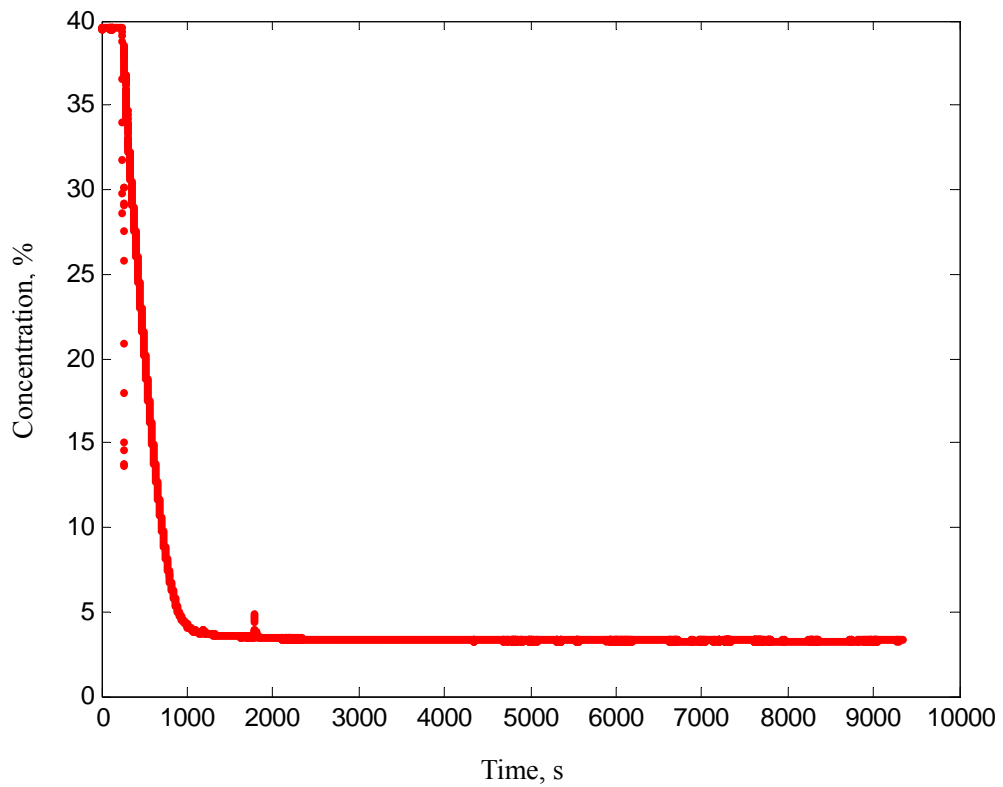


Figure 5-10 Concentration change for decomposition against time at 53.4°C



The discussion so far is about the kinetic characteristic of large pressure difference between the test rig and the condensing reservoir, which is at least 2bar. The dynamic experiments on small pressure difference are also operated at around 38°C, in which the pressures of the reactor and condensation are 4.7 and 4.5bar respectively. The concentration change against time is shown in figure 5-11. It takes around 400 minutes to complete the decomposition, which is around 20 times longer than that of large pressure difference. The change of the concentration is an exponential curve after a transition time of 250 minutes, which is also about 20 times longer than that of large pressure different. The pressure change against time is shown in figure 5-12. It shows that after the valve is open, the system pressure dropped quickly and then kept at the pressure of the condensing reservoir.

The temperature of reactor is almost kept constant even during the decomposition reaction, which was shown in figure 5-13. Due to small pressure differences between the reactor and the condensation, the time to complete decomposition becomes long. In this case, the oil bath will have enough time to keep the reactor at a constant temperature.

Figure 5-11 Concentration change for decomposition against time at 38°C

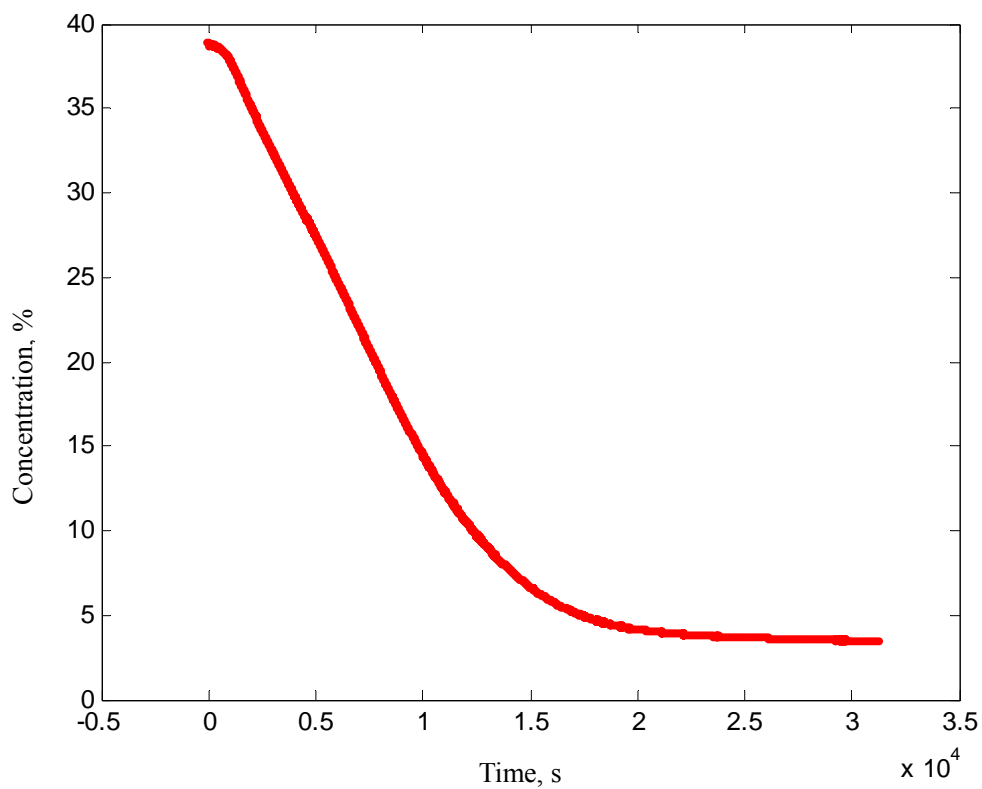


Figure 5-12 Pressure change for decomposition against time at 38°C

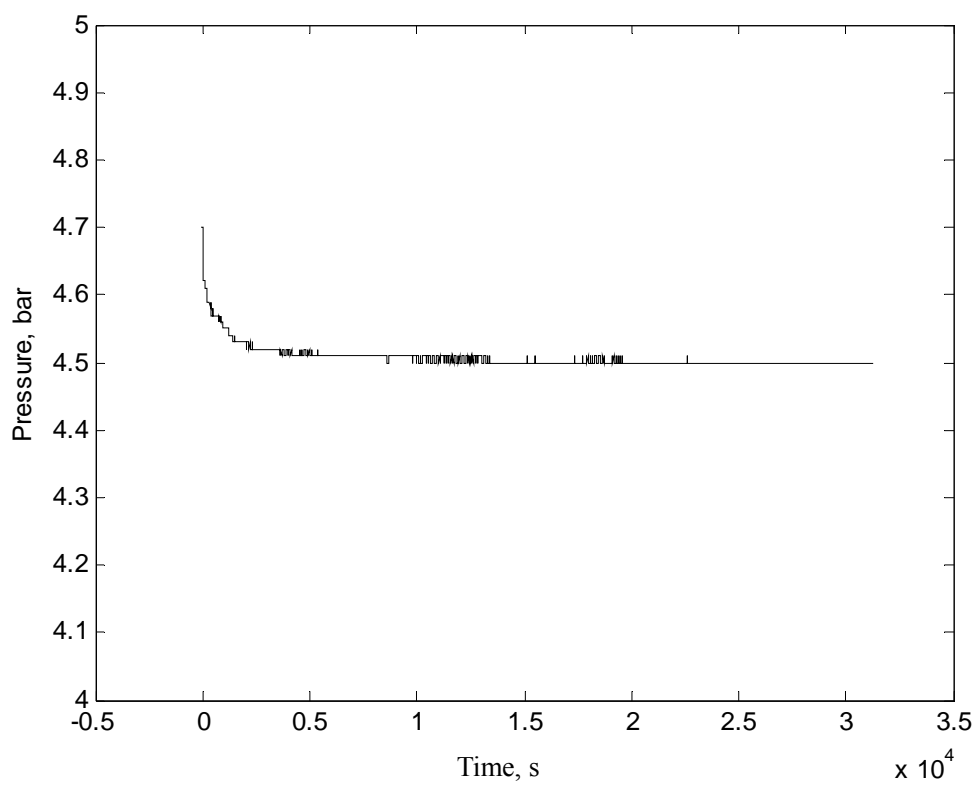
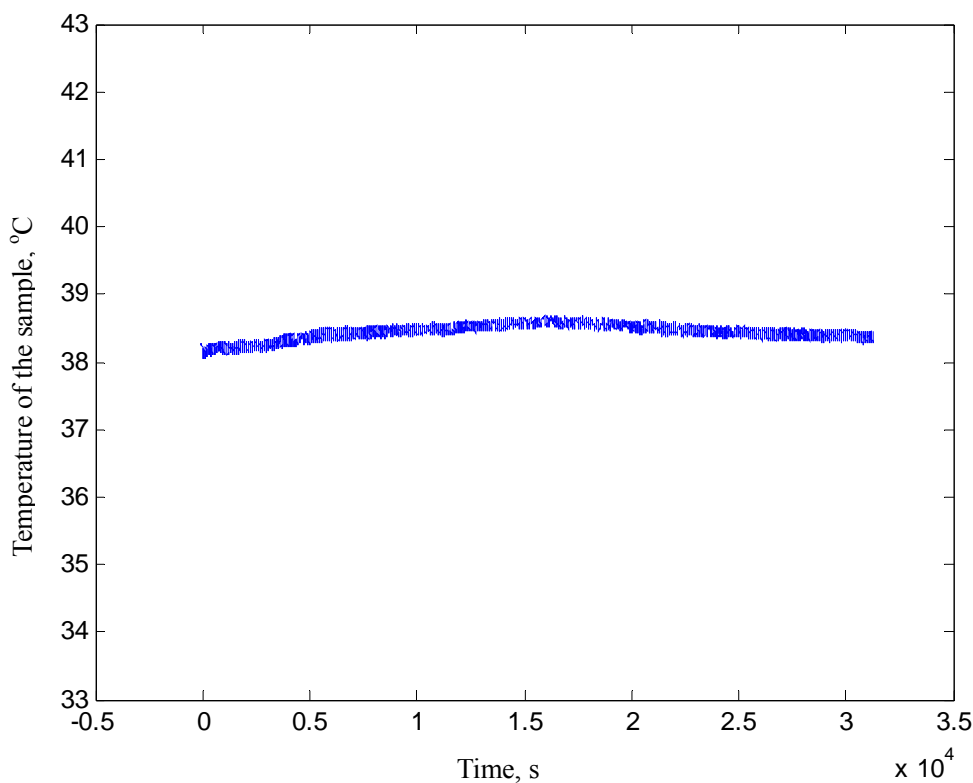


Figure 5-13 Temperature change for decomposition against time at 38°C



Similarly, the kinetic experiments for synthesis reaction are also operated at around 38 and 45°C. The concentration against time is shown in figure 5-14 and 5-15 respectively. The pressure difference between the reactor and the condensing reservoir is 6.63 and 8.25 bar respectively. The results show that it takes around 1500 seconds to complete the synthesis, which is similar for the decomposition.

The results of the kinetic experiments on $\text{BaCl}_2 - \text{NH}_3$ show that the pressure difference between the reactor and condenser plays an important role in the dynamics of adsorption pairs. The pressure difference affects the mass transfer of NH_3 through the pores of adsorbent and therefore the performance of the complete adsorption system.

Figure 5-14 Concentration change for synthesis reaction against time at 38°C

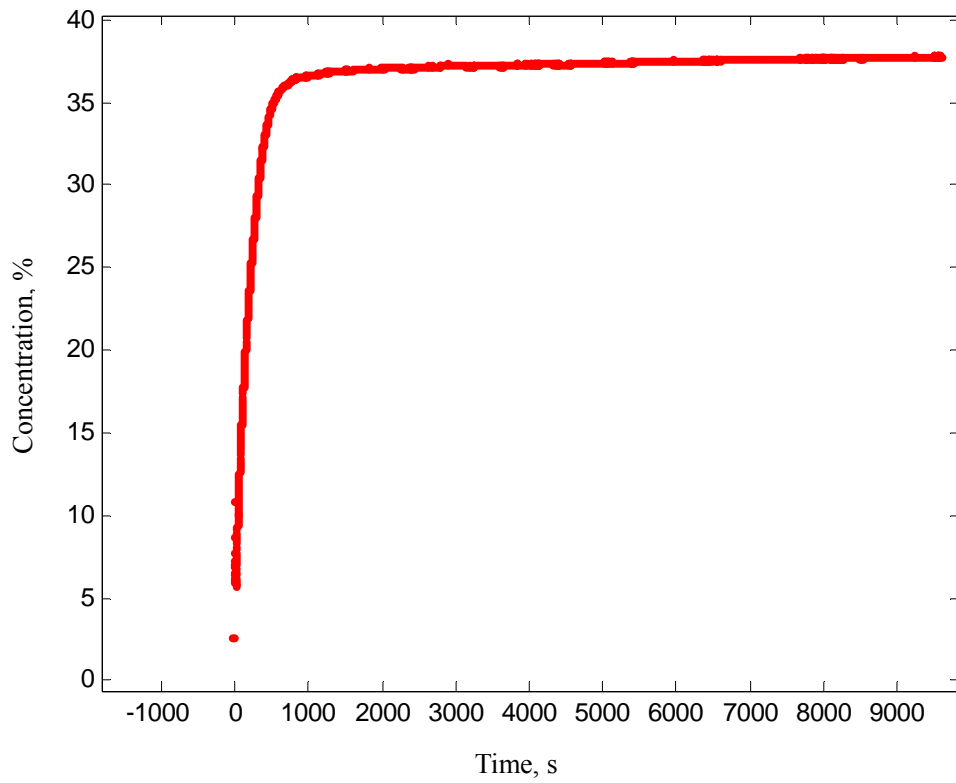
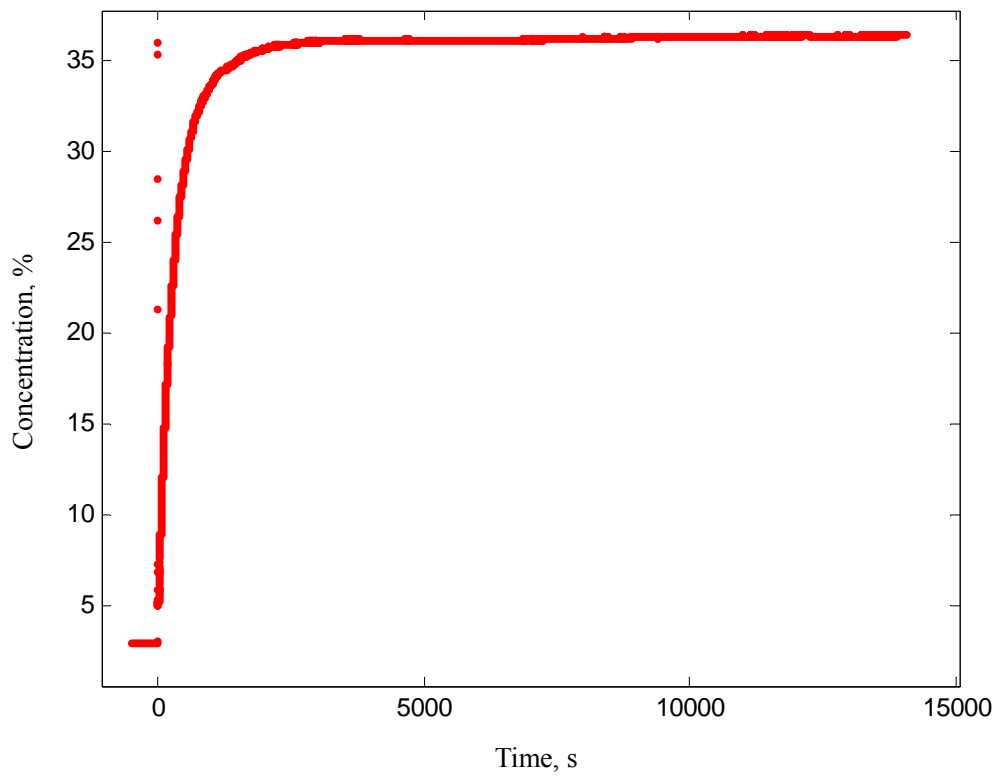


Figure 5-15 Concentration change for synthesis reaction against time at 45°C



5.4 Simulation of the dynamics of sorption in Vermiculite – BaCl₂

5.4.1 Description of the mathematical model

The design and modelling of the adsorption processes require numerical solutions of a set of partial differential equations involving time and spatial variables. The computations can be greatly simplified by using approximations for the intra-particle diffusion rates and the most frequently used models are Linear Driving Force (LDF) model and Fickian Diffusion (FD) model. Owing to its mathematical complication, analytical solution of the FD model is not practical for the simulation of a real adsorption process. The Linear Driving Force (LDF) model, on the other hand, is more suitable for practical analysis of dynamic data and for adsorptive process design because of its simple, analytical, and physically consistent.

As discussed in chapter 5.2, for a sorption process with step change in pressure at time zero, the dynamic curve only presents an exponent shape. However, a typical dynamic curve of NH₃ sorption on BaCl₂ which is presented in figure 5-8, shows the mixed shape of line and exponent that disagrees with the prediction of LDF model. The main reason is that the LDF model did not consider the chemical reaction of adsorbent and adsorbate during the sorption process. For chemisorption, the chemical reaction rate of adsorption pairs is also important as well as the diffusion of refrigerant into the adsorbent pores. To better match the experimental data, LDF

model is modified to predict the dynamics of BaCl₂ and NH₃ adsorption pair, which is given by,

$$\frac{dx}{dt} = \frac{-1}{K_1 + \frac{1}{K_2(x - x_{eq})}} \quad (5-14)$$

The experimental results show that the larger the pressure difference, the quicker the dynamic process. Therefore, the model used to describe the dynamics of sorption in vermiculite – BaCl₂ is expressed as,

$$\frac{dx}{dt} = \frac{-1}{\frac{C}{\Delta p} + \frac{1}{k(x - x_{eq})}} \quad (5-15)$$

where C is a resistant coefficient due to chemical reaction between the adsorbate and adsorbent, k is the mass transfer diffusion coefficient, x_{eq} is the final equilibrium adsorbed phase concentration, $\Delta p = p_{transition} - p$, p is the system pressure,

$p_{transition}$ is the onset pressure of the transition and given by,

$$\ln p_{transition} = 4.9767 \frac{-1000}{T} + 22.257 \quad (5-16)$$

where, T is the temperature of reaction bed.

The equation (5-15) shows that the mass transfer through the adsorbent particle is driven by two factors, one is the pressure difference and another one is the concentration difference.

Assume the two parameters are independent of the concentration, x . Then the equation

(5-15) can be written equivalently in the form,

$$dt = -dx \left[\frac{C}{\Delta p} + \frac{1}{k(x - x_{eq})} \right] \quad (5-17)$$

Integrate (5-16),

$$t|_0^\tau = - \left[\frac{Cx}{\Delta p} + \frac{1}{k} \ln(x - x_{eq}) \right]_{x_0}^x \quad (5-18)$$

$$\tau = - \frac{C}{\Delta p} (x - x_0) - \frac{1}{k} \ln \frac{x - x_{eq}}{x_0 - x_{eq}}$$

Set $X \equiv \frac{x - x_{eq}}{x_0 - x_{eq}}$, (X goes from 1 at $t=0$ to 0 at $t=\infty$)

Then $x - x_0 = (x_0 - x_{eq})(X - 1)$

So equation (5-18) becomes,

$$\tau = C \frac{\Delta x}{\Delta p} (1 - X) - \frac{1}{k} \ln X \quad (5-19)$$

where C is resistant constant, k is the mass transfer constant, $\Delta p = p_{transition} - p$, $p_{transition}$ is the onset pressure of the transition; p is the system pressure, $\Delta x = x_0 - x_{eq}$, x_0 is the initial equilibrium adsorbent phase concentration, and x_{eq} is the final equilibrium adsorbed phase concentration.

To find the reasonable range of C and k , experimental data are separated into the initial linear part and exponential part. Owing to the limitation of measuring equipment, the data in the first 25 seconds were eliminated from the fitting.

5.4.2 Data fits

The data fits of experimental data are shown in the following figures, in which the red lines are the data fits, the blue lines are the experimental data.

8/0 desorption, linear part, $t = a \frac{\Delta x}{\Delta p} (1 - X) + b$

Figure 5-16 Fitting results with $T=37.7^\circ\text{C}$, $\Delta p = 2.47\text{bar}$

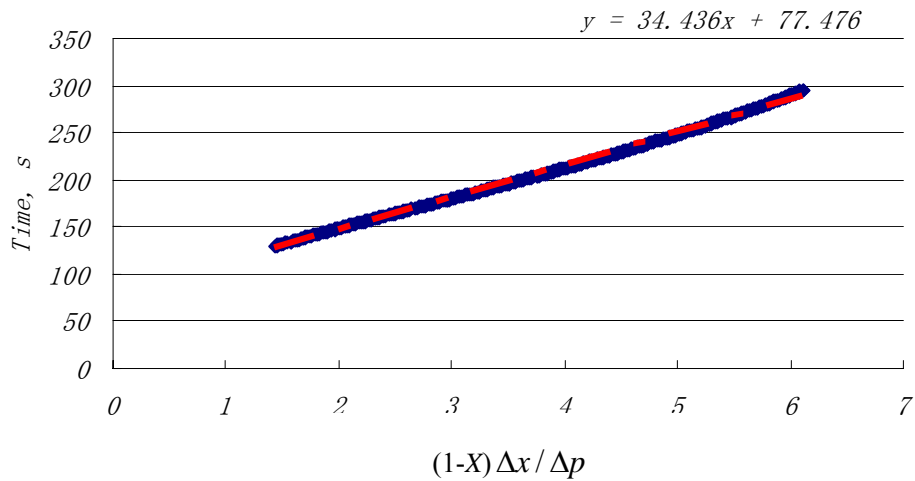


Figure 5-17 Fitting results with $T=38.2^\circ\text{C}$, $\Delta p = 0.12\text{bar}$

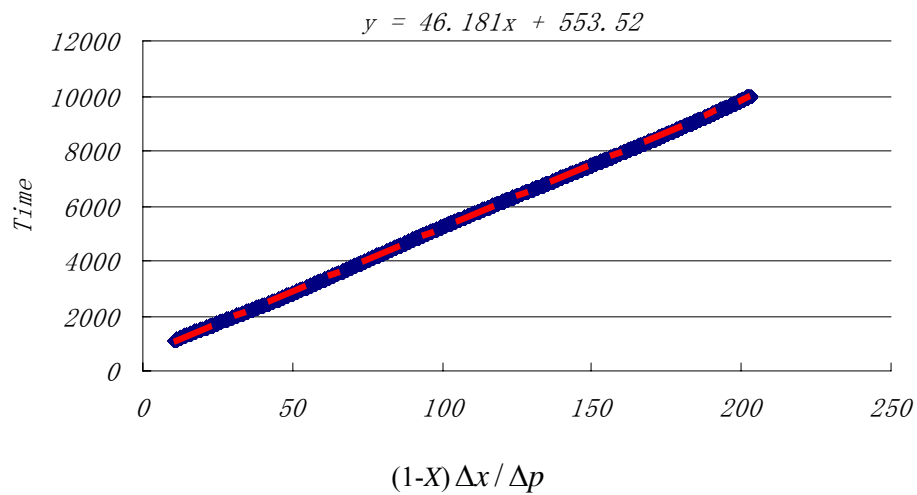


Figure 5-18 Fitting results with $T=44.8\text{ }^{\circ}\text{C}$, $\Delta p = 3.78\text{bar}$

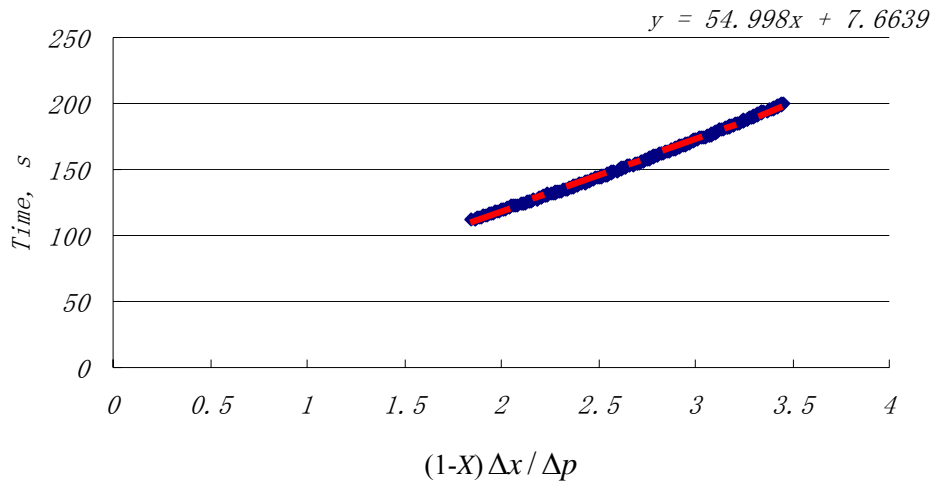


Figure 5-19 Fitting results with $T=44.65\text{ }^{\circ}\text{C}$, $\Delta p = 0.17\text{bar}$

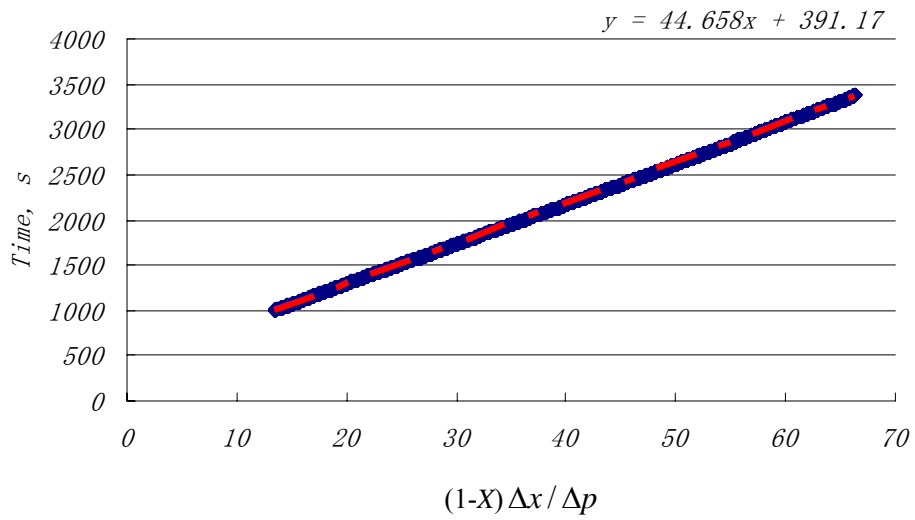


Figure 5-20 Fitting results with $T=53.4^{\circ}\text{C}$, $\Delta p = 5.4\text{bar}$

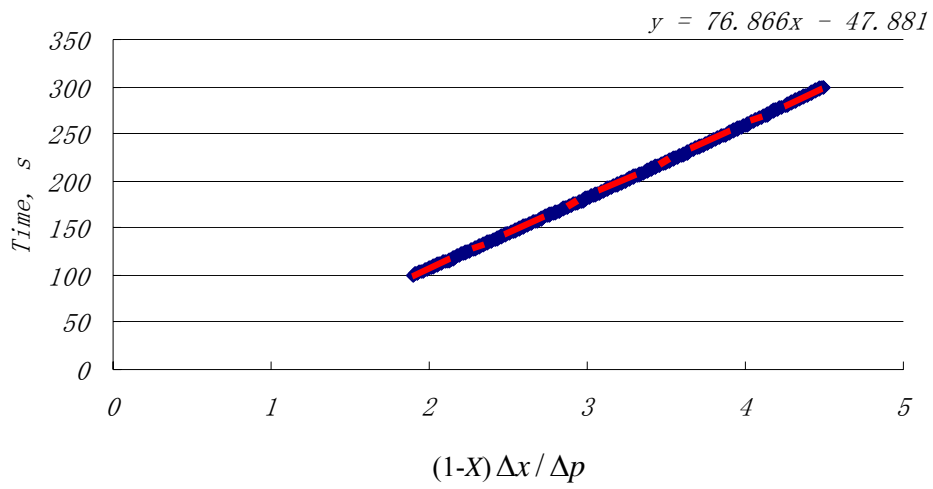


Figure 5-21 Fitting results with $T=51.4^{\circ}\text{C}$, $\Delta p = 0.1\text{bar}$

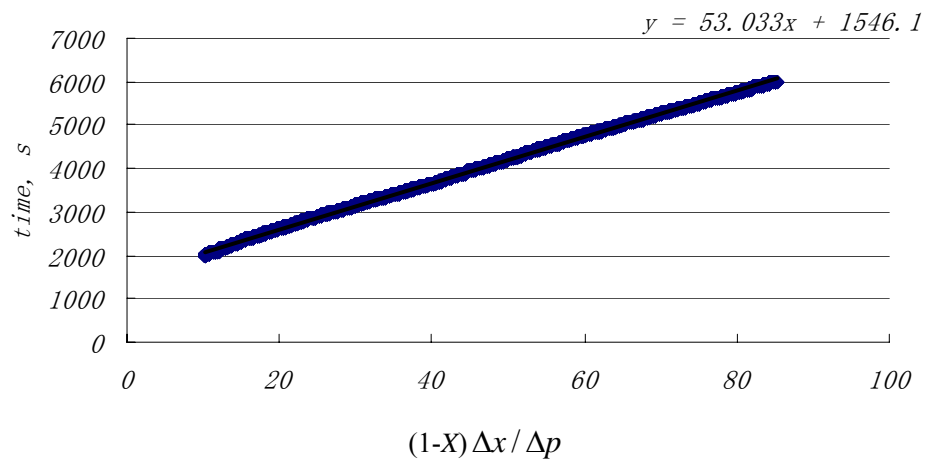


Table 5-1 Results of data fits for regression coefficient

$T, ^\circ\text{C}$	$\Delta p, \text{bar}$	<i>Regression coefficient, bar•s</i>
37.7	2.47	34.44
44.8	3.78	55
53.4	5.4	76.87
38.2	0.12	46.18
44.65	0.17	44.66
51.4	0.1	53

The results are summarized in table 5-1. From the results, we can draw a conclusion that the slopes, resistant constant (C), can be considered to be the same, which is around 50. This value is good for low pressure differences and something else happens at high pressure difference. The equation will be tested later.

8/0 desorption, exponential part, $t = K \ln X + b$

Figure 5-22 Fitting results with $T=37.7\text{ }^{\circ}\text{C}$, $\Delta p = 2.47\text{bar}$

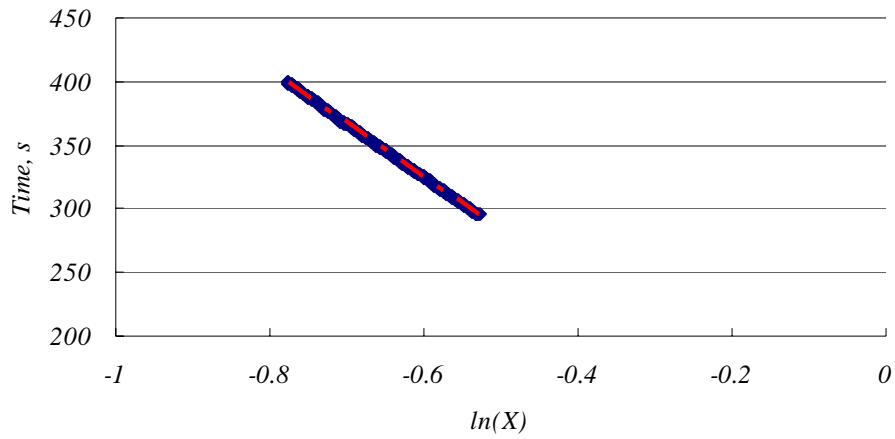


Figure 5-23 Fitting results with $T=38.2\text{ }^{\circ}\text{C}$, $\Delta p = 0.12\text{bar}$

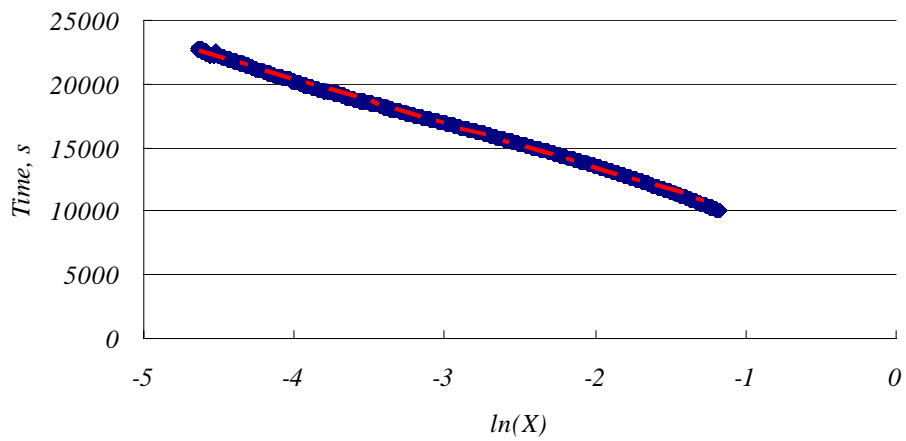


Figure 5-24 Fitting results with $T=44.8\text{ }^{\circ}\text{C}$, $\Delta p = 3.78\text{bar}$

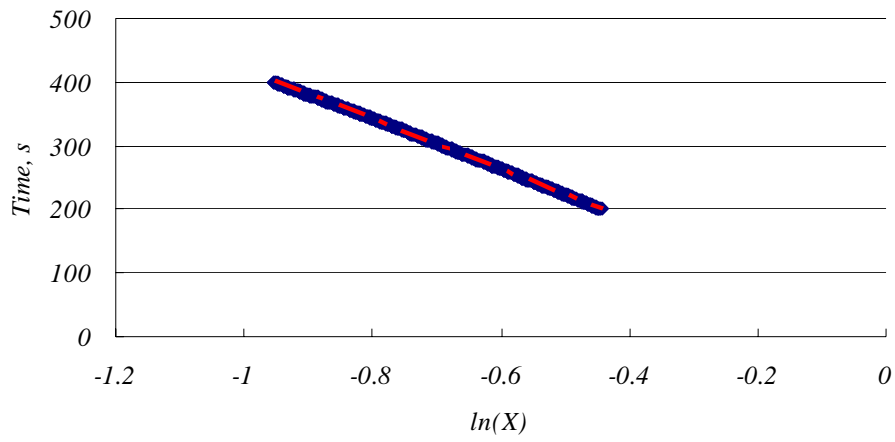


Figure 5-25 Fitting results with $T=44.65\text{ }^{\circ}\text{C}$, $\Delta p = 0.17\text{bar}$

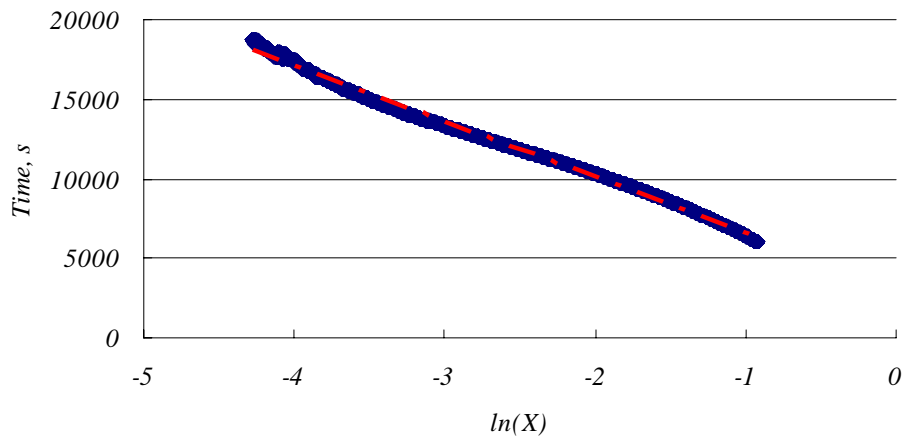


Figure 5-26 Fitting results with $T=53.4\text{ }^{\circ}\text{C}$, $\Delta p = 5.4\text{bar}$

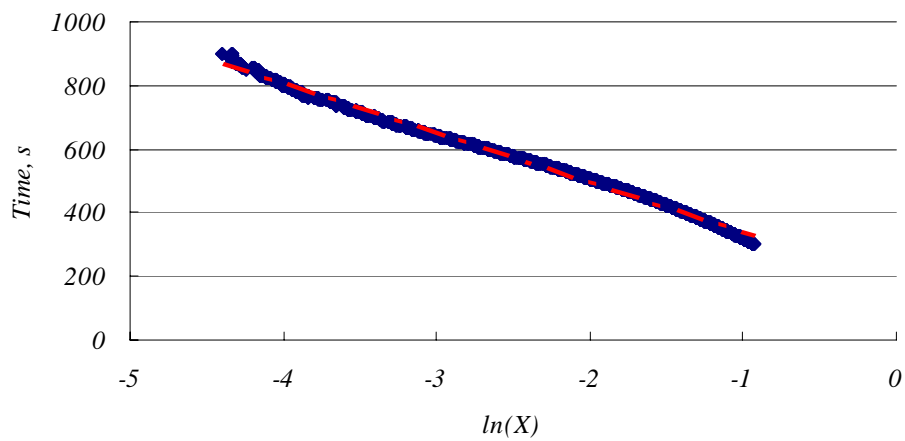


Figure 5-27 Fitting results with T=51.4 °C, $\Delta p = 0.1$ bar

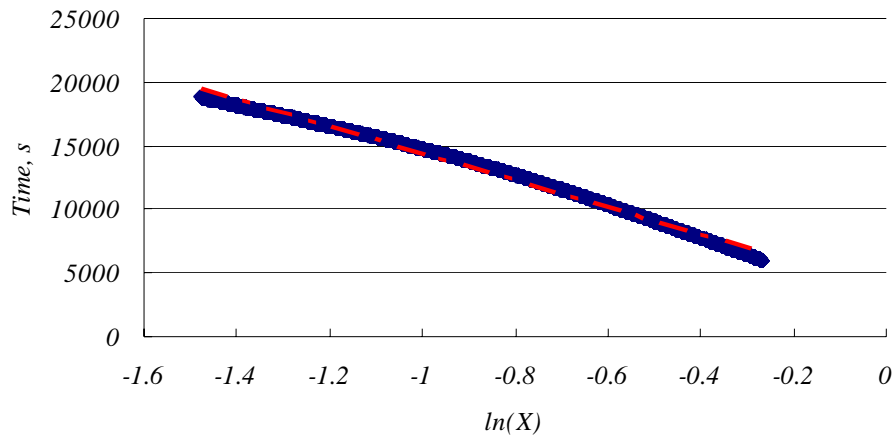


Table 5-2 Results of data fits for regression coefficient

$T, ^\circ\text{C}$	Δp	Regression coefficient, s	Regression coefficient $\times \Delta p$, bar \cdot s
37.7	2.47	-284.86	-703.6
38.2	0.12	-3488.3	-418.6
44.8	3.78	-208.12	-789.7
44.65	0.17	-3336	-567.1
53.4	5.4	-197.62	-1067
51.4	0.1	-8595.8	-859.6

From the results, we can get the conclusion that $\Delta p \times Slope$ is constant, which is set as K . In our tests, K is around -750. So, the equation can be modified as

$$t = \frac{K}{\Delta p} \ln X + b$$

0/8 adsorption, linear part, $t = a \frac{\Delta x}{\Delta p} (1 - X) + b$

Figure 5-28 Fitting results with $T=38.9\text{ }^{\circ}\text{C}$, $\Delta p = -5.88\text{bar}$

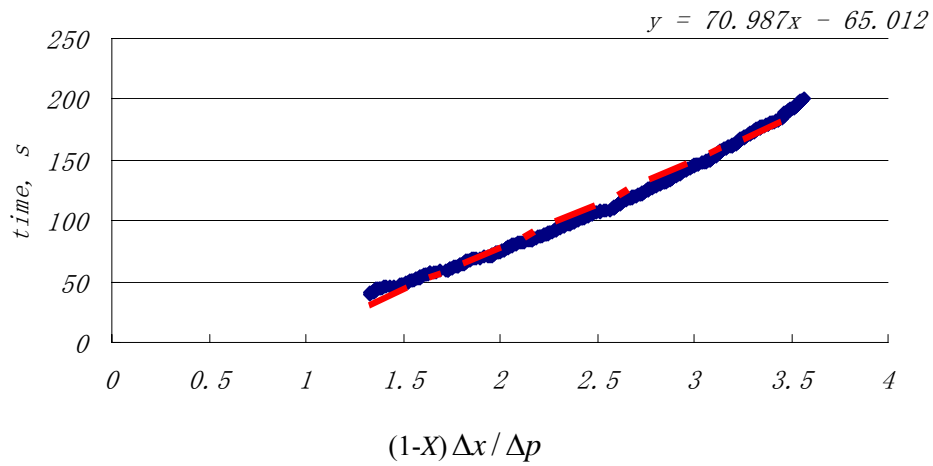


Figure 5-29 Fitting results with $T=37.9\text{ }^{\circ}\text{C}$, $\Delta p = -6.12\text{bar}$

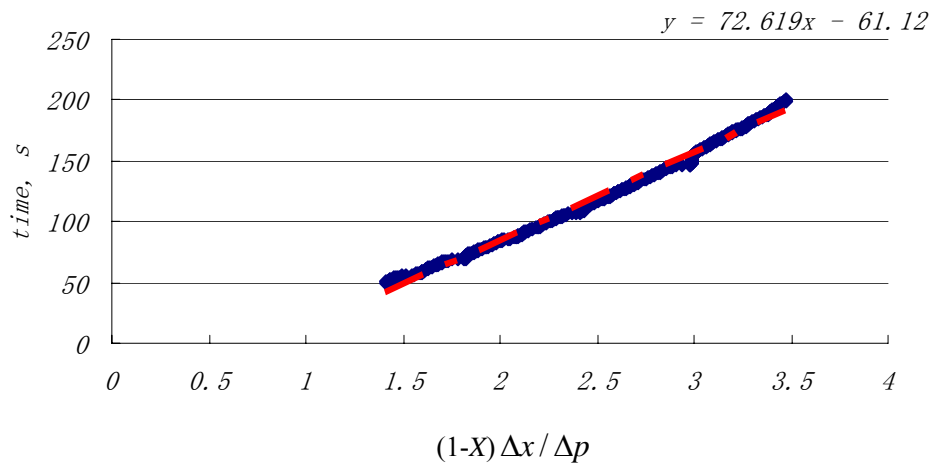


Figure 5-30 Fitting results with $T=45.5\text{ }^{\circ}\text{C}$, $\Delta p = -6.35\text{bar}$

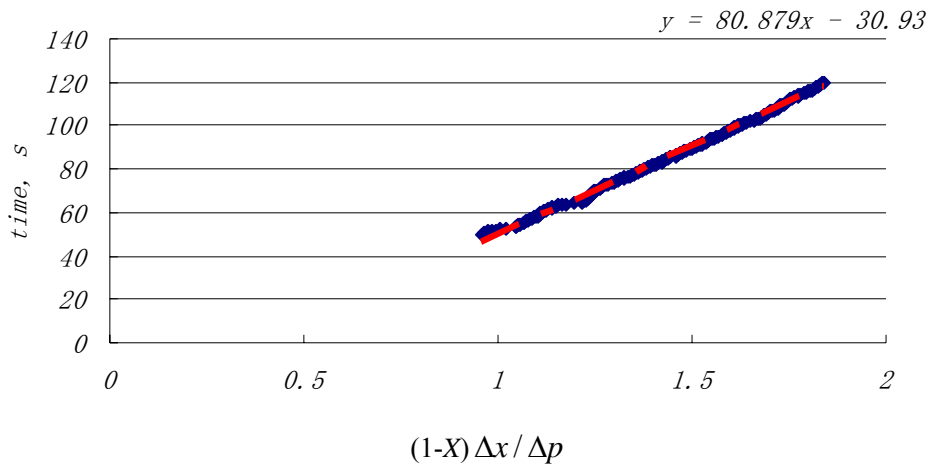


Table 5-3 Results of data fits for regression coefficient

$T, ^{\circ}\text{C}$	Δp	<i>Regression coefficient, bar•s</i>
38.9	-5.88	70.1
37.9	-6.12	72.6
45.5	-6.35	80.9

The results are summarized in table 5-3. From the results, we can draw a conclusion that the slopes, resistant constant (C), can be considered to be the same, which is around 75.

0/8 Adsorption, exponential part, $t = K \ln X + b$

Figure 5-31 Fitting results with $T=38.9\text{ }^{\circ}\text{C}$, $\Delta p = -5.88\text{bar}$

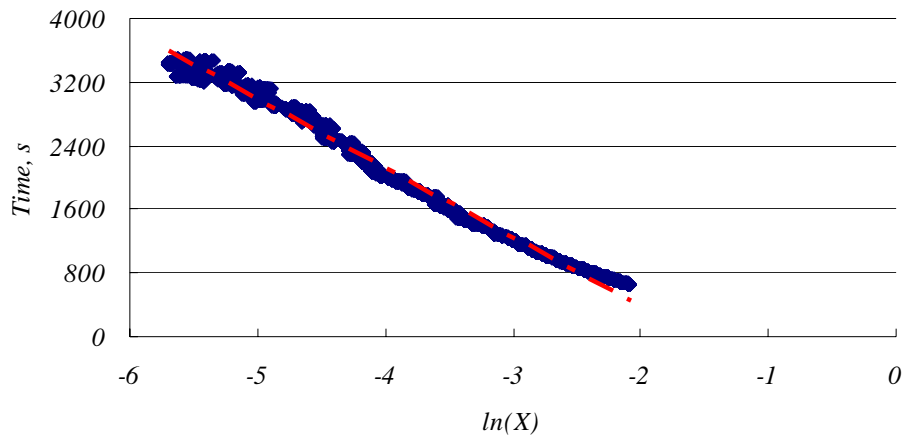


Figure 5-32 Fitting results with $T=37.9\text{ }^{\circ}\text{C}$, $\Delta p = -6.12\text{bar}$

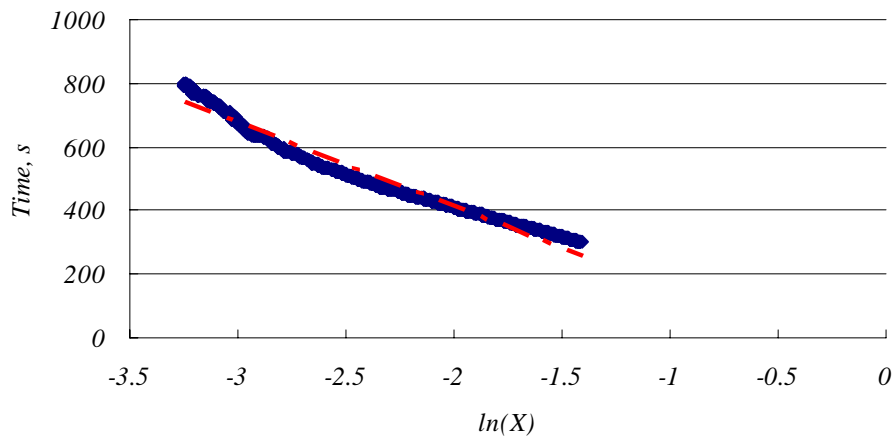


Figure 5-33 Fitting results with $T=45.5\text{ }^{\circ}\text{C}$, $\Delta p = -6.35\text{bar}$

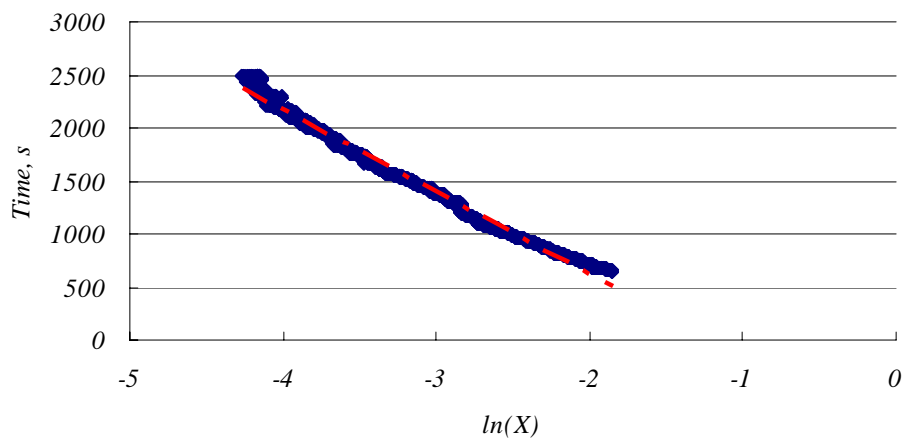


Table 5-4 Results of data fits for regression coefficient

$T, ^\circ\text{C}$	Δp	Regression coefficient, s	Regression coefficient $\times \Delta p$, bar*s
38.9	-5.88	-869.9	5115
37.9	-6.12	-819.9	5017.8
45.5	-6.35	-780.44	4955

From the results shown in table 5-4, we can get the conclusion that $\Delta p \times Slope$ is constant, which is set as K . In our tests, K is around 5000. So, the equation can be modified as

$$t = \frac{K}{\Delta p} \ln X + b$$

The resistant constant, C , and the mass transfer coefficient, K , from fitting the experimental data in above discussion just provide a reasonable range. For the whole experimental data, the C and K obtained above may not be applicable. By manually adjust the value, the best C and K is chosen to describe the dynamics of BaCl_2 and NH_3 .

In summary, the following equation is used to describe the dynamics of BaCl_2 and NH_3 ,

For adsorption,

$$\frac{\partial x}{\partial t} = \frac{p - p_{transition}}{C_{ad} + \frac{K_{ad}}{x - x_{eq}}} \quad (5-20)$$

For desorption

$$\frac{\partial x}{\partial t} = \frac{p - p_{transition}}{C_{de} + \frac{K_{de}}{x - x_{eq}}} \quad (5-21)$$

where,

C_{ad} - resistant constant during adsorption process, for $\text{NH}_3/\text{BaCl}_2$, $C_{ad} = 50$, bar•s

C_{de} - resistant constant during desorption process, for $\text{NH}_3/\text{BaCl}_2$, $C_{de} = 30$, bar•s

K_{ad} - mass transfer coefficient during adsorption process, for $\text{NH}_3/\text{BaCl}_2$,

$$K_{ad} = -2500, \text{ bar}\cdot\text{s}$$

K_{de} - mass transfer coefficient during desorption process, for $\text{NH}_3/\text{BaCl}_2$,

$$K_{de} = 500, \text{ bar}\cdot\text{s}$$

x - Ammonia mass concentration, kg ammonia / kg BaCl_2

x_{eq} - Ammonia mass concentration after adsorption/desorption, kg ammonia / kg BaCl_2

p - System pressure, bar

$p_{transition}$ - Pressure of the onset of 0/8 adsorption and 8/0 desorption transition, bar

The following figures are the comparison between experimental data and simulation, in which the black lines are the simulated results and the red lines represent the experimental data.

8/0 desorption: $C=30, K=500$

Figure 5-34 Comparison of experimental data and simulation at $T=37.7^{\circ}\text{C}$,

$\Delta p = 2.47\text{bar}$

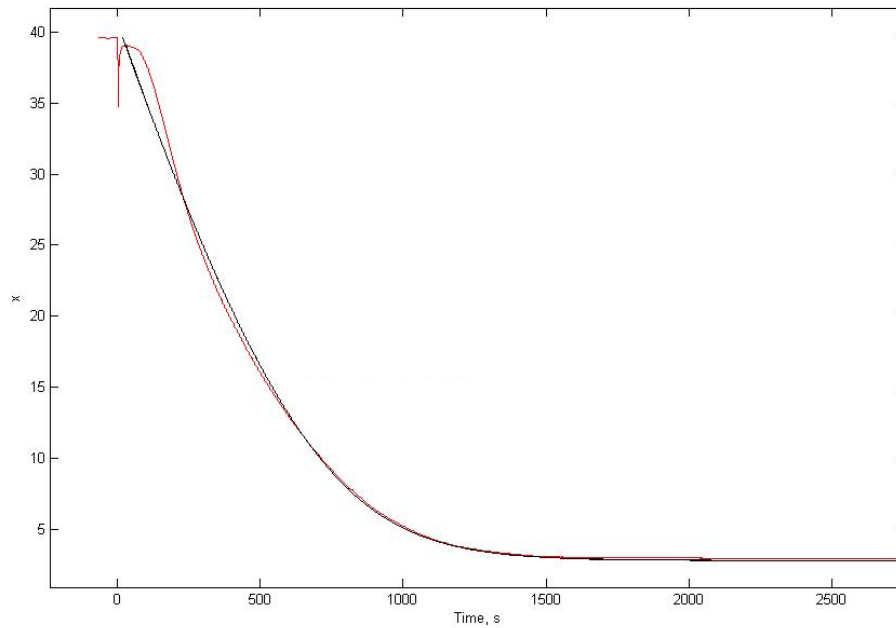


Figure 5-35 Comparison of experimental data and simulation at $T=38.2^{\circ}\text{C}$,
 $\Delta p = 0.12\text{bar}$

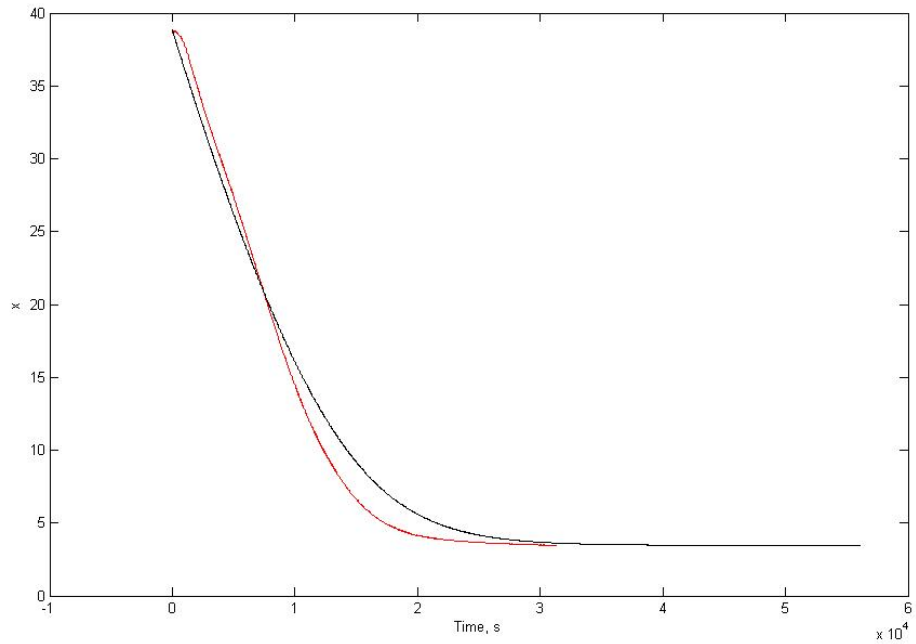


Figure 5-36 Comparison of experimental data and simulation at $T=44.8^{\circ}\text{C}$,
 $\Delta p = 3.78\text{bar}$

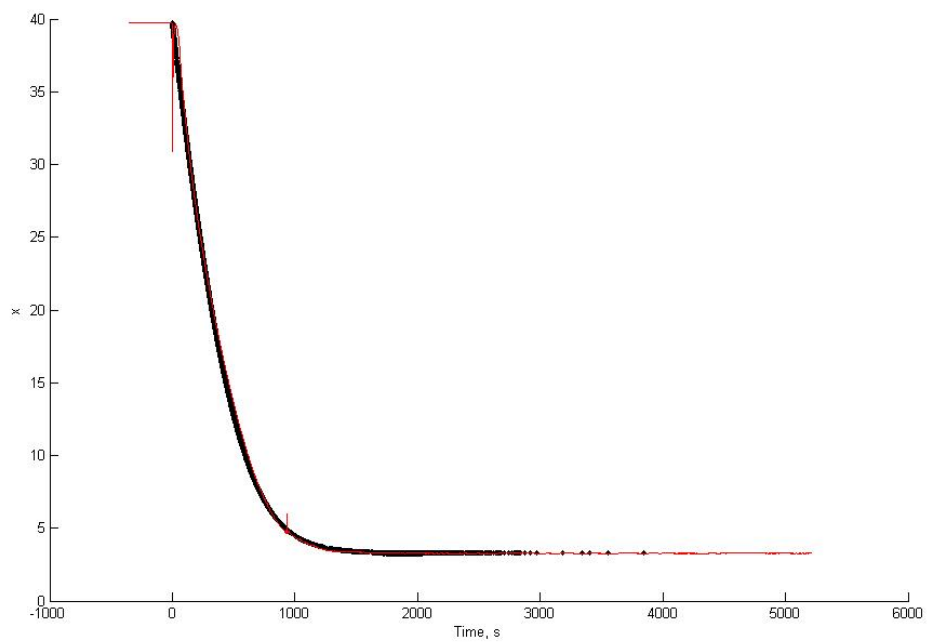


Figure 5-37 Comparison of experimental data and simulation at $T=44.65^{\circ}\text{C}$,
 $\Delta p = 0.17\text{bar}$

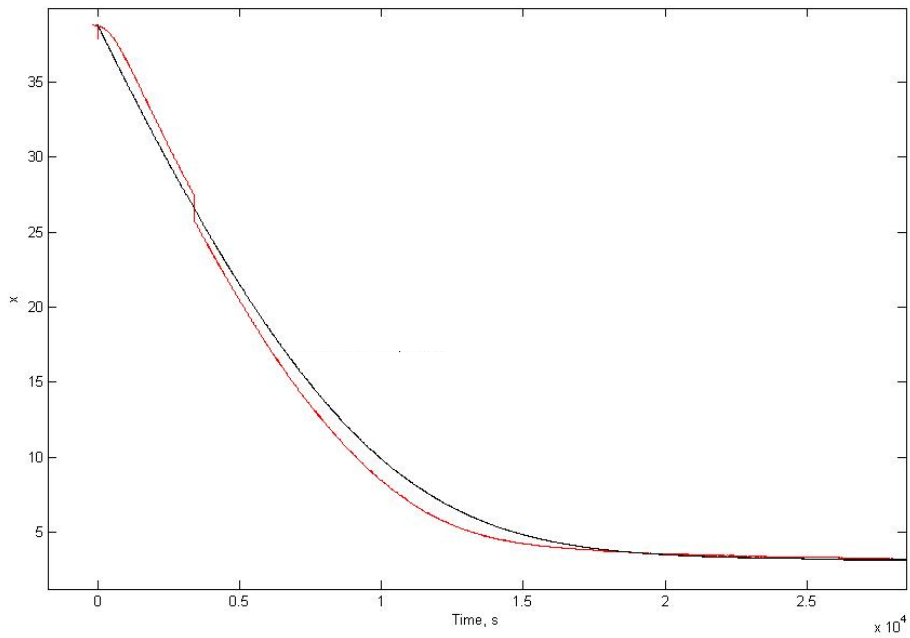
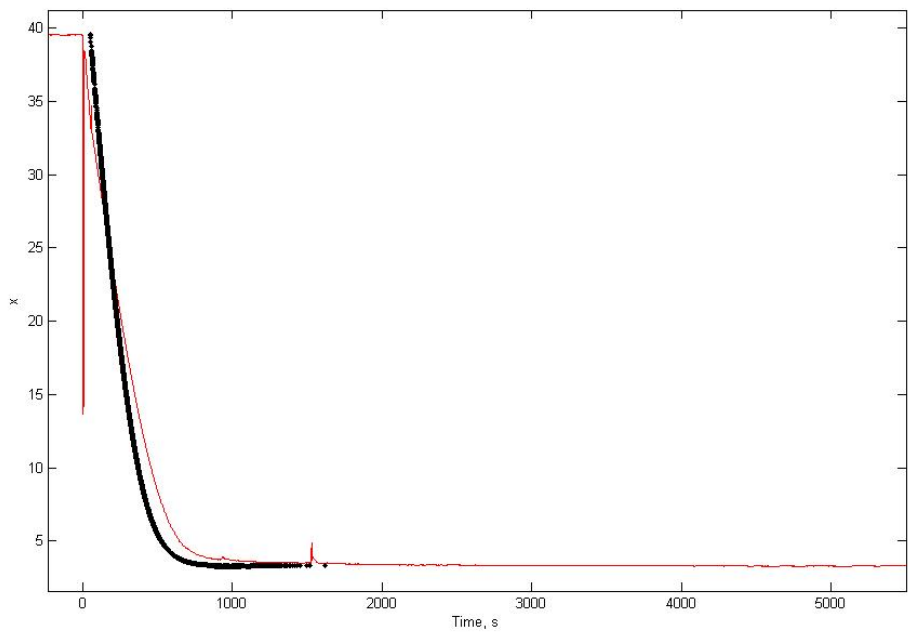


Figure 5-38 Comparison of experimental data and simulation at $T=53.4^{\circ}\text{C}$,
 $\Delta p = 5.4\text{bar}$



0/8 adsorption: $C=50, K=-2500$

Figure 5-39 Comparison of experimental data and simulation at $T=38.9^{\circ}\text{C}$,

$\Delta p = -5.88\text{bar}$

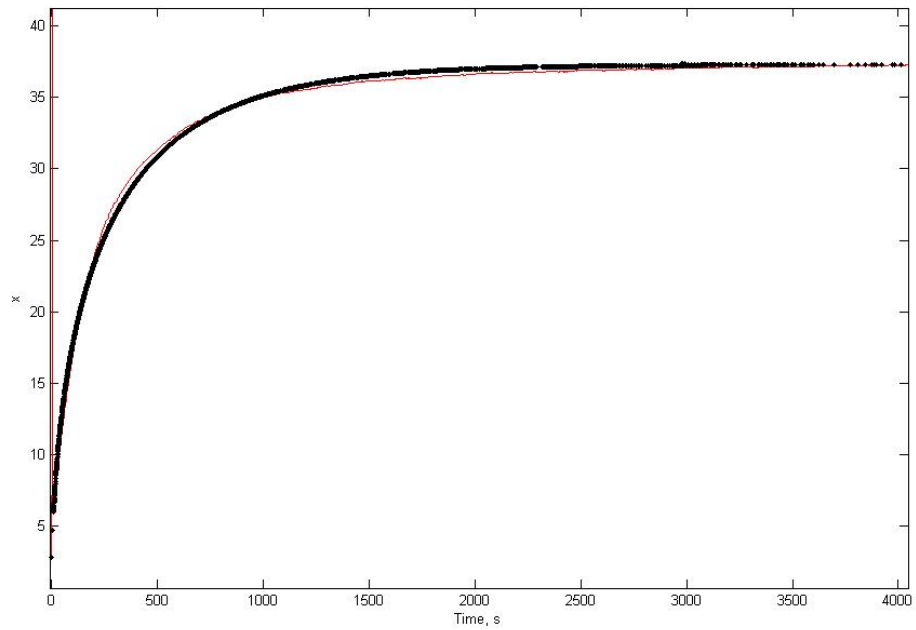


Figure 5-40 Comparison of experimental data and simulation at $T=37.9^{\circ}\text{C}$,

$\Delta p = -6.12\text{bar}$

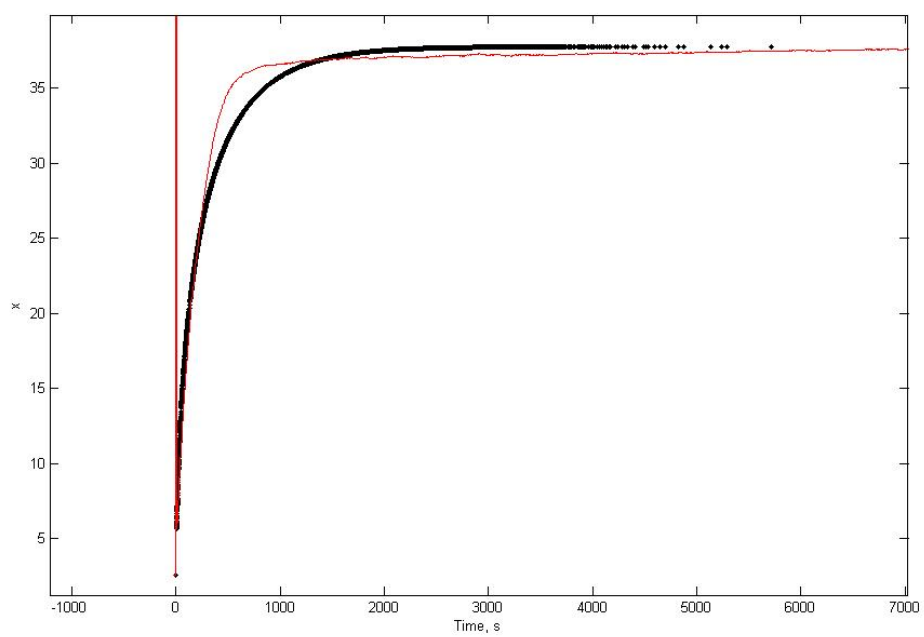
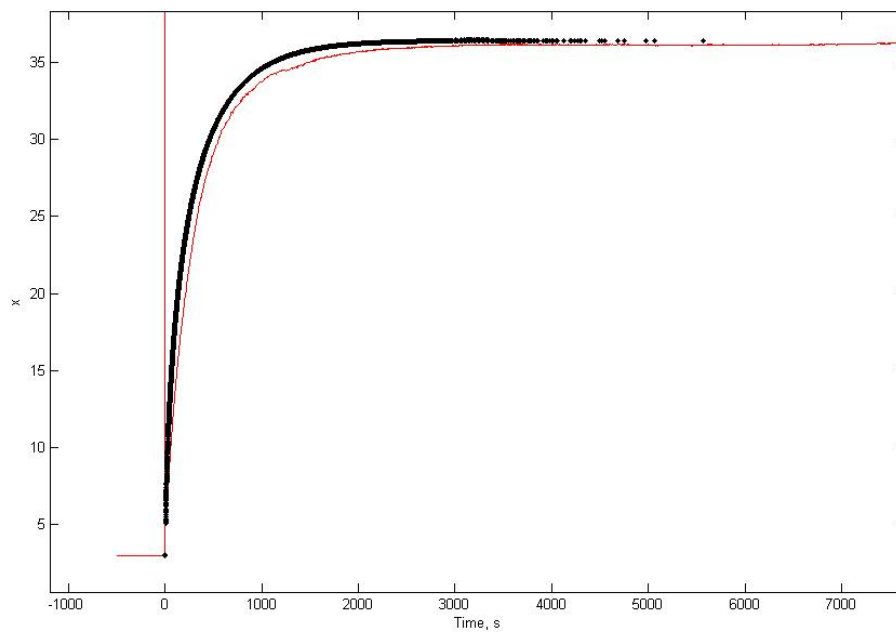


Figure 5-41 Comparison of experimental data and simulation at $T=45.5^{\circ}\text{C}$,
 $\Delta p = -6.35\text{bar}$



From the figures above, we can draw the conclusion that the mathematic model described in equation (5-20) and (5-21) can be used to predict the dynamics of BaCl_2 and NH_3 under isothermal conditions. The validity of the model will be tested out for a real adsorption system.

Reference:

- [1] C.H. Liaw, J.S.P. Wang, R.H. Greenkorn, and K.C. Chao, Kinetics of fixed bed adsorption: a new solution, *AIChE Journal*, vol.25, p.376, 1979
- [2] M.A. Buzanowski, R.T. Yang, Extended linear driving force approximation for intraparticle diffusion rate including short times, *Chemical Engineering Science*, vol.44(11), pp.2683 – 2689, 1989
- [3] B. Dawoud, Yu.I. Aristov, Experimental study on the kinetics of water vapor sorption on selective water sorbents, silica gel and alumina under typical operating conditions of sorption heat pumps, *International Journal of Heat and Mass Transfer*, vol.46, pp.273–281, 2003
- [4] Yu.I. Aristov, I.S. Glaznev, A. Freni , G. Restuccia, Kinetics of water sorption on SWS-1L (calcium chloride confined to mesoporous silica gel): Influence of grain size and temperature, *Chemical Engineering Science*, vol.61, pp.1453 – 1458, 2006
- [5] Z. Aidoun, M. Ternan, The synthesis reaction in a chemical heat pump reactor filled with chloride salt impregnated carbon fibres: the $\text{NH}_3\text{-CoCl}_2$ system, *Applied Thermal Engineering*, vol.22, pp.1943–1954, 2002
- [6] Z. Aidoun, M. Ternan, The unsteady state overall heat transfer coefficient in a chemical heat pump reactor: the $\text{NH}_3\text{-CoCl}_2$ system, *Chemical Engineering Science*, vol.59, pp.4023 – 4031, 2004
- [7] B. Dawoud, Yu.I. Aristov, Experimental study on the kinetics of water vapour

- sorption on selective water sorbents, silica-gels and alumina under typical operating conditions of sorption heat pumps. *Int.J.Heat & Mass Transfer*, vol.46(2), pp. 273-281, 2003
- [8] J.Kaerger, D.M.Ruthven, *Diffusion in zeolites and other microporous solids*, J.Willy, N.Y., 1992.
- [9] S. Sircar, J.R. Hufton, Why Does the Linear Driving Force Model for Adsorption Kinetics Work?, *Adsorption*, vol.6, pp.137–147, 2000
- [10] J. Crank, *Mathematics of Diffusion*, Oxford University Press, London, 1956
- [11] D.M. Ruthven, *Principles of Adsorption and Adsorption Processes*.Wiley, New York, 1984.
- [12] R.M. Rynders, M.B. Rao, and S. Sircar, Isotope Exchange Technique for Measurement of Gas Adsorption Equilibria and Kinetics, *AIChE J.*, vol.43, pp.2456–2470, 1997
- [13] R.J. Mohr, D. Vorkapic, M.B. Rao, and S. Sircar, Pure and Binary Gas Adsorption Equilibria and Kinetics of Methane and Nitrogen on 4A Zeolite by Isotope Exchange Technique, *Adsorption*, vol.5, pp.145–158, 1999
- [14] T. Vermeulen, Theory for Irreversible and Constant Pattern Solid Diffusion, *Ind. Eng. Chem.*, vol.45, pp.1664–1670, 1953
- [15] Y.I. Aristov, M.M. Tokarev, A. Freni, Restuccia, G., Comparative Study of Water Adsorption on Microporous Silica and SWS-1L: Equilibrium and Kinetics, International Sorption Heat Pump Conference, June 22-24, 2005; Denver, USA

- [16] K. Chihara, M. Suzuki, Air Drying by Pressure Swing Adsorption, J. Chem.Engn. Jpn., vol.16, pp.293-299, 1983
- [17] E. Glueckauf, Theory of chromatography, Part 10. Formula for diffusion into spheres and their application to chromatography, Trans. Faraday Soc., vol.51, pp.155-1551, 1955
- [18] J.H. Hills, An investigation of the linear driving force approximation to diffusion in spherical particles, Chem. Engng Sci., vol.41, pp.2779-2785, 1986
- [19] R.T. Yang, Gas Separation by Adsorption Processes, Butterworth, Boston, MA., 1987,
- [20] C.M. Liaw, J.S.P. Wang, R.A. Greenkorn, and K.C. Chao, Kinetics of fixed-bed adsorption: a new solution, A.I.Ch.E. J., vol.25, pp.376-381, 1979
- [21] T. Vermeulen, Theory for irreversible and constant pattern solid diffusion, Ind. Engng Chem., vol.45(1), pp.1665-1670, 1953
- [22] T. Vermeulen, and R.E. Quilici, Analytic driving-force relation for pore-diffusion kinetics in fixed-bed adsorption, Ind. Engng Chem. Fundam., vol.9, pp.179-180, 1970
- [23] D.D. Do, and R.G. Rice, Validity of the parabolic profile assumption in adsorption studies, A.I.Ch.E. J., vol.32, pp.149-154, 1986
- [24] D.D. Do, and P.L.J. Mayfield, A new simplified model for adsorption in a single particle, A.I.Ch.E. J., vol.33, pp.1397-1400, 1987
- [25] E. Glueckauf, Theory of chromatography, Part 10, Formula for diffusion into

- spheres and their application to chromatography, Transactions of the Faraday Society, vol.51, pp. 1540 – 1551, 1955
- [26] V.E. Sharonov, J.V. Veselovskaya, Yu.I. Aristov, Y. Zhong, R.E. Critoph, New composite adsorbent of ammonia “BaCl₂ in vermiculate” for adsorptive cooling, CHP (2006), Proc. HPC06, Newcastle, 2006
- [27] S. Nakao, M. Suzuki, Mass transfer coefficient in cyclic adsorption and desorption, J. them. Engineering Japan 16, pp. 114-119, 1983
- [28] D.W. Hand, J.C. Crittenden, W.E. Thacker, Simplified models for design of fixed-bed adsorbers, Journal of Env. Eng. Div., Proceedings of ASCE, 110 (EE2), 1984

Chapter 6 Dynamics of Vermiculite – BaCl₂ in a Lab-Scale Adsorption System

6.1 Introduction

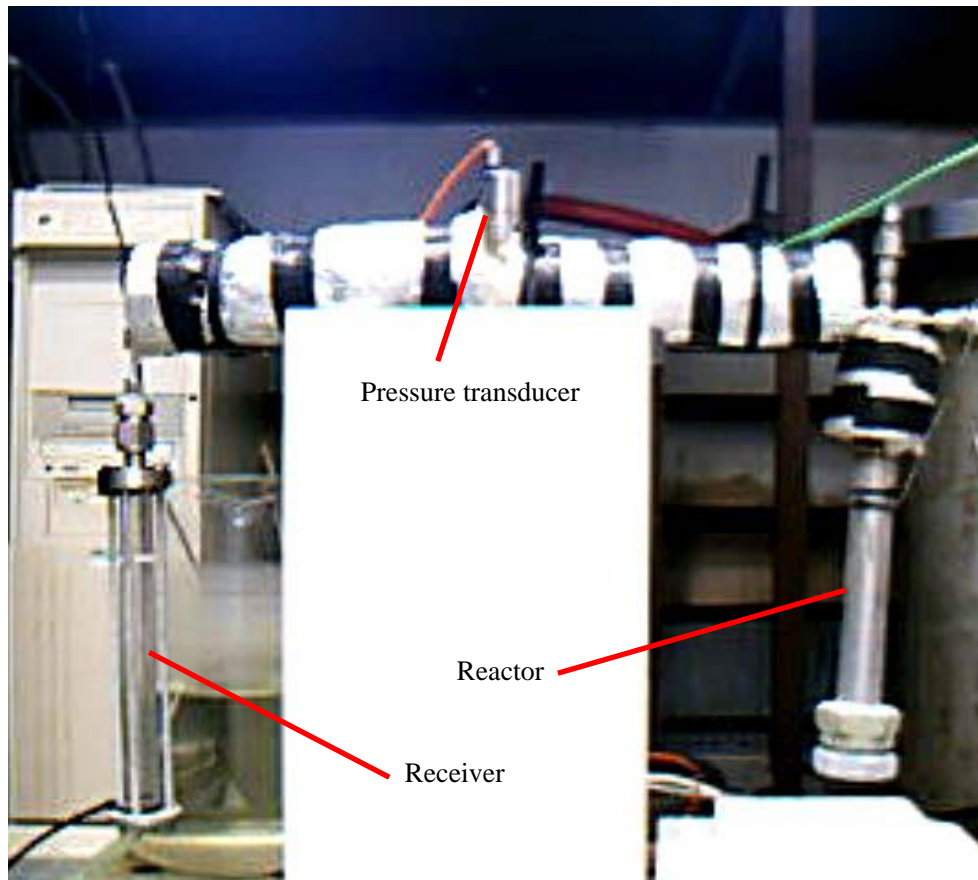
The study on dynamics in chapter 5 provided useful information for the kinetics of real adsorption systems and the mathematical model fitted well with the experimental data. However, during the experiments, the reactor was kept isothermal, which is not consistent with real adsorption systems. The accuracy of this model is still worth testing out for a real adsorption system.

This chapter focused on the dynamics of an experimental scale adsorption system utilizing hybrid material (BaCl₂ . vermiculite) and ammonia as adsorption pair. Adsorption and desorption dynamic data are collected and analyzed. A Matlab program is used to simulate the dynamics of the adsorption system. The measured reactor temperature and the concentration are compared with the simulated results.

6.2 Test rig description

The experimental rig consists of a reactor connected with a receiver and three water thermal baths, which are maintained at around 20°C (receiver water bath), 100°C (desorption water bath) and 20°C (adsorption water bath) respectively under atmospheric pressure. Four *K*-type thermocouples (two on the generator, which are placed in the centre and on the tube outer wall respectively; another one is placed on receiver outer wall, the other one is placed in the hot water bath) and a pressure transducer which is used to monitor the pressure within the generator are linked to a PC via an interface (Data Shuttle DA-16-TC-AO). A program written with Workbench 2.3 is used to monitor and record the temperatures and the pressure. The photograph and schematic diagram of the set-up are shown in figure 6-1 and 6-2.

Figure 6-1 Photograph of the test rig



In order to measure the amount of liquid collected during the dynamic test, a glass pressure tubing receiver (20mm OD and 12mm ID; water pressure tested in lab under 40bar at 20°C) supplied by Chemistry store in University of Warwick was manufactured by Engineering workshops and is connected with the generator. The schematic diagram of the receiver is shown in figure 6-3. The mass of ammonia collected in the receiver can be calculated by,

$$m = 36\pi\rho_{NH_3} 10^{-6} \Delta h \quad (6-1)$$

Where, m is the mass of ammonia collected in the receiver (g); ρ_{NH_3} is the density of ammonia liquid, Δh is the height of ammonia liquid level (mm).

Figure 6-2 Schematic diagram of the test rig

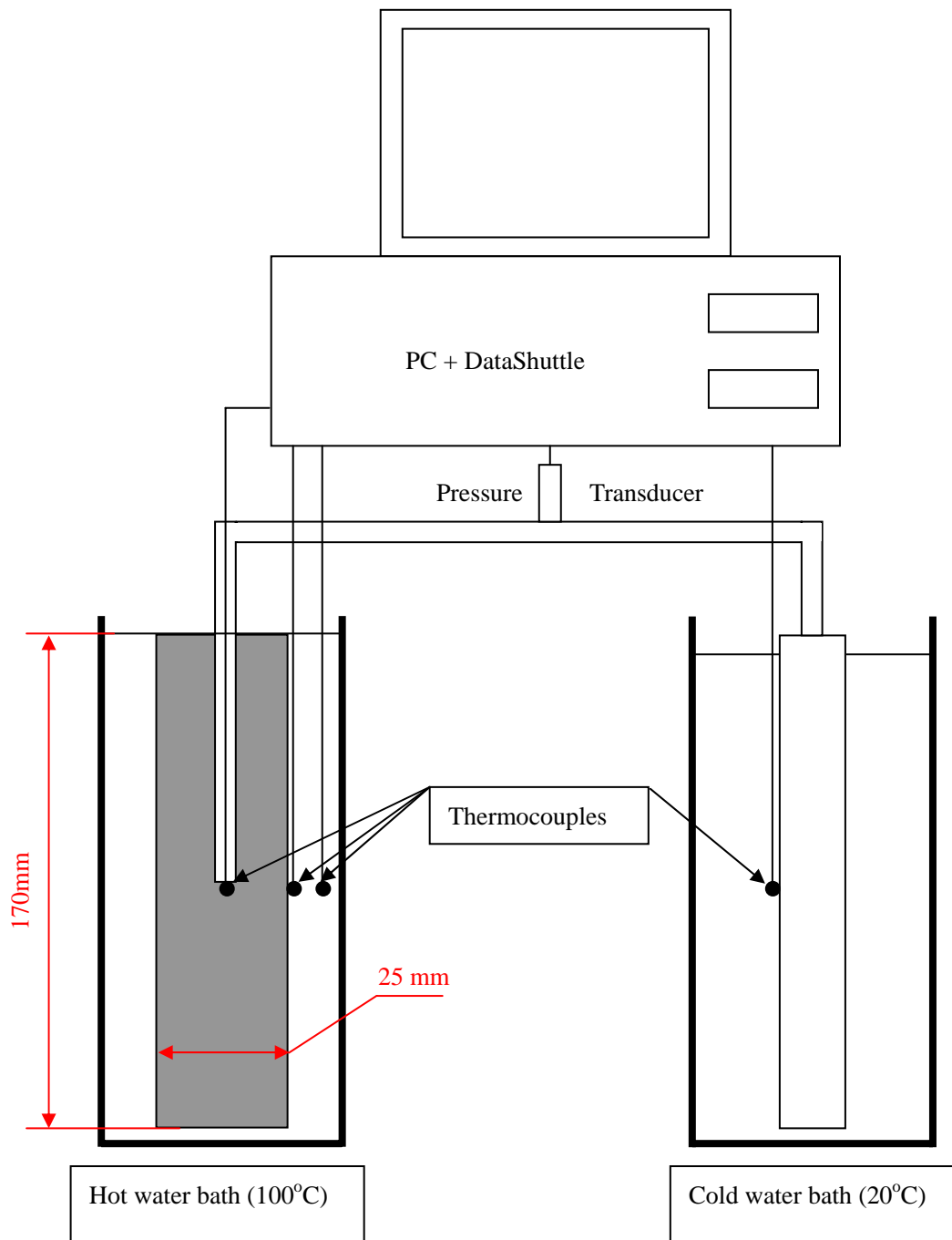
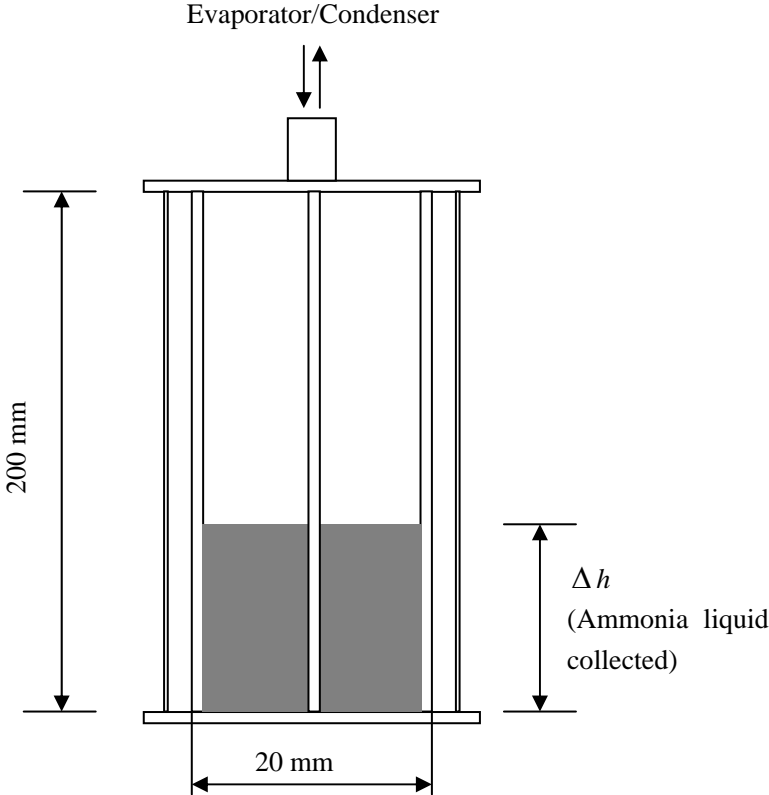


Figure 6-3 Schematic diagram of the glass tubing ammonia receiver



6.3 Test procedure and conditions

Initially, the test generator was at ambient temperature (typically 22°C). After long time (typically 16 hours) the system reaches equilibrium state and the test sample in the generator adsorbed the maximum amount of ammonia. Then the reactor was submerged suddenly into the boiling water bath (at about 100°C). The pressure and temperatures were recorded for the desorption procedure. After around 1 hour almost all of the ammonia in the reactor was desorbed and condensed in the receiver. The reactor was placed suddenly from hot water bath to cold water bath (at around 20°C) and the adsorption dynamic test was started. During the dynamic tests, the receiver was kept at around 20°C, controlled by the cold water bath. The pressure and temperatures were recorded at the rate of 5 data points/seconds during the experiments.

A one-dimensional transient heat conduction generator model was used to simulate the dynamics of the set-up. The thermal conductivity of the bed and the contact heat transfer coefficient between the bed and the tube wall were set to be 0.2 and 150 W/ (m K) [1]. The explicit scheme of finite difference was used in the modelling. The program was written in Matlab 7, which is shown in appendix E. To simplify the simulation, the pressure in a single control volume was assumed to be uniform. Therefore, the bed pressure was uniform and the resistance of mass diffusion through the sample pore in the reactor was neglected. The equations used to monitor the transient sorption characteristics were heat and mass conservation and the sorption dynamic equation.

The transient heat and mass transfer is given by the following equation:

$$\left[\rho_s r \Delta \theta \Delta z \Delta r (C_{ps} + C_{pa} x) + m_g C_{pg} \right] \frac{\partial T}{\partial t} = k_s A \frac{\partial T}{\partial r} - H \frac{\partial m_a}{\partial t} \quad (6-2)$$

where:

ρ_s is the sample density, kg/m³

r is the position of the sample cell from the centre, m

$\Delta \theta$ is the increment in angle, rad, for our one-dimensional models, $\Delta \theta = 2\pi$

Δz is the increment in height, m

Δr is the increment in radius, m

C_{ps} is the specific heat of the sample, J/(kg K)

C_{pa} is the specific heat of adsorbed ammonia, J/(kg K)

T is the sample temperature, K

t is the time, s

m_g is the mass of free gaseous ammonia, J/(kg K)

m_a is the mass of adsorbed ammonia, J/(kg K)

k_s is the thermal conductivity of the sample, W/(m K)

A is the area of conduction for sample = $2\pi(r + \Delta r/2) \Delta z$, m²

H is the heat of sorption, J/kg

x is the ammonia concentration, kg NH₃/ kg sample

The following equation is used to describe the dynamics of adsorption pair.

For adsorption,

$$\frac{\partial x}{\partial t} = \frac{P - P_{transition}}{C_{ad} + \frac{K_{ad}}{x - x_{eq}}} \quad (6-3)$$

For desorption

$$\frac{\partial x}{\partial t} = \frac{P - P_{transition}}{C_{de} + \frac{K_{de}}{x - x_{eq}}} \quad (6-4)$$

The mass of adsorbed ammonia m_a is a function of the ammonia concentration and is given

by:

$$\frac{m_a}{x} = M_s \quad (6-5)$$

where: M_s is the total mass of the sample, kg

$$\text{Then, } \frac{dm_a}{dt} = M_s \frac{dx}{dt} \quad (6-6)$$

To simplify the simulation, the wall is assumed to be isothermal and the relevant boundary

condition is:

$$T_{wallin} = T_{wallout} \quad (6-7)$$

where, T_{wallin} is the internal wall temperature, K; $T_{wallout}$ is the outer wall temperature which

can be measured by the thermocouples, K

During the experiments, the system is closed and the total mass of ammonia m_t remains

constant and is the sum of the mass of liquid ammonia in receiver, m_r , the free mass of

ammonia gas, m_g , and the adsorbed ammonia in the sample porosity, m_a :

$$m_t = m_a + m_r + m_g \quad (6-8)$$

The ammonia gas is assumed as perfect gas so that the free mass of ammonia gas can be calculated from the ideal gas law by,

$$m_g = \frac{p\nu}{RT} \quad (6-9)$$

where, p is the pressure of the system, Pa; ν is the void volume of the system, m^3 ; R is the gas constant, J/(K kg); T is the temperature of the ammonia gas.

The mass of liquid ammonia in receiver, m_r can be calculated by equation (6-1). Therefore, the rate of change in adsorbed ammonia in the sample porosity can be presented as:

$$m_a = m_r - m_r - m_g \quad (6-10)$$

The calculated mass of adsorbent ammonia is compared with the simulated results.

The simulation uses the measured tube wall temperature (boundary condition) and ammonia pressure as input. The heat transfer within the bed is based on the conduction through the bed and with the mass transfer. The initial temperature of the generator is assumed uniform. The simulated centre temperature of the reactor and the concentration of the sample are compared with the experimental results.

6.4 Experimental results and analysis

Figure 6-4 – 6-11 show the comparison of the centre temperature of the reactor bed and concentration of the sample between the experimental results and simulation for adsorption dynamic process.

Figure 6-4 Centre temperature of the reactor vs. time for adsorption dynamic data1 (red line is the measured centre temperature; blue line is the simulated centre temperature; black line is the measured wall temperature; the system pressure changed from 12.25 to 4.98 bar)

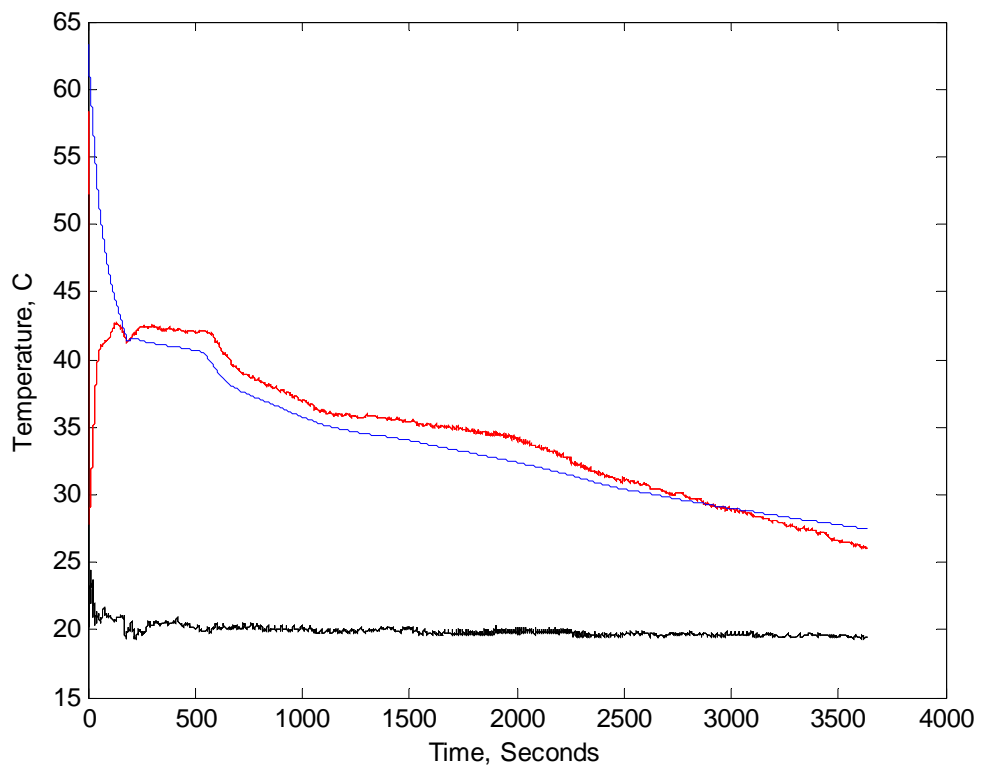


Figure 6-5 Concentration vs. time for adsorption data1

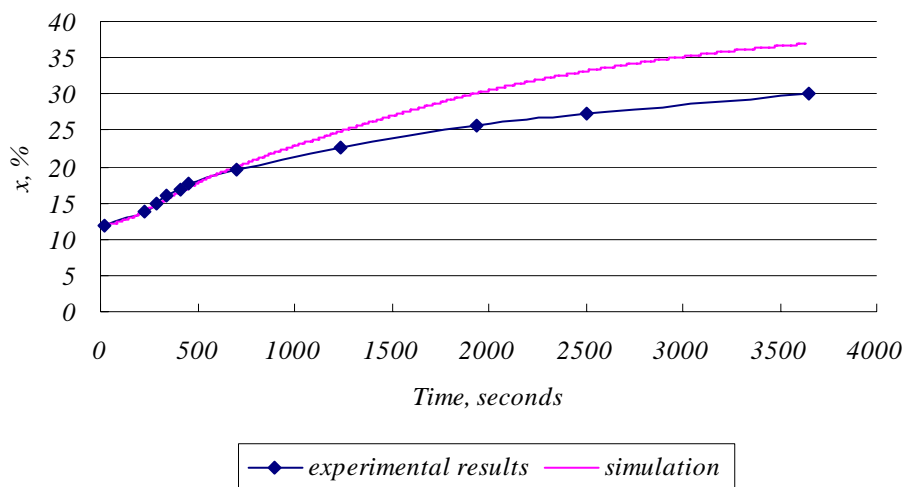


Figure 6-6 Centre temperature of the reactor vs. time for adsorption dynamic data2 (red line is the measured centre temperature; blue line is the simulated centre temperature; black line is the measured wall temperature; the pressure changed from 11.74 to 4.26 bar)

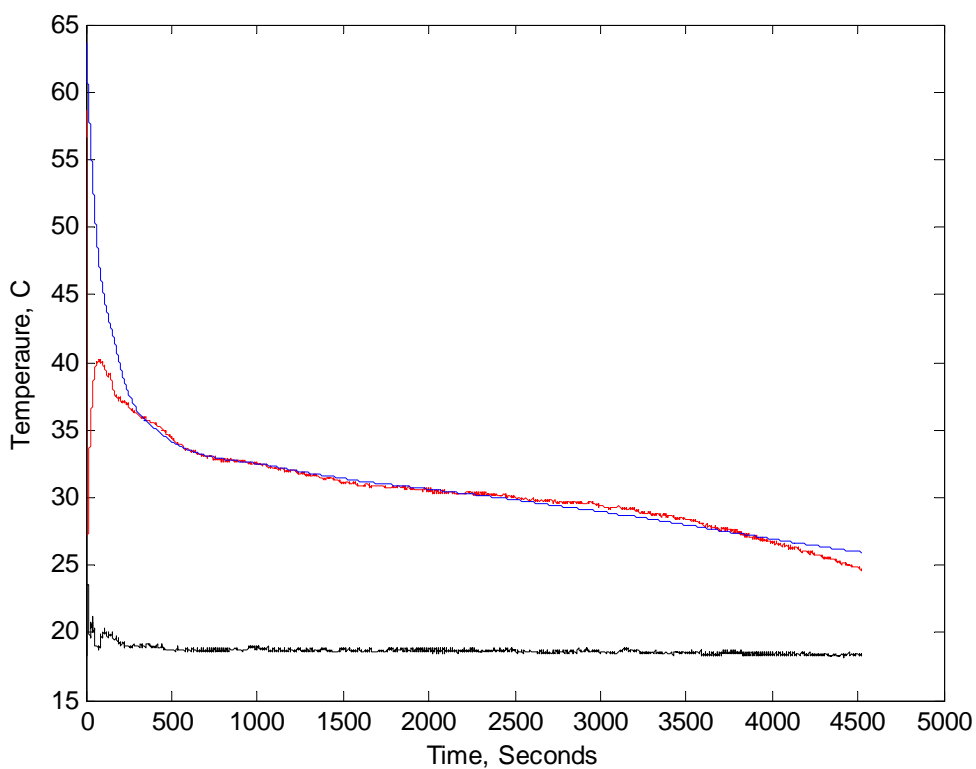


Figure 6-7 Concentration vs. time for adsorption data2

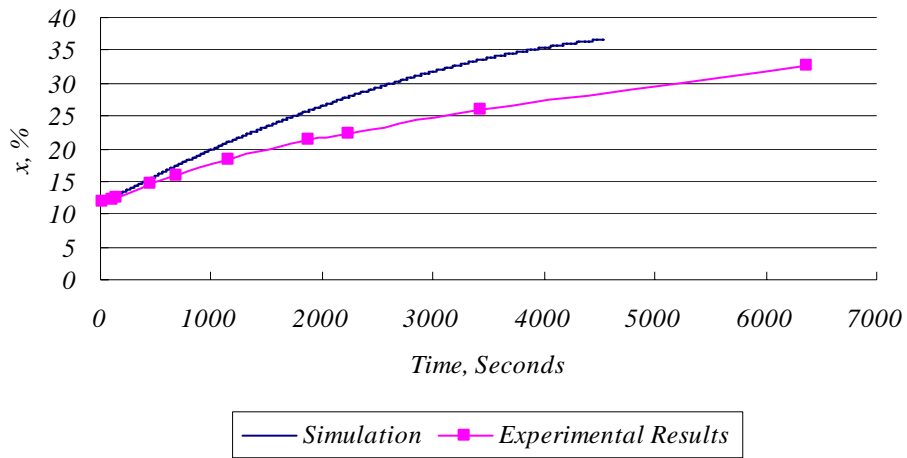


Figure 6-8 Reactor centre temperature vs. time for adsorption dynamic data3 (pink line is the measured centre temperature; blue line is the simulated centre temperature; green line is the measured wall temperature; the pressure changed from 12.8 to 7.62 bar)

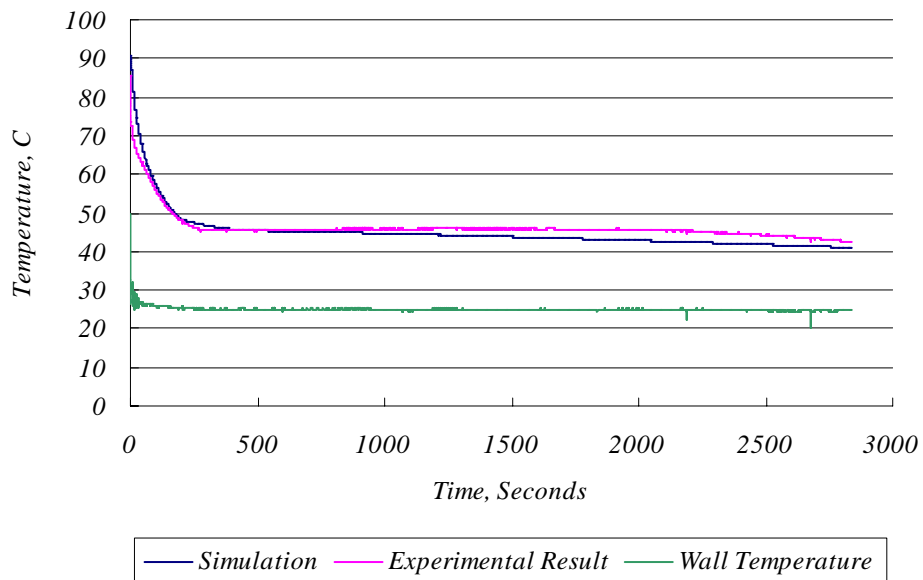


Figure 6-9 Concentration vs. time for adsorption data3

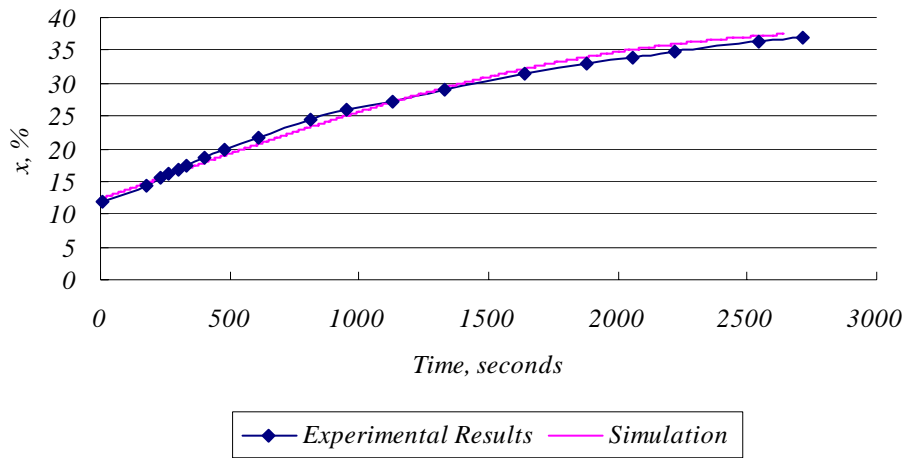


Figure 6-10 Temperature vs. time for adsorption dynamic data4 (red line is the measured centre temperature; blue line is the simulated centre temperature; and black line is the measured wall temperature; the pressure changed from 11.78 to 6.47 bar)

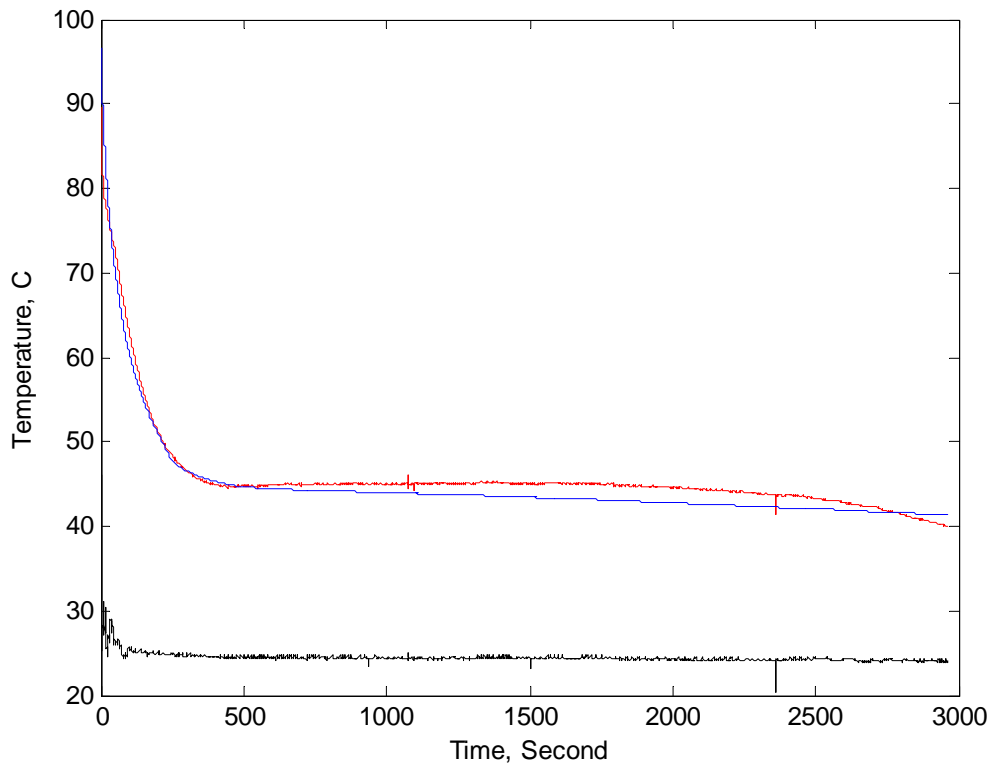
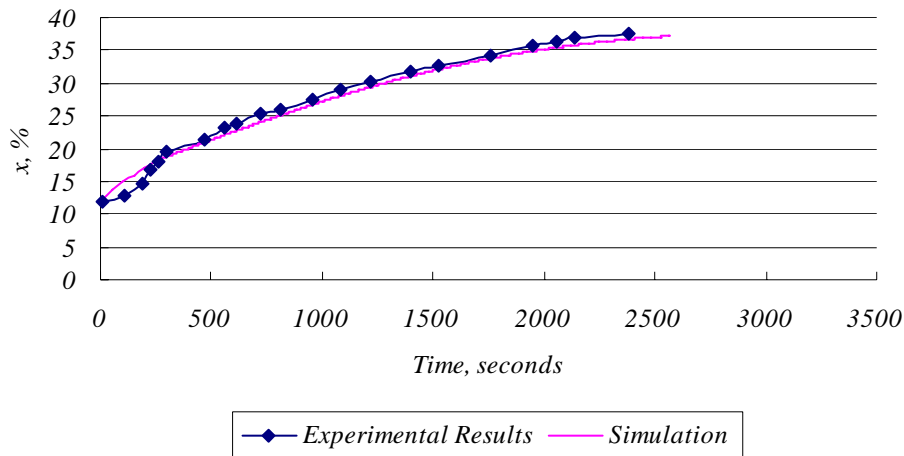


Figure 6-11 Concentration vs. time for adsorption data4



For the first two sets of adsorption data, in the first 10 seconds, there are sudden large decrements of the measured centre temperature, which is much lower than simulation. These may be due to the ammonia gas from the cold receiver flushing into the centre of the reactor and directly cooling the thermocouples. Except the first one or two minutes, the model can predict the centre temperature with great confidence. The maximum error is around $\pm 10\%$.

The simulated concentration of the first two adsorption data is larger than experimental data. The main reason is the inaccurate method of concentration measurement. Before the adsorption dynamic test, the void volume of the system is assumed to be full of ammonia gas. But the real situation may be that before the adsorption dynamic test there is some liquid ammonia condensed in the void volume, such as the horizontal tube connecting the generator and the receiver. When the reactor was placed into the cold water, the pressure drop drove the liquid ammonia evaporating from the receiver as well as the condensed

ammonia from the void volume. That is to say, the measured ammonia level change in the receiver will be smaller than expected.

For adsorption data 3 and 4, the model could simulate the concentration precisely. The initial centre temperatures of data 3 and 4 were around 90°C, which is much higher than those of data 1 and 2 (around 60°C). That is to say, the desorption procedures of data 3 and 4 are ended at higher temperature than those of data 1 and 2. And the hotter ammonia gas desorbed from the reactor flows through the void volume and condensed into the cold receiver. The hotter ammonia gas will reduce the chance of ammonia gas condensing in the void volume, which results in better simulation results.

Figure 6-12 – 6-19 present the comparison of the reactor centre temperature and concentration of the sample between the experimental results and simulation for desorption dynamic process.

Figure 6-12 Temperature vs. time for desorption data 1 (red line is the experimental results; blue line is the simulated results; the system pressure changed from 7.16 to 13.15 bar)

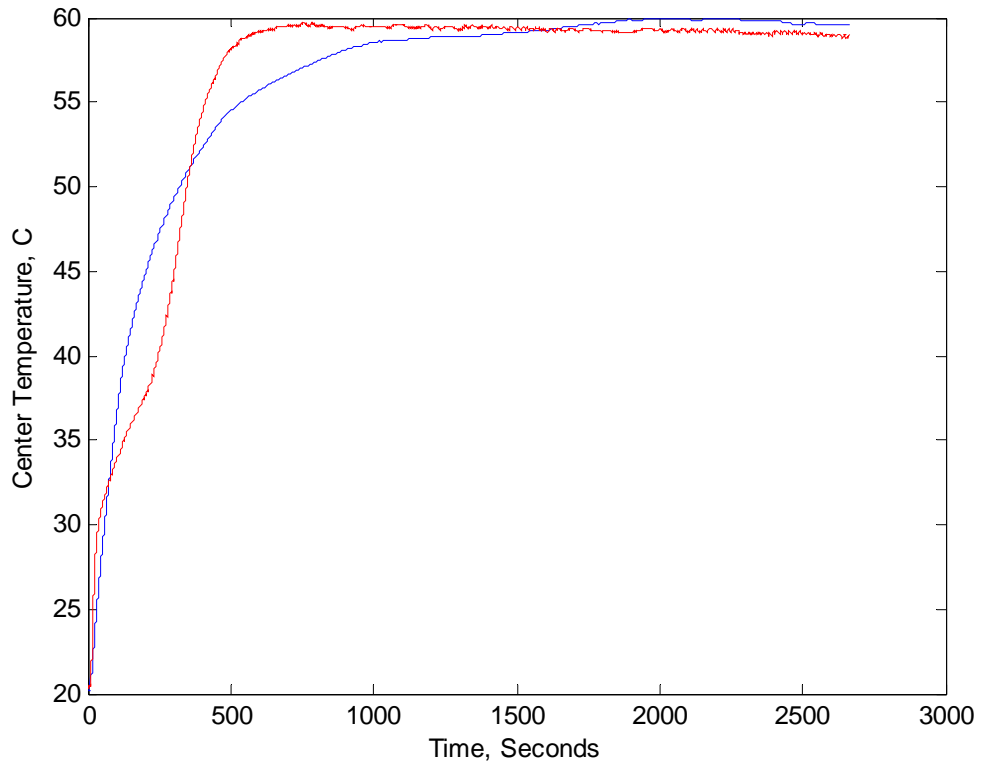


Figure 6-13 Concentration vs. time for desorption data 1

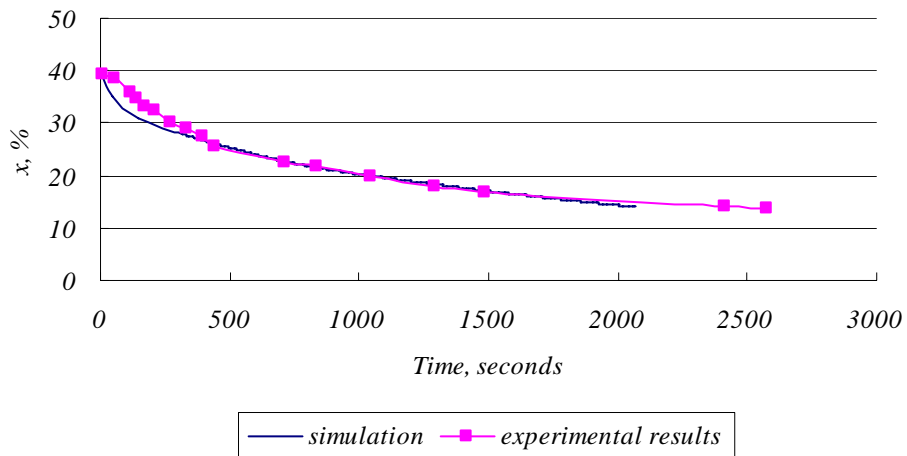


Figure 6-14 Temperature vs. time for desorption data 2 (red line is the experimental results; blue line is the simulated results; the system pressure changed from 7.27 to 12.11 bar)

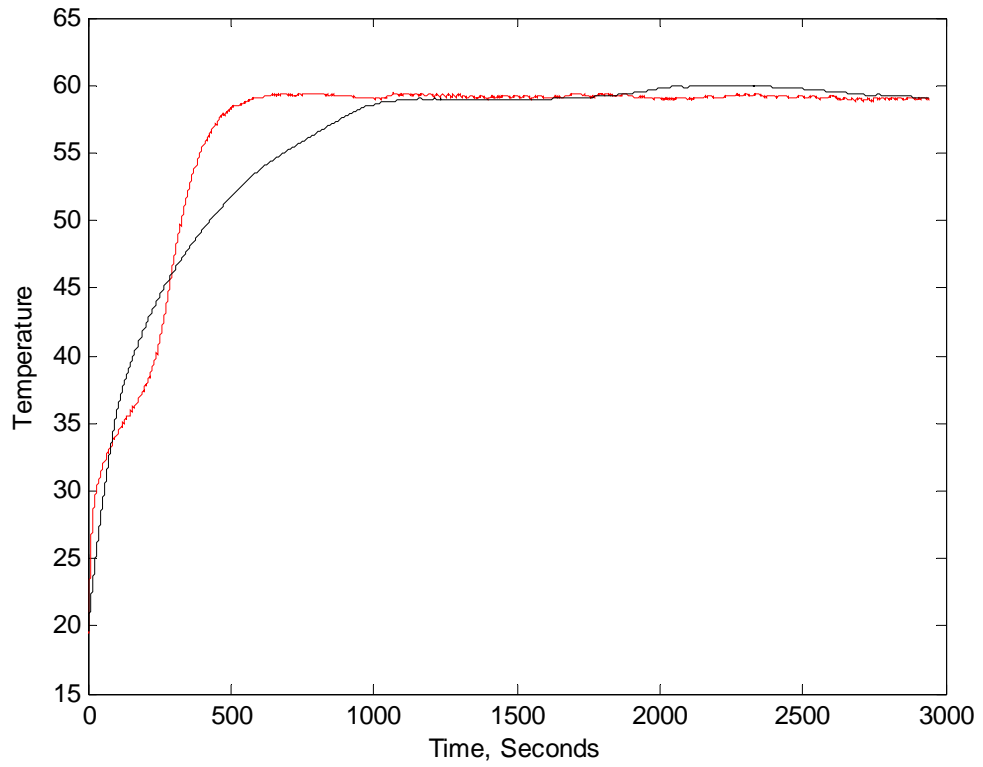


Figure 6-15 Concentration vs. time for desorption data2

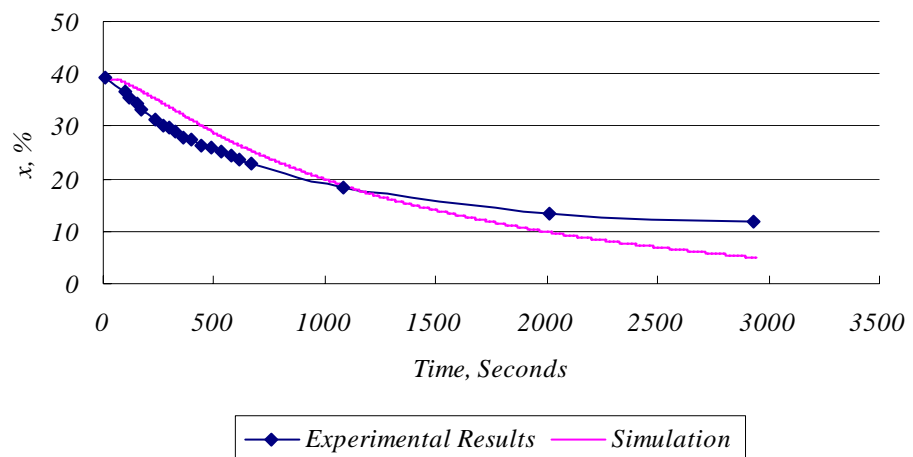


Figure 6-16 Temperature vs. time for desorption data 3 (red line is the experimental results; blue line is the simulated results; the system pressure changed from 7.62 to 12.55 bar)

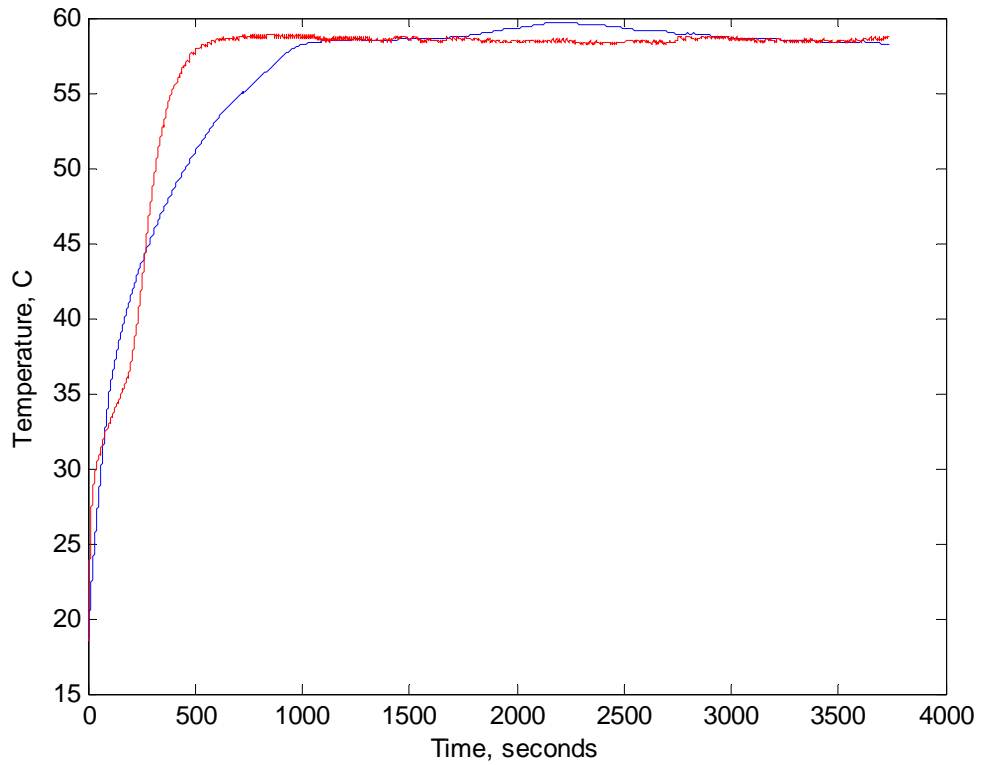


Figure 6-17 Concentration vs. time for desorption data3

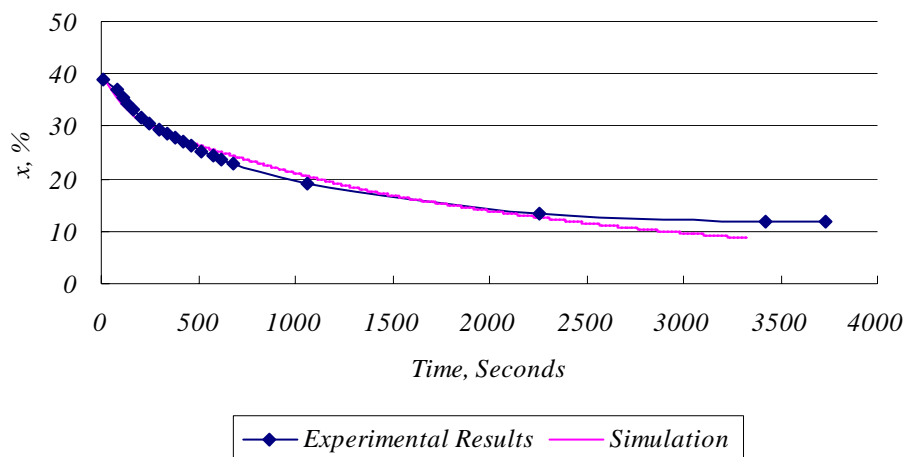


Figure 6-18 Temperature vs. time for desorption data 4 (red line is the experimental results, blue line is the simulated results, the system pressure changed from 7.99 to 12.78 bar)

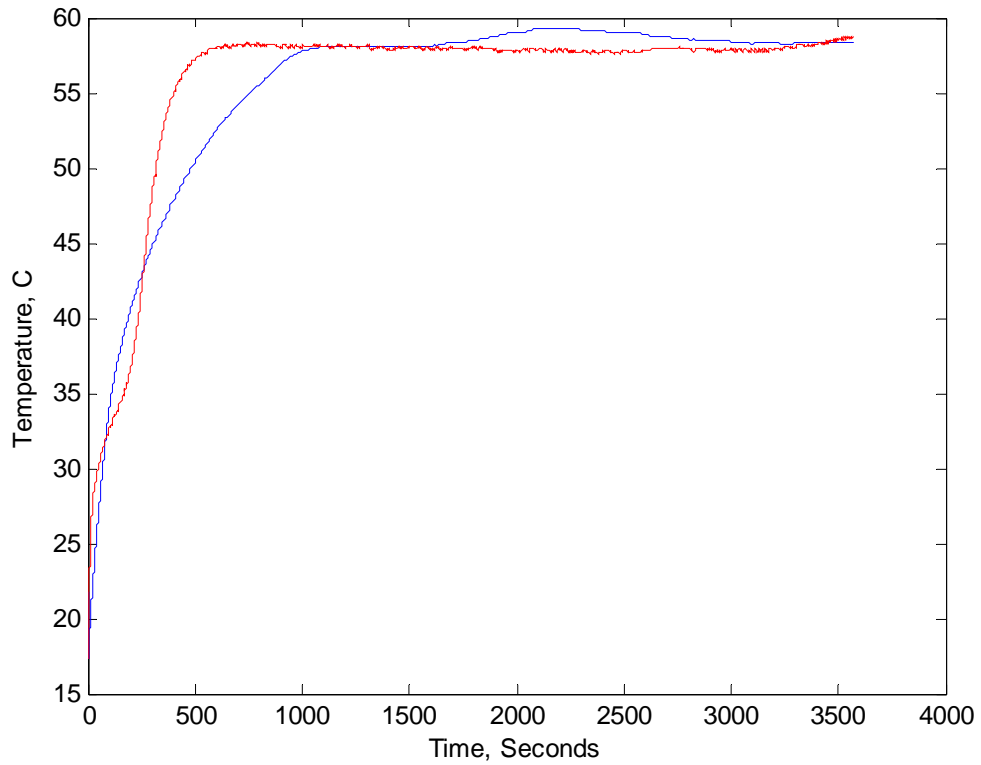
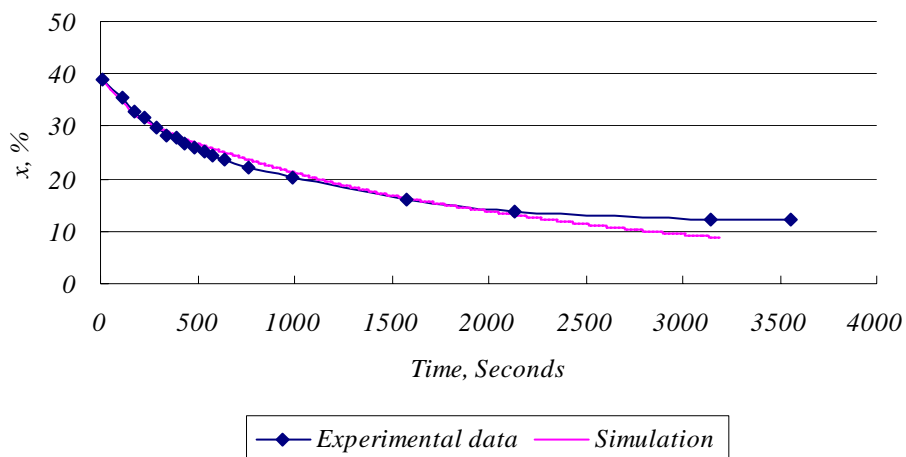


Figure 6-19 Concentration vs. time for desorption data4



For desorption dynamic test, the mathematical model can predict the centre temperature

well, while the model underestimated the concentration especially after 30 minutes. The main reason is that the ammonia gas might condense in the horizontal connecting tube or other void volume. Therefore the measured ammonia level in the receiver would be lower than that expected. In other words, the calculated concentration of the sample from experimental data will be greater than ideal situation.

In summary, through the comparison of the experimental data and simulation, the model can predict the dynamics of both adsorption and desorption fairly well. So it can be used for the modelling of real adsorption system and adsorption cycles.

Reference:

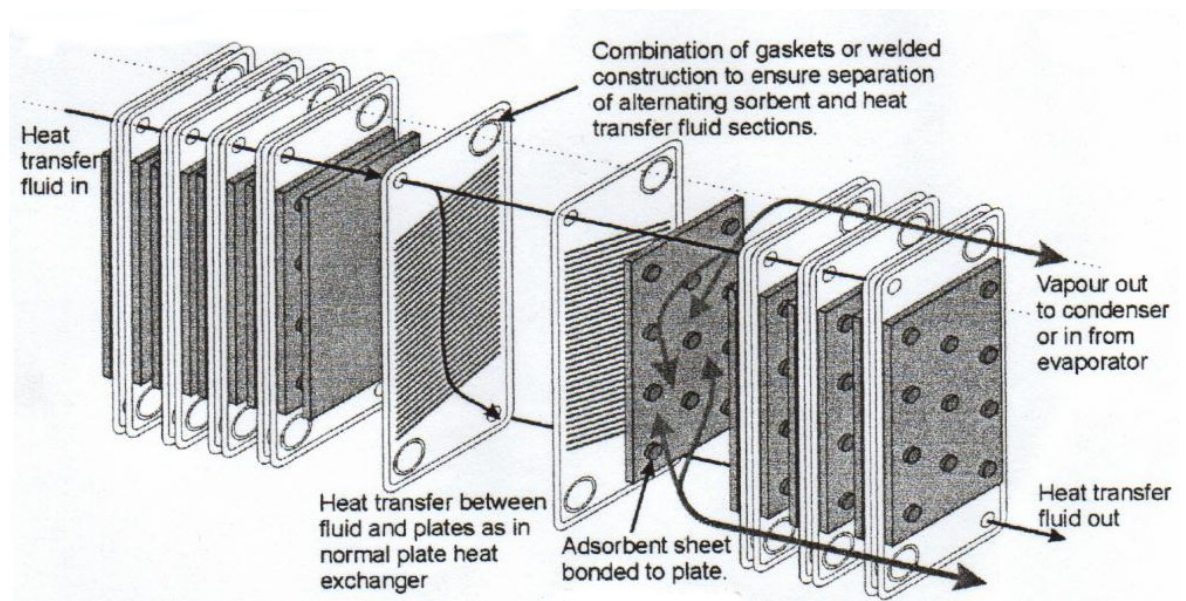
- [1] Z. Tamainot-Telto, R.E. Critoph, Cost effective carbon-ammonia generators, Report No ENK5-CT2002-00632-UW1, October 2003, School of Engineering, University of Warwick

Chapter 7 Simulation of Sorption in Vermiculite – BaCl₂

7.1 Physical model

A compact adsorption bed to improve the performance of adsorption systems has been designed at Warwick University. The structure of the plate heat exchanger which is used in the simulation is shown in figure 7-1. The heat transfer fluid is pumped between two metal plates to heat and cool the adsorbent beds. The refrigerant, ammonia, is condensed and evaporated in separate sections. The heat rejected from the condensing ammonia during desorption and the heat absorbed by the evaporating ammonia during adsorption is transferred to and from heat transfer fluid. The entire bed is constructed from many of these subsections placed side-by-side. The parameters have been optimized by Critoph and Metcalf [1].

Figure 7-1 Configuration of the plate heat exchanger for the generator bed [1]



This compact beds should have good heat transfer, especially if the adsorbent layers are made extremely thin, and it should be possible to achieve short cycle times and high specific heating and cooling powers. The metal plates which separated the sample layers may be made thin so that their thermal masses can thereby be low and less energy is wasted in heating up the plates every cycle, further decreasing the cycle time and improving COP.

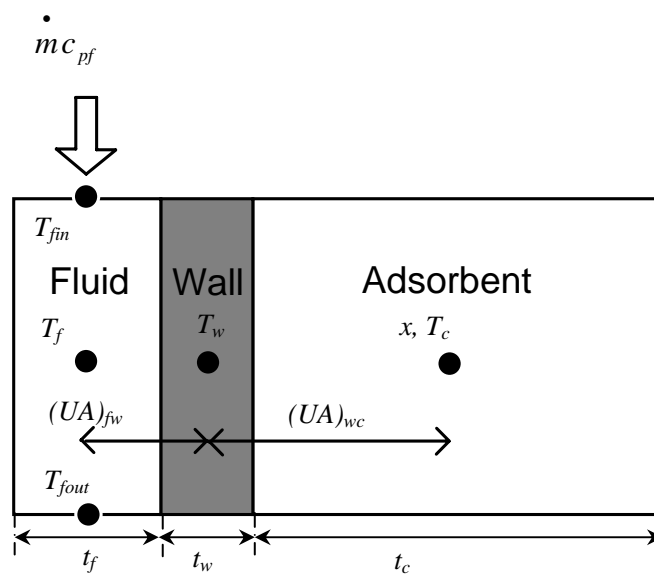
In the mathematical modelling of any physical system, it is necessary to make certain simplifying assumptions in order to reduce the complexity of the model and render it tractable without losing its physical validity. For this reason, we made the following simplifying assumptions:

1. The adsorbent retains its shape, size and porosity throughout the duration of the reaction;
2. The solid reactant (BaCl_2) is uniformly distributed throughout the volume of adsorbent;
3. The reaction rate throughout the volume of adsorbent depends upon the temperature, pressure and absorbed ammonia concentration;
4. The thermo-physical properties of the adsorbent do not change during the reaction;
5. The sample layers are assumed to firmly bond to the metal plates so that the thermal contact resistances are not considered during the simulation.

Based on these assumptions, the concept of the plate heat exchanger was simplified. The

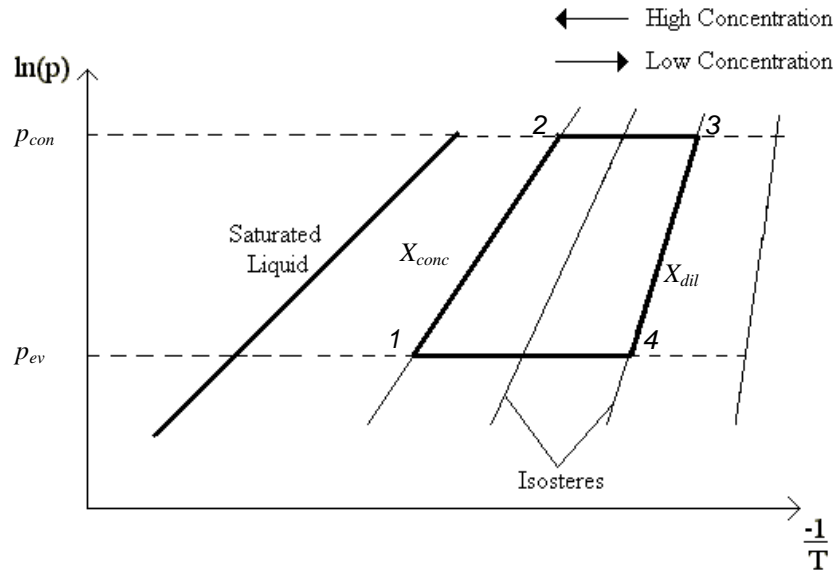
schematic of the simplifying generator to be modelled is shown in figure 7-2, in which, T_f is the mean temperature of heat transfer fluid; T_{fin}, T_{fout} is the inlet and outlet temperature of the heat transfer fluid respectively; T_w, T_c is the mean temperature of the wall and compound adsorbent respectively; $(UA)_{fw}$ is the heat transfer coefficient between the wall and heat transfer fluid; $(UA)_{wc}$ is the heat transfer coefficient between the wall and the adsorbent. t_f, t_w, t_c is the thickness of the heat transfer fluid channel, metal wall and adsorbent respectively.

Figure 7-2: Schematic diagram of the modelled generator bed



The model simulates a basic ideal cycle. An idealized cycle is assumed, as shown on the Clapeyron diagram in figure 7-3, which includes isosteric pressurization (1 - 2) and depressurisation stages (3 - 4) and isobaric adsorption (4 - 1) and desorption stages (2 - 3).

Figure 7-3: Idealised adsorption cycle



Firstly the generator was set in some initial condition, in which the adsorption system was at ambient temperature with the fully adsorbed ammonia within adsorbent. The total mass of refrigerant must remain constant since the system is sealed and will be constituted of the mass adsorbed in the adsorbent, and the mass as a gas and a liquid in the receiver.

A finite-difference method was used to accomplish the modelling. The parameters under the conditions of the system after a small interval of time or ‘time step’, denoted here by Δt , was calculated from those under the conditions at the previous time step. Starting from the initial conditions, the conditions of the system after any elapsed time may therefore be calculated by repeating an appropriate number of time steps.

7.2 Modelling equations

Overall value of heat transfer coefficient

Two heat transfer coefficients are considered in the model. One is the convection coefficient between the fluid and the wall, and the other is that between the wall and adsorbent. By selecting appropriate bed parameters, such as the heat transfer coefficients and the mass flow rate of heat transfer fluid within the control volume, it is possible to model any given bed design.

The overall heat transfer coefficient between the fluid and the wall depends on the convective heat transfer coefficient h . A table in Holman [2] provides useful information to calculate the convective heat transfer coefficient of laminar flow. Three values for the Nusselt number (Nu) are given under three different conditions:

- uniform heat flux in flow direction and uniform wall temperature at particular flow cross section, $Nu = 8.235$,
- uniform heat flux both in flow direction and around periphery, $Nu = 8.235$,
- and uniform wall temperature, $Nu = 7.541$.

But none of the three conditions given fit all the conditions in the heat transfer fluid flow channel. Therefore an average Nusselt number of 8.0 will be used in the model, which is quite reasonable because the calculations of convective heat transfer coefficient are seldom

accurate to real situation within 10%.

The Nusselt number is a non-dimensional value of the convective heat transfer coefficient, which is given by the relationship:

$$Nu = \frac{hD_h}{k}, \quad (7-1)$$

where:

h - convective heat transfer coefficient, W/m²K

k - thermal conductivity of the fluid, W/m K

D_h - hydraulic diameter of channel, m, calculated by

$$D_h = \frac{4A}{P} \quad (7-2)$$

A - cross-sectional area of flow, m²

P - wetted perimeter of flow channel, m

Considering the geometry of the heat transfer fluid channel, $A=2t_f$ and $P=(2+2t_f) \approx 2$ (since $t_f \ll 1$), from equation (7-1) and (7-2), the convective heat transfer coefficient for the heat transfer fluid channel is given by

$$h = \frac{Nu.kP}{4A} = \frac{2k}{t_f}. \quad (7-3)$$

So the heat transfer coefficient between the wall and heat transfer fluid is calculated by

$$U_{fw} = \frac{2k_f}{t_f} \quad (7-4)$$

Similarly, the heat transfer coefficient between the wall and adsorbent equals,

$$U_{wc} = \frac{2k_c}{t_c} \quad (7-5)$$

Temperature change in the heat transfer fluid

As the heat transfer fluid flows through the bed, its temperature will increase when cooling the bed in adsorption decrease when it is heating the bed during desorption. This temperature change is calculated using the log mean temperature (LMTD) method [2], where the log mean temperature difference is given by:

$$LMTD = \frac{T_{fin} - T_{fout}}{\ln \left[\frac{T_{fin} - T_{wall}}{T_{fout} - T_{wall}} \right]} \quad (7-6)$$

Governing equations

The governing equations for the model are

$$M_f c_{pf} \frac{\partial T_f}{\partial t} - \dot{m} c_{pf} (T_{fin} - T_{fout}) = -(UA)_{fw} T_{LMTD} \quad (7-7)$$

$$M_w c_{pw} \frac{\partial T_w}{\partial t} = (UA)_{fw} T_{LMTDfw} - (UA)_{wc} (T_w - T_c) \quad (7-8)$$

$$M_c (c_{pc} + x c_{pa}) \frac{\partial T_c}{\partial t} - M_c H \frac{\partial x}{\partial t} = (UA)_{wc} (T_w - T_c) \quad (7-9)$$

Where

M_f - Mass of the heat transfer fluid, kg

M_w - Mass of the wall, kg

- M_c - Mass of the compound adsorbent, kg
- c_{pf} - Specific heat capacity of the heat transfer fluid, $J\ kg^{-1}\ K^{-1}$
- c_{pw} - Specific heat capacity of the wall, $J\ kg^{-1}\ K^{-1}$
- c_{pc} - Specific heat capacity of compound adsorbent, $J\ kg^{-1}\ K^{-1}$
- \dot{m} - Heat transfer fluid mass flow rate, $kg\ s^{-1}$
- A_{fw} - Heat transfer area between the wall and heat transfer fluid, m^2
- A_{wc} - Heat transfer area between the wall and reaction bed, m^2
- U_{fw} - Heat transfer coefficient between the wall and heat transfer fluid, $W\ m^{-2}\ K^{-1}$
- U_{wc} - Heat transfer coefficient between the wall and reaction bed, $W\ m^{-2}\ K^{-1}$
- T_{LMTD} - Temperature change in the heat transfer fluid, calculated by equation 7-5, K
- T_{fin} - The inlet temperature of heat transfer fluid, K
- T_{fout} - The outlet temperature of heat transfer fluid, K
- T_f - The mean temperature of heat transfer fluid, K
- T_w - Temperature of the wall, K
- T_c - Temperature of the reaction bed, K
- x - Ammonia mass concentration, kg ammonia / kg adsorbent
- t - Time, seconds
- H - Heat of reaction, $J\ kg^{-1}$

H at any point on isobaric adsorption (4-1) and desorption stages (2-3) can be derived from the slope of the isostere on the Clapeyron diagram, which is given by equation(4-14) and (4-15).

In order to simplify the solution of the governing equations, the fluid thermal mass is lumped with the wall thermal mass [3], so that equations (7-7) and (7-8) become equations (7-12) and (7-13),

$$\dot{m}c_{pf}(T_{fin} - T_{fout}) = (UA)_{fw}T_{LMTD} \quad (7-12)$$

$$(M_w c_{pw} + M_f c_{pf}) \frac{\partial T_w}{\partial t} = (UA)_{fw}T_{LMTDfw} - (UA)_{wc}(T_w - T_c) \quad (7-13)$$

Adsorption characteristic of working pair

The equation of mass concentration change of adsorbate against time is vital to the simulation. In the model, the equations are obtained by fitting the dynamic experimental data,

For adsorption,

$$\frac{\partial x}{\partial t} = \frac{p - p_{transition}}{C_{ad} + \frac{K_{ad}}{x - x_{eq}}} \quad (7-14)$$

For desorption

$$\frac{\partial x}{\partial t} = \frac{p - p_{transition}}{C_{de} + \frac{K_{de}}{x - x_{eq}}} \quad (7-15)$$

Finite-difference methods

Finite-difference methods are used to discretize the differential equations. The finite-difference method calculates the condition of the system after a small interval of time

or ‘time step’, denoted here by Δt , based upon the conditions at the previous time step.

After discretization, the governing equations (7-12) – (7-15) become,

$$M_c (c_{pc} + x_{(t)} c_{pa}) \frac{(T_{c(t+\Delta t)} - T_{c(t)})}{\Delta t} - M_c \left(H \frac{\partial x}{\partial t} \right) \Big|_{(t)} = (UA)_{wc} (T_{w(t)} - T_{c(t)}) \quad (7-16)$$

$$(M_w c_{pw} + M_f c_{pf}) \frac{(T_{w(t+\Delta t)} - T_{w(t)})}{\Delta t} = (UA)_{fw} T_{LMTDfw} \Big|_{(t)} - (UA)_{wc} (T_{w(t)} - T_{c(t)}) \quad (7-17)$$

$$\frac{(x_{(t+\Delta t)} - x_{(t)})}{\Delta t} = \frac{\Delta p \Big|_{(t)}}{C + \frac{K}{\Delta x \Big|_{(t)}}} \quad (7-18)$$

where, the parameters with subscripts $(t + \Delta t)$ are the value at time $(t + \Delta t)$ and those with subscripts (t) mean the value at time (t) . So starting from the initial conditions the condition of the system after any elapsed time may therefore be calculated by repeating an appropriate number of time steps.

Cooling power and COP

The cooling power is evaluated by considering the mass of refrigerant desorbed and then adsorbed per unit mass of adsorbent during every cycle. The net concentration change is

$x_{dil} - x_{conc}$ (refer to figure 7-2). The useful cooling obtained from it is [4]:

$$q_{ev} = (x_{conc} - x_{dil}) (h_{gasev} - h_{liquidcon}) \quad (7-19)$$

where:

h_{gasev} - Specific enthalpy of gas leaving the evaporator, kJ/kg

$h_{liquidcon}$ - Specific enthalpy of the condensed liquid, kJ/kg

Hence, the COP for a basic refrigeration cycle can be calculated by

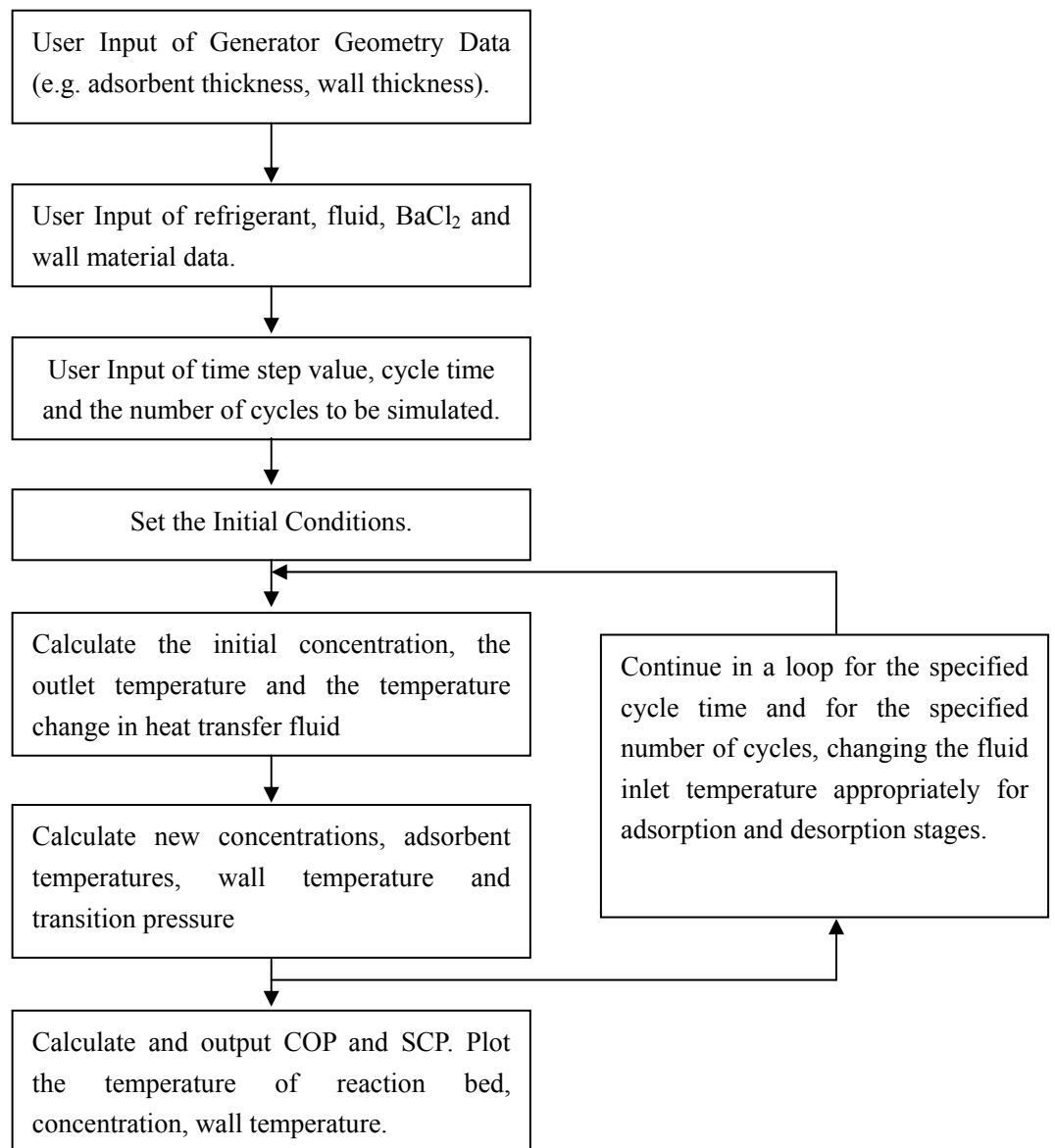
$$\text{COP} = \frac{q_{ev}}{q_{ad}} \quad (7-20)$$

q_{ad} - Heat input per unit mass of adsorbent in the desorption heating phase, which can be calculated by integrating equation (7-8) with time.

Block diagram of model

The steps in the model are probably best shown in a block diagram.

Figure 7-4: Simplistic block diagram of the program.



Modelling language

The model was produced using the Matlab computer language, which contains a variety of data visualization tools that enable the program output data to be plotted straightforwardly.

The functions that have been used to calculate the enthalpy and saturation temperature of ammonia were written for previous programs by my supervisor Prof. R.E. Critoph using MATLAB, which will further reduce the time required to produce the model. The original data of ammonia properties comes from reference [7]. The main program (named 'cycle') has been included in Appendix F.

7.3 Simulated results

Parameter combination

The following model parameters may be varied in the model:

- ✧ Thickness of the wall and adsorbent,
- ✧ Wall material and thereby the thermal conductivity, specific heat and density of the wall,
- ✧ Heat transfer fluid and thereby the thermal conductivity, specific heat, viscosity and density of the heat transfer fluid,
- ✧ Heat transfer fluid velocity,
- ✧ Fluid channel width,
- ✧ Fluid inlet temperature during desorption,
- ✧ Fluid inlet temperature during adsorption,
- ✧ Condensing temperature,
- ✧ Evaporating temperature,
- ✧ Adsorption and desorption cycle time

The adsorbent investigated in the model is the high-density BaCl_2 impregnated with vermiculate (mentioned in chapter 4.6.1) developed by the Boreskov Institute of Catalysis (Novosibirsk, Russia). The heat transfer fluid was selected as typical heat transfer oil and

the material of the wall was steel. The properties of these materials are,

Adsorbent material: BaCl₂-vermiculate, Density 230 - 750 kg/m³
Thermal Conductivity 0.1 - 0.4W/mK

The value of the density and thermal conductivity are varied for the various compactness of the compound material

Specific heat 1000 J/kgK

- Wall Material: Steel, Density 7818 kg/m³
Thermal Conductivity 16.3 W/mK
Specific heat 460 J/kgK

- Heat Transfer Fluid: Engine Oil from Holman
Density 900 kg/m³
Thermal conductivity 0.135 W/mK
Specific heat 2000 J/kgK
Viscosity 0.0065 Pa.s

The various parameters and the infinite number of combinations means that a few key parameters will have to be selected and investigated within a set range and the remaining parameters will have to fixed with reasonable values.

The thickness of adsorbent is one of the key parameters. In the model, the heat transfer coefficient between adsorbent and the wall, U_{wc} , represents the thickness of adsorbent. Several heat transfer coefficients are selected for the investigation of the effect of BaCl_2 thickness on the performance of the system.

The thickness of the wall is another key parameter. For maximum performance the wall should be as thin as possible within manufacturing and strength and rigidity constraints. The effect of wall thickness on the COP and the SCP was investigated in order to determine the maximum relative wall thickness that can be employed without causing a significantly adverse effect on performance.

The cycle time will affect both the COP and the specific cooling power. As the cycle time is increased, the COP will increase and will reach a maximum value. At that point, the cycle time is sufficient to complete the reaction of decomposition during desorption and synthesis during adsorption. Beyond this cycle time no more ammonia may be desorbed and reabsorbed during each cycle and therefore no further heating or cooling energy will be provided during each cycle and the COP will remain constant at its maximum value.

The SCP will also increase as the cycle time is increased from zero and reach a peak before the maximum COP is reached and will then continually decrease, tending asymptotically to zero [1]. With the increase of the cycle time, cooling energy will also increase. However, the increase of cooling energy will be compromised by the decrease of cooling power due to the increase the cycle time. So SCP will approach a maximum value before the reactions

of decomposition during desorption and synthesis during adsorption are complete. The cycle time must therefore be optimized to find this peak value of specific cooling power.

An analysis of performance under varied operating conditions is made for a generator bed similar in dimensions to that suggested as optimal by Critoph and Metcalf [5], as outlined in Table 7-1. Unless stated otherwise, all parameters are as detailed in Table 7-1.

Table 7-1: Base case parameter values

Parameter	Value	Unit
Sample	BaCl ₂	-
Sample mass, M_c	1.0	kg
Wall thickness, t_w	0.265	mm
Wall material	SS316	-
Wall mass, M_w	1.0	kg
Fluid channel width, t_f	0.29	mm
Heat transfer area, A	0.4717	m ²
UA_{wc}	250	W K ⁻¹
UA_{fw}	850	W K ⁻¹
$M_w C_{pw}$	460	W K ⁻¹
$M_f c_{pf}$	500	W K ⁻¹
Desorption fluid inlet temperature, T_{findes}	200	°C
Maximum adsorbent temperature, T_3	195	°C
Condensing temperature, T_{con}	40	°C
Adsorption fluid inlet temperature, T_{finads}	20	°C
Evaporating temperature, T_{ev}	30	°C

Effect of cycle time

Figure 7-5 Effect of cycle time on SCP

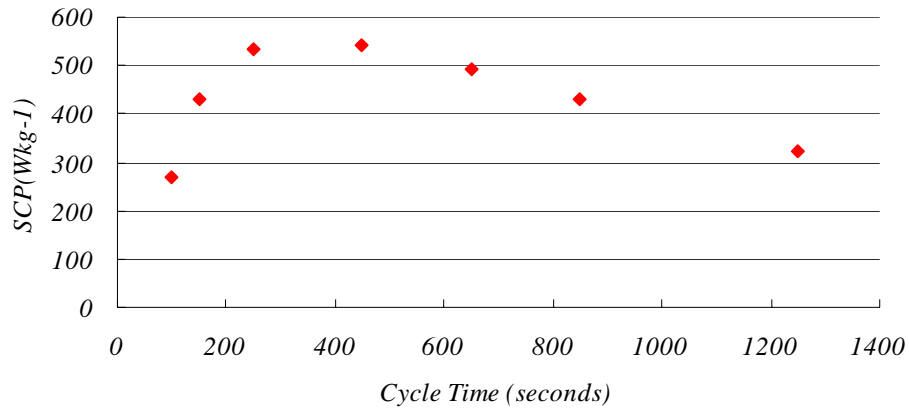
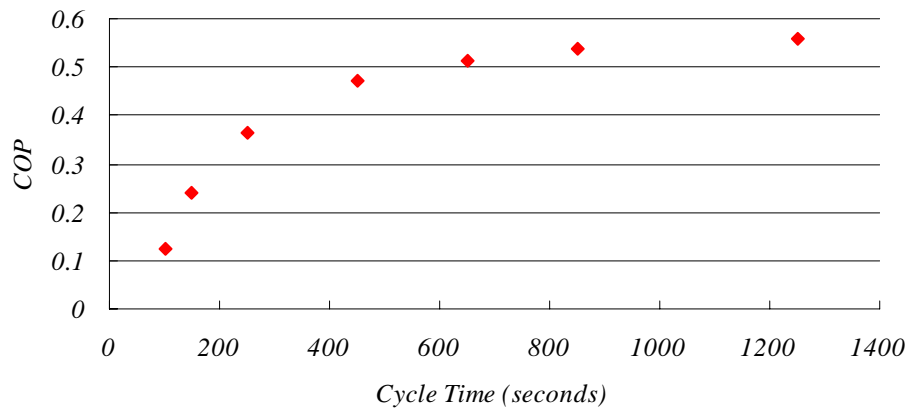


Figure 7-6 Effect of cycle time on COP



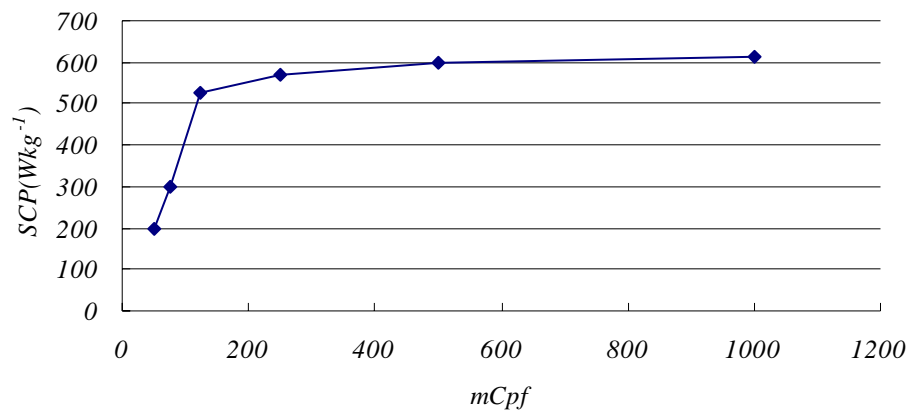
It can be seen that with the increase of the cycle time, the COP increased and reached a maximum value when the simulated reaction of synthesis and decomposition were fully completed during each cycle. While the SCP also increased as the cycle time was increased from zero. However, as the cycle time was further increased, the SCP began to approach its maximum value before the COP reached its maximum value and then continually

decreased because less additional cooling energy was provided each cycle with further increases in cycle time. The cycle time should therefore be optimized to find this peak value of specific cooling power.

Effect of heat transfer coefficients and fluid mass flow rate

Figure 7-7 plots the effect of the heat transfer fluid mass flow rate on SCP for the base case parameters in Table 7-1.

Figure 7-7 Effect of mass flow rate on SCP



It can be seen from the figure that the SCP tends to be zero when the thermal mass flow rate mC_{pf} inclines to zero. As the flow rate approaches zero, the outlet temperature of the fluid tends towards the wall temperature and the log mean temperature difference tends to zero. Thus, the cycle time tends to infinity so that the SCP to zero. As the flow rate increases, the log mean temperature difference increases and the cycle time decreases. Eventually, the fluid outlet temperature tends towards the inlet temperature and the log

mean temperature difference reaches a maximum at which a maximum SCP is reached, as can be seen in the figure 7-7.

To analyse the effect of heat transfer coefficient on the performance of the system, a ‘global’ heat transfer coefficient is applied by Critoph and Metcalf [5], which is calculated as the series combination of the wall-adsorbent and fluid-wall heat transfer coefficients [2],

$$(UA)_g = \frac{(UA)_{fw}(UA)_{wc}}{(UA)_{fw} + (UA)_{wc}} \quad (7-21)$$

This enables the definition of effectiveness for the heat transfer between the fluid and the adsorbent [2],

$$E = 1 - \exp(-NTU_g) \quad (7-22)$$

where, NTU_g are the ‘global’ number of heat transfer units [2],

$$NTU_g = \frac{UA_g}{\dot{m}C_{pf}} \quad (7-23)$$

In figure 7-8, this definition of the heat transfer effectiveness has been used to relate the heat transfer coefficients and the fluid mass flow rate to the *SCP*.

Figure 7-8 SCP Correlated against Emc_{pf} for various heat transfer coefficient values

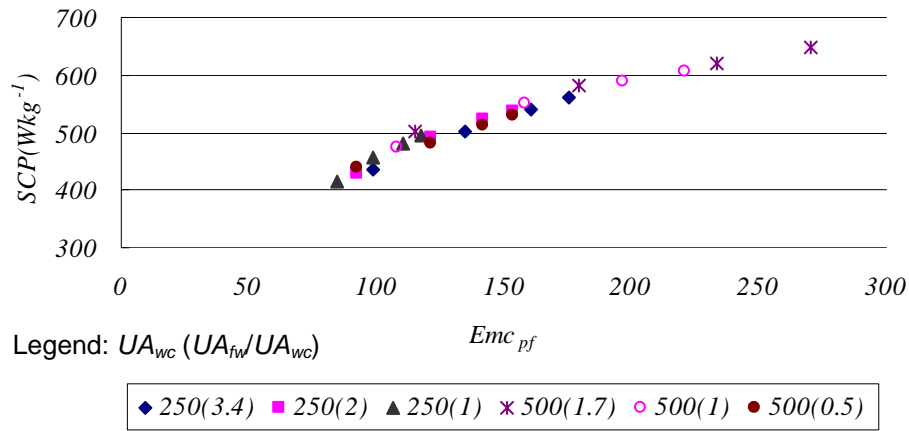
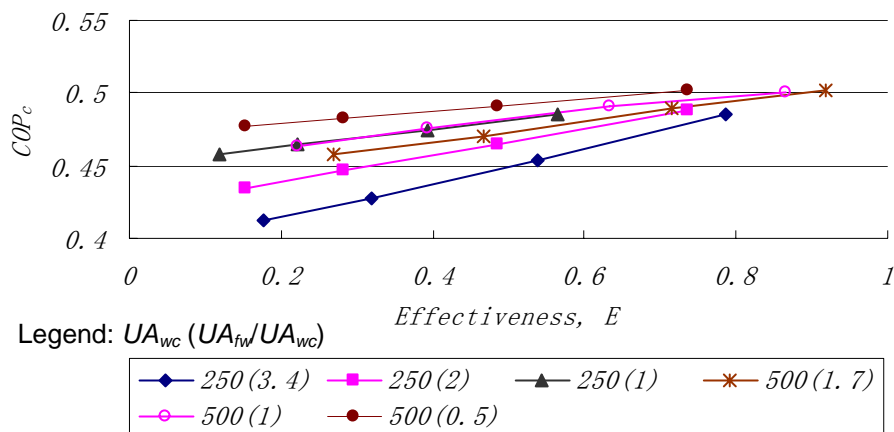


Figure 7-9 plots COP against heat exchange effectiveness, E , for various heat transfer coefficients. From the figure it can be seen that for each of the heat transfer coefficients, the relationship between the COP and the effectiveness, E , is linear. The gradient of the linear relationship is dependent upon the ratio of the fluid-wall heat transfer coefficient, UA_{fw} , and the wall-adsorbent heat transfer coefficient, UA_{wc} . For the same ratio $UA_{fw}:UA_{wc}$, which are 250(1) and 500(1) in the figure, their COP- E relationships are the same. At low effectiveness (i.e. high mass flow rate) the wall reaches a higher temperature during desorption and a lower temperature during adsorption. The additional energy transferred to the wall is not completely recovered and thus the COP is lower. As the effectiveness tends to 1, the wall temperature approaches the bed temperature throughout the cycle and the COP tends to be the same as less heat is transferred to and from the wall, regardless of the particular heat transfer coefficient values.

At the same ‘global’ effectiveness, if the ratio of the fluid-wall and wall-adsorbent heat

transfer coefficients differs, then the effectiveness of the heat transfer to the wall will be different and the wall temperatures will not be the same throughout the cycle. With a higher $UA_{fw}:UA_{wc}$ ratio, the wall reaches a higher temperature during desorption and a lower temperature during adsorption and the COP is lower. Thus, higher $UA_{fw}:UA_{wc}$ ratios result in a steeper gradient in the linear COP- E relationship, as shown in figure 7-9.

Figure 7-9 COP correlated against effectiveness for various heat transfer coefficients



Effect of wall mass

COP against effectiveness for three wall masses with fixed operating conditions are plotted in figure 7-10. It can be seen that the linear COP- E relationship is steeper at higher relative wall masses and the maximum COP at an effectiveness of unity is also lower.

Figure 7-11 plots SCP against EmC_{pf} for the three cases as figure 7-10. With greater

relative wall mass, the gradient of the linear relationship is shallower due to longer cycle times as a result of the greater quantity of heat transferred to the wall, however the effect on SCP of increased wall mass is significantly less than the adverse effect on the COP.

Figure 7-10 Effect of wall mass on COP

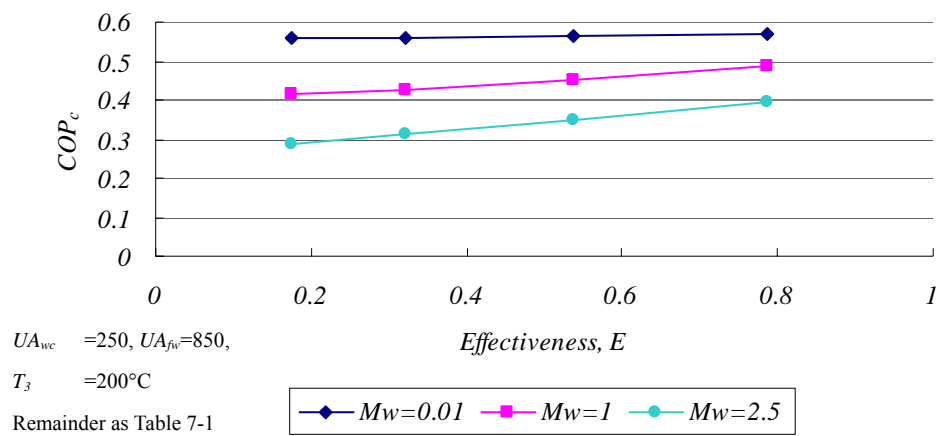
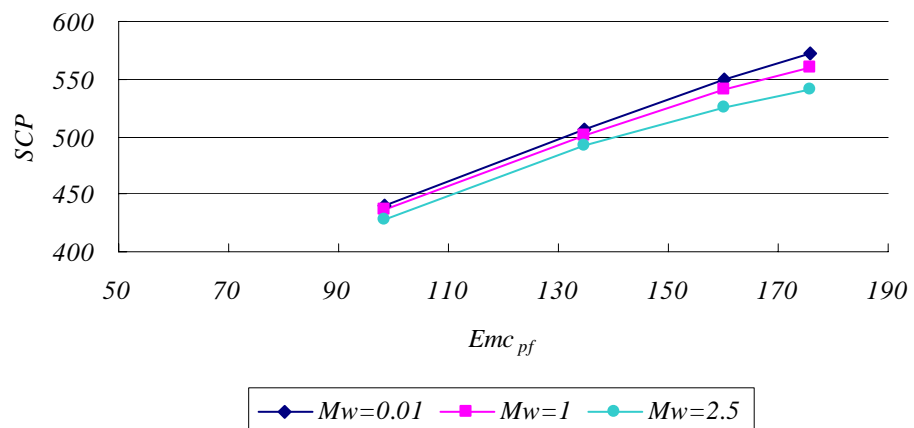


Figure 7-11 Effect of wall mass on SCP



Performance analysis under different operating conditions

The results presented so far have been for fixed cycle temperatures. They provide enough information for basic cycle. While in practice, multiple-beds cycles have to be applied for continuous cooling power output. Various maximum adsorbent temperature, T_3 , and minimum adsorbent temperature, T_1 will have to be applied. Also the evaporating temperature, T_{con} , and the condensing temperature, T_{ev} , affect the performance of the adsorption system remarkably.

Figure 7-12 Effect of condensing and driving temperatures on COP

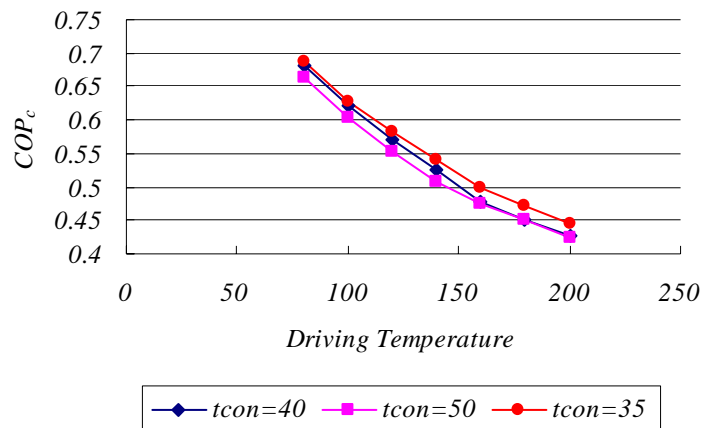


Figure 7-13 Effect of condensing and driving temperatures on SCP

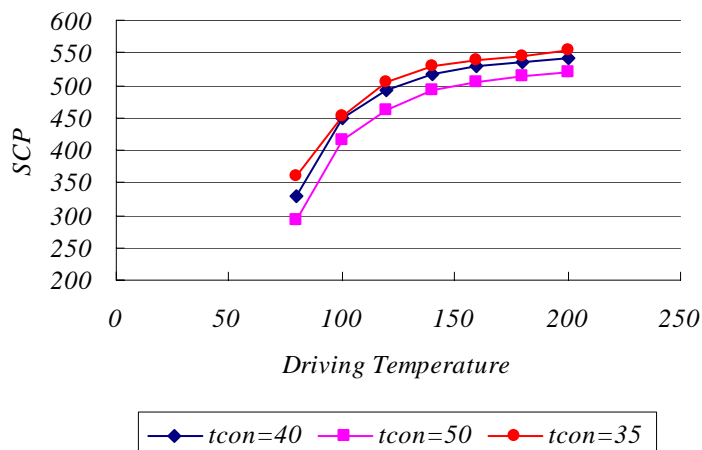


Figure 7-14 Effect of evaporating and driving temperatures on COP

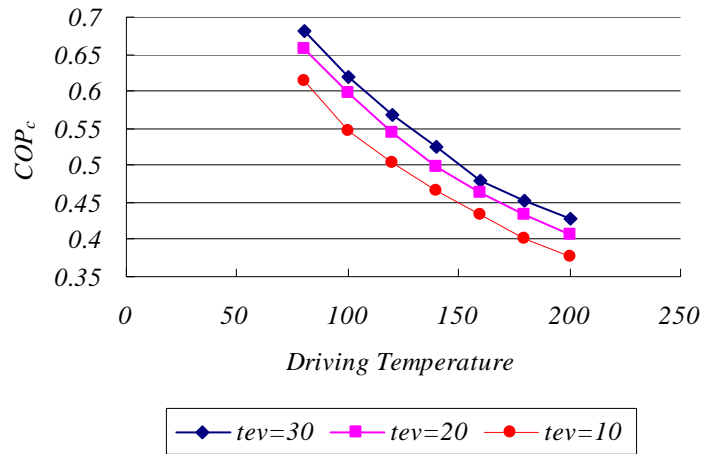


Figure 7-15 Effect of evaporating and driving temperatures on SCP

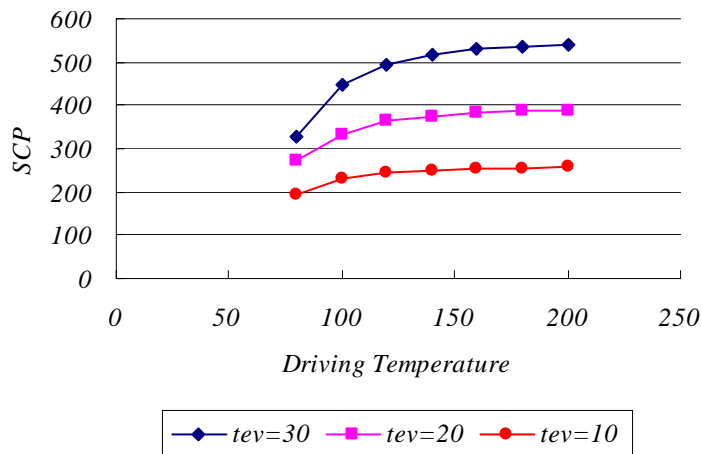


Figure 7-12 and 7-13 show the effect of condensing and driving Temperatures on COP and SCP and in figure 7-14 and 7-15 the COP and SCP have been plotted for a range of evaporating and driving temperatures. From the figures above, we can see that with the increase of condensing temperature or decrease of evaporating temperature, COP and SCP of adsorption system will decrease. Also for a fixed evaporating or condensing temperature, the less the driving temperature, the less SCP and the greater COP are. Also the figures

above provide obvious evidence that the effect of evaporating temperature on the performance of the system is much greater than that of condensing temperature.

These phenomena can be explained from the mechanics of the chemical adsorption system. Desorption happens when the transition pressure of desorption is greater than p_{con} , while adsorption happens when the transition pressure of adsorption is lower than p_{ev} .

As mentioned in chapter 5, the equation to describe the kinetic performance of adsorbent is:

$$dx/dt = \frac{\Delta p}{C + K/(x - x_{eq})} \quad (7-24)$$

where, for adsorption, $C = 50$, $K = -2500$, $\Delta p = p_{ev} - p_{transition}$; For desorption, $C = 30$, $K = 500$, $\Delta p = p_{con} - p_{transition}$

From the equation above, we can see, Δp , plays an important role to determine the rate of concentration change. The greater the pressure difference, the quicker the chemical reaction, which means the shorter cycle time and the larger SCP.

So, the decrease of the driving temperature causes the decrease of the corresponding transition temperature, which means the smaller Δp longer cycle time and smaller SCP. And with the increase of condensing temperature, $\Delta p = p_{con} - p_{transition}$ will decrease and cause the decrease of SCP. Similarly, the decrease of evaporating temperature and the increase of the minimum temperature cause the decrease of Δp and SCP.

For desorption, the corresponding transition pressure of the maximum temperature (T_3 in figure 7-3) is usually much higher than p_{con} , while for adsorption, the corresponding transition pressure of the minimum temperature (T_1 in figure 7-3) is not much lower than p_{ev} . So the Δp of desorption is relatively larger than that of adsorption, which means that the effect of the change of evaporating temperature on SCP will be more significant than that of the condensing temperature as are shown in the figures 7-12 and 7-15.

From figure 7-12 to 7-15, we can draw the conclusion that the higher the driving temperature, the higher the SCP; the lower the adsorbent temperature, the higher the COP. So it is possible to obtain both better COP and SCP at higher driving temperature but relatively lower adsorbent temperature. The performance of adsorption system with various adsorbent temperatures is shown in figure 7-16 and 7-17. In the figures, the driving temperatures are fixed at 180, 160, 140 and 120°C.

With the decrease of adsorbent temperature, the value of SCP kept rising until it reached maximum then drop down gradually. While the value of COP was almost a constant then decreased sharply at a specific adsorbent temperature with the decrease of adsorbent temperature.

The lower the adsorbent temperature, the less the heat transferred between heat transfer fluid and the generator, which also means the shorter cycle time. Less heat transfer means higher COP and shorter Cycle time will cause greater SCP. On the other hand, shorter cycle

time also means less NH_3 adsorbed on the adsorbent, so the cooling power produced through adsorption cycle will be less. With the decrease of the cycle time, the increase of SCP and COP will be compromised by the decrease of cooling power, as is shown in figure 7-16 and 7-17.

Figure 7-16 Effect of various adsorbent temperatures at fixed driving temperatures on COP

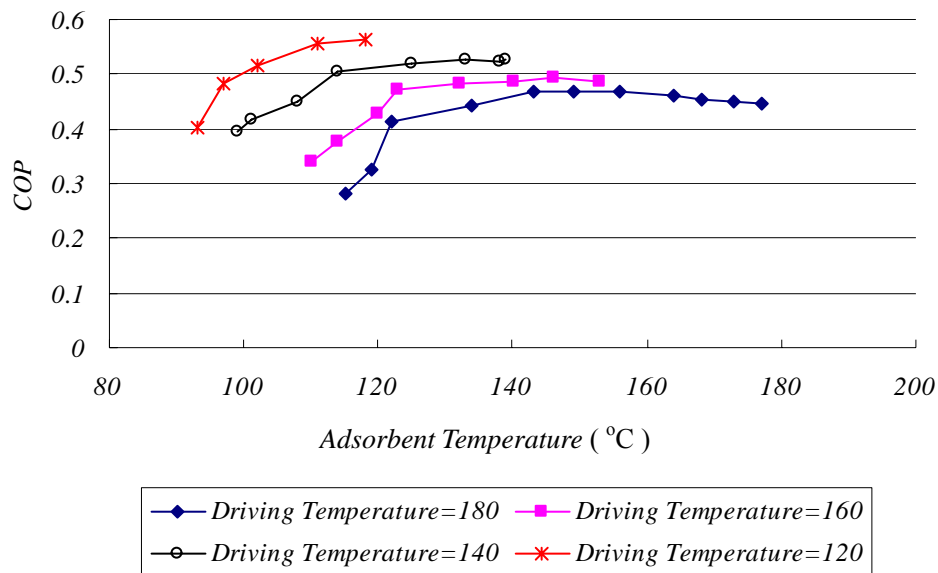


Figure 7-18 plotted driving temperature against adsorbent temperature when the SCP of adsorption system reached maximum at each driving temperature. Figure 7-19 plotted driving temperature against maximum SCP.

Figure 7-17 Effect of various adsorbent temperatures at fixed driving temperatures on SCP

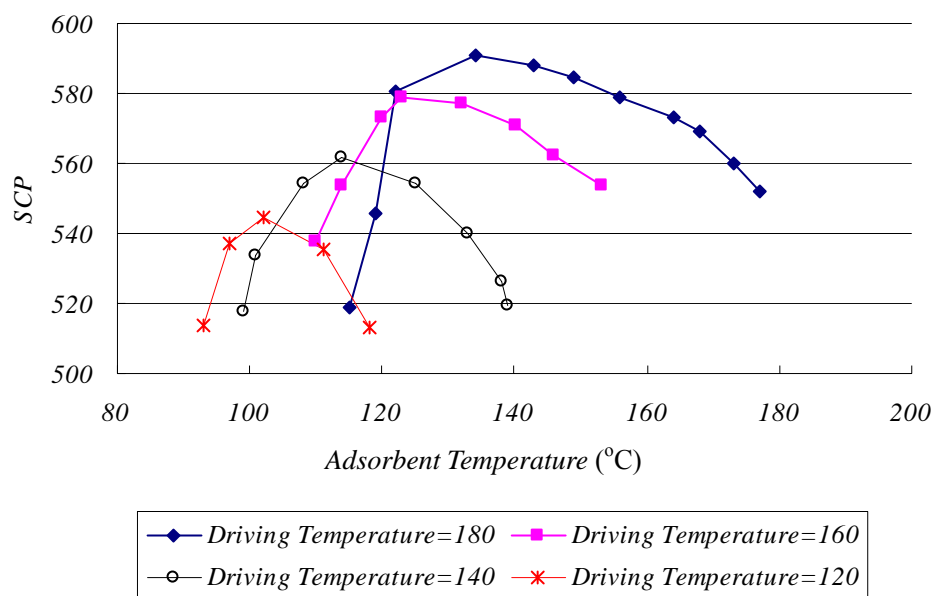


Figure 7-18 Adsorbent temperature correlated against driving temperature for maximum SCP

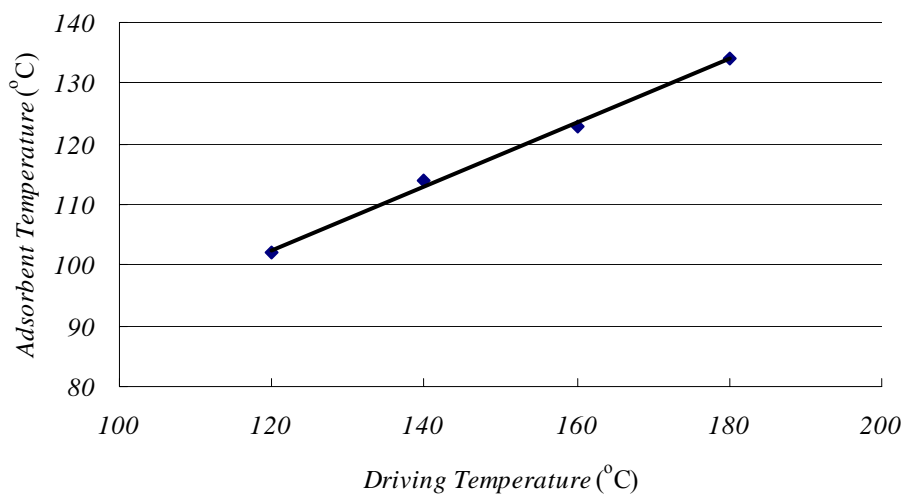
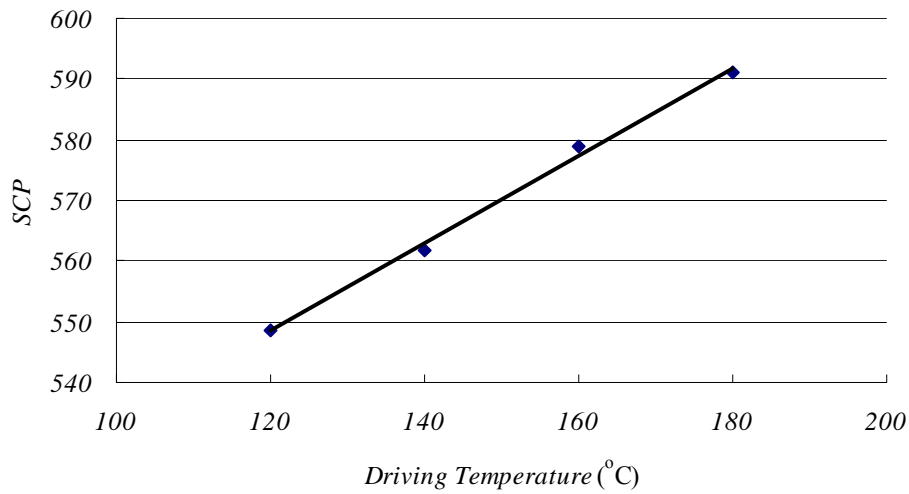


Figure 7-19 Maximum SCP correlated against driving temperature



From the figure 7-18 and 7-19, it can be seen that for each driving temperature, the relationship between adsorbent temperature and driving temperature and the one between SCP and driving temperature are all linear, which can be described in equation (7-25) and (7-26).

$$T_{ad} = 0.525T_{dr} + 39.5 \quad (7-25)$$

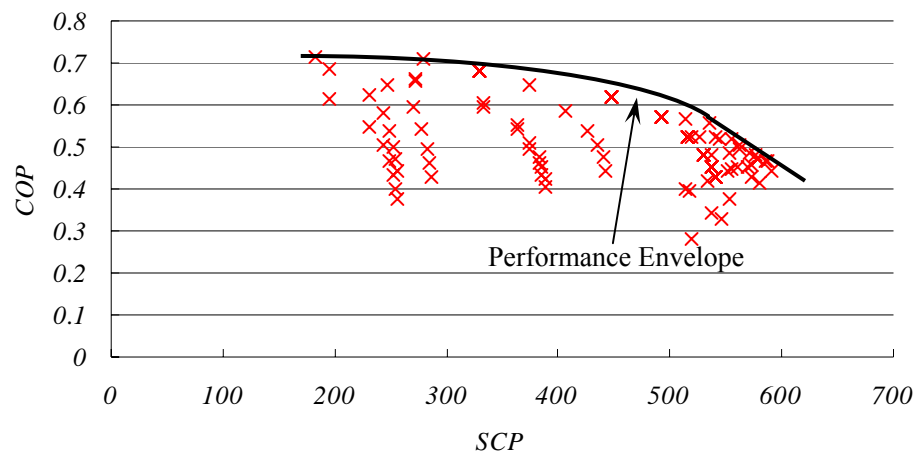
$$SCP = 0.7817T_{dr} + 451.82 \quad (7-26)$$

where T_{ad} is the adsorbent temperature, °C; T_{dr} is the driving temperature, °C; SCP is the maximum specific cooling power for each driving temperature, J/kgK. Equation (7-25) and (7-26) can be used to predict the best performance of adsorption system. For example, for a adsorption system with the maximum adsorbent temperature of 100°C, the best driving temperature should be 115°C and maximum SCP 540 J/kgK.

As mentioned before, the conditions for maximum COP are not the same as those for maximum SCP and a trade off must be made between the two. In figure 7-20, COP has

been plotted against SCP for various maximum adsorbent temperatures, approach temperature differences and fluid flow rates in order to obtain a ‘performance envelope’ which gives the optimal COP-SCP trade offs. This figure may not cover the full range of COP and SCP, but it can still provide useful information for the performance of adsorption system using BaCl_2 – vermiculite and ammonia.

Figure 7-20 ‘Performance envelope’ for the conditions and bed outlined in table 7-1



So far, the model has provided useful insights and relationships for the effects of various parameters on the performance of adsorption heat humps. For the cases mentioned above, the maximum COP of around 0.7 and maximum SCP of around 600 in an air conditioning application with one-bed basic cycle is encouraging. Although the use of an ideal cycle in the model means that performance is overestimated, the relationships should still hold.

7.4 Prediction of behaviour in a sorption generator

This compact bed can be used as car air conditioning in which the waste gas can be used to a heat generator bed. The driving temperature in this case is set to be 95°C. And the desorption inlet fluid temperature is set to be 30°C and the condensing and evaporating temperature are set to be 40°C and 10°C respectively. And due to the different compactness of adsorbent, the density will change from 230 to 750 kg/m³ and thermal conductivity will change from 0.1 to 0.4W/mK. To simplify the modelling, the density of 500 kg/m³ and two thermal conductivities, 0.1 and 0.4 W/mK, are assumed.

The simulating results are outlined in table 7-2. The temperature of adsorbent, the wall and the outlet of the fluid and the concentration are plotted against time in figure 7-22, 7-23 and 7-24 for a typical case, in which thermal conductivity is 0.4 Wm⁻¹K⁻¹ and the evaporating temperature is 20 °C.

Table 7-2 Simulating results of adsorption system using BaCl₂ – NH₃

Thermal conductivity, (W m ⁻¹ K ⁻¹)	Evaporating Temperature, (°C)	Adsorption cycle time, (seconds)	Desorption cycle time, (seconds)	COP	SCP
0.4	20	130	600	0.6158	260.89
	10	150	1000	0.5841	135.83
0.1	20	245	800	0.6477	203.35
	10	270	1200	0.6075	108.13

Figure 7-22 Temperature of adsorbent against time

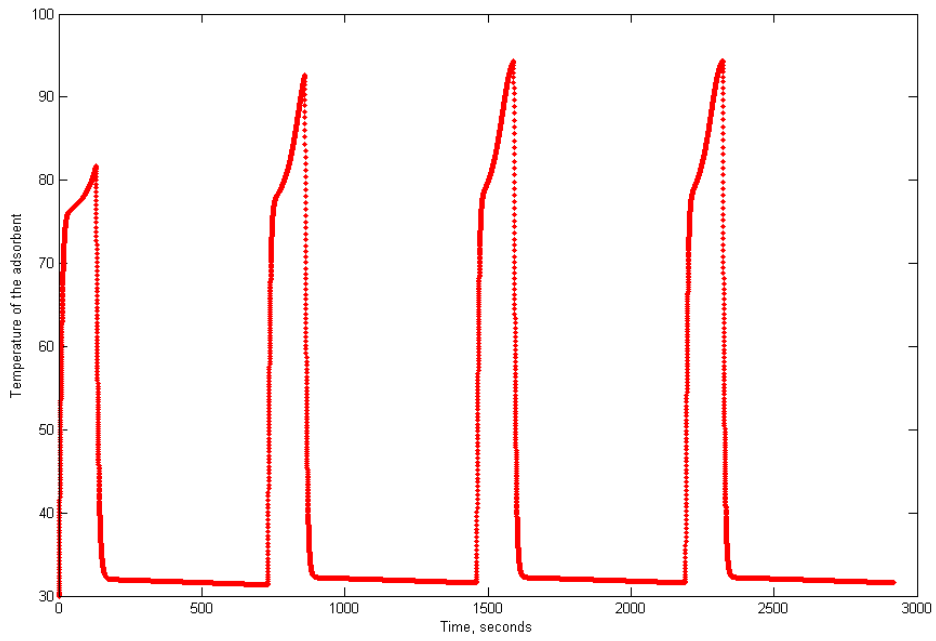


Figure 7-23 Temperature of the wall against time

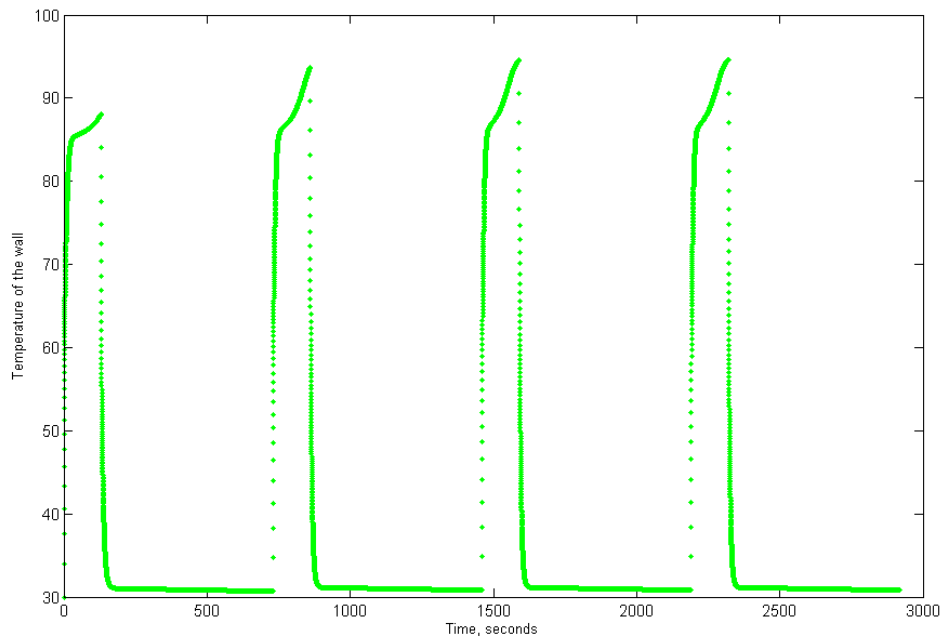


Figure 7-24 Outlet temperature of the heat transfer fluid against time

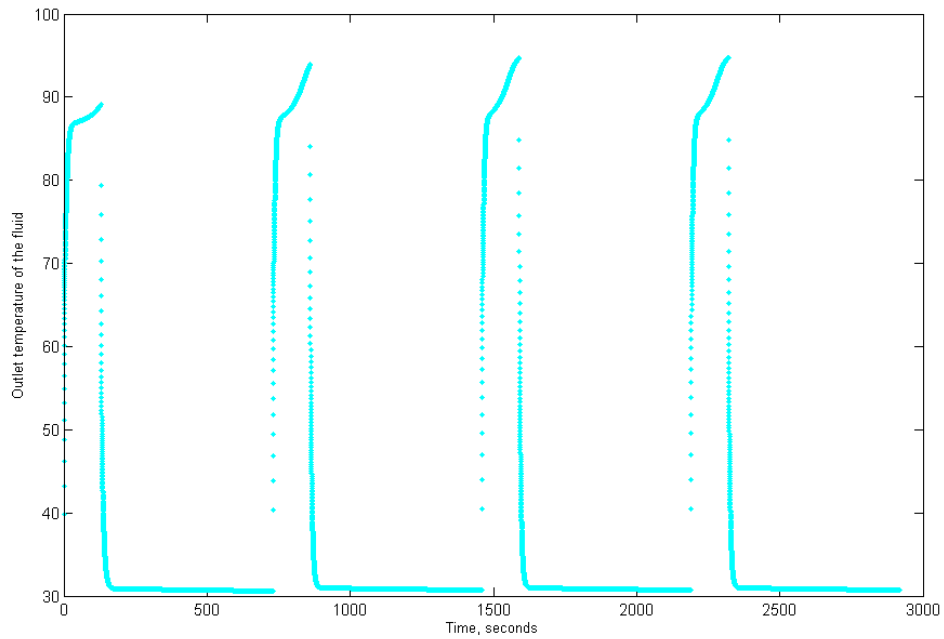
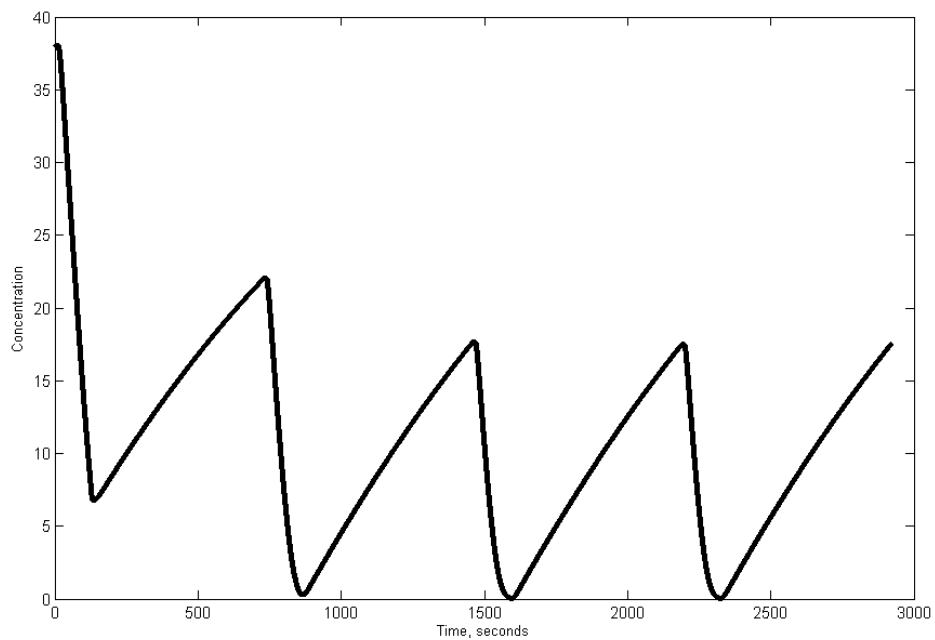


Figure 7-25 Concentration of adsorbent against time



Although the specific cooling power of 260 W/kgBaCl_2 in an air conditioning application is disappointing, such a machine could perhaps be used as auxiliary heat

pump when using waste heat or solar energy. Also multiple-bed regeneration can improve the performance remarkably.

Reference:

- [1] R.E. Critoph, and S.J. Metcalf, Specific cooling power intensification limits in ammonia-carbon adsorption refrigeration systems, *Applied Thermal Engineering*, vol. 24, pp. 661-678, 2004
- [2] J.P. Holman, *Heat transfer*, McGraw-Hill, 7th Edition in SI Units, p.289, 1992
- [3] S.J. Metcalf, Next generation of adsorption heat pumps utilizing monolithic carbon, 3rd year project report, 2003
- [4] S.J. Metcalf, Simulation of the effect of generator heat transfer parameters on power density and efficiency in multiple-bed regenerative carbon-ammonia sorption heat pump, *International Sorption Heat Pump Conference*, June 22-24, Denver, USA, 2005
- [5] R.E. Critoph, Adsorption refrigeration and heat pumps, In: *Carbon materials for advanced technologies*, Edited by Timothy D. Burchell, pp.303-340, PERGAMON, 1999
- [6] D.M. Ruthven, *Principles of adsorption and adsorption processes*, John Wiley and Sons, pp.29-30, 1984
- [7] IIR ammonia data book, *International Institute of Ammonia Refrigeration*, Washington, D.C., December 1992

Chapter 8 Conclusion

Sorption systems in some ways are considered as an ideal replacement for the classical vapour compression machines due to its energy saving and environmental benefits. They can efficiently use natural gas, solar energy or even waste heat as primary energy source, Also Sorption system can use environmentally friendly refrigerant such as ammonia, methanol and water, instead of CFCs, so that reduce the ozone layer depletion and global warming.

The sorption performance of a new adsorbate, CO₂, was studied with various adsorbent. The isosteres and isotherms of ammonia sorption were measured at T = 30-200°C and P = 2 – 20 bar. It was found that the performance of the adsorption system was poor due to lower latent heat of CO₂. So CO₂ is not practical for adsorption systems.

New composite ammonia sorbents, 59 wt. % BaCl₂/vermiculite, were synthesized and studied. The experiments were conducted under the conditions of T=20 - 60°C and P = 2 – 20bar. It was found that the modification of host matrices by the salt dramatically increases the ammonia uptake due to the formation of BaCl₂•8NH₃ complex. Hysteresis between the synthesis and decomposition reaction was found and investigated. The van't Hoff equation was used to fit the experimental data. It was found that the equations could predict the transition of synthesis and decomposition, and the hysteresis loop very well. As comparison, other hybrid materials consisting of CaCl₂ impregnated with various materials are also

made and studied. Hysteresis between adsorption and desorption was also observed. Four transition lines were observed and fitted by van't Hoff equation. For these composites the transition lines were close to the literature values under low pressure.

Dynamic tests under isothermal conditions were performed for the BaCl_2 composition salt. A modified Linear Driving Force (LDF) model was presented. The two constant in the model were empirical values which are determined by experimental data. The comparison between the experimental data and results from the model showed that the model can predict the dynamic process under isothermal conditions very well.

To test the validity of model for a real adsorption system, researches on the dynamics of a real pilot scale experimental rig were performed. The comparison showed that the model suitable under isothermal conditions could also be used for a real sorption system.

Due to its simple, analytical, and physically consistent, the modified LDF model with a lumped mass transfer coefficient could be used for practical analysis of dynamic data and for adsorptive process design. For a compact bed, which was designed and optimized by Critoph and Metcalf, this model is used to predict the performance of adsorption system utilizing BaCl_2 composite sorbent and ammonia as adsorption pairs. The simulation showed the encouraging performance of maximum *COP* of around 0.7 and maximum *SCP* of around 600 in an air conditioning application with one-bed basic cycle.

Further studies could focus on the commercial use of this promising material in air conditioning. Real lab scale compact bed could be set up and tested for the performance of adsorption pairs.